ARTICLES FOR FACULTY MEMBERS

The Application of Pyrolysis in Achieving UNs Sustainable Development Goals

TITLE/ AUTHOR	Reviewing the potential of Waste-to-Energy (WTE) technologies for Sustainable Development Goal (SDG) numbers seven and eleven / AlQattan, N., Acheampong, M., Jaward, F.M., (...), Vijayakumar, N., Bello, T.
SOURCE	Renewable Energy Focus Volume 27, December 2018, Pages 97-110 https://doi.org/10.1016/j.ref.2018.09.005 (Database : Science Direct)

TITLE/ AUTHOR	Application of GCMS-pyrolysis to estimate the levels of microplastics in a drinking water supply system / Gomiero, A., Øysæd, K.B., Palmas, L., Skogerbø, G.
SOURCE	Journal of Hazardous Materials Volume 416, 15 August 2021, 125708 https://doi.org/10.1016/j.jhazmat.2021.125708 (Database : Science Direct)

TITLE/ AUTHOR	Bio-based production of carbon nanotubes via co-pyrolysis of eucalyptus oil and ferrocene / Le, G.T.T., Mala, P., Ratchahat, S., Charinpanitkul, T.
SOURCE	Journal of Analytical and Applied Pyrolysis Volume 158, September 2021, 105257 https://doi.org/10.1016/j.jaap.2021.105257 (Database : Science Direct)

TITLE/ AUTHOR	Biochar for environmental sustainability in the energy-water-agroecosystem nexus / Malyan, S.K., Kumar, S.S., Fagodiya, R.K., (...), Singh, R., Singh, L.
SOURCE	Renewable & Sustainable Energy Reviews Volume 149, October 2021, 111379 https://doi.org/10.1016/j.rser.2021.111379 (Database : Science Direct)

27th January 2022
Source : Perpustakaan Sultanah Nur Zahirah

ARTICLES FOR FACULTY MEMBERS

The Application of Pyrolysis in Achieving UNs Sustainable Development Goals

TITLE/ AUTHOR	Nano-sized mesoporous biochar derived from biomass pyrolysis as electrochemical energy storage supercapacitor / Husain, Z., Shakeelur Raheman, A.R., Ansari, K.B., (...), Qyyum, M.A., Lam, S.S.
SOURCE	Materials Science for Energy Technologies Volume 5, January 2022, Pages 99-109 https://doi.org/10.1016/j.mset.2021.12.003 (Database : Science Direct)

TITLE/ AUTHOR	Strategic hazard mitigation of waste furniture boards via pyrolysis: Pyrolysis behavior, mechanisms, and value-added products / Foong, S.Y., Liew, R.K., Lee, C.L., (...), Tsang, Y.F., Lam, S.S.
SOURCE	Journal of Hazardous Materials Volume 421, 5 January 2022, 126774 https://doi.org/10.1016/j.jhazmat.2021.126774 (Database : Science Direct)

TITLE/ AUTHOR	Generating alternative fuel and bioplastics from medical plastic waste and waste frying oil using microwave co-pyrolysis combined with microbial fermentation / Wan Mahari, W.A., Kee, S.H., Foong, S.Y., (...), Lam, S.S., Sonne, C.
SOURCE	Renewable and Sustainable Energy Reviews Volume 153, January 2022, 111790 https://doi.org/10.1016/j.rser.2021.111790 (Database : Science Direct)

TITLE/ AUTHOR	**Reviewing the potential of Waste-to-Energy (WTE) technologies for Sustainable Development Goal (SDG) numbers seven and eleven / AlQattan, N., Acheampong, M., Jaward, F.M., (...), Vijayakumar, N., Bello, T.**
SOURCE	**Renewable Energy Focus Volume 27, December 2018, Pages 97-110 https://doi.org/10.1016/j.ref.2018.09.005 (Database : Science Direct)**

ELSEVIER

Reviewing the potential of Waste-to-Energy (WTE) technologies for Sustainable Development Goal (SDG) numbers seven and eleven

RESEARCH REVIEW

Nael AlQattan[a], Michael Acheampong[b,*], Foday M. Jaward[c], Funda Cansu Ertem[d], Nisha Vijayakumar[c] and Tolulope Bello[c]

[a] Qaisarat Al Dwaieh, 2nd Floor Al- Mobarakeia, Saud Ben Abdul Aziz Street, Kuwait
[b] Department of Geography, Oklahoma State University, 337 Murray Hall, Stillwater, OK 74078, USA
[c] College of Public Health, University of South Florida, 13201 Bruce B. Downs Blvd., MDC 56, Tampa, FL 33612, USA
[d] Department of Biotechnology, Technische Universität Berlin, Ackerstr. 76, ACK24, 13355 Berlin, Germany

Increasing global population and urbanization, coupled with rising standards of living have contributed to two of the world's most important challenges: a) increasing per capita energy consumption and global reliance on fossil fuels, and b) increasing per capita waste generation. The UN prominently featured addressing these two issues in goal numbers seven and eleven, respectively, of the SDGs. Waste-to-Energy (WTE) technologies have the potential to serve as a connecting link to support the successful pursuit of these two goals. They can control urban wastes and elevate waste as a necessary resource for energy production. This study reviews and presents an appraisal of the fast-evolving WTE technologies and their potential to harness energy potential of wastes in the pursuit of SDGs number seven and eleven. The study reveals illuminates the apparent inherent potential of WTE technologies to support the SDGs due to the considerable flexibility they present with their ability to utilize different forms of waste as feedstock. Environmental and economic performance of WTE incineration have steadily improved over the years, making it pivotal in pursuing these goals. Meanwhile, technologies such as gasification, anaerobic digestion, and pyrolysis have vastly expanded the array of waste products that are diverted from landfills for energy generation purposes. While there is lot more room for WTE technologies to grow into the mainstream in terms of their energy production capabilities, it is without doubt that investing and elevating WTE technologies will support the global drive towards achieving SDG numbers seven and eleven.

Introduction

Global population continues to accelerate at tremendous levels. Human populations are consuming significant amounts of energy through the production and consumption of resources as there is a general trend of increased per capita energy consumption due to rising standards of living [1]. The rapid rise in energy consumption is introducing high levels of GHG emissions into the atmosphere, which is known to be fundamental to climate change. Traditionally, the world has relied primarily on fossil fuels for energy supply [2–4]. While renewable energy has been advocated in recent years to mitigate climate change, fossil fuel contribution to total global energy supply has not reduced. Currently, as seen in Figure 1, traditional fossil fuels ranging from coal, crude oil, and natural gas account for about 13,700 TWh – about 84% – of electricity production in the world [2,5]. The high contribution of fossil fuels to primary energy supply remains an avenue of consternation for environmentalists and policy-makers alike, especially, given the continued dwindling of global fossil fuel reserves and fluctuating oil prices combined with climate change impacts [2,6]. The urgency of the need to continually pursue alternatives that will

*Corresponding author. Acheampong, M. (michael.acheampong@okstate.edu)

1755-0084/ https://doi.org/10.1016/j.ref.2018.09.005

Nomenclature

EC	European Commission
EPA	Environmental Protection Agency
EU	European Union
FAO	Food and Agriculture Organization
GHGs	Greenhouse Gas Emissions
IEA	International Energy Agency
LCA	Life Cycle Assessment
MACT	Maximum Available Control Technology
MDGs	Millennium Development Goals
MSW	Municipal Solid Waste
NACWA	National Association of Clean Water Agencies
OECD	Organization for Economic Cooperation and Development
PES	Primary Energy Savings
RDF	Refuse Derived Fuel
SDGs	Sustainable Development Goals
SRF	Solid Recovered Fuel
UN	United Nations
US	United States
WID	Waste Incineration Directive
WTE	Waste-to-Energy

rapidly wean the globe off fossil fuels is evident in predictions such as that of the U.S. Department of Energy that states that the earth is likely to warm by 1.7–4.9 °C over the period 1990–2100, due to carbon emissions [3,7].

The United Nations (UN) currently projects the world's population to top 9 billion people by 2050, with more than 50 percent inhabiting urban areas [8]. High energy consumption and waste generation are natural consequences of such rates of high population and urbanization. In fact, according to FAO [9], global energy demand will increase by nearly 60% by the year 2025. As far as waste generation is concerned, studies have estimated that municipal soil waste (MSW) generation levels will likely increase to about 2.6 billion tons by the year 2025 from its current level of 2.4, as urbanization and income levels increase [5,10,11]. Owing to this, the world is in dire need of sustainable urban development that will respond to high energy demand and waste levels [5]. The world acknowledges that continuing development and adoption of clean and sustainable energy are critical towards the drive for sustainable development, and has vigorously pursued alternative energy sources such as renewable bioenergy, solar radiation, wind, and waves among others [7,12,13].

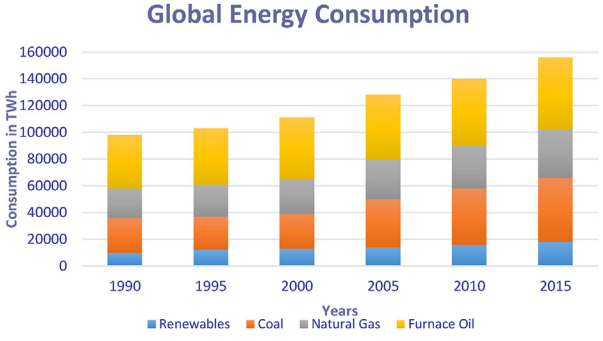

FIGURE 1

Contribution of Fossil Fuels and Renewables to Global Electricity Production [5].

While the UN Millennium Development Goals (MDGs) did not explicitly outline any targets in terms of global waste management and renewable energy development, these two issues featured prominently in the UN Sustainable Development Goals (SDGs) adopted in 2015, highlighting the recognition of their importance in achieving sustainable development. Specifically, the goal number 7 of the SDGs set the following targets in pursuit of sustainable and renewable energy: a) ensure universal access to affordable, reliable and modern energy services; b) to substantially increase the share of renewable energy to global energy mix by 2030; c) to double the rate of improvement of energy efficiency in countries around the globe by 2030; d) to facilitate access to renewable and clean energy technology and promote investment in energy infrastructure by 2030; and e) to increase supply of modern and sustainable energy services for all in developing countries through infrastructure expansion and technology upgrade by 2030 [14]. In a similar breadth, the sixth target in the goal number 11, which is to make cities inclusive, safe, resilient and sustainable, states the following: by 2030, reduce the adverse per capita environmental impact of cities, including by paying special attention to air quality and municipal and other waste management [14]. Tapping into waste materials to produce energy seems to be one of the most attractive options for future energy supply. This is because it holds the potential to aid in dealing with two crucial global challenges, which are namely: dealing with increased waste levels due to rising world population and urbanization; and mitigating fossil fuel driven GHG emissions [6,7]. Waste-to-Energy (WTE) technologies have shown enough promise in both of these directions.

The concept of WTE is not necessarily new as in renewable bioenergy development, using wastes from agricultural activities have been critical for the development of second generation biofuels. In recent years, however, WTE technologies have been increasingly developed to extract energy from an even wider array of wastes including MSW and sludge [6,7,15–17]. The appeal of WTE technologies has spurred many countries and world communities towards the quick adoption of these fast-evolving technologies [18]. Currently, the US and other developing countries around the world handle MSW in a hierarchy of preferred methodologies, where WTE far out-ranks landfilling.

Agricultural wastes, industrial and domestic wastes have been identified as endowed with renewable materials that are capable of producing energy in forms like biohydrogen, biogas, and bioalcohols [7,19–22]. Utilization of the growing levels of MSW and waste sludge for renewable energy finds the all-important string that connects providing a sustainable source of energy and transforming waste into a well-needed resource in the form of raw materials for energy generation [2,6]. In fact, many studies have been conducted by different authors regarding the potential of WTE technologies in country case studies [5,10,13,23,24] and advancements on the global level to support energy production [6,25–27]. However, there is currently no study assesses the potential of WTE technologies to support the SDGs. It is based on this observation that the authors of this study argue that if waste resources can be developed to be of such important value through WTE technologies, SDGs will be right on course to be able to achieve two of the

most notable additions as the globe transitioned from the MDGs to the SDGs era, while also contributing to the success of other goals. For this reason, in this paper, the authors present a critical appraisal of the quick-evolving WTE technologies and their breakthroughs and prevailing challenges; their trends and potential of adoptability in the quest to support the pursuit of the dual goals of SDG numbers 7 and 11; and how they will generally affect prospects of the renewable energy drive in the future. This article also outlines recommendations and research priorities for large scale adoption of WTE technologies around the globe to support the aforementioned SDGs. The rest of the paper is structured as follows: an overview of the quantities of wastes produced in the world, traditional waste disposal and management regimes, and waste as a renewable energy resource; a critical analysis of different WTE technologies; the benefits of large scale deployment of WTE; a summary of the paper; and areas of research and policy priorities.

Global waste as a renewable energy resource

Types of waste for energy generation

In the European Commission Waste Framework Directive (2008/98/EC), waste is defined as ''any substance or object which the holder discards or intends or is required to discard'' [2,28]. The umbrella of wastes is a broad one and covers a variety of items that includes those that are meant for further use, recycling or reclamation [3]. Wastes can be in the form of sludge or MSW.

MSW are wastes produced at household, commercial and industrial levels, under waste regulations [2,3]. Typically, waste management decisions as far as MSW are concerned are characterized by two components: a) how much waste to produce, and b) how to dispose of the waste [2]. While these two components are distinct, they are also significantly related, as the amount of waste produced may dictate the appropriate disposal method. MSW disposal can be undertaken by several means, including landfilling [29,30], recycling [31,32], and thermal and biological treatments [29,33,34]. MSW treatment can be quite different from the treatment of sludge [35].

Global waste quantities and regional variability

Currently, the amount of MSW generated around the world exceeds 1.3 billion tons per year, and averages about 1.2 kg person per day (1.2 kg/capita/day). This estimate is projected to increase to about 2.2 billion tons per year by 2025, with the average waste generated by increasing to nearly 1.5 kg/person/day [11]. The global averages, however, mask the inter-and-intra regional and country variabilities that prevail. Africa and South Asia produce the least amount of waste around the world, while the OECD countries, together, produce nearly half of the wastes generated as seen in Table 1. In sub-Saharan Africa, for instance, about 62 million tons of waste is produced annually, with an average of 0.65 kg/capita/day, and a wide intra-regional variation of 0.09–3.0 kg/capita/day [11,36].

The amount of waste generated from industrial nations, both on the household level and by industry, far outweigh that of their non-industrialized counterparts. In recent decades, the amount of wastes produced in industrial regions has seen a significant increase. For instance, in a period of about 25 years, OECD countries increased their MSW per capita from about 415 kg in 1980 to 560 kg in 2006 [27,37]. The EU alone produced a total of 250 million tons of waste in 2005, with per capita topping over 520 kg in 2007 as shown in Figure 2 below [26,38]. Similar to trends registered in the EU, the US has substantially its waste produced per capita, by raising it from 444 kg in 1960 to 725 kg by 2012 [27,39]. It was estimated that MSW generated in the US increased by more than 15 million tons in a two year period: an annual growth rate of 2.5%, from 335.80 million tons in 2002 to 351.90 million tons in 2004 [24,40,41].

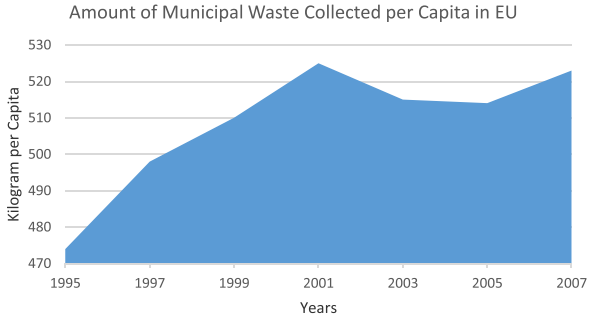

FIGURE 2

Waste Collected in the EU per Capita [38].

TABLE 1

Current and Projected Waste Generation around the Globe [11].

Region	Current Figures			Projected 2025 Figures		
	Total Urban Population (Millions)	Per Capita Waste Generation (kg/Capita/Day)	Total (Tons/Day)	Total Urban Population (Millions)	Per Capita Waste Generation (kg/Capita/Day)	Total (Tons/Day)
Sub-Saharan Africa	260	0.65	169,119	518	0.85	441,840
East Africa and the Pacific	777	0.95	738,958	1,229	1.5	1,865,379
Eastern and Central Asia	227	1.1	254,389	239	1.5	354,810
Latin America and the Caribbean	399	1.1	437,545	466	1.6	728,392
Middle East and North Africa	162	1.1	173,545	257	1.43	369,320
OECD	729	2.2	1,566,286	842	2.1	1,742,417
South Asia	426	0.45	192,410	734	0.77	567,545
Total	**2980**	**1.2**	**3,532,252**	**4285**	**1.4**	**6,069,703**

Increased waste generation around the world is a socioeconomic and ecological problem, and an issue of public health concern, especially in developing countries [25]. It has therefore been the preoccupation of scientists and policy makers alike to find more sustainable means of disposal. Over the last decade, however, there has been a significant drive towards developing technology that utilize waste as a needed resource in energy production.

Waste as raw material for energy generation

Traditionally, resources that are considered inexhaustible or replenished by nature are those that are classified under renewable energy sources. These sources energy normally include hydro [42], solar [43–45], geothermal [46], wind [43], and biomass, among others [10,47]. According to the US DOE [48], the term biomass encapsulates wide range of organic matter, plant and animal derived, that are available on renewable basis. This includes energy crops, agricultural wastes and residues, forest and wood wastes and residues, animal wastes, and others. MSW is currently classified under the broad umbrella of biomass it normally contains significant proportions of materials such as food waste, wood and yard trimmings, paper, and others. The US EPA also classifies MSW as a renewable resource because it is a constantly produced biogenic material that would be destined for landfills, if not channeled towards energy generation purposes [7,10,24,49].

Sludge has critical characteristics, including high energy and nutrient content. These two critical components of sludge make it technically and economically feasible to recycle nutrients and carbon from it [6,50]. The energy recovery potential of sludge is directly dependent on its composition. Sludge is mainly a mixture of volatile organic matter, inert inorganic matter, and water. The volatile solid component is the storehouse of the energy content inherent in sludge [6,51]. When dewatered, sludge can be incinerated for energy generation [27].

Waste treatment hierarchies

Historically, MSW has been primarily disposed of in landfills or dumpsites in many countries around the globe. This means of disposal has, however, oftentimes raised environmental and public health concerns [5]. Similarly, landfilling has also been a popular means through which waste sludge is disposed [6]. Other means of dealing with MSW are composting [52], recycling [31], and mechanical-biological treatment [24], while incineration, ocean disposal, and application as soil conditioner are also other common methods of sludge disposal [6].

Due to the concerns related to traditional disposal methods, many countries especially the developed ones are pursuing the objective of managing and controlling waste through a hierarchical system of preference. In this hierarchy, priority is assigned to ultimately reducing waste stream [2,53]. As seen in Figure 3, the hierarchy consists of five main steps in order of preference, namely: 1) waste prevention; 2) reuse; 3) recycling; 4) recovery (including energy recovery); and 5) safe disposal [2,53]. This hierarchy provides a useful framework for enactment policies related to waste management.

After waste prevention and reuse that are meant to reduce the waste stream is recycling in the hierarchy of preference. After recycling is the energy recovery. Overall lifecycle assessments carried out by several researchers have shown that recycling is

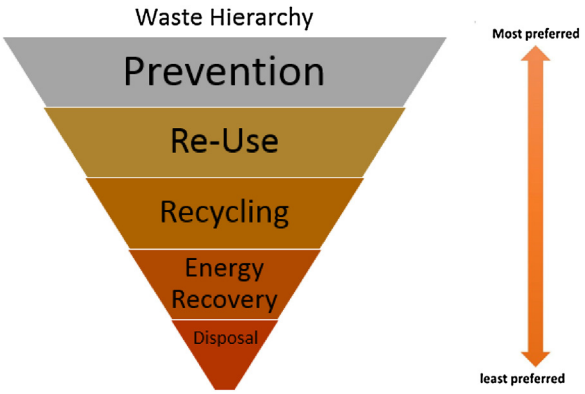

FIGURE 3

Waste Treatment Hierarchy in Order of Preference [2].

the most environmentally friendly waste management option in terms of the carbon savings and costs [2]. However, recycling does not provide the benefit of energy recovery, and materials that cannot be recycled are usually candidates for the process of energy recovery, preferable to traditional landfilling.

The potential of WTE to recover energy from unrecyclable components of the waste stream has made it an indispensable part of the concept of circular economy that has been on the rise for over a decade. The concept of circular economy is a concept developed to achieve a closed-loop economy in which industrial and economic growth are decoupled from environmental degradation [54,55]. The increasing recognition of the need for renewable energy to play a central role in a circular economy has increased the core principles from the 3R (reduction, reuse, and recycling) [54] to 5R (reduction, reuse, recycling, recovery, and reclamation) [55]. Pan et al. [55] observed that the inclusion of WTE in the quest of closing the loop in a circular economy has enhanced industrial symbiosis in ecological industrial parks where businesses coordinate their operations to reduce waste to improve environmental quality and increase economic gains.

At this juncture, it is important to present an overview of the process of recycling (as it could also be an important component to WTE as it will be explained later in a subsequent section) before focusing on a critical appraisal of various WTE technologies.

Overview of recycling

Recycling products is a green and environmentally friendly approach to minimize waste and produce final materials that serve as biomass from waste for renewable energy. According to the US Environmental Protection Agency, recycling is the development of collecting and processing previously manufactured materials that would be otherwise disposed in a landfill and turning them into new products [56]. Recycling is typically understood to be a continuous cycle of three steps, which is classically defined by the three arrowed recycling symbol as seen below in Figure 4.

The first step of the recycling procedure requires the recovery of previously manufactured and used resources, which would otherwise be disposed of. Methods of resource recovery include curbside collection, buy-back centers, drop-off centers and deposit/refund programs [56]. The next step of the loop entails recyclable items to be sent to a ''recovery facility'' where they are sorted, cleaned and

FIGURE 4
Symbol of the Recycling Process [56].

processed into raw materials that can be used in the manufacturing new, marketable products [56]. This step of the process varies depending on the type of product being recycled (glass, aluminum, paper, e-waste, etc.). However, all recovered products go through a method that breaks down the original material, either through a melting or liquefying process, before it can be made into a new material. Recycled materials can be used to manufacture an assortment of products and are constantly being tested in new ways, such as using recycled glass to pave roadways [56].

The final step of the recycling sequence relies on the consumer or businesses to continuously purchase products made from recycled materials. These products include aluminum cans, carpeting, motor oil, newspapers, trash bags, nails and much more [56]. After these products have outlived their intended lifespan, the expectation is for the materials to once again be recovered by recycling facilities in order to begin this process over again.

The idea behind recycling has always been a practical concept due to the economic benefits of using recycled or recovered materials versus new, ''virgin'' materials [57]. With an ever increasing demand for consumable materials, societies have had to explore options, which offer extra sources of materials [57,58]. The importance recycling from MSW as a precursor in the WTE process, and a critical factor in the loop of a circular economy is demonstrated in Figure 5 below.

Evolution of WTE technologies from the rudimentary to the revolutionary — assessing their pros and cons

With the dwindling reserves of global oil and dangers posed by climate change, the fact that global demand for energy is expected to increase six fold by 2100 needs immense innovation and approaches that attempt to revolutionize the global energy sector [7]. WTE technologies are viewed as potential alternatives to the traditional fossil fuel production.

As represented in Figure 6 below, there are three main routes through which energy is recovered from wastes, namely; 1) biochemical, 2) thermochemical, and 3) Physicochemical. In the biochemical pathway, organic wastes are converted to liquid or gaseous forms of energy primarily through biomethanation and fermentation [59,60]. For the thermochemical pathway, through processes such as incineration, gasification and pyrolysis, waste feedstocks are converted to energy in the form of electricity and heat, by applying high temperatures [61,62]. In the physicochemical pathway such as transesterification, organic wastes are converted to energy by the use of chemical agents [38,63].

At this juncture, the different technologies are appraised for their performance and influence on global energy systems.

Waste incineration/combustion

Waste incineration is simply the oxidation of combustible components of waste, which is employed as the most integral part of waste management around the globe [5,26,64]. Traditionally, the appeal of incineration as a waste management technique lied in the fact that it could vastly reduce the weight and volume of wastes by approximately 80% and 70%, respectively, and contribute to public health by destroying harmful substances [5,10,26]. In recent years, however, the appeal of incineration is its combination with energy recovery. Incineration is the most conventional WTE in heat and electricity generation [26]. Typically, organic materials that are recovered from wastes have sizeable deposits of energy of which about 65–80% can be tapped for heat and deployed in thermal supplies [65,66].

Of all WTE technologies, the method of incineration is the most mature and widely adopted around the globe, with the major differentiating characteristics being the different levels of advancement between countries [2,5,10,26,67,68]. The efficiency level of the process of incineration is said to be about 25–30% and can largely be determined by the composition of waste stream, especially for MSW as waste can be very heterogeneous [2,5,26]. Increasingly, advancements in incineration technologies are increasing the potential for thermal treatment and the efficacy of high energy retrieval from sewage sludge [6,26,69,70].

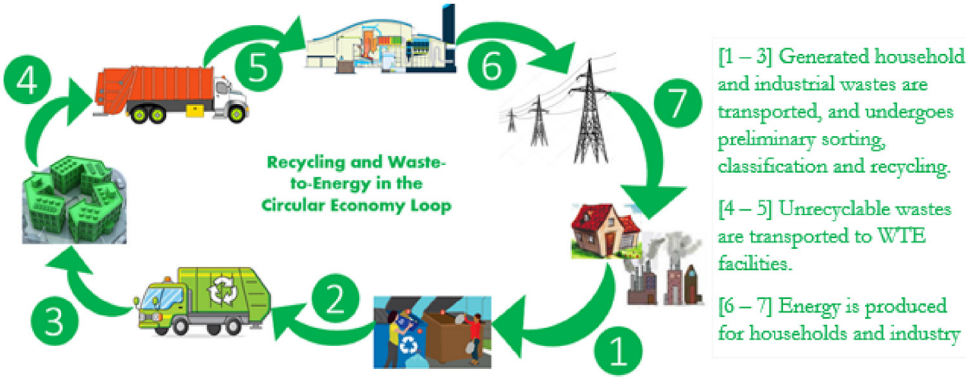

FIGURE 5
Schema of a Recycling and WTE as components of a circular economy.

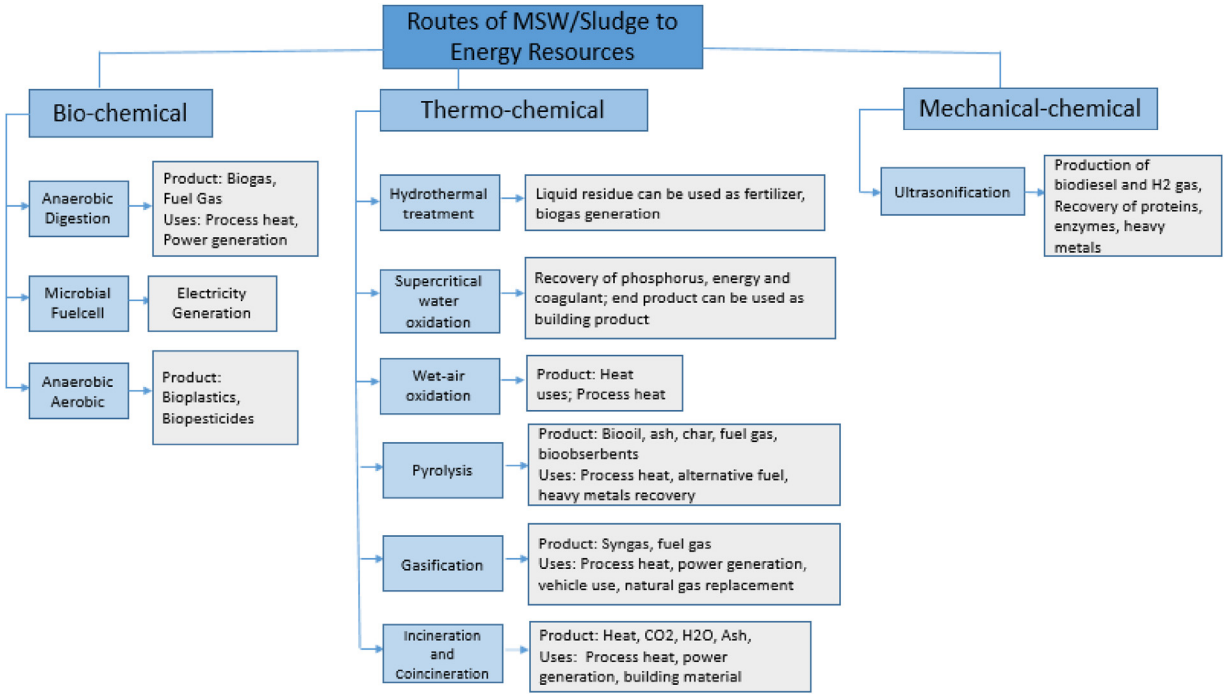

FIGURE 6

WTE Conversion Routes [5,6].

Generally, incineration WTEs are categorized into two. They are the mass-burn and refuse derived fuel (RDF). The main difference between the two is that mass-burn undergo little to no pre-processing of waste before incineration, while RDF undergoes pre-processing by carefully sorting materials with low heat value and low calorie content, such as glass and metals. For RDF, uniform waste content is produced after the pre-processing to be shredded to produce fuel with relatively more uniform characteristics compared to mass-burn. While RDF may be more efficient, mass-burn facilities are more common [18].

In the incineration WTE process, while there several different deployed for the combustion, there are three main incinerator types used in the combustion phase of the process, namely; a) grate incinerators or moving grates, b) rotary kilns, and c) fluidized bed. In grate incinerators, the grate, in a tumbling manner, moves the waste in the combustion chamber through different zones. Through this tumbling motion, wastes are well-mixed and uncombusted materials are readily exposed to the heat [18,26]. Rotary kilns are similar to moving grates in process except that the incineration occurs in a rotating chamber. In the rotary kiln, a cylindrical vessel spinning around its axis, by means rollers that are located under it, conveys waste by means of gravity [18,26]. In the fluidized bed incineration, there is a bed of inert material that is fluidized with at the lower section of the combustion chamber into which waste is constantly fed. Air flowing constantly beneath bed allows the waste to keep moving, in order to ensure a more complete combustion. It is normally used for processing sludge or waste that has gone through a great deal of pre-processing and therefore, finely divided like RDF [18,26,71].

While incineration has traditionally been viewed as a costly method for waste processing, the advent of WTE that makes it possible to collect heat generated from steam for heating and power generation. Funds generated from selling by-product electricity and steam improves the cost performance of incineration. It is also worth noting that efficient WTE incineration plants possess higher positive externalities through improvement in energy security and reduction of GHG emissions [2,10]. This notwithstanding, when WTE incineration is considered for its electricity generation potential only, it is found to be less efficient compared to fossil fuel-based conventional electricity plants. In fact, electrical power production efficiency in WTE incineration can be lower than 20% [2,27,72]. This, as Stehlik [27] and Pavlas et al. [38] explain, could be attributed to improvement in equipment requirements for waste incineration and cogeneration of heat and electricity. Combined heat and power (CHP) can raise efficiency of WTE incineration to about 80% [2]. A study conducted by Cucchiella et al. [23] also showed that only electric configuration of a WTE plant produced emissions greater than cogenerative configuration by 14% i.e. environmental savings of 430 kg CO2eq per ton of waste and 370 kg CO2eq per ton of waste, respectively.

Some researchers have conducted studies that have revealed that the environmental and economic performance of WTE incineration as against conventional power and heating plants is improving with time as the technology is improved. In a study conducted by Pavlas et al. [38], the primary energy savings (PES) performance of stand-alone WTE systems defeated natural gas-based cogeneration systems in PES, revealing the potential to successfully substitute fossil fuels, with better environmental gains [38].

While WTE incineration's environmental and economic performance has vastly improved over time, several challenges persist. To overcome these challenges, it is important to fully understand their nature and the inherent trade-offs that exist in the development of incineration technologies. Additionally, it is pertinent to illuminate some of the steps that have been and/or are being

developed to mitigate the shortcomings. The subsequent subsections are dedicated to assessing the challenges and followed by the mitigating steps.

Understanding the challenges of incineration

Emissions of GHGs and air pollutants

One of the biggest challenges with incineration is the emissions of GHGs and other pollutants that is contrary to the environmental benefits being some of the primary reasons for which it is pursued. While WTE incineration have been found to perform better in CO and particulate matter emissions than other technologies, it has been found to perform worse in SO_X, carbon dioxide (CO_2) and nitrous oxide (N_2O) emissions, which can have significant negative effect on climate [5,10,73,38].

During the incineration process, the composition of the materials may result in the formation of particulate and acid gas pollutants, including SO_2, VOCs, PCBs, CO, HCl, HF, HBr, and heavy metal compounds among others [18,26,68]. Concerns about dioxin emissions have prompted more stringent regulations in many countries, developed and developing, such as Germany, China and Taiwan, among others to limit dioxin emissions to 1 ng toxic equivalent per cubic meter for incinerators [10,18,68,74,75].

Fly ash public health concerns from WTE emissions

While one of the central arguments of WTE incineration has been the potential to positively contribute to public health by killing pathogens and other bacteria that may accumulate in garbage in landfills, there are externalities relating to pollution from incineration that may be detrimental to public health [18,38]. However, fly ash from incineration poses an existential health risks, including respiratory ones, through carriage of toxic heavy metals such as mercury and lead, along with other pollutants such as furans and dioxins. Besides, incineration plants can be unsightly and could also produce unpleasant odors [2,10,55,76]. Incineration facilities can cause significant water and soil pollution through leaching, as in the case of landfilling [24,68].

High operational cost

The cost of operating a WTE incineration plant can be steep especially if operated without the possibility of CHP which can improve its efficiency and increase financial gains [10]. Even with CHP, the initial capital investments involved in WTE incineration can be deterring for poor countries [10,26]. Incineration equipment with greater capacities are normally imported by low-technology countries, which are accompanied by high operating and maintenance costs for complex pollution control mechanisms for modern facilities [10].

Meanwhile, other studies have revealed that running the most environmentally efficient WTE systems may not always be the most financially prudent, leaving proponents with a dilemma. As previously noted, Cucchiella et al. [23] found that cogenerative configurations in WTE systems perform better environmentally; however, they found that it has worse financial performance compared to the electric only configuration. In the study, profit generated by 150 kt plant in electrical configuration was significantly higher than a 300 kt plant with cogenerative configuration (25.4 € vs. 4 € per kiloton of treated waste).

Overcoming incinerator challenges with increased regulations and technological advancements to support SDGs

One of the concerns that has surrounded incineration, as previously explained, has been the enormous air pollution they can cause [18,27]. Over the years, the US and the EU have passed stringent air quality legislations such as maximum available control technology (MACT) regulations and the waste incineration directive (WID), respectively, which have contributed better environmental performing WTE incineration plants [3,18,24].

To meet the new emission standards, new age incineration plants are equipped with modern combustion, additional pollution control technologies and flue gas cleaning systems, which result in retrieving substantial amounts of energy from combustion and reduction of emissions [18,24,27]. The implementation of the MACT regulations in the US resulted significant reduction of mercury emissions, and other volatile heavy metals, furans, and dioxins by over 99% [24,77].

Performance of new generation WTE incinerators have improved so much that the USEPA considers it as one of the cleanest sources of energy in the US, and this has helped shift public perception about WTE incineration favourably [10,18,24,27,78–81]. While they may come with additional costs, advancements such as introduction of secondary combustion chambers, low-NO_X burners, dioxin filters, heat exchangers, waste heat recovery systems, wet scrubbers, and flue gas recirculation systems help ensure that emissions are reduced, and contribute to the improved environmental performance [26,27,82]. Additionally, leaching of heavy metals resulting post-combustion is also being counteracted with advanced technologies that reprocesses and recycles plant ash, rather than disposing of under traditional landfill conditions. Many countries have advanced technologies that utilize this ash by-product as cement substitute, road aggregate, and fill material [18].

Without a doubt, these advancements chalked in WTE incineration especially those designed for CHP, and further developments are increasing its viability to supporting the renewable energy drive and sustainable cities target by 2030. Besides incineration, however, a range WTE technologies have been developed since the 1970s that have the potential to complement or serve as useful alternatives to incineration. Some of these approaches are also thermochemical but arguably more advanced and not adopted on the same scale as incineration [26,53,83]. Technologies such as thermal gasification, pyrolysis, and biogas development can be applied to different forms of waste streams to achieve specific and different range of desired products. Additionally, they are able to increase efficiency that may not be achieved with incineration, due to their greater flexibility in the energy system compared with incineration that is characterized by high and constant heat production [26,53]. Sections that follow sheds light on some of these technologies and their advancements.

Gasification

Gasification is simply a process whereby organic substances are partially oxidized at elevated temperatures, typically in the range of 500–1800 °C and reduced amount of oxygen. Besides, very high pressure is required for the process of gasification, in the range of 0.6–2.6 MPa (MPa). The substances are broken down in ash that

forms a molten slag, which is subsequently quenched at the bottom of the gasifier, and incombustible gases [6,26,84]. As Tyagi and Lo [6] and Bosmans et al. [26] have indicated, the main products of gasification are heat and a high quality synthetic gas (syngas) that is formed after resultant raw gas is cleaned by removing CN, NH_3 and H_2S. Being an indirect process of combustion, in gasification, an exothermic reaction takes place in a reactor as a result of a reaction between carbon and O_2 that produces energy to drive the reaction [5,6]. In regard of the above, it is safe to say that the process of gasification has three main driving parameters, which are temperature, O_2 concentrations, and pressure [5].

In the process of gasification, the waste to be treated is converted into a secondary energy carrier in the form of either a combustible liquid, gas or solid. Subsequently, the secondary carrier is combusted in a turbine to produce heat or electricity or both [26]. The first part of the process is carried out in an oxy-steam fluidized bed reactor at relatively low temperatures of around 600–800 °C. This is to ensure that metals like aluminum that may be part of the waste stream are not melted, and are successfully collected at the bottom of the gasifier. In the second phase, higher temperature gasifiers that have the capacity to deal with flows that have a significant content of solids above their melting point of 1300–1500 °C. Unlike WTE incineration which is only useful energy recovery, gasification may be used for the recovery of the chemical value of wastes. The product syngas can, therefore, be used as a feedstock in the chemical industry after adequate processing [26].

Apart the possibility of recovering chemical value, gasification is known to have several other advantages over WTE incineration. Being a partial combustion process, it only requires a fraction of the oxygen amount needed in incineration. This limits the amount of dioxins, SO_2 and NO_x, which reduces or eliminates the need to purchase expensive gas cleaning equipment that is needed to enhance environmental performance in incineration [26,85]. Additionally, gas generated by gasification is combustible and can be integrated with gas engines and fuel cells for electricity, among others. As far as the benefit of waste treatment is concerned, gasification is also said to fare even better than incineration in terms of reducing waste volume, with lower energy consumed [26,86]. As Ouda et al. [5] noted, gasification can save between 1.9 and 3.8 MW per ton of waste. Though relatively nascent compared to incineration, the above-listed advantages have increased the adoption of the technology in many countries albeit on a relatively smaller scale. In the US for instance, the number of gasification plants has seen more than a 100% increase since 2010 [5].

The feedstock in gasification immensely affects its efficiency and the chemical composition of the end products. In principle, biosolids are well placed to yield greater amounts of energy. However, gasifiers that can process biosolids and treat MSW are still developing, as the most common forms of gasifiers are only suitable for treatment of sludge, serving as the main drawback of gasification. To emphasize the potential of greater energy yield with biosolids, dry materials like green waste and wood are normally mixed in sludge gasification to meet the needed characteristics for energy production [6,26].

The potential of gasification is further demonstrated by the rising prominence of its utility of Solid Recovered Fuel (SRF). While SRF is similar to RDF, they fundamentally differ in terms of the source, components and pre-processing involved. While RDF is basically composed of wastes generated from domestic and business activities, including biodegradables and plastics, SRF is a much more homogenous waste derived fuel from MSW and commercial wastes that have gone through additional pre-processing to improve quality and calorific value, and meet the European CEN/TC 343 standards [87]. It is normally composed of plastic, paper, wood, and textiles, among others. Many researchers [87–89] have conducted studies that SRF can be conveniently gasified to produce high quality syngas, which can be utilized in energy applications.

While gasification may still be relatively nascent compared to incineration, continuous advancements in the technology hold a great potential to complement modern forms of energy and support SDG number 7. Furthermore, even in its current state, the ability to process sludge without the externalities that are associated with incineration can contribute greatly to sustainable cities as stipulated by SDG in the face of exploding urban populations worldwide.

Pyrolysis

Similar to gasification, pyrolysis is a process that can process waste – sewage sludge and MSW – for both energetic and chemical values. Simply, the process is an innovative and sophisticated method that manages waste through thermal degradation under high pressure in an oxygen deficient environment, or limited supply of oxidizing agent. Temperatures applied in pyrolysis can be relatively low compared to those of gasification (350–900 °C), but usually kept under 700 °C [6,26,90]. However, according to Ouda et al. [5], a typical pyrolysis reactor is designed with a two-stage chamber in terms for temperature operation like in gasification. In the first chamber, lower temperatures are applied, while the temperature is ramped up in the second chamber to ensure complete combustion. The principal parameters driving the pyrolysis process include temperature, operating pressure and characteristics of raw materials, along with reaction time. These factors considerably affect the yields of the process of pyrolysis [6,91].

In the process of pyrolysis, there are three main products that result – pyrolysis gas, pyrolysis liquid and solid coke – depending on the method of pyrolysis and the parameters of the reaction process [26]. The process is gaining significant traction in the WTE research agenda because of its regarded relatively higher efficiency, as it has the potential to recover as much as 80% of stored energy in carbonaceous wastes [5,92]. In pyrolysis, the molecular structure of solids are altered. During this alteration, CO_2 is released and causes about 40% reduction in the mass of the solids. The carbonized solids that are produced are then transformed into slurry, which is dried by applying thermal energy and converted to solid fuels in the form of pellets. The pelletized solid fuel, also known as E-fuel, can be combusted directly in gasifiers, fluidized bed incinerators and pulverized coal boilers, or deployed for alternative fuel purposes off-site [6,51].

Apart from the solid product, as noted previously, some pyrolysis processes produce liquid products or combustible gases. The gases is basically made up of CO and H_2 for which reason they could be used in gas turbines, gas engines and fuel cells. Sharing some other advantages of gasification, the resultant synthesis gas can also be used as chemical feedstock. In addition, it also produces lower volume of flue gas, No_x emissions, dioxins and furans [6,26].

The potential of pyrolysis adoption to help in production of environmentally friendly energy and contribute to sustainable cities through alternative treatment of waste in line with SDGs 7 and 11 is conspicuous and deserve to be researched and developed to eliminate bottlenecks and constraints. This is because the commercial viability of the process is saddled with a number of shortcomings. For instance, final products of pyrolysis may be unsuitable for use as secondary fuel after all if they contain high level of pollutants. Additionally, homogenizing waste streams that are typically very heterogeneous to meet the inherent stringent conditions for the pyrolysis process can incur costly pretreatment, thereby, rendering the process economically undesirable.

Biofuel technologies

Biofuels are arguably the most advanced renewable source of energy to serve as alternative to fossil fuels in dealing with the global energy crisis, and as such is expected to be pivotal in the pursuit of renewable energy targets set per SDG number seven [7,93–96]. Biofuels are simply fuels that are produced from biomass, and can be the in solid, liquid or gaseous state [6]. Biofuels are produced from a myriad of feedstocks ranging from edible oil like palm oil, non-edible oil like jatropha, lignocellulosic biomass, and biological material from animals, plants, microorganisms and wastes [93,97]. The use of food and energy crops can, however, result in significant negative trade-offs in terms of GHG emissions that have thrown the whole renewable and sustainability argument of biofuels in doubt. Nevertheless, biofuels obtained from waste biomass such as traditional and urban forest residues, wastes from wood industry, food scraps and sewage sludge are still regarded as purely renewable feedstock [13,98–101].

Several types of biofuels can be produced from wastes including but not limited to bioethanol, biodiesel, biogas, and biohydrogen among others [6,102]. One of the most common approaches used to process wastes into energy products is anaerobic digestion or biomethanation as presented in Figure 7. Under anaerobic conditions, organic materials, such as the biodegradable-organic matter content of MSW and sewage sludge, are converted through microbial reactions into gases and manure [5–7,65]. The biomethanation process is a complex one that is characterized by four main stages. The first stage is hydrolysis in which complex organic materials in the form of proteins, fats and carbohydrates are converted into soluble organic materials such as sugars, and amino and fatty acids by extracellular enzymes. The second stage of the process is acidogenesis where products from the hydrolysis phase are broken down into acetate, hydrogen, and higher molecular-weight volatile fatty acids. The third stage is called acetogenesis in which products that result from acidogenesis are further processed into acetic acid, CO_2 and hydrogen by acetate-forming bacteria. The last stage methanogenesis where methane and CO_2 are produced from and acetic acid and H_2 [5,6,103–105].

The principal component of the resultant gas is methane within which about 90% of substrates' energies are retained. The amount of biogas generated by anaerobic digestion per ton of biodegradable waste is estimated to be about 250–350 m^3, and can be deployed for different uses such as cooking, lighting and fuel electric generators and internal combustion engines [7]. In regions like Europe, anaerobic digestion is one of the most preferred technologies for energy recovery from waste biomass, operated under two main conditions: mesophilic digestion under lower temperature conditions and longer retention time, and thermophilic digestion under higher temperature conditions and longer retention time [5,7].

The use of wastes and sewage sludge for production of biodiesel has also increasingly gained prominence research and practice in recent years around the world. In the biodiesel production process, lipids react with alcohol in the presence of a catalyst through the

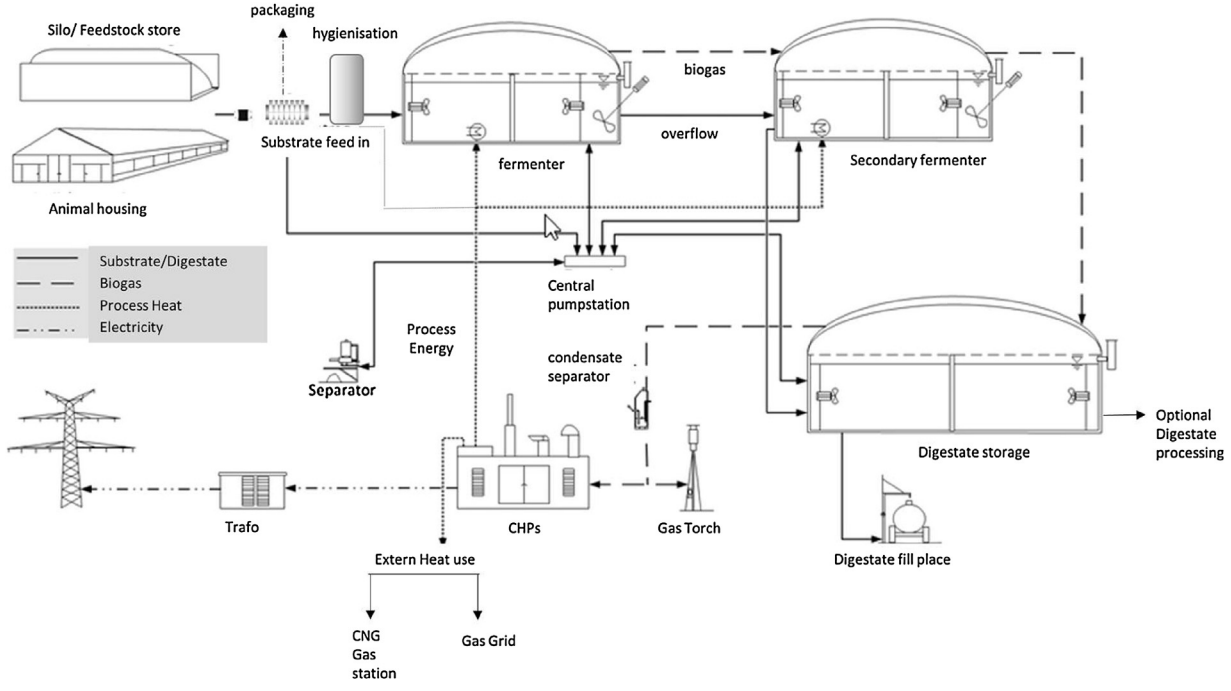

FIGURE 7

Schematic Diagram of a Biogas Plant.

process of trans-esterification to produce the esters of simple alkyl fatty acids [6]. Biodiesel production from sludge is regarded as even more lucrative due the fact that oil and fats in them are saturated with energy-rich lipids, including monoglycerides, diglycerides, triglycerides, phospholipids and free fatty acids [7,106].

Biohydrogen, a product of the biological process that produces hydrogen, is considered as another form of biofuel that serves as a promising alternative to fossil fuels. By deploying suitable bioprocess technologies, wastes from agricultural and food industry that are rich in carbohydrates are used as feedstocks to produce biohydrogen [6,7]. Besides the biological pathway, hydrogen can also be produced through chemical processes. One of the main advantages of hydrogen fuel is that, as Tyagi and Lo [6] indicates, water, rather than GHGs, is the by-product of its combustion with oxygen. Additionally, it has nearly three times the energy content embedded in hydrocarbon fuels [6,107].

The potential of utilizing wastes for energy products by biofuel technologies is established and one of the most widely adopted among the various WTE technologies. Inherent energy potential of different forms of energy has been well studied. For instance, in NACWA [51], it was revealed that setting up CHP plants in all wastewater treatment facilities in the US would be able to power over 260,000 homes. Just focusing on the inherent energy potential of garden wastes, Shi et al. [13] also estimated that the total potential of biofuel that could be produced from them in China is 260 petajoules (PJ), which translates into over one-fifth of the country's urban residential electricity consumption or over 12% of gasoline used in its transport sector. Using anaerobic digestion to produce biogas also offers one of the cleanest routes in WTE as it captures methane, which is one of the potent GHGs, for fuel.

Making WTE technologies central for SDGS 7 and 11 — highlighting other accompanying benefits

While renewable energy advocacy is on the increase, so is the rising mantra of ''sustainable cities'' as SDG number 11 seeks to achieve. Waste management is pivotal and can be the definitive difference between a sustainable city and one that is not. Given these, WTE technologies can have the dual advantage of contributing immensely to both SDG numbers one and eleven. Besides, highlighting and increasing adoption of WTE technologies in the quest to achieve the two goals may also have several concomitant benefits. There are several ways in which adopting WTEs to make good on achieving SDG number seven and 11 can benefit the countries and the world at large, and we have elaborated on some of the critical ones below.

Environmental protection and benefits

Due to the over-reliance on fossil fuels to sustain the global economy, the world is currently at a place where it lives under the constant threat and harsh realities of climate change. Combatting the continuous emissions of GHGs is goal of the renewable energy drive as embedded in SDG number seven [108]. Implementing WTE technologies and strategies can largely offset negative repercussions associated with burning fossil fuels and enhance waste utilization. For instance, as Psomopoulos et al. [24] has indicated, every metric ton of waste used in WTE industry to produce electricity serves to substitute 1/4 of a ton of high quality coal or a barrel of oil, which can reduce GHGs in the US alone by about 26 million tons of CO_2. Additionally, advancing WTE in developing countries can drastically reduce the amount of woodfuels burned for energy purposes, which can in turn reduce GHG emissions from burning and forest degradation [109].

Another means through which WTE contributes to reducing GHG emissions is the capture of methane for fuel. Methane has a higher global warming potential (GWP) as it is 21 times more potent than CO_2 in terms of its ability to trap heat in the atmosphere. This gas primarily escapes into the atmosphere in landfills during waste decomposition. Therefore, using anaerobic digestion to capture the gas in the form of biogas serves to produce clean energy and safe waste management and disposal [110–112].

Besides reduction in GHG emissions, WTE technologies can also have other ecological benefits. For instance, sludge is one of the richest sources of nutrients such as nitrogen and phosphorus, which can be recovered in the WTE processes for other purposes. Specifically, during the process of anaerobic digestion of wastes to produce biogas, by-products such as biogas slurry, which is a high-value fertilizer alternative, is produced and can be used to fertilize agricultural soils [6,113–116].

Health benefits and implications

Developing WTE technologies and increasing their adoption can contribute to improved public health, especially in developing countries. In many developing countries, as previously alluded to, household cooking and heating is carried by burning biomass. This can cause many health problems that arise from inhalation of smoke from burning biomass. Children are especially for vulnerable to respiratory diseases caused by exposure to smoke, since they have relatively less body weight. WTE technologies such as biogas produced from waste to replace woodfuels in households will improve health of a population [117,118].

Reducing GHG emissions through the wide-scale adoption of products from WTE technologies to replace fossil fuels will contribute to mitigating climate change. The extreme weather conditions predicted under climate change scenarios are expected to come with severe health consequences, which will be minimized if the rate of climate change is reduced by the aid of WTE substituting fossil fuels. Lane et al. [119] have predicted that climate change will likely increase floods, which are in turn likely to increase the spread of water-borne pathogens into drinking water sources and the discharge of untreated sewage into rivers and other freshwater bodies. These developments hold significant potential to adversely threaten public health, which will be minimized WTE technologies can contribute to cutting down global GHG emissions. Per the foregoing, there is little doubt that there will be significant health benefits for global populations if WTE technologies are developed to take central position in the quest to achieve SDGs number seven and eleven.

Rural development and women empowerment

Wide-scale and global level deployment of WTE technologies and implementation of enabling policies can contribute to the decentralization agenda of energy production in developing countries. Being able to fill gaps in electricity production for off-grid, rural communities with electricity generated from WTE technologies via mini-grids will increase the use of renewable energy, while ensuring their development at the same time. This is because the

positive relationship between energy use socioeconomic indicators is widely known [120].

Additionally, achieving breakthroughs with using wastes for household level biogas plants can contribute to women empowerment in many poor countries. In such countries where there is a fine delineation of gender roles, women are mostly in charge of the upkeep of the household including chores such as cooking. Since gathering of woodfuel to carry out this responsibility can take a toll on the quality of life that women enjoy [109,121], women can dedicate the significant amount of time that they dedicate to other productive purposes such as education and active engagement in formal employment where they can increase their standards and quality of lives as well as that of their offspring.

Benefits of land savings

Traditional landfilling demands large-scale land acquisition that is accompanied by high cost. The land requirement for landfills can also increase with time, sometimes far surpassing what is initially required. However, WTE technologies can drastically cut back on such vast land requirements, as they usually do not require more land than what is initially required. This is even besides the fact that WTE facilities generally require less amount of land to process waste as compared to landfilling [24].

Another shortcoming of landfills that can mitigated by WTE technologies is that every new landfill require a new parcel of land, meaning that lands that can be productive for other purposes must be relinquished for waste processing. Landfill sites are virtually useless after their closure. However, a new WTE plant can be sited on an already existing WTE facility, which saves the capital cost for land in every new plant. It is also worth noting that every saved land contributes to net decrease in GHG emissions released from cleared land, while also reducing formation of urban heat islands.

Recycling and recovery of heavy metals

There is a huge presence of heavy metals in both MSW and sludge alike. The presence of these metals such as Zn, Ni, Cd, Pb and Hg, among others is one of the main drawbacks in WTE approaches such as incineration, since it poses a great health risk to humans and ecosystems if not properly carried out. However, when done under the right conditions, WTE technologies such as pyrolysis and incineration offer a greater chance of recycling high-grade metals from wastes [6,18].

The metal content of the resultant ash after WTE incineration is about 8–12% ferrous metals and 0.5–1.5% non-ferrous metals in both the bottom and fly ash combined, which can be readily collected under controlled conditions. In fact, nearly 80% of WTE plants in the US is said to have on-site ferrous metal recovery programs that recover over 700,000 t of metals on a yearly basis, primarily from bottom ash after combustion. Overall, these recoveries have been found to contribute to greater recycling rates for communities with WTE incineration systems than those without at about 33% and 28%, respectively [6,18,24].

Source of innovative construction material

Many authors have acknowledged the potential of converting WTE technology by-products into durable building materials. As mentioned preciously, many modern-day incineration facilities install extensive emissions control systems such as electro-filters that capture the fly ash. One of the main issues involved with the process is the appropriate disposal of the resulting ash, which contemporary technologies combines with slag from the bottom of furnace into cement and other building materials [5,26,64].

Sewage sludge is also known to be made up of substantial portions of valuable materials such as organic carbon-containing complexes and the inorganic composites, which as has been demonstrated in Japan and elsewhere that can be used successfully in building materials upon thermal solidification [6,26]. Apart from the fact that reusing by-products in construction materials helps deal with disposal issues, it is also worth noting that it also contributes to conservation of non-renewable natural resources that will otherwise be mined for construction.

Summary and priorities for research and Policy

Globally, renewable energy advocacy is on the increase and their percent contribution to total energy supply has been rising in many countries and regions. However, this has had little to no impact on the total amount of fossil fuel contribution, owing to several factors including exploding global population and increased consumption patterns. Meanwhile, the growing global population is contributing to unprecedented levels of urbanization that is increasing the amounts of waste generated in cities around the world, making them unsustainable. In the SDGs, the UN dedicated goals number seven and eleven, respectively, to increasing the renewable energy share of global energy supply and making cities more sustainable, by the year 2030. While these two goals may look rather disparate on the surface, there is a common thread that connects the two: waste.

When cities generate uncontrollable amounts of waste, it makes them unsustainable. However, these wastes have huge deposits of energy that can be tapped into for their renewable energy potential. For this reason, expanding WTE technologies will help to find a sustainable means of waste disposal while contributing the renewable energy development, thereby, advancing the world on the path to achieving SDGs number seven and eleven. This study has presented an in-depth appraisal of various WTE technologies along with their strengths and inherent challenges, as well as how they may affect prospects of renewable energy drive in the future.

While landfilling may be least desired in the hierarchy of waste treatment options, it is still the leading means of disposal around the world and poses significant health risk to populations and ecosystems. Recycling, per LCA studies, offers the most environmentally friendly means of disposing of wastes. However, WTE presents the extra incentive of energy production that increases its overall performance in carbon savings. There are a myriad of WTE technologies currently in deployment or development around the world of which incineration is the most common, with varying levels of technological advancement. Incineration generally has lower efficiency (25–30%) when considered for only its electricity generation potential. However, current improvements and the advent of CHP with WTE incineration is drastically increasing its performance, by raising its efficiency to up to 80%.

Even though the environmental and economic performance of modern-day WTE incineration has significantly increased compared to their predecessors in the 1960s and 70 s, it is still fraught with many challenges such as high levels of GHG emissions and air

pollutants. The passage of MACT and the WID in the US and EU, respectively, as more stringent air quality legislations have spurred the evolution of relatively simpler incineration systems into more complex and efficient systems. These new systems have upgraded incineration technology with modern combustion systems, additional pollution control technologies and flue gas cleaning systems to meet air quality standards.

Besides improvements in WTE incineration, the review has shown that the wide range of other WTE technologies such as thermal gasification and pyrolysis, as well as biogas development are ably complementing incineration and in some cases, serving as even more effective alternatives. These technologies can be applied to different forms of waste streams to achieve specific and different range of desired products. In addition, these technologies can offer greater flexibility in the energy system.

Per the foregoing discussion, there is certainly a lot more room for WTE technologies to grow into the mainstream in terms of their energy production capabilities and be able to contribute to finding a lasting solution to the global waste crisis. However, the inherent potential for these objectives to be realized is apparent, especially considering the flexibility it presents with the different forms of technologies and their ability to utilize different forms of waste as raw materials and feedstock. While the SDGs may have set some very ambitious goals, it is without doubt that investing and elevating WTE technologies into the mainstream sets the world on the desired course in its drive to achieving goal numbers 7 and 11.

While WTE is primed to support the current targets for renewable energy and sustainable cities as within the SDGs number 7 and 11, respectively, a wider-scale adoption of these technologies can be challenged from different perspectives. It therefore should be pursued with diligence in order to forestall any potential negative aspects. This is especially important as countries around the world have different levels of economic and technological development. In this regard, there are number of suggestions to towards making wastes central to achieving the targets set in the dual goals of SDGs number 7 and 11.

First of all, exploitation of wastes for energy is still constrained with technological challenges and high operational costs. Incineration, which is the most common WTE technology, is characterized by low efficiency with its electricity generation potential. While the efficiency is improved with CHP, such efficiency may not be achieved in countries with warm climates (e.g. those in most parts of Africa), where household heating is rarely a necessity. It is therefore incumbent on developers and engineers to optimize the technology to improve its electricity generation potential to make it more attractive and economically feasible for poorer countries. In the interim, however, many less developed countries still rely on drying as a method of food preservation, so heat generated can be channeled towards artificial drying that will help to significantly cut down on food wastes. Secondly, one of the major issues that have characterized biofuel development is the phenomenon of land grabbing in developing countries and the interference of energy crops with cultivation of food crops. The 2007 food crisis is evidence of the shocks in food market that can ensue when biofuels interfere with food. These issues, aside from infringing on the fundamental human rights of some of the world's poorest and most vulnerable, also decreases the environmental performance of biofuels due to the negative trade-offs that result. It is, therefore, suggested that developed countries channel investments that optimize wastes, both MSW and sludge, as a resource for biogas and other biofuel products, to reduce the need for land for cultivation of energy crops.

On another note, it is important to recognize the importance of coordination between technologically advanced countries and less advanced countries to achieve the set global goals as they pertain to renewable energy expansion. In the SDG number 7, the last target is to expand renewable energy infrastructure and technology upgrade in developing countries, in order to increase supply of modern and sustainable energy services for all in developing countries. This target acknowledges the need to pursue SDGs with ''the whole is greater than the sum of its parts'' approach, where the goals are pursued with the world as a unit than as individual countries. With this said, subsidized transfer of technologies from advanced countries to developing countries is central. Since WTE technologies are farther advanced in industrialized countries, it is important that these countries support their developing counterparts to develop their capabilities by sharing their technologies and training local human resources for sustenance, maintenance, and further development of such technologies. Additionally, one of the greatest challenges that developing countries face is the electrification gap between urban and rural areas. Mostly, it is very expensive for governments to get distant, rural areas onto national grids to meet energy targets, such as those embedded with the SDGs. It will, therefore, be beneficial for governments in developing policies that support community-and-WTE-based mini-grid systems to provide such communities with electricity. This will provide viable alternatives to the placement of such areas on fossil fuel-based national grids.

In many countries, governments subsidize conventional energy systems that gives it undue advantage over emerging renewable energy systems, as far as their competitiveness in the energy market is concerned. For this reason, it is imperative that governments show commitment to achieving the SDG targets by revisiting their national energy policies, in order to expand subsidies to cover renewable energies such WTE. The offer of such subsidies could have significant medium-to-long term impacts on the cost-effectiveness of mini-grids to support rural electrification. Finally, it is important to reconcile recycling and WTE in disposal of wastes. This is because of the extensive pre-processing that is required for some WTE technologies such as incineration, pyrolysis and gasification. Since the essence of the pre-processing is to eliminate low calorie materials including glasses, it will be beneficial to have recycling facilities ready to take such by-products into the recycling stream. Otherwise, such materials are more likely to go back into the waste stream.

Conflicts of interest

The authors wish to declare that we have no conflicts of interest.

References

[1] H. Schandl, S. Hatfield-Dodds, T. Wiedmann, A. Geschke, Y. Cai, J. West, D. Newth, T. Baynes, M. Lenzen, A. Owen, J. Clean. Prod. 132 (September) (2016) 45–56.
[2] T. Jamasb, R. Nepal, Resour. Conserv. Recycl. 54 (October (12)) (2010) 1341–1352.
[3] A.M. Omer, Renew. Sustain. Energy Rev. 12 (December (9)) (2008) 2265–2300.
[4] I. Dincer, Renew. Sustain. Energy Rev. 4 (June (2)) (2000) 157–175.

[5] O.K. Ouda, S.A. Raza, A.S. Nizami, M. Rehan, R. Al-Waked, N.E. Korres, Renew. Sustain. Energy Rev. 61 (August) (2016) 328–340.
[6] V.K. Tyagi, S.L. Lo, Renew. Sustain. Energy Rev. 25 (September) (2013) 708–728.
[7] R. Kothari, V.V. Tyagi, A. Pathak, Renew. Sustain. Energy Rev. 14 (December (9)) (2010) 3164–3170.
[8] R.M. Smith, Asian Geogr. 32 (July (2)) (2015) 73–84.
[9] FAO: Food and Agriculture Organization of the United Nations, Energy Supply and Demand: Trends and Prospects, Report available from:, 2007 www.fao.org/tempref/docrep/fao/010/i0139e/i0139e03.pdf.
[10] H. Cheng, Y. Hu, Bioresour. Technol. 101 (June (11)) (2010) 3816–3824.
[11] World Bank, What a Waste: A Global Review of Solid Waste Management. Urban Development Series – Knowledge Papers, 2012.
[12] R.D. Ionescu, M. Ragazzi, L. Battisti, E.C. Rada, G. Ionescu, WIT Trans. Ecol. Environ. 176 (2013) 245–253.
[13] Y. Shi, Y. Ge, J. Chang, H. Shao, Y. Tang, Renew. Sustain. Energy Rev. 22 (June) (2013) 432–437.
[14] Nations U, Sustainable Development Goals, 2015.
[15] A. Milbrandt, T. Seiple, D. Heimiller, R. Skaggs, A. Coleman, Resour. Conserv. Recycl. 137 (2018) 32–47.
[16] E.C. Rada, L.I. Cioca, G. Ionescu, Energy recovery from municipal solid waste in EU: proposals to assess the management performance under a circular economy perspective, in: MATEC Web of Conferences, 121,05006, 2017.
[17] A. Soufali, M. Bashiri, A comprehensive closed loop supply chain model; environmental, technology and energy concerns, in: IEEE International Conference on Industrial Engineering and Engineering Management, 2016, pp. 1498–1502 7798127.
[18] M.L. Miranda, B. Hale, Energy Policy 25 (May (6)) (1997) 587–600.
[19] G.K. Dinesh, R. Chauhan, S. Chakma, Renew. Sustain. Energy Rev. 92 (2018) 807–822.
[20] M. Melikoglu, V. Singh, S.-Y. Leu, C. Webb, C.S.K. Lin, Biochemical production of bioalcohols, in: Handbook of Biofuels Production: Processes and Technologies, second edition, 2016, 237–258.
[21] E.C. Rada, M. Ragazzi, S. Villotti, V. Torretta, Waste Manag. 34 (5) (2014) 859–866.
[22] V.K. Tyagi, L.A. Fdez-Güelfo, Y. Zhou, C.J. Álvarez-Gallego, L.I.R. Garcia, W.J. Ng, Renew. Sustain. Energy Rev. 93 (2018) 380–399.
[23] F. Cucchiella, I. D'Adamo, M. Gastaldi, Energy Convers. Manag. 131 (January) (2017) 18–31.
[24] C.S. Psomopoulos, A. Bourka, N.J. Themelis, Waste Manag. 29 (May (5)) (2009) 1718–1724.
[25] H.D. Beyene, A.A. Werkneh, T.G. Ambaye, Renew. Energy Focus 24 (March) (2018) 1–11.
[26] A. Bosmans, I. Vanderreydt, D. Geysen, L. Helsen, J. Clean. Prod. 55 (September) (2013) 10–23.
[27] P. Stehlik, J. Clean. Prod. 17 (July (10)) (2009) 919–931.
[28] European Commission, Off. J. Eur. Union (November) (2008).
[29] A. Nabavi-Pelesaraei, R. Bayat, H. Hosseinzadeh-Bandbafha, H. Afrasyabi, K.W. Chau, J. Clean. Prod. 148 (April) (2017) 427–440.
[30] N. Yang, A. Damgaard, P. Kjeldsen, L.M. Shao, P.J. He, Waste Manag. 46 (December) (2015) 362–372.
[31] S.P. Gundupalli, S. Hait, A. Thakur, Waste Manag. 60 (February) (2017) 56–74.
[32] Y. Sadef, A.S. Nizami, S.A. Batool, M.N. Chaudary, O.K. Ouda, Z.Z. Asam, K. Habib, M. Rehan, A. Demirbas, Energy Sources Part B Econ. Plan. Policy 11 (July (7)) (2016) 569–579.
[33] T.F. Astrup, D. Tonini, R. Turconi, A. Boldrin, Waste Manag. 37 (March) (2015) 104–115.
[34] A.P. Tom, R. Pawels, A. Haridas, Waste Manag. 49 (March) (2016) 64–72.
[35] K. Hii, S. Baroutian, R. Parthasarathy, D.J. Gapes, N. Eshtiaghi, Bioresour. Technol. 155 (March) (2014) 289–299.
[36] D. Hoornweg, P. Lam, M. Chaudhry, Waste management in China: issues and recommendations, in: Urban Development Working Papers, 2005 issue (9).
[37] OECD Environment Directorate, OECD Key Environmental Indicators, Available from:, 2008 (Last accessed 23 November 2008) www.oecd.org/dataoecd/20/40/37551205.pdf.
[38] M. Pavlas, M. Tou, L. Bébar, P. Stehlík, Appl. Therm. Eng. 30 (November (16)) (2010) 2326–2332.
[39] United States Environmental Protection Agency, Municipal Solid Waste in the United States. Facts and Figures, available online, 2012 https://archive.epa.gov/epawaste/nonhaz/municipal/web/html/msw99.html.
[40] P. Simmons, N. Goldstein, S.M. Kaufman, N.J. Themelis, J. Thompson Jr., BioCycle 4 (47) (2006) 26–43.
[41] N.J. Themelis, S.M. Kaufman, BioCycle 45 (4) (2004) 22.
[42] K. Aroonrat, S. Wongwises, Renew. Sustain. Energy Rev. 46 (June) (2015) 70–78.
[43] V. Khare, S. Nema, P. Baredar, Renew. Sustain. Energy Rev. 58 (May) (2016) 23–33.
[44] N.S. Lewis, Science 351 (January (6271)) (2016) aad1920.
[45] G. Najafi, B. Ghobadian, R. Mamat, T. Yusaf, W.H. Azmi, Renew. Sustain. Energy Rev. 49 (September) (2015) 931–942.
[46] W.E. Glassley, Geothermal Energy: Renewable Energy and the Environment, CRC Press, 2014 Oct 13.
[47] I.G. Mason, S.C. Page, A.G. Williamson, Energy Policy 38 (August (8)) (2010) 3973–3984.
[48] US Department of Energy. Homepage http://energy.gov/engine/content.do?bt_code=bioenergy.
[49] U.S. Environmental Protection Agency, Electricity from Municipal Solid Waste, 2006 http://www.epa.gov/cleanenergy/muni.htm.
[50] H.W. Campbell, Water Sci. Technol. 41 (8) (2000) 1–8.
[51] NACWA: National Association of Clean Water Agencies, Renewable Energy Resources: Banking on Biosolids, 2010 http://www.nacwa.org.
[52] C. Montejo, C. Costa, M.C. Marquez, J. Environ. Manag. 162 (October) (2015) 240–249.
[53] M. Münster, H. Lund, Waste Manag. 30 (July (7)) (2010) 1251–1263.
[54] P. Ghisellini, C. Cialani, S. Ulgiati, J. Clean. Prod. 114 (February) (2016) 11–32.
[55] S.Y. Pan, M.A. Du, I.T. Huang, I.H. Liu, E.E. Chang, P.C. Chiang, J. Clean. Prod. 108 (December) (2015) 409–421.
[56] US Environmental Protection Agency, Recycling Basics, 2016 EPA.gov.
[57] Patrick Degryse, Jens Schneider, U. Haack, V. Lauwers, Jeroen Poblome, M. Waelkens, Ph. Muchez, J. Archaeol. Sci. 33 (4) (2006) 494–501.
[58] Tim Cooper, Hist. Res. 81 (214) (2008) 710–731.
[59] M. Esen, T. Yukse, Energy Build. 65 (2013) 340–351.
[60] E. Thorin, E.D. Boer, O. Belous, H. Song, Waste to energy – a review, Proceedings of the International Conference on Applied Energy, ICAE (2012), Paper ID: ICAE2012-A10544.
[61] IEA: International Energy Agency, Waste to Energy. Summary and Conclusions From the IEA Bioenergy ExCo71 Workshop. IEA Bioenergy, Available from:, 2013 http://www.ieabioenergy.com/wp-content/uploads/2014/03/ExCo71-Waste-to-Energy-Summary-and-Conclusions-28.03.14.pdf.
[62] A. Tozlu, E. Özahi, A. Abuoğlu, Renew. Sustain. Energy Rev. 54 (2016) 809–815.
[63] M. Münster, H. Lund, Energy 34 (2009) 636–644.
[64] U. Arena, Waste Manag. 37 (2015) 1–2.
[65] M. Chakraborty, C. Sharma, J. Paney, P.K. Gupta, Energy Convers. Manag. 75 (2013) 249–255.
[66] S. Kathirvale, M.N.M. Yunus, K. Sopian, A.H. Samsuddin, Renew Enegy 29 (2003) 559–567.
[67] H. Kleis, S. Dalagar, 100 Years of Waste Incineration in Denmark – From Refuse Destruction Plants to High-technology Energy Works, 2007.
[68] W.T. Tsai, Y.H. Chou, Renew. Sustain. Energy Rev. 10 (October (5)) (2006) 491–502.
[69] D. Luts, K. Devoldere, B. Laethem, W. Bartholomeeusen, P. Ockier, Water Sci. Technol. 42 (9) (2000) 259–268.
[70] W. Rulkens, Energy Fuels 22 (2008) 9–15.
[71] C. Rhyner, L. Schwartz, R. Wenger, M. Kohrell, Waste Management and Resource Recovery, CRC Press, Boca Raton, Florida, 1995.
[72] Reimann D.O. CEWEP energy report (status 2001–2004). Result of specific data for energy, efficiency rates and coefficients, plant efficiency factors and NCV of 97 European W-t-E plants and determination of the main energy results; Updated July 2006. Bamberg, Germany.
[73] P.H. Brunner, H. Rechberger, Waste Manag. 37 (2015) 3–12.
[74] Y. Nie, Front. Environ. Sci. Eng. China 2 (2008) 1–7.
[75] M. Xu, J. Yan, S. Lu, X. Li, T. Chen, M. Ni, H. Dai, F. Wang, K. Cen, Environ. Sci. Technol. 43 (2009) 1023–1029.
[76] E. Ares, P. Bolton, Waste incineration, Research Paper 02/34.9 May, House of Commons Library. House of Commons, London, 2002.
[77] D. Albina, Theory and Experience on Corrosion of Waterwall and Superheater Tubes of Waste to Energy Facilities. M.S. Thesis, Columbia University, 2005.
[78] G. McKay, Chem. Eng. J. 3 (2002) 343–368.
[79] K. Millrath, F.J. Roethel, D.V. Kargbo, Waste-to-energy residues – the search for beneficial uses, 12th North American Waste to Energy Conference (NAWTEC 12) (2004) 1–812.
[80] N.J. Themelis, Waste Manag. World 3 (2003) 40–47.
[81] US Environmental Protection Agency, Letter to President of Integrated Waste Services Association, February, 2003 www.wte.org/docs/epaletter.pdf.
[82] S. Zuboff, Dioxin and Waste Combustion: It's Not What You Burn- It's the Way You Burn It! Chlorine Chemistry Division of the American Chemistry Council, 2018
[83] T. Kolb, H. Seifert, Thermal Waste Treatment: State of the Art E a Summary. Waste Management 2002: The Future of Waste Management in Europe, VDI GVC, Strasbourg, France (Düsseldorf, Germany), 2002.

[84] M. Jaeger, M. Mayer, Water Sci. Technol. 41 (8) (2000) 37–44.
[85] EBARA, TwinRec - Fluidized Bed Gasification and Ash Melting, 2017 (Accessed December 2017) http://www.eep.ebara.com/en/products/melting.html.
[86] G. Genon, V. Tedesco, P. Urso, Assessment of the feasibility of an innovative technology plant aimed at the energetic valorization of municipal waste in the Province of Turin, Third International Symposium on Energy from Biomass and Waste (2010).
[87] U. Arena, F.D. Gregorio, Fuel 117 (2014) 528–536.
[88] U. Arena, F.D. Gregorio, Waste Manag. 50 (2016) 86–92.
[89] J. Recari, C. Berrueco, S. Abelló, D. Montané, X. Farriol, Fuel Process. Technol. 142 (2016) 107–114.
[90] P. Stolarek, S. Ledakowicz, Water Sci. Technol. 44 (10) (2001) 333–339.
[91] B. Khiari, F. Marias, F. Zagrouba, J. Vaxelaire, Desalination 167 (2004) 39–47.
[92] R. Hogg, Energy from waste by pyrolysis and gasification the experience and performance of an operational plant, Proceedings of the International Conference on Sustainable Solid Waste Management (2007) 385–392.
[93] M. Acheampong, F.C. Ertem, B. Kappler, P. Neubauer, Renew. Sustain. Energy Rev. 75 (August) (2017) 927–937.
[94] M. de Wit, M. Londo, A. Faaij, Renew. Sustain. Energy Rev. 15 (2011) 2397–2412.
[95] N. Scarlat, J.-F. Dallemand, O.J. Skjelhaugen, D. Asplund, L. Nesheim, Renew. Sustain. Energy Rev. 15 (2011) 3388–3398.
[96] T. Yusaf, S. Goh, J.A. Borserio, Renew. Sustain. Energy Rev. 15 (2011) 214–221.
[97] N.R. Singh, in: G. Speight James (Ed.), The Biofuels Hand Book. RSC Energy Seriesno. 5, Royal Society of Chemistry, 2011, pp. 160–198[chapter 5].
[98] J. Fargione, J. Hill, D. Tilman, S. Polasky, P. Hawthorne, Science 319 (2008) 1235–1238.
[99] R. Spinelli, N. Magagnotti, C. Nati, Biosyst. Eng. 105 (2010) 316–322.
[100] D. Tilman, R. Socolow, J.A. Foley, J. Hill, E. Larson, L. Lynd, et al. Science 325 (2009) 270–271.
[101] B. Velazquez-Martı, E. Fernandez-Gonzalez, I. Lopez-Cortes, D.M. Salazar-Hernandez, Renew. Energy 36 (2011) 621–626.
[102] M.F. Demirbas, M. Balat, H. Balat, Energy Convers. Manag. 52 (2011) 1815–1828.
[103] M. Krishania, V.K. Vijay, Comparison of various pretreatments of wheat straw for biomethanation, in: PRoceedings of the World Congress of Sustainable Technologies, WCST, 2012.
[104] A.S. Nizami, J.D. Murphy, Environ. Sci. Technol. 45 (17) (2011) 7561–7569.
[105] J. Winter, Biotechnol. Adv. 2 (1) (1984) 75–99.
[106] D.M. Kargbo, Energy Fuels 24 (2010) 2791–2794.
[107] S.K. Han, H.S. Shin, Int. J. Hydrogen Energy 29 (2004) 569–577.
[108] G. Afrane, Energy Policy 40 (2012) 444–451.
[109] R. Arthur, M.F. Baidoo, E. Antwi, Renew. Energy 36 (5) (2011) 1510–1516.
[110] M.H. Duku, S. Gu, E.B. Hagan, Int. J. Hydrogen Energy 15 (1) (2011) 404–415.
[111] R. Gautam, S. Bara, S. Herat, Renew. Sustain. Energy Rev. 13 (1) (2009) 248–252.
[112] Wetlands International, Biofuels in Africa. An Assessment of Risks and Benefits for African Wetlands, AID Environment, 2008 May.
[113] Biogas Team, Biogas for Better Life, an African Initiative, 2007 Business plan 2006e2020.
[114] P.H. Liao, W.T. Wong, V. LoK, J. Environ. Eng. Sci. 4 (2005) 77–81.
[115] L. Spinosa, Water Sci. Technol. 50 (9) (2004) 1–8.
[116] W.T. Wong, W.I. Chan, P.H. Liao, K.V. Lo, D.S. Mavinic, J. Environ. Eng. Sci. 5 (2006) 459–465.
[117] F.H. Abanda, Renew. Sustain. Energy Rev. 16 (7) (2012) 4557–4562.
[118] Ghana Energy Commission, Ghana Sustainable Energy for All Action Plan, 2012.
[119] K. Lane, K. Charles-Guzman, K. Wheeler, Z. Abid, N. Graber, T. Matte, J. Environ. Public Health (2013).
[120] S. Kankam, E.K. Boon, Energy Sustain. Dev. 13 (3) (2009) 212–218.
[121] Kumasi Institute of Technology, Energy and Environment (KITE). Feasibility Study Report on Domestic Biogas in Ghana, Submitted to Shell Foundation, Accra, Ghana, 2008.

TITLE/ AUTHOR	Application of GCMS-pyrolysis to estimate the levels of microplastics in a drinking water supply system / Gomiero, A., Øysæd, K.B., Palmas, L., Skogerbø, G.
SOURCE	Journal of Hazardous Materials Volume 416, 15 August 2021, 125708 https://doi.org/10.1016/j.jhazmat.2021.125708 (Database : Science Direct)

Journal of Hazardous Materials 416 (2021) 125708

Contents lists available at ScienceDirect

Journal of Hazardous Materials

journal homepage: www.elsevier.com/locate/jhazmat

Application of GCMS-pyrolysis to estimate the levels of microplastics in a drinking water supply system

Alessio Gomiero [a,*,1], Kjell Birger Øysæd [a], Luca Palmas [b], Geir Skogerbø [c]

[a] NORCE-Environment, Mekjarvik 12, 4070 Randaberg, Norway
[b] Ztrong Partner AS, Bergliveien 25A, 4020 Stavanger, Norway
[c] IVAR Iks, Breiflåtveien 16/18, 4017 Stavanger, Norway

ARTICLE INFO

Editor: Dr. Rinklebe Jörg

Keywords:
Microplastics
Drinking water treatment plants
Pyr-GCMS

ABSTRACT

Communities value water and aquatic environments for a many diverse reasons. Ensuring safe drinking water is prioritized on the political agenda with a dedicated focus on safe and affordable drinking water under the 6th of the UN sustainable development goals. The occurrence of micron sized plastic fragments has been confirmed even in very remote areas. In the present study we analysed drinking water of a medium-sized Norwegian urban area for the presence of microplastics ≥ 1 μm. A modular filtering sampling devices was developed allowing a sequential in-situ enzymatic and mild oxidizing driven sample preparation prior to pyrolysis gas chromatography-mass spectrometry sample's analysis (pyr-GCMS). Samples were taken at different stages of the drinking water supply chain. The total amount of polymers per sites ranged from 6.1 to 93.1 μg/m^3. Higher levels were detected in the raw water, but significant reduction rates ranging from 43% to 100% depending on the polymer type were scored after the water treatment processes. Polyethylene, polyamide, and polyester were the most frequently detected polymer types. Overall, the levels of MPs in the raw water influence the occurrence and polymer type occurrence and distribution is the drinking water supply net. This study contributes to the emerging field of plastics pollution in drinking water supply systems by providing effective methods helping with future routine monitoring of this source of human plastic uptake.

1. Introduction

Unquestionably plastic has significantly contributed to the development of societal well-being. However, improper or ineffective waste management systems as well as deliberate spill actions have caused a continuous and progressive environmental release of ever larger quantities of plastic items. Nowadays occurrence of microplastics (MPs) has been documented in nearly all investigated terrestrial and marine environments including urban areas, freshwater and marine ecosystems, shores of remote uninhabited islands, alpine lakes and mountains, rivers, seawater column, deep seafloor and trenches (Li et al., 2020; Strafella et al., 2020; Peng et al., 2020; Parolini et al., 2021). The ubiquitous occurrence of plastics in both the natural and urban environment will unavoidably lead to human exposure to MPs. Even so, knowledge about the main routes of exposure, the actual exposure levels, as well as the potential human health effects related to MP exposure is still limited (Prata et al., 2020). Thus, to be able to assess the risk associated with microplastics exposure, exposure concentrations and uptake pathways need to be characterized.

The human body is exposed to microplastics through inhalation of microplastics in the air and by direct ingestion of food, drinks and water containing microplastics, (Cox et al., 2019; Vianello et al., 2019; Revel et al., 2018). A recent study on human stool confirmed human ingestion and pointed out that MPs bigger than 50 μm may be ingested but are also completely excreted (Schwabl et al., 2019). On the other hand, little is known about the fraction of smaller sized particles. MPs smaller than 150 μm have been suggested to be capable of passing the gut wall (Lusher et al., 2017) and MPs smaller than 20 μm have been demonstrated to accumulate in several organs of mice (Deng et al., 2017). Thus, it is crucial to characterize the occurrence of MPs in identified exposure routes with trusted analytical methods able to provide reliable exposure dose measurements in order to correctly assess toxicological and human health risks associated with microplastics. Water is essential for human life and wellbeing, is critical to food production, and is a part of many

* Corresponding author.
E-mail address: algo@norceresearch.no (A. Gomiero).
[1] Present address: NORCE-Environment dep, Mekjarvik, 12, 4070 Randaberg, Norway.

https://doi.org/10.1016/j.jhazmat.2021.125708
Received 1 December 2020; Received in revised form 10 March 2021; Accepted 18 March 2021
Available online 23 March 2021

manufacturing and industrial processes. High drinking water quality depends on its preservation against contaminations, including that of plastics microlitter.

While drinking-water treatment provides an effective barrier to a wide range of waterborne particles, probably including microplastics, components in the treatment-plant and the distribution networks are made from plastics and their wear and tear may contribute to microplastics release into the drinking water (Mintenig et al., 2019; Pivokonsky et al., 2018). To date, only a few studies have reported on the occurrence and concentrations of microplastics in drinking-water or their removal in the drinking water treatment processes (Pivokonsky et al., 2018; Uhl et al., 2018; Strand et al., 2018; Mintenig et al., 2019; Kirstein et al., 2021). However, a lack of standardized methods for sampling and analysis as well as QA/QC procedures hamper comparisons across studies (Koelmans et al., 2019a, 2019b). To obtain reliable data from freshwater and drinking water studies large volume samples are needed, and accurate extraction and purification procedures are required to avoid sample contamination. Additionally, detection of the smallest particle sizes is largely dependent on the size of the available mesh, which is currently limited to a few microns, thus prohibiting assessment of nano-sized plastic particles occurrence/concentrations.

Among available analytical methods, the spectroscopic, the thermoanalytical and the chemical oriented ones show greatest potential for characterization of MPs in environmental matrices. They all present advantages and disadvantages. Fourier Transform Infrared Spectroscopy (FTIR) and Raman spectroscopy are well established and reliable methods that can identify particle sizes down to 10 and 1 μm, respectively, but dirty samples and residual unprocessed organic matter may slow down the analysis and hamper polymer identification.

Thermal analytical methods such as pyrolysis-GC-MS tend to require larger particle masses compared to the spectroscopic methods. However, it is a fast approach and enables simultaneous assessment of additives, and if the sample is large enough it may also identify the polymer composition of nanoplastic particles.

The present study aimed at investigating microplastics occurrence in water samples from the raw water up to the water meter step in the drinking water supply network. This was supported by the implementation of sampling solutions aiming at processing large amounts of water, by the reduction of any source of plastic contamination during the sampling and sample preparation steps as well as by the application of a thermoanaytical (pyr-GCMS) oriented method for the chemical characterization of MPs in the investigated samples. A case study was carried out focusing on MPs in freshwaters that directly enter Water Treatment Plants (WTPs), and subsequently on microplastics determination in treated water at different collection points in the supply grid in a medium-sized Norwegian urban area.

2. Materials and methods

2.1. Study area

The study investigated microplastic pollution in raw and treated drinking water in an area with a population of approximately 300.000 in the south-western part of Norway (Fig. 1). The main drinking water treatment facility provides 41 million cubic meters of drinking water. Water collected from two mountain lakes hereafter referred to using the technical term ‘raw water’, is transported to the drinking water treatment plant (DWTP) located 5 km from the collection point by a tunnel dug in the rocky bed, passed through marble beads filtration, UV disinfection and clorination (Fig. 1 – Supplementary). In the DWTP, all

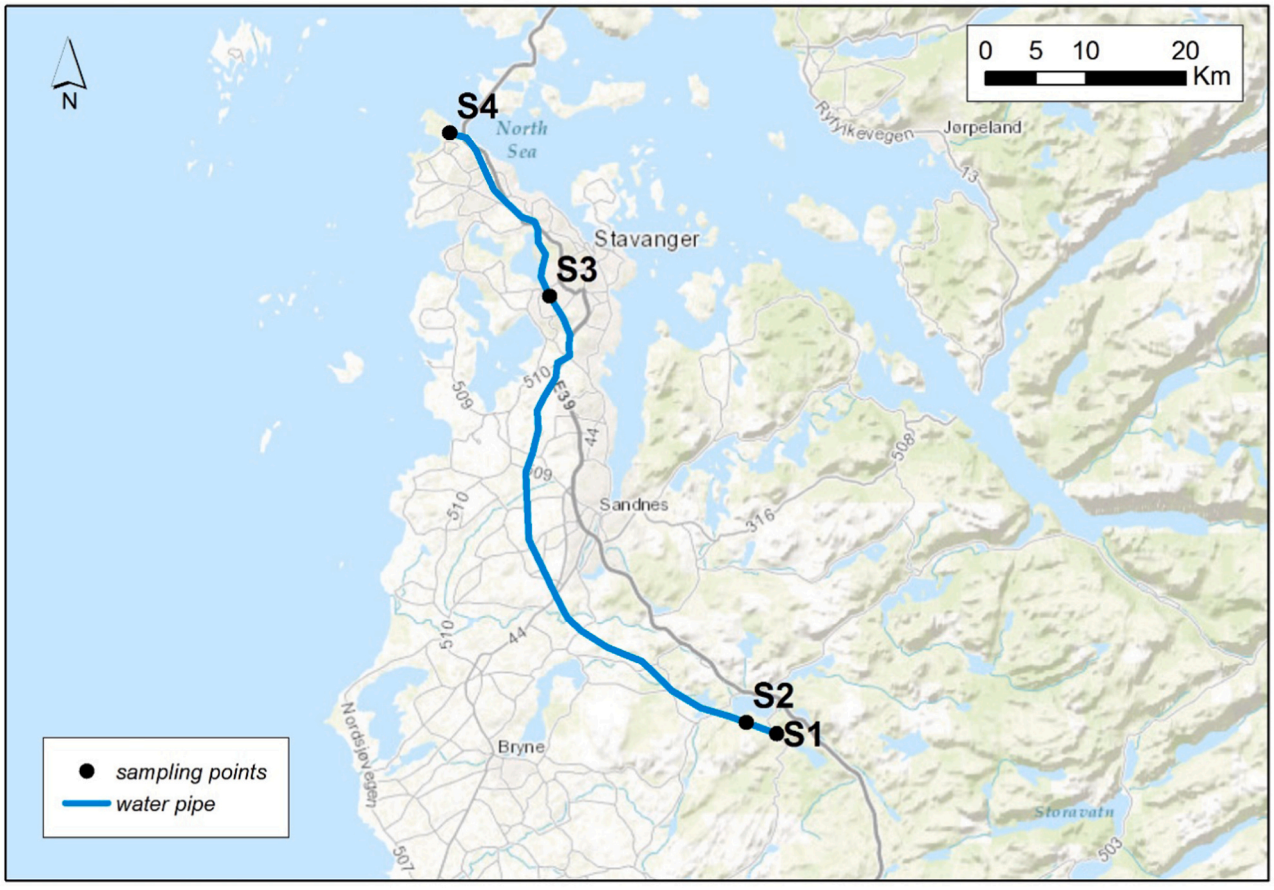

Fig. 1. Location of the drinking water suppling grid and localization of the sampling sites. S1 = Raw water collection site, Ålgard lakes; S2 = Sampling site after raw water treatmen plant; S3 = Sampling site before entering the urban area; S4 = Sampling site after the urban area.

reaction and storage tanks have an inner layer of epoxy resin to avoid corrosion, and aeration tanks have built in rings of polypropylene (PP) to enlarge the surface area. After purification, the drinking water is fed into the distribution system and transported to the Sandnes and Stavanger urban area through high-density polyethylene (HDPE), polyvinylchloride (PVC), concrete or cast iron pipes.

2.2. Water samples collection

The goal was to follow treated drinking water produced and supplied by the WTP in order to cover variability in MP abundance throughout the process. Water samples were collected from various points along the process and transport chain. Samples were first taken from the raw water reservoir at Langevatn lake via an inspection valve within the line connecting the reservoir to the DWTP (St-1, raw water). The next samples were obtained from the stainless steel outflow of the water treatment plant, immediately prior to its entry into the distribution grid (St-2). A third set of samples were taken from a pressurization station located within the Stavanger urban area (St-3), with a final set taken at a more distant sampling station, beyond the main urban area, from an hydrant located in Mekjarvik (St-4, Fig. 1). To avoid potential contamination of the water during sampling no additional mechanical pumping systems were used. The sampling device was connected by metal junctions to stainless steel valves and the water samples were collected from gravity fed or pressurized supplies. Three replicates were collected per site during each sampling session. In detail, sampled water was passed through a portable stainless steel multi-layered filtering system specifically designed for the study. The inlet connection of the sampling device was attached directly to the supply network (Fig. 1A- Supplementary material). A jack up module allowing direct connection to the water system outlets was fitted to the filtration module. Each filtration module accommodates a cryo-welded 47 mm framed stainless-steel filter of a defined mesh size. Every filtration module can be connected and sealed to each other's by a thread and a copper O-ring to realize a cascade of filtering modules (Fig. 2- Supplementary material). The sampling device in its largest set up can consist on a jack up module, six filtration modules arranged in sequence and an outlet module. A flow meter counter is connected to the outlet of the last filtering module to measure the amount of filtered water. The sampling task was set stopping after reaching a filtered volume of 1 m^3 per replica. Having several operating modules with decreasing filter sizes in series it offers the advantage of reducing clogging and pressure on the finer meshes filtering modules. Thus, in the present study the sampling system was configured by connecting the jack up module to a cascade of three filtering modules: $\geq$ 1 μm (D_1), $\geq$ 10 μm (D_2) and $\geq$ 100 μm (D_3), with D_2 and D_3 intended to physically protect the main filtering unit (D_1) from rapid clogging due to the occurrence of solid particles i.e., sandy materials, biofilms and algae aggregates occurring in the sample and the consequent back-pressure in the filter surface. This solution aimed at limiting the clogging of the filters and extending the filtration time, thus increasing the amount of processed water. The assembly was further designed to apply in-situ sample purification from interferents (i.e., particulate organic matter organic matter, algae, bacteria, etc). This was realized by directly injecting into the internal fractionation chambers the solutions used for the sample's preparation by a stainless steel ball valve located in the first module of the sampling device (jack up module), and the discarding of the degraded interferents through a valve lock outlet set in the last filtering module using a vacuum system (Fig. 2- Supplementary material). The device enabled both the collection and pre concentration of large quanitities of water and the sample preparation in the same device. This limits any possible source of location and/or operator derived contamination during the sample preparation phases). In addition it helps minimizing the elapsed time between the sample collection and the purification/extraction phase as the sample treatment starts immediately right after the collection at the sampling site. The recovery efficiency of the sampling device was tested by flowing 1 m^3 of tap water spiked with $\approx$ 50 μg of uneven shaped Ø 20 $\pm$ 10 μm deuterated polyethylene (PE-d_4, # 487007, Sigma Aldrich, Germany) and performing all the sample preparation steps up to the analysis. The recovery test was performed five times. After each sample collection the sampling device was disconnected from the water supply grid and the primary inlet/outled sealed by stainless steel bolts. The valve of the secondary inlet was carefully connected by a corrugated stainless steel pipe to a 2 L pyrex bottle filled with 5% sodium dodecyl sulfate solution (SDS) kept at RT. In the meantime, the secondary outlet was connected to a vacuum pump by a teflon tube (secondary inlet – Sin; Fig. 2- Supplementary material). Vacumm was applied to fill the inner chambers of the sampling device and both inlet/outlet valves closed afterwards. The device was carried from the sampling site to a specifically designed area of the research facility dedicated to the plastic pollution research.

2.3. Contamination control measures

To reduce at best any possible airborne plastic contamination during the final phases of the sample preparation and analysis such area is equipped with high efficiency ultra-low penetration HEPA filtration class H 13 (Bravida, Norway) with an efficiency of $>$ 99% for the most penetrating particle size (0.3–0.5 μm particles). The laboratory has overpressure and the entrance is set with an airlock with a sticky floor mat to avoid dust entry. The laboratory is entered with dedicated low-abrasion shoes and a certified full cotton laboratory coat. Either no gloves or nitrile gloves are worn. By the exeption of the teflon tube connecting the vacuum pump with the sampling device's secondary outlet, non-plastic equipment is used within the clean lab.

Furtermore, to reduce samples cross-contamination phenomena the stainless steel sampling device was disassemblend and every module burned on a muffle oven at 500 °C for 3 h and re-assembled afterwards after every samping session.

All tools and glasswarebeing potentially in contact with the samples were pre-burned at 500 °C for 3 h and carefully rinsed with twice-distilled water filtered through 0.7 μm GF/F fiberglass filters (Whatman, Milan, Italy). All reagents and solutions involved in every step of the sample preparation were pre-filtered through simlar fiberglass membranes.

Furthermore, a total of six procedural controls consisting on each of all enzymes and strong oxidizing solutions being flown in the sampling device during the sample's preparation steps were analyzed for microplastics content. Furthermore, each working day open beakers filled with 250 ml of 0.7 μm GF/F filtered Milli-Q water were placed in the area where the sampling device was open to evaluate any contribution of airborne plastics contamination. Both procedural controls and dust deposition wet traps samples were analyzed and results reported as part of the routine plastics contamination QA/QC assessment (Dehaut et al., 2019).

2.4. Sample processing

In the clean lab and after 3 h of incubation at RT the SDS solution was discarded from the secondary outlet and the sampling device refilled with protease enzyme (P3111 Sigma-Aldrich, Germany) 1:10 (v:v) in 0.1 M glycine buffer at pH 9.0. The device was kept in an oven set at 50.0 $\pm$ 1.0 °C overnight. After incubation the digestate was discarded and the sampling device internally flushed with 1 L of MillQ from a Pyrex bottle connected to the secondary inlet by applying vacuum from the secondary outlet. Using the same strategy, a solution of 15% hydrogen peroxide (H_2O_2) was loaded afterward. The inlet and outlet valves were closed and the device kept at 50 °C for 3 h. After H_2O_2 incubation the strong oxidant solution was discharged, and the inner chambers of the sampling device flushed with 1 L of filtered MilliQ water. Before disassembling the device by unscrewing each filtering module the sampler was externally washed with 2 L of MilliQ and 1 L of an ethanolic solution (EtOH; 50:50, v/v).

Each filtering module was open and capsized in a clean beaker, filled with 200 ml of EtOH and sonicated for 5 min to facilitate the release of the trapped particles from the filtering surface to the EtOH solution. The module was collected from the solution and the filtering surface gently scratched and backflushed with an aliquot of EtOH solution. The obtained EtOH solution was gently concentrated by means of a TurboVap 500 (Zymark, Norway) to a final volume of 1 ml. The 1 ml sample was transferred to a pre-burned 25 mm GF/F (0.7 μm mesh size) fiberglass filters by means of a glass microanalysis vacuum filtration unit (#10665961, Millipore-Merck, Norway). As described in Gomiero et al. (2019) such vacuum filtration equipment was coupled with a glass micro funnel specifically designed to reduce the filtering surface of the membrane from Ø25 mm to Ø10 mm. The filters were then cut using a sharp metal cylinder reducing their size to Ø 15 mm thus enabling their easier folding and placement into stainless steel cups suitable for pyr-GCMS analysis.

2.5. Samples analysis - GCMS Pyrolysis

Pyrolysis GCMS measurements were performed by a Shimazu Optima 2010 C GCMS controlled by GCMS solution V 4.45, equipped with a Rxi-5 ms column (RESTEC, Bellefonte, PA) and coupled with Frontier Laboratories Multi-Shot Pyrolizer EGA/PY-3030D with auto-shot sampler (BioNordika, Norway). Pyrolysis was performed at 590 °C on a stainless steel pyrolytic target cup. Thermochemolysis was performed by adding 10 μL of tetramethylammonium hydroxide (TMAH, 25% in water) in stainless steel cups pre-loaded with samples, allowing it to dry at 40 °C on a heat plate prior to pyrolysis. Eight of the most commonly used plastic polymers polyethylene - PE, polypropylene - PP, polystyrene - PS, polyvinyl chloride - PVC, polyammide - PA, polymethyl methacrylate - PMMA, Polycarbonate - PC and polyethylene terphtalate - PET of purity > 99% were purchased from Goodfellow Ltd (Huntingdon, England) to set up the calibration and quantification curves (Table 1–Supplementary material). Furtermore, deuterated polyethylene - PE-d_4 was used as internal standard to asses the overall efficiency of the analytical method. To unambiguously identify single polymers in complex environmental samples specific indicator compounds were chosen pyrolizing the polymer standards of interest according to the instrumental condition reported in Table 2 (Supplementary material). Furthermore, to allow the mass spectrometer to detect the compounds of interest with the highest sensitivity, the SIM (Selected Ion Monitoring) acquisition mode was used. This implis that only a limited mass-to-charge ratio range is transmitted/detected by the instrument, as opposed to the full spectrum range. SIM is a major application for GC–MS and allows the instrument to be used in its most sensitive mode for quantitative measurements (Harvey, 2005). SIM instrumental conditons are presented in Table 3 (Supplementary material).

The obtained pyrograms were compared to a customized database and cross-checked with literature data following reccomendations and selection criteria from Gomiero et al. (2019), Hermabessiere et al. (2018) and Matsui et al. (2020). The most abundant and/or polymer-specific compounds from TMAH pyrograms selected as indicators for polymer specific qualitative and quantitative analysis in this study are listed in Table 4 (Supplementary material). To obtain calibration curves, standards were weighed at between ≈ 0.4 and 310 μg of polymer directly into the pyrolysis stainless steel cups using a XPE205 DeltaRange Mettler Toledo balance coupled with an Compact Anti Static Excellence Kit discharger tool (Mettler-Toledo, Germany). Individual polymers were calibrated by means of preselected combination of retention time and mass markers by integrating chromatograms of their associated indicator ions and respective integration results. The standards were directly weighed into the pyrolysis stainless steel cups. For the lowest calibration points the anti-static discharge tool efficiently helped to measure polymers in the 0.4–1.0 μg range. To date the methodological limitations in calibration curve range are represented by the lowest trustable mass measurable by the adopted balance. The obtained calibration curves were used to quantify the polymers of interest in the processed environmental samples. The evaluation of the signal to noise ratios (S/N) of the detected peaks at the lowest concentration levels in the calibration curves allowed the extrapolation to a 10:1 ratio pointing to the LOQ (Kirstein et al., 2021; Krauskopf et al., 2020; Table 4 - Supplemetary material). Values calculated by the S/N estimation range from ≈ 0.5 to ≈ 1.1 μg.

2.6. Statistical analysis

Statistical data analysis was performed using Statistica 13.5 (StatSoft Inc., USA). All of the data were log-transformed to reduce the skewed distribution. The homogeneity of variance and the distributions were analyzed using Levene and Kolmogorov–Smirnov tests, respectively. The data were then subjected to analysis of variance (ANOVA) to identify differences in polymer type levels between the different investigated sampling sites. When the ANOVA test indicated significant differences, the sampling sites were compared using Tukey's test to determine significant differences based on $p < 0.05$. Furthermore, the spatial distribution of the targeted polymer levels was investigated by a Principal Componet Analysis (PCA) using Primer 6.1.16 (Primer-E, Ltd, UK).

3. Results

In the deuterated polyethylene spiked water sample the estimated recoveries ranged from 98,5–99.0% validating the field application of the designed sampling device. A total of 12 m^3 of water and a total of 5 m^3 of recovery testing samples were analyzed within the study. Using the pyr- GCMS method, a total of 29 pyrograms were analyzed (four sampling points with three samples each, six procedural blank, six airborne contamination samples colleted during analyses as well as five samples from the recovery testing).

The total amount of polymers ranged from 6.1 to 93.2 μg/m^3 observed in the S4 and S1 site, respectively (Fig. 2). Within all analyzed samples, the predominat polymer type in the drinking water supply system was PE (21–82%) followed by PA (0–36%) and PET (0–35%, Fig. 3). Furthermore, PP (13%) and PS (2%) where only detected in the raw water samples. While comparing the distribution across the investigated collection points, a significant reduction of the polymers levels was observed for all detected polymer types after the raw water sanitation process. PE and PA showed the higest reduction values of - 92% and - 89%, respectively. Meanwhile, a reduction of – 80% and - 43% was observed for PET and PVC, respectively. A complete reduction was observed for PP and PS. However, this result may be correlated to the already limited amounts present in the raw water samples before the raw water treatment processes.

This trend is further pointed out by the results of the Principal Component Analysis (PCA), a two-dimensional representation enabling a simple visualization of the data distributionn. The PCA analysis described most of the variance (≈ 99%) by using the first two principal components, PC1 and PC2 (Fig. 4). A clear separation was shown between the results of the raw water samples (S1) and a cluster of samples represented by the remaining sampling sites located at increasing distances from the raw water collection in the drinking water supply grid (S2, S3 and S4). The relatively high factorial weights of all detected polymer types in the PC1 axis (total explained variance of 91%) contributed to explaining the horizontal separation of the sampling sites. The factorial weights of PE and partially of PET and PS contributed to separating S4 from S2 and S3 in the PC2 axis (total explained variance of 8%). To evaluate the contribution of the water supplying grid the "polymer type" vs "distance" factors were compared using ANOVA. Only PE showed a significant distance related increment throught the sampling sites with low values after the sanitation step and higher avearage values in the most distant north most sampling site ($F(3, 8) = 28{,}28$; p value = 0,0012).

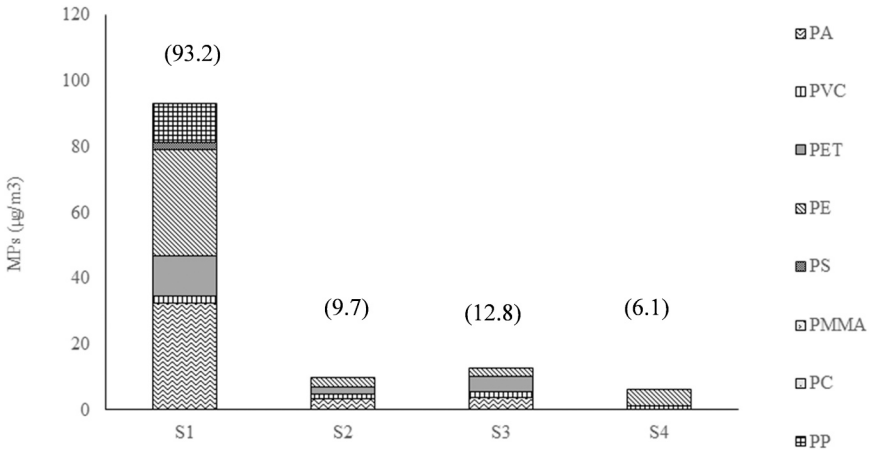

Fig. 2. Total and relative mass estimation (µg/m^3) of the identified polymer types. PE = polyethylene, PP = polypropylene, PS = polystyrene -, PVC = polyvinyl chloride -, PA = polyammide -, PMMA polymethyl methacrylate -, PC = Polycarbonate - and PET = polyethylene terphtalate. S1 = Raw water collection site, Langavatnet; S2 = Sampling site after raw water treatmen plant; S3 = Sampling site before entering the urban area; S4 = Sampling site after the urban area. Values in brakets are the total sum of the detected polymers (µg/m^3).

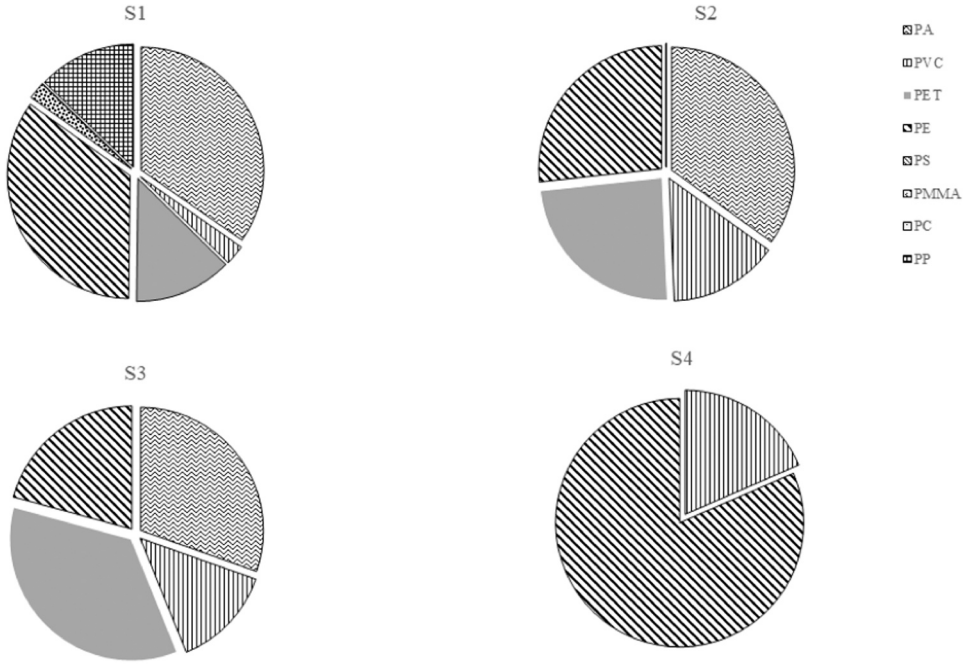

Fig. 3. Relative abbundance of detected polymers in the investigated sampling sites. S1 = Raw water collection site, Langavatnet; S2 = Sampling site after raw water treatmen plant; S3 = Sampling site before entering the urban area; S4 = Sampling site after the urban area. PE = polyethylene, PP = polypropylene, PS = polystyrene -, PVC = polyvinyl chloride -, PA = polyammide -, PMMA polymethyl methacrylate -, PC = Polycarbonate - and PET = polyethylene terphtalate. S1 = Raw water collection site, Langavatnet; S2 = Sampling site after raw water treatmen plant; S3 = Sampling site before entering the urban area; S4 = Sampling site after the urban area.

4. Discussion

The present study aimed at strengthening the knowledge on MP characterization and quantification in drinking water production and supply systems analysing masses of particles up to very small sizes based on the applied smaller pore size of the sampling device (≥ 1 µm).

A novel and versatile sampling device focusing on both the quantitative collection of MPs from a representative sample size of 1 m^3 per replica (Koelmans et al., 2019a, 2019b) and reduction of plastics contamination during sampling and sample preparation phases presented a promising solution to overcome the limitations of current sampling methodologies. Furthermore, the processing of large volumes of sample water contributed towards minimizing the analytical limitations of the pyrolysis- gas chromatography mass spectrometry which tends to require larger particle masses compared to other spectroscopic oriented analytical methods such as µ-FTIR and µ-Raman (World Health Organization, 2019). To overcome such critical limitation the application of a selected-ion monitoring chromatogram strategy focuses on a defined core of ions instead of the summed intensity across the entire range of masses being detected at every point in the analysis and offers an increase in analytical performance in terms of sensitivity in respect to previous performed studies in drinking water systems (Kirstein et al., 2021).

Hence, through the combination of a large volumes sampling strategy, solutions toward stringent contaminations controls during sample's collection and preparation and mass spectrometry based on SIM acquisition mode, MPs could be identified and quantified in all analysed drinking water sampling sites.

The highest occurrence of MPs was observed in raw water with an overall amount of 93.2 µg/m^3. In the present study the raw water was collected from a pristine lake used as a source for drinking water production. Microplastics frequently occur in freshwater environments, including rivers and lakes used as open reservoirs for drinking water production. Being open systems, these freshwater water bodies may be potentially exposed to several type of MPs sources i.e., atmospheric deposition, surface runoff and marginally by human activities. Hence the occurrence of MPs in raw water in the present study was expected.

PE, PET, PVC, PA and PS were the most recurring polymer types in the analyzed reservoir water confirming previous observations in similar water bodies used for drinking water production. In a monitoring study

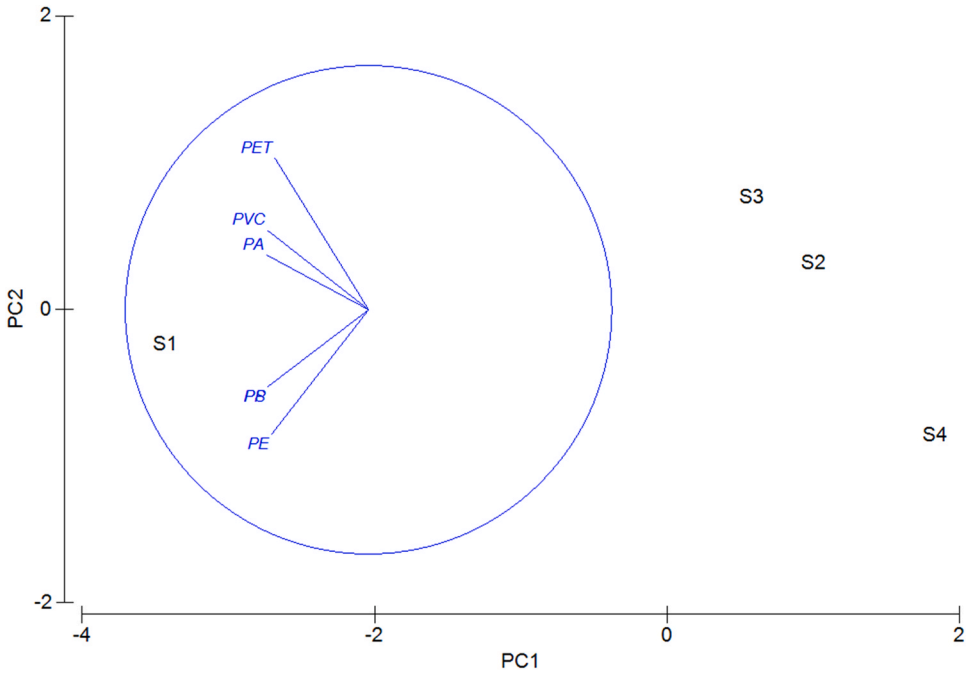

Fig. 4. PCO ordination plot with projection of polymer types contribution onto the ordination axes. PE = polyethylene, PP = polypropylene, PS = polystyrene -, PVC = polyvinyl chloride -, PA = polyammide -, PMMA polymethyl methacrylate -, PC = Polycarbonate - and PET = polyethylene terphtalate. S1 = Raw water collection site, Langavatnet; S2 = Sampling site after raw water treatmen plant; S3 = Sampling site before entering the urban area; S4 = Sampling site after the urban area.

assessing the occurrence of MPS in the Rhine river Mani et al. (2015) identified a weighted average of 892,777 MPs/Km^2. More recently Di and Wang (2018) estimated an abundance of 1597–12,611 MPs/m^3 and 3400–25,800 MPs/m^3 respectively in the Three Gorges Reservoir and in Taihu Lake, using a combination of visual observation followed by SEM microscopy or μ-FTIR analysis. According to the authors of the studies, PS, PP and PE were the major polymer types of the selected plastic particles, indicating that domestic sewage and fishing activities might be the main sources of microplastics in the investigated lakes.

Nevertheless, very few studies have analyzed particles as small as those detected in the present study (≥ 1 μm). Among them, two studies from Pivokonsky et al. (2018, 2020) reported higher levels of MPs in three separate lakes and in the Úhlava river located in the Czech Republic all acting as raw water reservoirs. Using a combination of μ-FTIR and μ-RAMAN imaging analysis 1384–4464 MPs/L in the lakes and 23−1296 MPs/L in the river were identified, with most of the characterized particles smaller than 10 μm. Similar to what was observed within our study, these authors reported the predominant occurrence of PET (27–68%) followed by PP (16–26%) and PE (≈ 24%). However, the general physical conditions and the magnitude of the input sources controlling the MPs contamination and the level of anthropogenic activities in the different water basins may be different. The MPs total masses level obtained by converting the no of particles per volume (MPs/ m^3) and their relative sizes into a mass balance (μg/m^3) falls in the range of hundreds of μg which tend to show higher values that those reported in this study.

Few recent studies have attempted to directly correlate the outcomes of particles enumeration vs mass-based estimation characterizing techniques in critical environmental matrices (Primpke et al., 2020) including drinking water (Kristein et al., 2021). Both μFTIR imaging and pyr-GCMS are reported to have successfully determined very low MP loads in comparable concentrations. Some discrepancies in some samples with very low levels of MPs showed a general underrepresentation of specific plastic types. This was mainly related to limitation in the polymer-specific detection limit of pyr-GCMS rather than in the FTIR imaging technique. The present study overcomes such limitation by using a selected ion chromatogram strategy to improve the sensitivity of the thermoanalytical method, targeting the mass estimation of limited amounts of MPS most likely brought by the smaller MPs size fraction.

With respect to the raw water, lower concentration for all the detected polymers were found in the drinking water sanitation process and in the following distribution system indicating an efficient removal of MPs during drinking water treatment by simple conventional sand filtration technology. Removal efficiency was partially affected by the initial amounts of MPs in raw water and it varied from 43% for PVC to 100% for PS If compared with other studies, limited data are available about MPs removal rates for such water treatment systems as few research initiatives have investigated the occurrence of MPs along the whole drinking water treatment process. Only Pivokonsky et al. (2018) reported an overall MPs removal rate ranging from 70% to 82% in a conventional coagulation-clarification-filtration driven DWTP. In another study Uhl and co-workers (2018) assessed the occurrence of MPs in 24 Norwegian DWTPs however levels in the raw water were below the detection limits of the applied visual analyse oriented method while an average of 4.1 MPs/L were found in the tap water. However, the absence of MPs in the raw water as well as the limited amount found in the treated water might be due to the small sample volumes used (3 L/sample) or the missing identification of particles. Overall, no firm conclusion can be drawn. However, even if drinking water treatment systems are not specifically designed for MPs removal; they are considered highly effective in removing particles with characteristics similar to those of MPs. Properties playing a central role in the removal effectiveness are mainly the particle's surface charge, size, shape, density and biofilm formation in sand beads and drinking-water pipes. Biofilms in drinking-water are formed when microorganisms grow on drinking-water pipes and other surfaces. Furthermore, microorganisms responsible for biofilm formation attach more rapidly to hydrophobic, nonpolar surfaces, such as plastics, than to hydrophilic surfaces. Large quantities are formed in the sand beads used for raw water filtration. Such biologically formed films may attract particles, including MPs by their strong surface charge, and act as a collector in the sanitation process. This leads to another environmental issue as plastics are not usually destroyed, but rather moved from the liquid phase to a solid one. Thus, attention should be given to waste associated with water treatment processes as they could be considered an underestimated source of microplastics contamination in the environment.

Overall, although there are only limited data available on the efficacy of microplastic removal during drinking-water treatment, such

treatment has proven effective in removing far more particles of smaller size and at far higher concentrations than those of microplastics. Conventional treatment, when optimized to produce treated water of low turbidity, can remove particles smaller than a micrometre through processes of coagulation, flocculation, sedimentation/flotation, and filtration (Pivokonsky et al. (2018, 2021). After water treatment process a total of 6.1–12.8 μg/m^3 of plastics polymers were detected in the distribution grid. This distribution system consists of a combination of cement, stainless steel, PE and hardened glass pipes. Overall, the present study identified four polymer types in the treated drinking water: PA, PET, PVC and PE. Despite of the levels of most of the investigated polymers remained similar through the distribution network, PE showed a significant increase through the distribution line. As such points out to a minor contribution of the distribution line which is likely to be explained by the mechanical abrasion of PE based pipes. Abrasion phenomena are also reported by Pivokonsky et al. (2018, 2020) as a main driving factor in the observed distribution of MPs on a drinking water suppling system fed by groundwater in the north of Germany. This study characterized the occurrence of an average of 0.7 MPs/m^3 of PE, PA, PVC and epoxy resin particles falling in the range from 50 to 150 μm, with 1–3 particles scored at the water meter sampling sites. If converting the reported particle size to mass-based estimations using the density of PE as guiding value, the obtained results, in the range of few μg, are lower respect to those observed in the present study. However, this should be put in relation with the different origin of the raw water in the two different drinking water supply systems and the higher vulnerability of open water bodies to plastic pollution contamination than that of groundwater reservoirs. Conversely, the assessment recently performed by Kristien et al. (2021) on a Swedish drinking water distribution system concluded reporting that the age of pipes had no significant impact on MPs load.

The occurrence of MPs in products designated for human consumption such as drinking water is receiving increasing attention due to the discovery of small MPs translocating to inner organs (Deng et al., 2017). Cartus and Schrenk (2017) estimated 5 mg/kg body weight per day as the level of no concern for humans strictly related to the Tolerable Daily Intake (TDI) value. Comparing the results obtained by the present study and considering an adult's daily water consumption of 2 litres of tap water (World Health Organization, 2017) for an adult having a default body weight of 60 kg and a day intake of 0.02–0.2 μg MPs /L day it may be concluded that the risk to human health associated with the consumption of the analysed drinking water is limited. Higher daily intake values of about 2.0 μg/L are extrapolated by using the same above presented assumptions on particle numbers and shape results obtained from the study of Oßmann et al. (2018) and Schymanski et al. (2018) on bottled mineral water as well as from drinking water systems by Pivokonsky et al. (2018). In contrast, estimated MPs intake from drinking water based on the work of Mintenig et al. (2019) provide more comparable estimations (≈0.01 μg MPs /L day) to the present study. However, more research is needed before being able to provide a reliable human risk assessment for MPs uptake.

Overall, future efforts need to address a better understanding of the occurrence of plastic particles in potable water systems that obtain raw water from different sources, their levels and polymer type composition as well as their relative and total masses. Such data are essential for toxicologist to define exposure routes and create natural exposure scenario to investigate realistic biological effects and define reliable toxicity thresholds to be adopted at regulatory level.

5. Conclusions

In this study a total of 12 individual m^3 drinking water samples were examined resulting in a total amount of polymers ranging from 6.1 to 93.2 μg/m^3 as microplastic particles > 1 μm based on the pore size of the adopted sampling device. The most dominant polymer type in the analyzed samples were PE>PA>PET>PP>PS. Despite some significant contributions from the drinking water suppling system in increasing the final levels of PE at the water meter step in the sampling grid, no general and firm conclusion can be drawn about the aging effect of the supply grid as some conflicting outcomes are reported by other authors on the topic (Mintenig et al., 2019; Kirstein et al., 2021). Furtermore, even though of drinking water treatment systems are not specifically designed for MPs removal, the performances of the investigated system as well as of others compared within the present study are considered highly effective in removing MPs. In this context, the level of MPs pollution in raw water appears to be a more relevant factor influencing the final levels in the supplied drinking water as results from the present study indicate, with this further supported by previous observations (Mintenig et al., 2019; Pivokonsky et al., 2018). Further research is needed in tracking the MPs fluxes of MPs in the various processes within drinking water production i.e., those procedures aimed at routinely removing biofilm from sand filtration beads or flocculator reactors as formed biofilms are likely to act as major trap of floating MPs in the processed raw water (World Health Organization, 2019). Such research is likely to lead to a better understanding of the significance of treatment related waste streams as contributors of microplastics to the environment. Overall, the outcomes of the present study showed low MPs loads in the drinking water sample up to the water meter stage in the supply grid suggesting a low risk to human health. The introduced combination of enhanced sampling and analytical detection techniques support future tailored, quality-controlled investigative studies to better understand the sources and occurrence of microplastics in both produced tap and bottled water, the efficacy of different treatment processes and combinations of processes, and the significance of the potential return of microplastics to the environment from treatment waste streams.

CRediT authorship contribution statement

Alessio Gomiero: Conceptualization, Data curation, Writing - original draft, Funding acquisition, Project administration. **Kjell Birger Øysæd**: Investigation, Formal analysis, Data curation. **Luca Palmas**: Sampling device engineering, Writing - original draft. **Geir Skogerbø**: Conceptualization, Writing - review & editing, Supervision.

Declaration of Competing Interest

The authors declare that they have no known competing financial interests or personal relationships that could have appeared to influence the work reported in this paper.

Acknowledgments

The authors are grateful to the staff of the water utilities at IVAR iks for organisational and technical assistance during the sampling campaign to Asle Sikveland and Unni Synnøve Lea. The authors are grateful to dr. Shaw Bamber for English proofreading and the staff members at NORCE for valuable technical assistance. Furthermore, the authors thank dr. Marta Bertolaso for the GIS data analysis This work was supported by the Norwegian Regional Fund for Rogaland and Hordaland (RFF-Vest) grant#283135.

Appendix A. Supporting information

Supplementary data associated with this article can be found in the online version at doi:10.1016/j.jhazmat.2021.125708.

References

Cartus, A., Schrenk, D., 2017. Current methods in risk assessment of genotoxic chemicals. Food Chem. Toxicol. 106, 574–582.
Cox, K.D., Covernton, G.A., Davies, H.L., Dower, J.F., Juanes, F., Dudas, S.E., 2019. Human consumption of microplastics. Environ. Sci. Technol. 53 (12), 7068–7074.

Dehaut, A., Hermabessiere, L., Duflos, G., 2019. Current frontiers and recommendations for the study of microplastics in seafood. TrAC Trends Analyt. Chem. 116, 346–359.
Deng, Y., Zhang, Y., Lemos, B., Ren, H., 2017. Tissue accumulation of microplastics in mice and biomarker responses suggest widespread health risks of exposure. Sci. Rep. 7, 46687.
Di, M., Wang, J., 2018. Microplastics in surface waters and sediments of the Three Gorges Reservoir, China. Sci. Total Environ. 616, 1620–1627.
Gomiero, A., Øysæd, K.B., Agustsson, T., van Hoytema, N., van Thiel, T., Grati, F., 2019. First record of characterization, concentration and distribution of microplastics in coastal sediments of an urban fjord in south west Norway using a thermal degradation method. Chemosphere 227, 705–714.
Harvey, D.J., 2005. Chapter "gas chromatography | mass spectrometry". In: Worsfold, P., Townshend, A., Poole, C. (Eds.), Encyclopedia of Analytical Science, Second ed. Elsevier, pp. 106–116. ISBN 9780123693976.
Hermabessiere, L., Himber, C., Boricaud, B., Kazour, M., Amara, R., Cassone, A.L., Duflos, G., 2018. Optimization, performance, and application of a pyrolysis-GC/MS method for the identification of microplastics. Anal. Bioanal. Chem. 410 (25), 6663–6676.
Kirstein, I.V., Hensel, F., Gomiero, A., Iordachescu, L., Vianello, A., Wittgren, H.B., Vollertsen, J., 2021. Drinking plastics?–Quantification and qualification of microplastics in drinking water distribution systems by μFTIR and Py-GCMS. Water Res. 188, 116519.
Koelmans, A.A., Nor, N.H.M., Hermsen, E., Kooi, M., Mintenig, S.M., De France, J., 2019. Microplastics in freshwaters and drinking water: critical review and assessment of data quality. Water Res. 155, 410–422.
Koelmans, A.A., Nor, N.H.M., Hermsen, E., Kooi, M., Mintenig, S.M., De France, J., 2019. Microplastics in freshwaters and drinking water: critical review and assessment of data quality. Water Res. 155, 410–422.
Krauskopf, L.M., Hemmerich, H., Dsikowitzky, L., Schwarzbauer, J., 2020. Critical aspects on off-line pyrolysis-based quantification of microplastic in environmental samples. J. Anal. Appl. Pyrolysis 152, 104830.
Li, C., Busquets, R., Campos, L.C., 2020. Assessment of microplastics in freshwater systems: a review. Sci. Total Environ. 707, 135578.
Lusher, A., Hollman, P., Mendoza-Hill, J., 2017. Microplastics in Fisheries and Aquaculture: Status of Knowledge on Their Occurrence and Implications for Aquatic Organisms and Food Safety. FAO.
Mani, T., Hauk, A., Walter, U., Burkhardt-Holm, P., 2015. Microplastics profile along the Rhine River. Sci. Rep. 5 (1), 1–7.
Matsui, K., Ishimura, T., Mattonai, M., Iwai, I., Watanabe, A., Teramae, N., Watanabe, C., 2020. Identification algorithm for polymer mixtures based on Py-GC/MS and its application for microplastic analysis in environmental samples. J. Anal. Appl. Pyrolysis 149, 104834.
Mintenig, S.M., Löder, M.G.J., Primpke, S., Gerdts, G., 2019. Low numbers of microplastics detected in drinking water from ground water sources. Sci. Total Environ. 648, 631–635.
Oßmann, B.E., Sarau, G., Holtmannspötter, H., Pischetsrieder, M., Christiansen, S.H., Dicke, W., 2018. Small-sized microplastics and pigmented particles in bottled mineral water. Water Res. 141, 307–316.
Parolini, M., Antonioli, D., Borgogno, F., Gibellino, M.C., Fresta, J., Albonico, C., Cavallo, R., 2021. Microplastic Contamination in Snow from Western Italian Alps. Int. J. Environ. Res. Public Health 18 (2), 768.
Peng, G., Bellerby, R., Zhang, F., Sun, X., Li, D., 2020. The ocean's ultimate trashcan: hadal trenches as major depositories for plastic pollution. Water Res. 168, 115121.
Pivokonsky, M., Cermakova, L., Novotna, K., Peer, P., Cajthaml, T., Janda, V., 2018. Occurrence of microplastics in raw and treated drinking water. Sci. Total Environ. 643, 1644–1651.
Prata, J.C., da Costa, J.P., Lopes, I., Duarte, A.C., Rocha-Santos, T., 2020. Environmental exposure to microplastics: an overview on possible human health effects. Sci. Total Environ. 702, 134455.
Primpke, S., Fischer, M., Lorenz, C., Gerdts, G., Scholz-Böttcher, B.M., 2020. Comparison of pyrolysis gas chromatography/mass spectrometry and hyperspectral FTIR imaging spectroscopy for the analysis of microplastics. Anal. Bioanal. Chem. 412, 8283–8298.
Revel, M., Châtel, A., Mouneyrac, C., 2018. Micro (nano) plastics: A threat to human health? Curr. Opin. Environ. Sci. Health 1, 17–23.
Schwabl, P., Köppel, S., Königshofer, P., Bucsics, T., Trauner, M., Reiberger, T., Liebmann, B., 2019. Detection of various microplastics in human stool: a prospective case series. Ann. Intern. Med. 171 (7), 453–457.
Schymanski, D., Goldbeck, C., Humpf, H.U., Fürst, P., 2018. Analysis of microplastics in water by micro-Raman spectroscopy: release of plastic particles from different packaging into mineral water. Water Res. 129, 154–162.
Strafella, P., López Correa, M., Pyko, I., Teichert, S., Gomiero, A., 2020. Distribution of microplastics in the marine environment. Handb.of Microplast. Environ. 1–35.
Strand, J., Feld, L., Murphy, F., Mackevica, A., Hartmann, N.B., 2018. Analysis of Microplastic Particles in Danish drinking water (p. 34). DCE-Danish Centre for Environment and Energy.
Uhl, W., Eftekhardadkhah, M., Svendsen, C., 2018. Mapping Microplastic in Norwegian Drinking Water. Atlantic 185, 491–497.
Vianello, A., Jensen, R.L., Liu, L., Vollertsen, J., 2019. Simulating human exposure to indoor airborne microplastics using a Breathing Thermal Manikin. Sci. Rep. 9 (1), 1–11.
World Health Organization, 2017. Guidelines for drinking-water quality: fourth edition incorporating the first addendum. Geneva:. Licence: CC BY-NC-SA 3.0 IGO.
World Health Organization. (2019). Microplastics in drinking-water. ISBN: 978–92-4–151619-8; Licence: CC BY-NC-SA 3.0 IGO.

TITLE/ AUTHOR	**Bio-based production of carbon nanotubes via co-pyrolysis of eucalyptus oil and ferrocene / Le, G.T.T., Mala, P., Ratchahat, S., Charinpanitkul, T.**
SOURCE	**Journal of Analytical and Applied Pyrolysis Volume 158, September 2021, 105257 https://doi.org/10.1016/j.jaap.2021.105257 (Database : Science Direct)**

Journal of Analytical and Applied Pyrolysis 158 (2021) 105257

Contents lists available at ScienceDirect

Journal of Analytical and Applied Pyrolysis

journal homepage: www.elsevier.com/locate/jaap

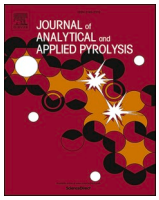

Bio-based production of carbon nanotubes via co-pyrolysis of eucalyptus oil and ferrocene

Giang T.T. Le [a], Phanatchakorn Mala [a], Sakhon Ratchahat [b], Tawatchai Charinpanitkul [a,c,*]

[a] Center of Excellence in Particle Technology and Material Processing, Faculty of Engineering, Chulalongkorn University, Bangkok, 10330, Thailand
[b] Department of Chemical Engineering, Faculty of Engineering, Mahidol University, Nakhon Pathom, 73170, Thailand
[c] Research Network of NANOTEC-KU on Nanocatalyst and Nanomaterials for Sustainable Energy and Environment, Bangkok, 10900, Thailand

ARTICLE INFO

Keywords:
Pyrolyzing
Eucalyptus oil
CNT
Ferrocene
SDG

ABSTRACT

To comply with the sustainable development goals (SDGs), bio-based production of carbon nanotubes (CNTs) was investigated using co-pyrolysis of eucalyptus oil and ferrocene instead of non-valorizable petroleum-based hydrocarbons. Attributed to high carbon content of eucalyptus oil, CNTs with substantial yield could be produced within a pyrolyzing temperature (T_p) range of 800−900 °C and different molar ratios of eucalyptus oil to ferrocene (R_{of}) including 1:1, 2:1 and 3:1. Typical FESEM analyses of as-produced CNTs revealed that CNTs with agglomeration of amorphous carbon could be produced at low T_p and low R_{of}. Meanwhile higher T_p and R_{of} could provide CNTs with lower content of amorphous carbon. TGA analyses could confirm the superior thermal stability of the resultant CNTs which were produced at high T_p and R_{of}. The highest CNT yield of about 45 % was obtained at T_p of 850 °C and R_{of} of 1:1. It could be confirmed that T_p of 900 °C and R_{of} of 3:1 was the optimal condition for production of high quality CNTs from valorizable eucalyptus oil.

1. Introduction

With an aim of contribution to the Sustainable Development Goals (SDG) of the United Nation, Goal No. 12: ensuring sustainable consumption and production patterns has stimulated various emerging research and development works in many countries [1]. Accordingly, there are many technological progresses in resource usage, sustainable and responsible consumption with decreasing waste generation as well as CO_2 emissions. Exploration on finding alternative renewable resources for production of novel materials is also a crucial issue for stimulating many research teams around the world. At presence, various biomass-based precursors have become an attractive precursor for production of some high value-added products, which could promote the Bio-Circular-Green (BCG) economy for the SDGs [2]. Accordingly, pyrolysis with strategic usage of alternative raw materials, especially biomass, would provide new potential of resource valorization [3].

Meanwhile, the discovery of carbon nanotubes (CNTs) by Iijima in 1991 has stimulated a sky-rocketing increase in investigation on effective production of CNTs [4]. Since then, CNT growth mechanism has been debatable issue, resulting in many different models have been proposed regarding to components and physical states of raw materials and operating conditions. So far, CNTs could be produced from hydrocarbon-based precursors, such as alcohol, methane, which are non-valorizable resources [5–9]. Some works with focus on utilizing polymeric waste were also reported previously [10]. Meanwhile, there was only a limited amount of previous studies in the use of renewable biomass. Based on our literature review, the use of biomass-based carbon feedstock for CNT synthesis via pyrolysis method has been reported in several studies [11–13]. However, lack of systematic investigation on effect of various synthesis variables on CNT properties is still a remaining issue. It should be noted that high carbon contents in eucalyptus oil could make it become a potential carbon precursor for CNT synthesis [14]. A simple technique of co-pyrolysis of eucalyptus oil with commercially available metallocene provides a large-scale production, low investment cost, and high-quality CNTs when compared with other techniques, such as arc discharge and laser ablation techniques [5, 15–18]. Herein, a novel aspect on using a combination of eucalyptus oil and ferrocene which were subject to pyrolysis for examining possibility to synthesize CNTs with controllable properties was raised. Accordingly, two major variables, which were pyrolyzing temperature and molar ratio of eucalyptus oil to ferrocene, were experimentally examined and discussed. The CNT production via co-pyrolysis of eucalyptus oil and

* Corresponding author at: Center of Excellence in Particle Technology and Material Processing, Faculty of Engineering, Chulalongkorn University, Bangkok, 10330, Thailand.
E-mail address: ctawat@chula.ac.th (T. Charinpanitkul).

https://doi.org/10.1016/j.jaap.2021.105257
Received 20 December 2020; Received in revised form 20 June 2021; Accepted 1 July 2021
Available online 3 July 2021

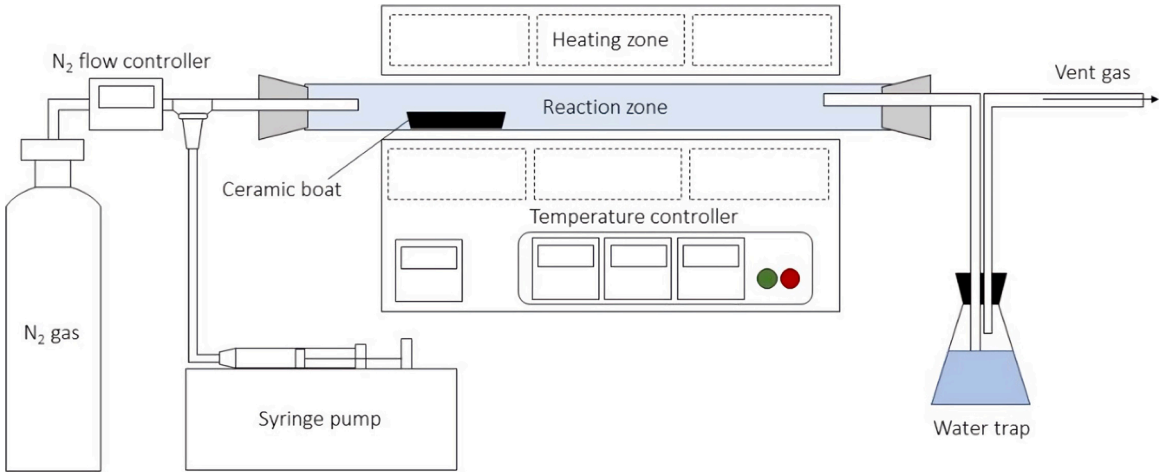

Fig. 1. Experimental setup for producing CNTs by co-pyrolysis of eucalyptus oil and ferrocene.

ferrocene was conducted using a tubular reactor equipped with an electrical furnace and temperature controller. All resultant CNTs produced under each condition were comprehensively characterized using field-emission scanning electron microscopic, N_2 adsorption/desorption, thermogravimetric, and Raman spectroscopic analyses for clarifying their properties. Finally, dependence of production yield and characteristics of resultant CNTs on pyrolyzing temperatures and molar ratio of eucalyptus oil to ferrocene were discussed.

2. Experimental

For production of CNTs, eucalyptus oil and ferrocene were vaporized within a quartz tube reactor using an electrical furnace equipped with a temperature controller. Eucalyptus oil (70 % proportion of eucalyptol, Peerasuk Chemicals, Thailand) and ferrocene (98 % purity, Aldrich, Germany) were used without additional purification. Based on CHNS/O elemental analysis (FlashSmart Elemental Analyzer, Thermo Scientific, USA), the main elemental composition of typical samples of eucalyptus oil was carbon of 85.23 %, oxygen of 12.14 %, and hydrogen of 2.63 % with negligible amount of nitrogen.

Schematic diagram of the quartz tube reactor and relevant equipment was depicted in Fig. 1. With this setting, it could be confirmed that pyrolyzing temperature (T_p) could be controlled at the designated range of 800–900 °C. With the set of the electrical furnace and temperature controller, the quartz tube reactor (diameter of 3 cm and length of 100 cm) was heated from room temperature to a designated T_p in 30 min under nitrogen (99.9 % purity, Linde, Thailand) flow of 1.2 L/h at atmospheric pressure. When temperature inside the reactor reached the set-point temperature, the ceramic boat containing 1 g ferrocene was shifted into a position which could vaporized it gradually. Then, eucalyptus oil with a designated molar ratio of oil to ferrocene (R_{of}) including 1:1, 2:1, and 3:1 was supplied into the heating zone of the reactor with a constant flow rate 0.01 L/h. After 30 min of operating time and cooling down to room temperature, black particulate products were collected from the inner wall surface of the tubular reactor and taken out for comprehensive analyses. In each experiment, it could be observed that all raw materials (eucalyptus oil and ferrocene) were completely converted without any remaining residue. Characteristics and production yield of CNTs produced under each condition were reported and discussed in the following sections.

Microscopic structure and morphology of CNTs was characterized by field emission scanning electron microscope (FESEM, S-3400 N, Hitachi,

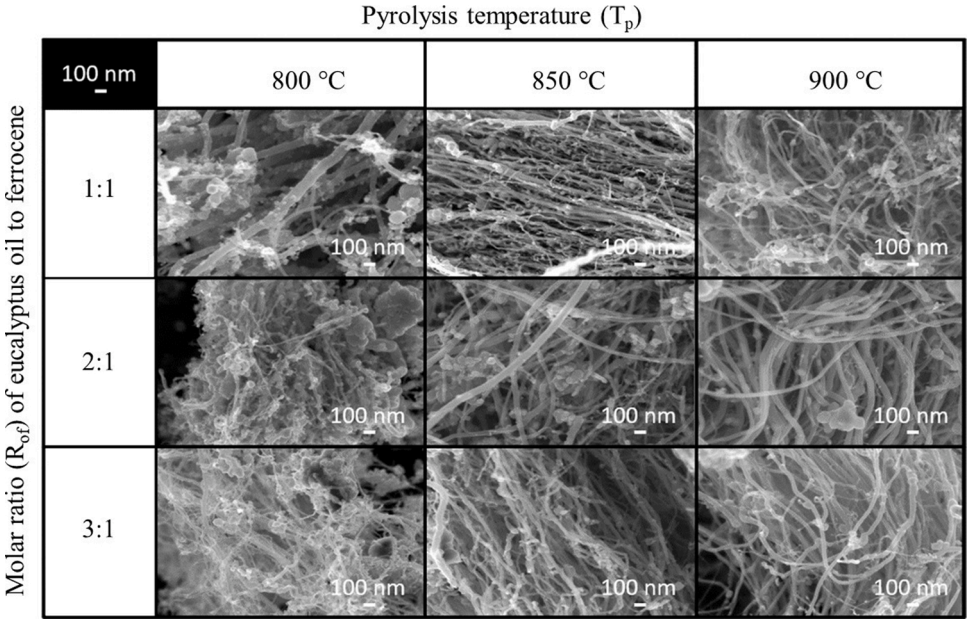

Fig. 2. Microscopic structure of CNTs produced at different T_p and R_{of}.

Japan) at an accelerated voltage of 20 kV and their specific surface area was determined by N_2 adsorption/desorption (3Flex, Micromeritics, USA). Thermal stability of CNTs produced under each condition was analyzed by Thermogravimetric analyzer (TGA, TGA8000, Perkin-Elmer, USA) under nitrogen atmosphere with a heating rate of 10 °C/min up to 900 °C. Graphitic and amorphous carbons content of the resultant CNTs was characterized by Raman spectroscopy (NTEGRASpectra, NT-MDT, USA) with a wavelength of 633 nm. Based on Eq. (1), production yield of resultant CNTs (wt%) could be confirmed based on the ratio of the total weight of collected products against the summation of total weight of eucalyptus oil and ferrocene.

$$\text{CNT Production yield} = \frac{W_c}{W_{oil} + W_{fer}} \quad (1)$$

whereas W_c represented weight of carbon product

W_{oil} represented weight of eucalyptus oil

W_{fer} represented weight of ferrocene

Meanwhile, production yield of resultant CNTs per unit mass of ferrocene was determined based on Eq. (2):

$$\text{CNT Yield per unit mass of ferrocene} = \frac{W_c}{W_{fer}} \quad (2)$$

3. Results and discussion

3.1. Dependence of CNT microscopic property on T_p and R_{of}

Typical FESEM images in Fig. 2 exhibit microscopic structure and morphology of CNTs produced at different T_p and R_{of}. Such FESEM images revealed that there were both CNTs (tubular structure) and carbon nanoparticles (irregular structure) in all resultant products. In general, quality of produced samples could be estimated by the proportion of well-aligned CNT structure in such micrographs. With a designated R_{of} of 1:1, an increase in T_p from 800 to 900 °C could provide the resultant product with higher content of well-aligned CNTs. Meanwhile, an increase in R_{of} from 1:1 to 3:1 with any designated T_p could also lead to the resultant products with higher contents of well-aligned CNTs. Accordingly, higher content of well-aligned CNTs in typical samples produced with higher T_p and R_{of} suggested their higher quality. Using more complicated catalyst of cobalt on titanium boride ($Co@TiB_2$), Lin et al. also reported that a synthesizing temperature could improve the excitation growth rate of CNTs when compared to that of carbon nanoparticles [7]. Thermodynamically, an increase in pyrolyzing temperature could enhance the decomposition of amorphous carbon nanostructure because of their higher reaction activity and higher specific surface area [10]. Hence CNTs became dominant species in the resultant samples produced at a higher T_p.

It should be noted that an increase in eucalyptus oil content (higher R_{of}) could provide a certain amount of carbon dioxide (CO_2) as a by-product, which could contribute to the decomposition of amorphous carbon content via oxidation [19]. The use of CO_2 as selective oxidant of amorphous and defective carbon has been reported with remarkable efficiency and selectivity [20,21]. It is reasonable that a higher content of eucalyptus oil would provide more CO_2 as one of the major gaseous products after its decomposition. Therefore, such CO_2 generated from decomposition of eucalyptus oil could engage in reacting with amorphous carbon content in the resultant products at an elevated temperature above 800 °C. As confirmed by FESEM analyses, a decrease in amount of carbon nanoparticles together with an increase in CNTs could be observed when R_{of} was increased from 1:1 to 3:1. Therefore, these morphological analyses would suggest that regulation of T_p and R_{of} could provide effective CNT production via co-pyrolysis of eucalyptus oil with the presence of ferrocene. In addition, further confirmation using Raman spectroscopy and TGA analyses would be discussed in the following sections.

Meanwhile, nominal diameter of CNTs produced under each condition was analyzed via Image Processing by employing the ImageJ software. Statistical analyses of a few hundred CNTs in typical FESEM images were conducted for acquiring their nominal diameter distribution. As a result, the nominal diameter distribution of the CNTs produced at T_p of 900 °C R_{of} of 3:1was depicted in Fig. 3 while Table 1 summarizes the average diameter of all as-synthesized samples (the nominal diameter distribution of all CNT samples was provided in Supporting Information). It could be clearly observed that the resultant CNTs exhibited a normal distribution in their nominal diameter within a range of 30−70 nm, which is defined as MWCNTs [12–14]. When T_p was increased from 800 to 900 °C and R_{of} was increased from 1:1 to 3:1 while the average nominal diameter was shifted from 39 to 59 nm, respectively. The increment of the nominal diameter of the resultant CNTs would be attributed to the growth of catalytic Fe nanoparticles at a higher temperature. With an increase in synthesizing temperature, the

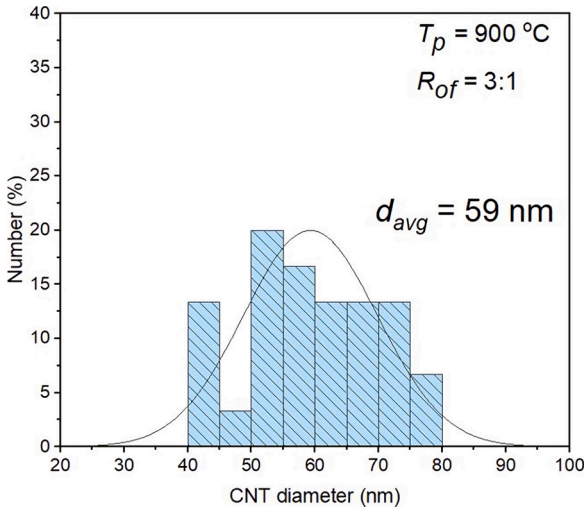

Fig. 3. Size distribution of typical samples of CNTs produced with R_{of} of 3:1 at T_p of 900 °C.

Table 1
Average diameter of as-synthesized CNTs at various T_p and R_{of}.

T_p	Average diameter (nm)		
	R_{of} = 1:1	R_{of} = 2:1	R_{of} = 3:1
800 °C	39	44	45
850 °C	44	49	55
900 °C	42	51	59

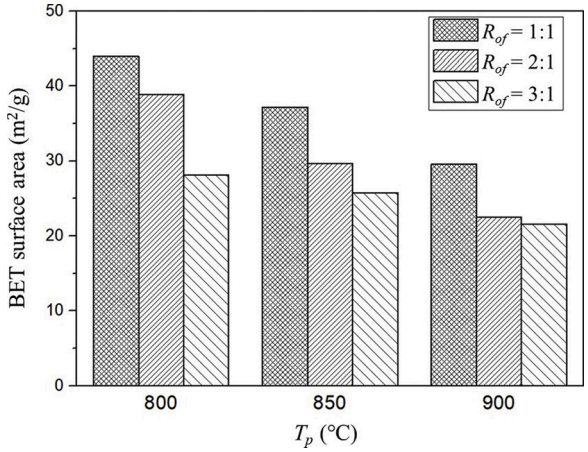

Fig. 4. Specific surface area of CNTs produced at different T_p and R_{of}.

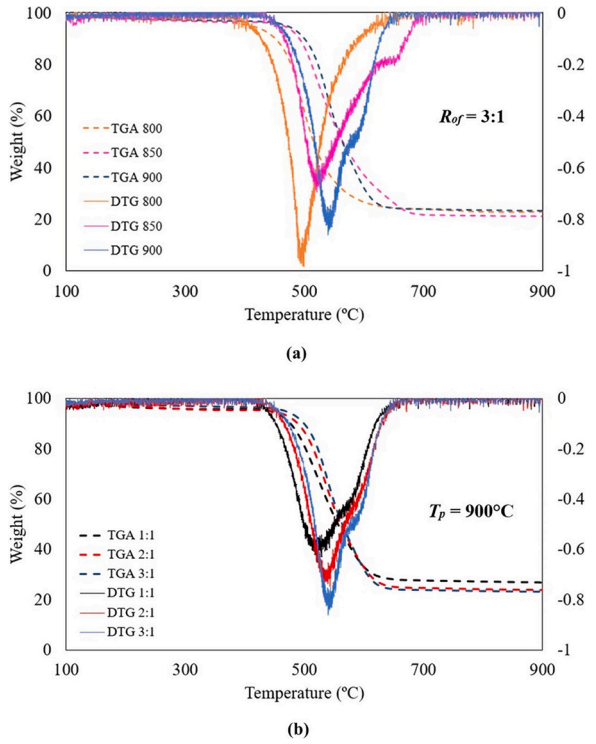

Fig. 5. (**a**) Effect of T_p on Thermal stability of CNTs produced at R_{of} of 3:1 and (**b**) effect of R_{of} on Thermal stability of CNTs produced at T_p of 900 °C.

nominal diameter of synthesized CNTs would be increased with an increase in the graphene layer induced by the catalytic particles with a larger size [15]. Based on TEM analyses, Li et al. also reported that a higher synthesizing temperature could result in CNTs with higher graphitic content depositing on the surface of agglomerated Fe nanoparticles doped on SiO_2 support [22]. In addition, an increase in diameter of synthesized CNTs with increasing molar ratio of carbon precursor to ferrocene had also been reported by Thonganantakul et al. [23].

Furthermore, specific surface area measurements of all resultant CNT samples were conducted by N_2 adsorption/desorption method as shown in Fig. 4. It could be observed that when T_p was increased from 800 to 900 °C, the specific surface area of CNTs produced with R_{of} of 1:1 was shifted from 44.1 to 29.6 m^2/g, respectively. Repeated tendency of dependence of the specific surface area of the produced CNTs on the eucalyptus oil content was also confirmed with different R_{of}. An increase in T_p and R_{of} could result in a decrease in the specific surface area of the produced CNTs. Lee et al. also reported that an increase in synthesizing temperature would stimulate a decrease in amorphous carbon content which was more reactive due to its higher surface area [24,25]. In addition, it should be noted that an increase in eucalyptus oil content with a fixed amount of ferrocene would certainly attribute to an increase in CO_2 content generated from eucalyptus oil decomposition. Such CO_2 content would attribute to the oxidation of reactive amorphous carbon. As also confirmed by the analytical results in Fig. 3, the increase in the nominal diameter of the CNTs produced at a higher T_p would also attribute to their lower specific surface area. Consistency in all microscopic analyses mentioned above would suggest that co-pyrolysis of eucalyptus oil and ferrocene could attribute to production of CNTs with regulatable quality. Anyway, further confirmation of thermal stability and production yield of CNTs produced by this method would also be examined and discussed.

3.2. Dependence of thermal stability of CNTs on T_p and R_{of}

Thermal stability of all CNT samples produced with regulated T_p and

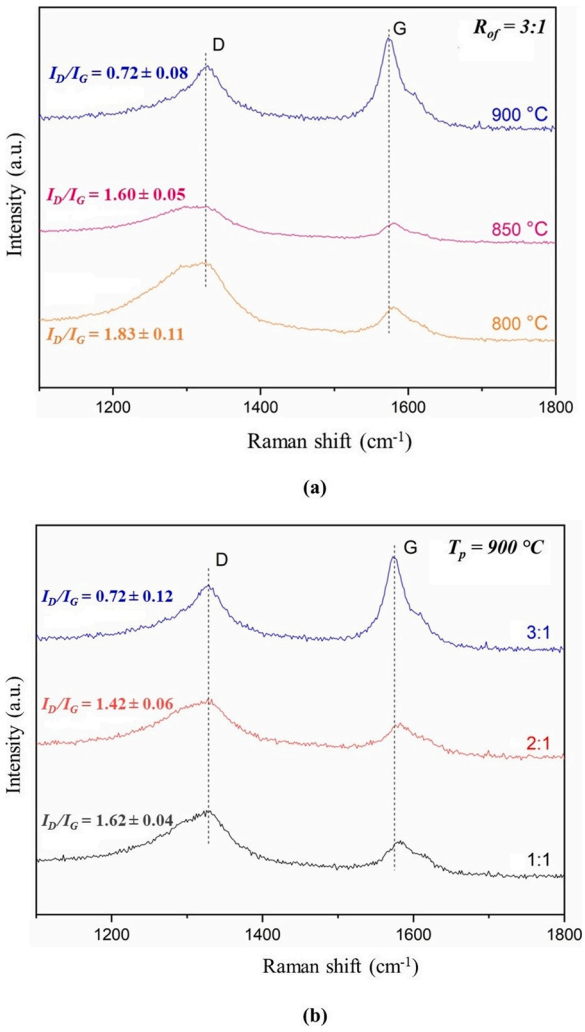

Fig. 6. (**a**) Effect of T_p on I_D/I_G of CNTs produced at R_{of} of 3:1 and (**b**) effect of R_{of} on I_D/I_G of CNTs produced at T_p of 900 °C.

R_{of} could be confirmed by thermogravimetric analyzer (TGA) under O_2 atmosphere. Fig. 5(**a**) exhibits TGA and DTG curves of CNT samples obtained from co-pyrolysis at R_{of} of 3:1 with T_p in the range of 800−900 °C. Significant weight loss of CNT samples observed at 430−600 °C could be attributed to the decomposition of carbon content within the samples [24]. Meanwhile, the remaining residue (24 ± 2 wt%) could be assigned to the Fe content which was obtained from ferrocene during the co-pyrolysis of carbon precursor and ferrocene [26–28]. Such slight difference in residual content would be due to the fixed amount of loaded ferrocene.

Furthermore, effect of R_{of} on the thermal stability of CNTs produced at a pyrolyzing temperature of 900 °C is depicted in Fig. 5(**b**). Similar thermal stability could be observed that significant weight loss of CNT samples took place in the treating temperature range of 430–600 °C. Also, DTG analysis was employed to figure out a peak temperature with maximum weight loss rate. It could be confirmed that the peak temperature was shifted from 525 to 542 °C when R_{of} was increased from 1:1 to 3:1, indication greater thermal stability of CNTs synthesized at higher R_{of}. These results would be ascribed to the different portion of amorphous carbon content in the CNT samples. Basically, amorphous carbon is more reactive than graphitic structure because of its less stable microscopic structure and larger specific surface area [28]. Within the accuracy of the TGA analyzer, it should be noted that there was a detectable decrease in the residue content when the CNTs produced with the higher R_{of} was subject to TGA analyses. The residue content was

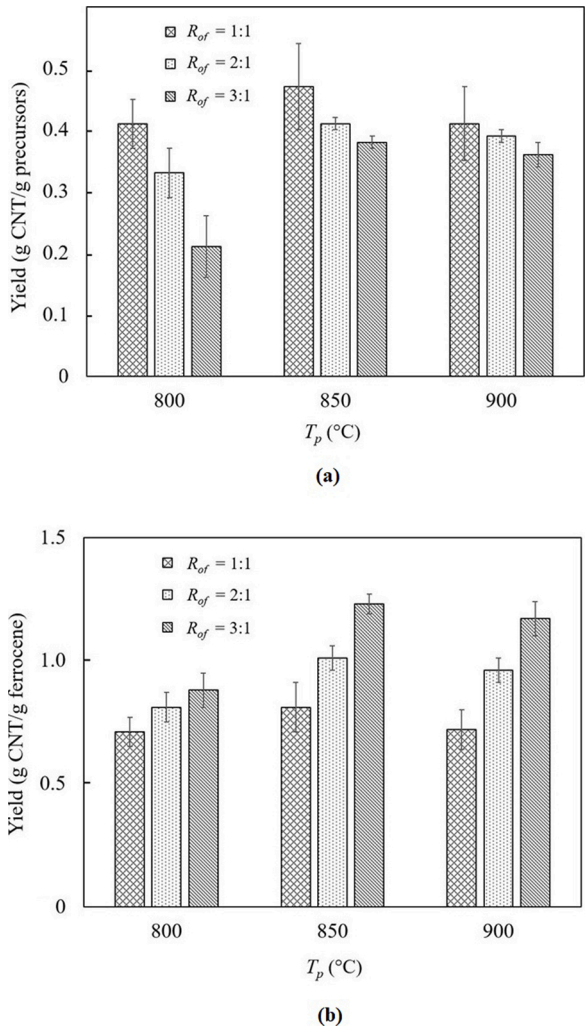

Fig. 7. (**a**) Dependence of yield of CNTs on T_p and R_{of} and (**b**) Dependence of CNT yield per unit mass of ferrocene on T_p and R_{of}.

decreased from 29 to 24 wt% when the R_{of} was increased from 1:1 to 3:1, respectively. These results would be attributed to the relative content of carbon and Fe within CNTs produced with the different loading of carbon source and metal catalyst [27]. An increase in R_{of} could be implied that higher amount of carbon could be supplied to the CNT formation with lower amount of Fe. As a result, CNTs produced at 900 °C with R_{of} of 3:1 possessed the lower residual content.

Raman spectroscopy is widely applied to investigate the structural property of carbon-based materials, which could be employed for supporting their thermal stability. The graphitization/crystallinity of CNTs produced at regulated T_p and R_{of} could also be confirmed by Raman spectrum as shown in Fig. 6(**a**) and (**b**), respectively. The dominant band (G-band), which appeared at a Raman Shift of 1576 cm^{-1}, could be assigned to the vibration of sp^2 bonded carbon atom. In general, such G-band was applied to identify graphitic structure in CNTs. Meanwhile, the other dominant band (D-band) at a Raman shift of 1344 cm^{-1} could be assigned to the vibration of non-sp^2 bonded carbon atom which could identify amorphous configuration of carbon clusters within a sample [28]. The intensity ratio of D-band to G-band (I_D/I_G) was used to evaluate the quality of carbonaceous material based on its crystallinity or graphene layer. In general, carbonaceous material including CNTs which contain more graphene layers in their tubular structure would be identified by lower I_D/I_G.

Accordingly, Fig. 6(**a**) reveals effect of T_p on I_D/I_G of CNTs produced at R_{of} of 3:1. An increase in T_p from 800 to 900 °C resulted in a significant decrease in I_D/I_G from 1.83 to 0.72. Meanwhile, effect of R_{of} on I_D/I_G of CNTs produced at T_p of 900 °C was depicted in Fig. 6(**b**), suggesting that an increment of eucalyptus oil portion when compared to ferrocene could also result in a decrease of I_D/I_G from 1.62 to 0.72. These analytical results are consistent evidence for supporting the TGA analyses which could confirm that CNTs produced at a higher T_p and a higher R_{of} would exhibit superior thermal stability due to the availability of higher graphitic content [14,28]. Based on all analytical results discussed above, it could be confirmed that high quality CNTs could be produced by co-pyrolysis of eucalyptus oil and ferrocene by regulating two key variables, which are T_p and R_{of}.

3.3. Dependence of production yield of CNTs on T_p and R_{of}

In addition to the quality of CNTs produced by co-pyrolysis of eucalyptus oil and ferrocene, its productivity is also an important issue worth for investigation. Based on Eq. (1), Fig. 7(**a**) reveals effect of T_p and R_{of} on dependence of yield of resultant CNTs with respect to the total amount of precursors which were eucalyptus oil and ferrocene. With a designated R_{of} of 1:1, an average CNT production yield was increased from 41.4 % to 46.8 % when T_p was increased from 800 to 850 °C, respectively. On the other hand, the CNT production yield was decreased from 46.8 % to 41.7 % when T_p was further increased from 850 to 900 °C, respectively. With R_{of} of 2:1 and 3:1, a similar tendency was also confirmed. These results were in a good agreement with some previous works which used other hydrocarbon precursors. Using acetylene (C_2H_2) as precursor, Li et al. reported that an increase in pyrolyzing temperature from 600 to 900 °C could lead to a significant increase in the CNT production yield. Meanwhile, a further increase in the pyrolyzing temperature resulted oppositely in the lower CNT production yield [29]. It is well recognized that CNTs could be produced through multiple steps of dissolving, diffusing, and precipitating of carbon clusters, which were affected by both pyrolyzing temperature and supplying of precursor [29]. An increase in T_p in a lower range could enhance the thermal decomposition of both eucalyptus oil and ferrocene, which played an important role in sufficient supply of carbon and catalytic Fe clusters for promoting the CNT production yield. However, the excessive increase in T_p would attribute to enhancing agglomeration of Fe clusters and decomposition of amorphous carbon content, which resulted oppositely in a decrease in the CNT production yield.

Meanwhile, a distinct decrease in the CNT production yield was confirmed when R_{of} was increased from 1:1 to 3:1 with a designated T_p. These results would be ascribed to the role of excessive amount of CO_2 and insufficient amount of Fe catalysts due to the increase in eucalyptus oil content when compared to ferrocene. When R_{of} was increased from 1:1 to 3:1, higher amount of CO_2 decomposed from eucalyptus oil would engage in oxidation of emerging carbon clusters while lower amount of Fe clusters would be insufficient for accommodating the formation of CNTs [30]. These quantitative analyses would also be in a good agreement with the analytical results of TGA and Raman spectroscopy as discussed in previous section.

It should be noted that consideration on CNT yield with respect to the total amount of eucalyptus oil and ferrocene would not provide a viewpoint of ferrocene utilization. In fact, the cost of ferrocene (8.60 baht/g), which is employed as catalyst is more expensive than that of eucalyptus oil (2.25 baht/g). A focus on the unit mass of ferrocene would suggest the efficiency of ferrocene utilization. Based on Eq. (2), Fig. 7(**b**) reveals effect of T_p and R_{of} on yield of resultant CNTs per unit mass of ferrocene. Consistent tendency of dependence of CNT yield per unit mass of ferrocene could be confirmed with respect to all T_p and R_{of}. With a designated T_p, the increase in R_{of} resulted in an increase in the CNT yield unit mass of ferrocene, indicating there was higher possibility of CNT growth when supplying more content of eucalyptus oil into the reactor. The lowest R_{of} of 1:1 could provide limited carbon content when compared to the excessively available amount of active surface of Fe clusters, resulting in the lowest CNT yield unit mass of ferrocene.

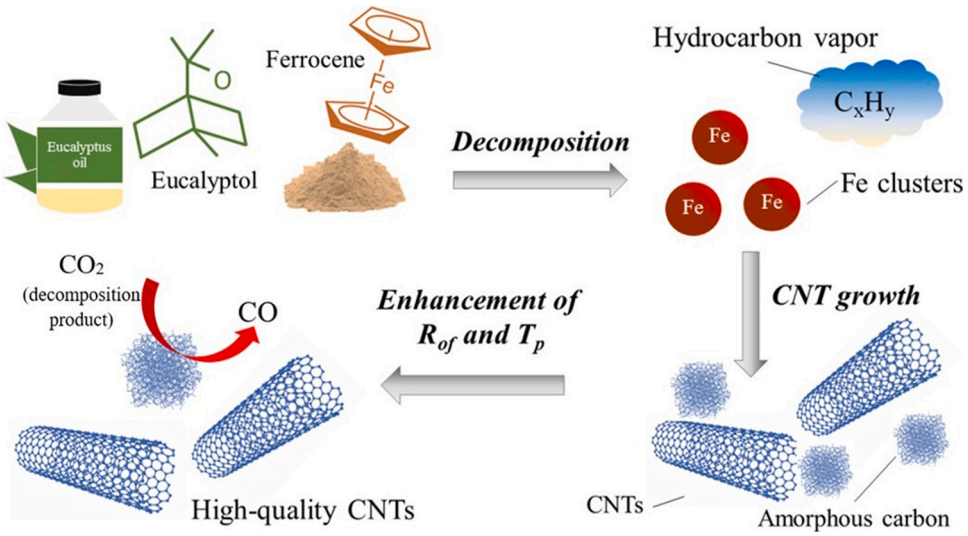

Fig. 8. Schematic diagram of CNTs produced by co-pyrolysis of eucalyptus oil and ferrocene.

Meanwhile, the increase in T_p from 800 to 900 °C with a designated R_{of} of 1:1 could also lead to the increase in the CNT yield per unit mass of ferrocene from 0.722 to 0.897. These results would be ascribed to the enhancement of eucalyptus oil decomposition, which would play an important role in sufficient supply of carbon atoms for CNT growth [24–27].

Based on all analytical results which were discussed above, schematic diagram of CNT formation mechanism via co-pyrolysis of eucalyptus oil and ferrocene was illustrated in Fig. 8. At a designated T_p, above 800 °C which is higher than decomposition temperatures of eucalyptus oil and ferrocene, both precursors would be decomposed to provide carbon and Fe clusters. Self-assembly of CNTs would take place on the catalytic surface of Fe clusters while amorphous carbon would also competitively be formed as impurities. Under the condition of lower T_p (800 °C) and R_{of} (1:1), fewer amount of CNTs would be obtained due to the insufficient dissolution, diffusion, and precipitation of carbon and Fe clusters emerging from decomposition of both precursors. Meanwhile, an increase in T_p and R_{of} could lead to an increment in both carbon and Fe clusters, resulting in production of CNTs with higher quality and promoted production yield. As a supporting evidence, TGA and Raman spectroscopic analyses suggested that the increase in T_p would attribute to enhancing decomposition of amorphous carbon content. According to all consistent analytical results and discussion, it would be summarized that co-pyrolysis of renewable eucalyptus oil with the presence of ferrocene is a promising technique to valorize eucalyptus oil for bio-based production of CNTs.

4. Conclusions

Eucalyptus oil is one of the promising biomass-based carbon feedstocks for bio-based production of CNTs via co-pyrolysis with ferrocene. The synthesizing conditions at low pyrolyzing temperature (T_p) and low molar ratio (R_{of}) could provide the regulatable CNT yield of 41.38 % and specific surface area of 44.1 m^2/g. On the other hand, despite its lower product yield and surface area, high T_p and R_{of} could provide high content of CNT yield with higher thermal stability as confirmed by FESEM, TGA and Raman spectroscopic analyses. The increase in R_{of} could enhance the CNT quality due to the enhanced oxidation of amorphous carbon content while the increase in T_p could promote the thermal stability of the resultant CNTs. In summary, T_p of 900 °C and R_{of} of 3:1 was the optimal condition for production of high quality CNTs from co-pyrolysis of eucalyptus oil and ferrocene.

Declaration of Competing Interest

The authors report no declarations of interest.

Acknowledgements

This research project has been supported by the Second Century Fund (C2F), Chulalongkorn University for Postdoctoral Fellowship (G.T.T.L.). T.C. is grateful to partial support of the National Nanotechnology Center (NANOTEC), NSTDA. Ministry of Science and Technology, Thailand through the program of Research Network of NANOTEC (RNN). Also, the Ratchadapisek Sompoch Endowment Fund (2015), Chulalongkorn University (CU-58-064-CC) and partial support from the Institutional Research Grant (IRG5780014) of TRF and Chulalongkorn University (Contract No. RES_57_411_21_076) was acknowledged.

Appendix A. Supplementary data

Supplementary material related to this article can be found, in the online version, at doi:https://doi.org/10.1016/j.jaap.2021.105257.

References

[1] B.F. Giannetti, F. Agostinho, J.J. Cabello Eras, Z. Yang, C.M.V.B. Almeid, Cleaner production for achieving the sustainable development goals, J. Clean. Prod. 271 (2020), 122127.
[2] W.L. Filho, U. Azeiteiro, F. Alves, P. Pace, M. Mifsud, L. Brandli, S.S. Caeiro, A. Disterheft, Reinvigorating the sustainable development research agenda: the role of the sustainable development goals (SDG), Int. J. Sustain. Dev. World Ecol. 25 (2018) 131–142.
[3] P. Thomas, C.W. Lai, M.R. Bin Johan, Recent developments in biomass-derived carbon as a potential sustainable material for super-capacitor-based energy storage and environmental applications, J. Anal. Appl. Pyrolysis 140 (2019) 54–59.
[4] S. Iijima, Helical microtubules of graphitic carbon, Nature 354 (1991) 56–58.
[5] N. Arora, N.N. Sharma, Arc discharge synthesis of carbon nanotubes: comprehensive review, Diam. Relat. Mater. 50 (2014) 135–142.
[6] S. Inoue, S. Lojindarat, T. Kawamoto, Y. Matsumura, T. Charinpanitkul, Spontaneous and controlled-diameter synthesis of single-walled and few-walled carbon nanotubes, Chem. Phys. Lett. 699 (2018) 88–91.
[7] J. Lin, Y. Yang, H. Zhang, F. Li, G. Huang, C. Wu, Preparation of CNT–Co@TiB2 by catalytic CVD: effects of synthesis temperature and growth time, Diam. Relat. Mater. 106 (2020), 107830.
[8] A. Hussain, Y. Liao, Q. Zhang, E.X. Ding, P. Laiho, S. Ahmad, N. Wei, Y. Tian, H. Jiang, E.I. Kauppinen, Floating catalyst CVD synthesis of single walled carbon nanotubes from ethylene for high performance transparent electrodes, Nanoscale 10 (2018) 9752–9759.
[9] A. Yahyazadeh, B. Khoshandam, Carbon nanotube synthesis via the catalytic chemical vapor deposition of methane in the presence of iron, molybdenum, and iron–molybdenum alloy thin layer catalysts, Results Phys. 7 (2017) 3826–3827.

[10] J. Gong, X. Chen, T. Tang, Recent progress in controlled carbonization of waste polymers, Prog. Polym. Sci. 94 (2019) 1–8.
[11] A. Luís, A. Duarte, J. Gominho, J. Domingues, A.P. Duarte, Chemical composition, antioxidant, antibacterial and anti-quorum sensing activities of Eucalyptus globulus and Eucalyptus radiata essential oils, Ind. Crops Prod. 79 (2016) 274–282.
[12] M. Robaiah, M. Rusop, S. Abdullah, Z. Khusaimi, H. Azhan, M.Y. Fadzlinatul, M. J. Salifairus, N.A. Asli, Synthesis of carbon nanotubes from palm oil on stacking and non-stacking substrate by thermal-CVD method, in: AIP Conference Proceedings, 1963, 2018, 020027.
[13] K. Awasthi, R. Kumar, R.S. Tiwari, O.N. Srivastava, Large scale synthesis of bundles of aligned carbon nanotubes using a natural precursor: turpentine oil, J. Exp. Nanosci. 5 (2010) 498–508.
[14] R. Kumar, R.M. Yadav, K. Awasthi, R.S. Tiwari, O.N. Srivastava, Sffect of nitrogen variation on the synthesis of vertically aligned bamboo-shaped C-N nanotubes using sunflower oil, Int. J. Nanosci. 10 (2011) 809–813.
[15] R. Das, Z. Shahnavaz, Md.E. Ali, M.M. Islam, S.B.A. Hamid, Can we optimize arc discharge and laser ablation for well-controlled carbon nanotube synthesis? Nanoscale Res. Lett. 11 (2016) 510–533.
[16] J. Chrzanowska1, J. Hoffman, A. Małolepszy, M. Mazurkiewicz, T.A. Kowalewski, Z. Szymanski, L. Stobinski, Synthesis of carbon nanotubes by the laser ablation method: effect of laser wavelength, Phys. Status Solidi B 252 (2015) 1860–1867.
[17] Y.M. Manawi, Ihsanullah, A. Samara, T. Al-Ansari, M.A. Atieh, A review of carbon nanomaterials' synthesis via the chemical vapor deposition (CVD) method, Materials 11 (2018) 822–858.
[18] T. Charinpanitkul, N. Sano, P. Puengjinda, J. Klanwan, N. Akrapattangkul, W. Tanthapanichakoon, Naphthalene as an alternative carbon source for pyrolytic synthesis of carbon nanostructures, J. Anal. Appl. Pyrolysis 86 (2009) 386–390.
[19] F.G. Mendonça, J.D. Ardisson, R.M. Lago, J.C. Tristão, Selective oxidation of amorphous carbon by CO_2 to produce Fe@C nanoparticles from bulky Fe/C matrices, J. Braz. Chem. Soc. 26 (2015) 11.
[20] M. Smith Jr, S.W. Hedges, R. LaCount, D. Kern, N. Shah, G.P. Huffman, B. Bockrath, Selective oxidation of single-walled carbon nanotubes using carbon dioxide, Carbon 41 (2003) 1221–1230.
[21] S.C. Tsang, P.J.F. Harris, M.L.H. Green, Thinning and opening of carbon nanotubes by oxidation using carbon dioxide, Lett. Nat. 362 (1993) 520.
[22] W.Z. Li, J.G. Wen, Z.F. Ren, Effect of temperature on growth and structure of carbon nanotubes by chemical vapor deposition, Appl. Phys. A 74 (2002) 397.
[23] O. Thonganantakul, W. Chaiwat, S. Srinives, K. Suttiponparnit, T. Charinpanitkul, Effect of preloaded ferrocene in co-pyrolysis of kerosene/ferrocene on CNT synthesis, J. Jpn. Inst. Energy 97 (2018) 180–185.
[24] C.J. Lee, J. Park, Y. Huh, J.Y. Lee, Temperature effect on the growth of carbon nanotubes using thermal chemical vapor deposition, Chem. Phys. Lett. 343 (2001) 33–38.
[25] C.J. Lee, J. Park, J.A. Yu, Catalyst effect on carbon nanotubes synthesized by thermal chemical vapor deposition, Chem. Phys. Lett. 360 (2002) 250–255.
[26] J.P. Huo, H.H. Song, X.H. Chen, Preparation of carbon-encapsulated iron nanoparticles by co-carbonization of aromatic heavy oil and ferrocene, Carbon 42 (2004) 3177–3182.
[27] P. Puengjinda, N. Sano, W. Tanthapanichakoon, T. Charinpanitkul, Selective synthesis of carbon nanotubes and nanocapsules using naphthalene pyrolysis assisted with ferrocene, J. Ind. Eng. Chem. 15 (2009) 375–380.
[28] M.S. Shamsudin, N.A. Asli, S. Abdullah, S.Y.S. Yahya, M. Rusop, Effect of synthesis temperature on the growth iron-filled carbon nanotubes as evidenced by structural, micro-Raman, and thermogravimetric analyses, Adv. Condens. Matter Phys. 2012 (2012), 420619.
[29] R.T.K. Baker, Catalytic growth of carbon filaments, Carbon 27 (1989) 315–323.
[30] H. Ming, D. Peiling, Z. Yunlong, G. Jing, R. Xiaoxue, Effect of reaction temperature on carbon yield and morphology of CNTs on copper loaded nickel nanoparticles, J. Nanomater. 2016 (2016), 8106845.

TITLE/ AUTHOR	**Biochar for environmental sustainability in the energy-water-agroecosystem nexus / Malyan, S.K., Kumar, S.S., Fagodiya, R.K., (...), Singh, R., Singh, L.**
SOURCE	**Renewable & Sustainable Energy Reviews Volume 149, October 2021, 111379 https://doi.org/10.1016/j.rser.2021.111379 (Database : Science Direct)**

Renewable and Sustainable Energy Reviews 149 (2021) 111379

Contents lists available at ScienceDirect

Renewable and Sustainable Energy Reviews

journal homepage: www.elsevier.com/locate/rser

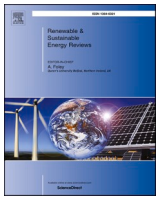

Biochar for environmental sustainability in the energy-water-agroecosystem nexus

Sandeep K. Malyan [a], Smita S. Kumar [b], Ram Kishor Fagodiya [c], Pooja Ghosh [d], Amit Kumar [e], Rajesh Singh [f], Lakhveer Singh [g,*]

[a] Research Management and Outreach Division, National Institute of Hydrology, Jalvigyan Bhawan, Roorkee, Uttarakhand, 247667, India
[b] Department of Environmental Sciences, J.C. Bose University of Science and Technology, YMCA, Faridabad, 121006, Haryana, India
[c] ICAR-Central Soil Salinity Research Institute, Karnal, Haryana, 132001, India
[d] Centre for Rural Development & Technology, Indian Institute of Technology Delhi, Hauz Khas, 110016, India
[e] Central Muga Eri Research and Training Institute, Central Silk Board, Jorhat, Assam, 785000, India
[f] Environmental Hydrology Division, National Institute of Hydrology, Jalvigyan Bhawan, Roorkee, Uttarakhand, 247667, India
[g] Department of Environmental Science, SRM University-AP, Amaravati, Andhra Pradesh, 522502, India

ARTICLE INFO

Keywords:
Biochar
Climate change
Carbon sequestration
Bioenergy
Emerging pollutants
Soil management

ABSTRACT

Global warming, management of soil health, remediation of contaminated wastewater,and sustainable alternate source of energy are the major challenges of the 21st century. Biochar has an enormous potential in addressing these global issues and can act as a catalyst in achieving sustainable development goals (SDGs). Biochar produced from waste biomass (crop residues, algal biomass, municipal waste, etc.) has dual advantages of waste management along with its application in different sectors. The mineral contents and buffering capacity of biochar make it an ultimate catalyst for anaerobic digestion which significantly enhances bioenergy production. Supplementing anaerobic digestion with biochar can increase biogas and biological hydrogen production up to 57% and 118% respectively, over control. Biochar addition to soil improves soil health, porosity and aeration which mitigates greenhouse gas emission from soil. Addition of biochar at the optimum level in rice can reduce cumulative methane emission up to 60%. In this manuscript, the potential of biochar for bioenergy production (biogas and biological hydrogen production), greenhouse gases mitigation, carbon sequestration in soils, and waste water remediation is discussed in detail along with the challenges and future prospects of biochar. This review identifies the key issues which need to be addressed for sustainable utilization of biochar.

1. Introduction

The increasing global human population is the foremost culprit for several environmental problems such as global warming, water scarcity, shortage of quality food and shelter, waste management, loss of biodiversity, and others. The sustainable development goals (SDGs) have been introduced for wise utilization of natural resources for fulfilling the present human needs and to conserve these resources for future generations. The hasty development of cities, industries, and agricultural practices has led to deterioration in environmental quality. The rapid increase in the ambient greenhouse gases (GHGs) concentration (CO_2, CH_4, and N_2O) is the main culprit for the enhanced greenhouse effect. Enhanced global warming is triggering several adverse impacts such as flash floods, severe droughts, high fluctuation of day-night and seasonal temperatures, land inundation in coastal areas, and loss of biodiversity. Secondly, drinking water is a rare resource on planet Earth and good quality drinking water is not distributed uniformly and is scarce in several countries. According to the World Health Organization (WHO), 80% of global diseases are related to water contamination. Globally, crop production is adversely affected by global warming and poor soil health. Thus, mitigation of GHG emission, remediation of contaminated water, and soil health management is extremely important for achieving the SDGs.

A vast range of remedial methods for these issues have been suggested by scientists worldwide. Biochar, ("*black carbon*") is a rich carbon source. It is derived from the heating of lignocellulosic biomass like plant and crop residues, municipal solid waste, algal biomass, etc. in the partial presence or absence of oxygen via pyrolysis. Application of biochar in agriculture can potentially mitigate the concentration of

* Corresponding author.
E-mail address: lucki.chem09@gmail.com (L. Singh).

https://doi.org/10.1016/j.rser.2021.111379
Received 31 July 2020; Received in revised form 12 June 2021; Accepted 14 June 2021
Available online 23 June 2021

Abbreviations

SDGs	sustainable development goals
GHGs	Greenhouse gases
N_2O	Nitrous oxide
CH_4	Methane
CO_2	Carbon dioxide
HM	Heavy metals
AD	Anaerobic digestion
MFCs	Microbial fuel cells
v/v	Volume per volume
g/g	gram per gram
g VS/L^{-day}	gram volatile solid per liter per day
m^2/g	meter square per gram
H_2S	hydrogen sulfide
MJ/Nm	Megajoule per newton meter
ppb	part per billion
MJ/kg	Megajoule per kilogram
g/L	gram per liter
mg/L	Milligram per liter
mW/m^2	Milliwatt per square meter
W/m^3	Watt per meter cube
Pt/C	Platinum/carbon
Mg ha^{-1}	Megagram per hectare; kg ha^{-1}, Kilogram per hectare
kg CH_4–C ha^{-1}	Kilogram methane-carbon per hectare
kg N_2O–N ha^{-1}	Kilogram nitrous oxide-nitrogen per hectare
g CH_4 m^{-2}	Gram methane per meter square
g N_2O m^{-2}	Gram nitrous oxide per meter square
kg C ha^{-1}	kilogram carbon per hectare
kg CO_2–C ha^{-1}	kilogram carbon dioxide-carbon per hectare
NH_4^+	Ammonium ion
NO_3^-	Nitrate
mg/g	Milligram per gram
mg/kg	Milligram per kilogram
Cd	Cadmium
Cu	Copper
Zn	Zinc
Cr	Chromium
Pb	Lead
Ni	Nickel
Ti	Thallium
As	Arsenic
ppm	art per million

potential GHGs such as CH_4, CO_2, and N_2O emissions from soils [1,2]. Biochar due to its slow degradation rate is the best available option for long-term carbon seizure in agricultural soils. Plants directly uptake atmospheric CO_2 and fix it in the form of plant biomass. Biochar produced from plant biomass has a significant amount of organic carbon and this carbon can be sequestered up to 2000 years mean residence time in soil via biochar application [3,4]. Biochar application to agricultural soils hinders the production and emissions of GHGs and thereby checks global warming. Further, biochar application improves soil health by enhancing soil porosity, soil moisture retention, enhances the nutrient supply capacity of soils, and thereby enhances the overall crop production. Besides this, it also removes heavy metals from soils [5]. Wastewater pollutants, such as pesticides [6], antibiotics [7], heavy metals (HMs) [8], dyes [9], and nutrients, can be efficiently and easily fixed through biochar application. Biochar has a high surface area which is helpful for the removal of water contaminants through various mechanisms such as sorption, pore filling, ion exchange, electrostatic interaction, etc. [10].

The versatile application of biochar for hydrosphere (wastewater contamination), lithosphere (soil health management), and atmosphere (GHGs mitigation) related problems has led to a growing global interest in its application to solve environmental issues. Scattered literature/information is available thus justifying its importance for the decontamination of wastewater, soil health management, and GHGs mitigations. However, an inclusive holistic review article discussing all these issues together and taking up the complete utilization of biochar in various environmental issues is presently lacking. To the best of our knowledge, a review article covering the role of biochar in energy (biogas, biological hydrogen, and ion-based batteries), climate change mitigation options (carbon sequestration and CH_4, and N_2O mitigation), and wastewater treatment has not been published yet. Therefore, this manuscript presents the potential applications of biochar pertaining to wastewater management, soil health management, mitigation of GHGs emission from soils, and carbon sequestration, so as to comprehensively present a mechanistic understanding of the same.

2. Techniques of biochar production

Pyrolysis, gasification, and torrefaction are the main thermochemical processes through which biomass is converted into valuable products such as biochar, biofuel, and syngas [11]. Biomass is decomposed into biochar at high temperature, and pressure, in the presence of negligible oxygen. The percentage of valuable products (biochar, biofuel, and biogas) formation is affected by the pyrolysis conditions (Fig. 1). In the following section, different biochar production technologies are described.

2.1. Pyrolysis

Pyrolysis (complex thermochemical process) involves thermal decomposition of biomass into biochar (carbon-rich), gases, and condensed liquids (bio-oils/biofuel). Pyrolysis is carried out in an oxygen-free environment at a high temperature ranging between 300 and 1000 °C. This oxygen-free environment prevents the combustion of biomass and allows heating above the limit of thermal stability. The composition of biochar, gases, and bio-oil products varies depending

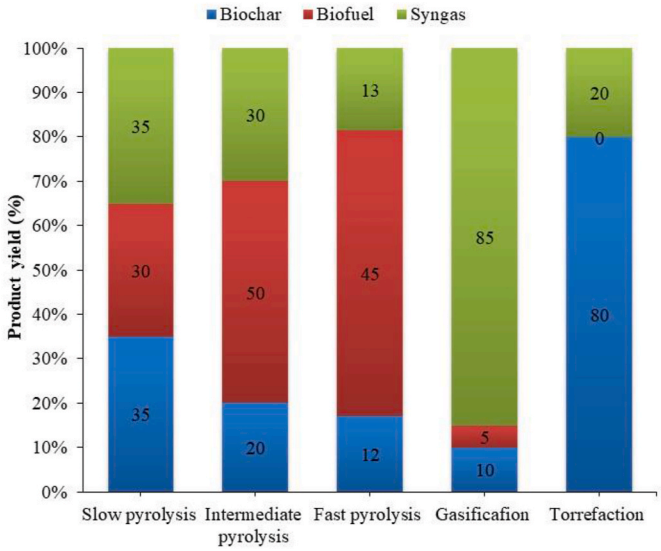

Fig. 1. The production of biochar, bio-oil, and gases obtained from different pyrolysis techniques (Data from Qambrani et al. [11] and Roy and Dias, [12]).

upon feedstock, temperature, residence time, heating rate, etc. (Fig. 1). The solid product of pyrolysis is carbon (C) rich, but is not pure C. Rather, it is a mixture of C, oxygen (O), nitrogen (N), calcium (Ca), sulfur (S), and other elements depending on the composition of the biomass employed for the formation of biochar [13]. Further, pyrolysis is classified as slow and fast depending on the basis of temperature, pressure, residence time, and heating rate. The yield of major products of slow and fast pyrolysis vary, thus resulting in the production of biochar and bio-oil as major products, respectively [12].

2.1.1. Slow pyrolysis

Slow pyrolysis is a conventional method of producing biochar (BC) from biomass. Under slow pyrolysis process, biomass is heated for a longer residence time (ranging from min to hours) at a low temperature as compared to fast pyrolysis. The heating rate ranges from 0.1 to 0.8 °C per second or less than 50 °C per min [12]. Again, the production of BC and bio-oil depend upon the feedstock properties, heating rate and processing temperature, and gaseous environment of pyrolysis. BC yield gets reduced with the amplifying pyrolysis temperature (Fig. 1), and residence time. It has been found that the rate of BC production at a low heating rate is higher as compared to a high heating rate in the pyrolysis process [14]. Angin [14] reported that at 400 °C, the biochar yield got reduced from 34.18 to 29.70% on increasing the rate of heating from 10 °C/min to 50 °C/min. Hossain et al. [15] reported that biochar production from wastewater sludge feedstock reduced from 72.3% of original feedstock to 52.4% on raising the temperature of pyrolysis from 300 °C to 700 °C. The study conducted by Angin [14] and Hossain et al. [15] clearly indicate that the yield of biochar decreased with the increase in the temperature of pyrolysis and the highest biochar yield can the achieved with slow pyrolysis. In slow pyrolysis, almost 50% of feedstock carbon is stored in a stable form in the biochar [16].

2.1.2. Intermediate pyrolysis

The amount of biochar produced through slow pyrolysis is relatively higher than biochar production through fast, and intermediate pyrolysis. Intermediate pyrolysis is usually followed to obtain a balanced concentration of different pyrolysis products such as biochar, biofuel, and syngas (Fig. 1). Operating conditions such as heating temperature (500–600 °C), residence time (300–1000 s), etc., lie between fast and slow pyrolysis [17]. Concentration of by-products generated during intermediate pyrolysis was reported to be 15–25% of biochar, 20–30% of syngas, and 40–60% of biofuel [17,18]. However, Ahmed et al. [19] observed a higher content of biochar (38.78%) on intermediate pyrolysis (temperature-500 °C, and heat rate-25 °C/min) of *Acacia holosericea* and *Accacia cincinnata* species. The production of biochar from agro-residues and woody biomass under intermediate pyrolysis (temperature-500 °C) ranged from 27.5 to 40% of total pyrolysis product [20]. Yakub Mohammed et al. [21] also investigated the intermediate pyrolysis of Napier grass and observed 20.06% of biochar yield at 600 °C temperature with a heating rate of 50 °C/min.

2.1.3. Fast pyrolysis

Heating of feedstocks above 500 °C/min for less than 2 s of vapor residence time in the absence of oxygen is known as fast pyrolysis [22]. Under such operating conditions, mostly vapors (bio-oil) are produced with some amount of charcoal (Fig. 1). Fast pyrolysis is an advanced process to obtain a high yield of bio-oil, and a low amount of biochar and gases. Usually, in fast pyrolysis, peak temperature is maintained in the range 500–550 °C to produce high bio-oil [22]. The major product of fast pyrolysis i.e. bio-oil is miscible in water (~20–25 wt %) and polar organics (~75–80 wt %) [23]. Fast pyrolysis is preferred over slow and intermediate to prevent the polymerization of intermediates, secondary cracking, and condensation during the process [24]. One of the crucial factors that affect the process of fast pyrolysis is particle size and it is recommended to reduce the feedstock particle size to less than one mm. In pyrolysis reactors, the feedstock is heated rapidly to decompose the biomass into gases and short-chain molecules. The gases produced are cooled down to form bio-oil. The fraction of gases that do not condense is used as fuel gases in the process of reheating the pyrolysis reactors [25]. The desired product of fast pyrolysis is mainly bio-oil (40–70%), but biochar (10–25%) and gaseous products (20–40%) are also obtained in the process.

2.2. Gasification

In gasification (thermochemical process), small size carbonaceous feedstock (<5 mm) is heated (>650 °C) in a partially oxidative atmosphere under controlled air (gasification agent) supply by air/steam-air/CO_2/steam/steam-oxygen/steam-air. The products generated during gasification include syngas/synthetic gas/producer gas (low down heating of 3.5–10.0 MJ Nm^{3-}), and small amounts of ash, char, and tar [22,26]. The fraction percentage of the by-products generated during gasification depends on the moisture percentage and biomass composition of the feedstock [27]. The burn-off percentage (30–55%) and activation temperature (700–850 °C) are important parameters for syngas production. The gasification process occurs in three phases (1) endothermic pyrolysis-heat converts biomass into volatile matter and char (methanol, steam, tars, and acetic acids), (2) exothermic process-oxidation of carbon into CO_2 (3) reduction of volatiles, steam, and some CO_2 into CO, H_2 and CH_4 which is further diluted with the N_2 present in the air and unreduced CO_2. The syngas chiefly consists of CO_2, CO, H_2, and hydrocarbons [28]. The syngas produced during gasification can be used as a direct source of energy in gas turbines or boilers, or gas engine after some purification or converted into high-quality chemical/fuel products such as H_2, CH_4, C_2H_5OH, and CH_4OH [28]. Biochar production from gasification is significantly lower than slow pyrolysis (Fig. 1) due to high operating temperature conditions. Based on the feedstock composition, metals, minerals, and ash content may differ in charcoal. Gasification can also be used to improve the textural properties of charcoal produced during pyrolysis process and the production of activated carbon for adsorption and catalytic uses.

2.3. Torrefaction

Torrefaction is a thermal decomposition and biomass treatment process that produces biochar from the biomass/waste feedstock in an inert atmosphere at 1 atmosphere pressure. Torrefaction decreases the volatiles and water content from biomass thus improveing fuel properties in terms of higher energy density, elimination of biological activity, hydrophobic behaviour, easier grindability, and homogeneous composition, etc. [29]. Torrefaction efficiency mainly depends on temperature (200–300 °C) and retention time (15–60 min). Torrefaction feedstocks are lignocellulosic (crop residue, chips, wood pellets, and tree bark, etc.), organic non-lignocellulosic (cattle manure, paper sludge, poultry waste, olive mill waste, and bagasse, etc.), and other feedstocks including sewage sludge, digestate from biogas plants, food waste, and spacecraft solid wastes consisting of low/or no lignocellulose content. In torrefaction, the lignocellulosic compounds (cellulose, hemicellulose, and lignin) are degradation products in which removal of CO_2 and H_2O takes place, thus reducing O and H and in turn increasing C contents in the remaining torrefied residue. Cellulose and lignin degradation depends on the torrefaction temperature [30]. The torrefied biomass contains initial mass (60–70%) and low heating value (90%). Torrefaction biochar has a high energy density (potential energy - 80–90%) and a further 30% can be increased through decreasing biochar mass up to 70–80% [31]. Torrefied biochar is a hydrophobic reducing agent with increased fixed carbon content (25–40%) and reduced oxygen and O/C ratio making it an attractive substrate for incineration, co-combustion, and gasification [32].

3. Biochar and bioenergy

Biochar has a significant role to play in energy perspectives. It can be utilized either as a feedstock for biogas production [33,34] or can be utilized for biogas enrichment (for the removal of impurities from biogas) [35,36]. Other than biogas production and purification, it can be utilized for biological hydrogen production or for enhancing bioenergy production in microbial fuel cells. Also, it can be utilized in ion batteries. The application of biochar in each of these sectors is described in the section below.

3.1. Role of biochar in biogas production

The decomposition of organic matter in an anaerobic environment produces biofuel known as biogas which is a mixture of CH_4 (40–65% v/v), CO_2 (35–55% v/v), hydrogen sulfide (H_2S) (0.1–3% v/v), moisture and other trace gases [37]. Anaerobic digestion (AD) is a multiple-stage complex process which is affected by temperature, pH, feedstock composition (C/N ratio), hydraulic retention time, and organic loading rate [38,39]. To achieve the optimum C/N (20:1–30:1) required for biogas production, feedstocks are often co-digested or specific amendments are added [37,40]. Biochar along with other organic matter can be used as an amendment in AD for the enhancement of biogas production [33,34]. C/N ratio of substrate and pH of AD significantly affect biogas production [41]. Zhao et al. [42] investigated the effect of pH on methanogenesis, hydrolysis, and acidogenesis in AD and reported that pH 8 is suitable for all three processes in AD. Addition of highly biodegradable substrates having a low C/N ratio reduces process pH and thus leads to acidogenenic processes.

Acidogenesis suppresses the activity of methanogenic (CH_4 producing) bacteria and results in lower biogas production. Under the acidic environment of AD, the methanogenesis recovery takes a long time. However, the application of biochar balances the C/N ratio as well as pH thus resulting in quick restoration of the methanogenesis process [41]. Cerón-Vivas et al. [40] investigated the influence of substrate C/N ratio on CH_4 production in AD and observed the highest CH_4 production at a 14.2 balanced C/N ratio. Higher and lower C/N ratio also plays a negative role and inhibits CH_4 production in AD. Higher C/N ratio

Table 1
Role of biochar in biogas (biological methane) and biological hydrogen production.

Reference	Organic matter/substrate used	Duration of experiments	Biochar feedstock	Increase in Methane/ hydrogen production (%)	Remarks
Biogas					
Sánchez et al. [60]	Swine waste	8 days	Wheat and corn straw	25–37%	Biochar supplies several trace metals to the methanogenesis process.
Sugiarto et al. [61]	Food wastes	40 days	Pine sawdust	33.2–46.9%	Biochar is leached with Fe and it enhances CH_4 production.
Sharma and Suthar, [44]	Water hyacinth	35 days	Cow dung	40.6–57.6%	In this study, three level of biochar doses (v/v) (0.5%, 1.0% and 1.5%) were used.
Qin et al. [49]	Sludge of kitchen waste	25 days	Bamboo Corn stalk Oak Wood Pine wood Apple wood Rice straw	2.13% −2.82%* 11.95% 10.18% 15.36% 1.18%	Biochar was synthesized at 500 °C. Incubation experiment was conducted at 35 °C. *Note: Negative sign indicates a decrease in CH_4 production over control (without biochar).
Wei et al. [45]	Primary sludge	116 days	Corn stover	Up to 17.8%	Incubation experiment conducted at 55 ± 1 °C.
Pan et al. [47]	Chicken manure	72 days	Fruitwood	69%	Biochar was produced at 550 °C. Anaerobic digestion was conducted at 35 ± 1 °C
Wang et al. [50]	Sludge + food waste (4:1)	55 days	Sawdust	22.4–40.3%	Pyrolysis temperature for biochar production was 500 °C.
Sunyoto et al. [48]	Aqueous carbohydrates	39 days	Pine sawdust	10–41%	Aqueous carbohydrate culture with biochar was incubated at pH 7 at 35 °C. Biochar was produced at 650 °C.
Biological hydrogen					
Li et al. [62]	Clostridial growth medium	40–60 h.	Rice straw	79.6–118.4%	Biochar was produced at 700 °C pyrolysis temperature.
Sugiarto et al. [63]	Food waste	6 days	Pinewood	45–54%	Leached biochar was used in this study.
Zhao et al. [64]	Cow dung compost	30 h.	Cornstalk	7–69%	Biochar was prepared from cornstalk residue after pretreatment and hydrolysis.
Yang and Wang [65]	Grass biomass (*Lolium perenne* L)	48 h.	Sawdust	89.8%	Biochar was produced at 500 °C pyrolysis temperature
Wang et al. [66]	Dewater activated sludge and food waste (1:4 ratio)	7 days	SD300 SD500 SD700 SS300 SS500 SS700 PS300 PS500 PS700 WB300 WB500 WB700	27.89% 32.66% 110.05% 109.80% 60.80% 63.82% 57.29% 18.59% 70.35% 31.41% 64.32% 61.81%	SD-Sawdust; SS-Sewage sludge; PS-peanut shell; WB-wheat bran. Biochar was produced at 300 °C, 500 °C, and 700 °C pyrolysis temperature.
Zhang et al. [67]	Glucose	27 h.	Corn-bran residues	48.35%	Biochar was produced at 600 °C.
Sharma and Melkania [68]	Municipal solid waste	12 h.	Woody mass	44.59–76.65%	15 batch experiments using 100% organic biochar produced at 400–500 °C pyrolysis was used.
Sunyoto et al. [48]	Aqueous carbohydrates	08 days	Pine sawdust	31–36%	Aqueous carbohydrate culture with biochar was incubated at pH 5 at 35 °C. Biochar was produced at 650 °C.

provides optimum nitrogen to methanogenic bacteria enough for its protein demand, and at lower C/N ratio, nitrogen is present in ammonia form which suppresses the activity of methanogenic bacteria [40,43]. Recently, Sharma and Suthar [44], observed that the addition of biochar at the rate of 1.0%(v/v) reduced the C/N ratio of AD setup from 21.80 to 14.28 which simultaneously enhanced biogas production by 57.6% over non-biochar treatment (Table 1).

Balanced biochar addition in AD is a feasible option for maintaining an optimum C/N ratio. Shen et al. [34] found that the addition of corn stover feedstock biochar in AD increased CH_4 production rate and biogas CH_4 percentage got enhanced by 37% and 25% respectively, over control. Addition of corn stover biochar (1.82, 2.55, and 3.06 g/g total solid) into the primary sludge feedstock in AD enhanced CH_4 production from 67.5% to 81.3–87.3% [45]. Addition of biochar increased the hydrolysis of primary sludge along with conductivity, buffering capacity, and alleviated ammonia inhibition resulting in higher CH_4 production (Fig. 2) [45,46]. Giwa et al. [46] used both commercial biochar and local biochar in the anaerobic digester with high organic load (6.0 g VS/L^{-day}) in a long-run (365 days) experiment and observed a 5% higher CH_4 production over the control (Table 1). In the laboratory AD batch experiment, Pan et al. [47] biochar derived from air-dried chicken manure, fruitwood, and wheat straw, and observed that CH_4 production improved by 69% with fruitwood biochar (Table 1).

The addition of biochar in two-phase digestion of liquid carbohydrates (obtained from food waste) at 35 °C pH 7 for 39 days enhanced CH_4 yield from 10 to 41% over control [48]. In another study, Sunyoto et al. [48] found that the addition of biochar in the AD system stimulated the methanogenic population which boosted CH_4 yield over control. Physicochemical properties of biochar such as electron donor capacity and specific surface area play an important role in improving biogas production yield [49]. Qin et al. [49] investigated the effect of adding biochar produced from seven different feedstocks of corn stalk, rice straw, applewood, oak wood, bamboo, and pinewood on AD process. The properties of biochar differed in the surface area ranging from 77.14 to 253.39 m^2/g. The addition of woody biochar (oak, bamboo, and pinewood) enhanced CH_4 production from 10.18 to 15.35% over no biochar although no significant difference in CH_4 yield was observed among woody biochar (Table 1). The highest increase in CH_4 production was observed with the addition of applewood biochar may be due to higher C content and lower ammonia formation in AD (Table 1).

Biochar addition in AD is also known to shorten the lag phase of biogas formation [50]. A study of Wang et al. [50], found that addition of sawdust biochar to food waste and sludge in AD reduced the lag phase time from 27.5 to 64.4% and improved CH_4 production from 22.4 to 40.3% over conventional operation and AD without sawdust biochar, respectively. Biochar amendment in AD has a great potential for maximizing the biogas recovery with several other benefits such as sludge reduction, sludge nutrient enhancements and pH buffering.

The addition of biochar to AD also promotes the direct interspecies electron transfer (DIET) and sustains the methanogenic population [51,52]. Wang et al. [52] investigated the effect of biochar addition in up-flow anaerobic sludge blanket reactor and reported that the addition of biochar maintains the balance between acidogenesis and methanogenesis. High loading shock without biochar reduced biogas production while biogas production is rapidly restored in high organic loading with biochar. The addition of biochar helps in balancing the C/N ratio, buffering capacity, moisture content, pH, methanogenic population, shortening lag phase, etc., which in combination improve the overall biogas production efficiency of AD.

3.2. Role of biochar in biogas enrichment

Biogas enrichment involves the removal of CO_2 and other impurities (H_2S and other trace gases) from biogas for increasing its energy efficiency and application as a vehicular fuel. This process increases the methane content to more than 90%. Consequently, the enriched biogas has an approximate heating value of 35.8 MJ/Nm^3 which is comparable to natural gas [39]. Conventional biogas enrichment technologies such as pressure swing adsorption, membrane separation, and water scrubbing suffer the drawback of high operating costs ranging between \$0.15–0.4/Nm^3 of biogas [53]. Comparatively, biological enrichment technologies are more cost-efficient and easier to operate [35]. Biochar-based biogas enrichment can be done either *in-situ* wherein the biochar is added to an anaerobic digester serving a dual purpose of enhancing biogas production as well as adsorption of impurities or *ex-situ* where the biogas produced is allowed to pass through a column packed with biochar for effective adsorption of the impurities. In-situ enrichment has the advantage of cost-reduction but suffers from various technological challenges such as increased pH and gas–liquid mass transfer of H_2 [54]. However, studies have reported that biochar is highly efficient in *in-situ* biogas enrichment resulting in the production of biomethane with >90% purity and <5 ppb of H_2S [55].

Shen et al. [56]utilized biochar derived from corn stover during *in situ* biogas enrichment for removal of CO_2 and H_2S from biogas and reported high adsorption efficiency of the biochar resulting in >95% methane content. The CO_2 removal efficiency was found to vary

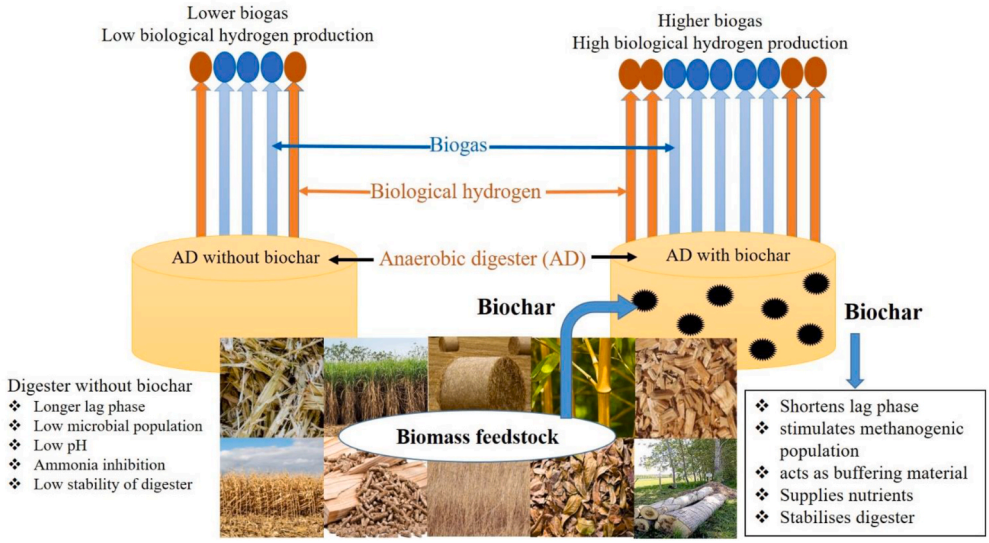

Fig. 2. Impact of biochar on biogas and biological hydrogen production in anaerobic digestion.

between 54.9 and 86.3% based on the dosage of biochar. The *in-situ* removal of CO_2 was attributed to the micropores existing in biochar, higher surface area, electrostatic interaction, and polarity attraction. With the increase in biochar dose, an increase in methane content and substrate degradation was observed. However, at a higher dose, process inhibition was observed, which was attributed to high concentrations of alkali-metal beyond the acceptable limits thus leading to cation toxicity. Under thermophilic conditions, the cationic toxicity was observed to be lower as compared to mesophilic conditions as efficient hydrolysis and microbial activity occur prior to cation release [57].

Biochar has also been utilized for the adsorption of biogas impurities under *ex-situ* conditions. Sahota et al. [58], utilized leaf waste biochar for ex-situ biogas cleaning and observed that biochar synthesized at different temperatures (200, 300, and 400 °C) varied in their H_2S adsorption efficiency. Biochar produced at 400 °C showed highest H_2S removal efficiency of 84.2%. This was attributed to the fact that higher carbonization temperature results in the generation of a greater number of micro-/meso-pores resulting in increased pore volume and surface area leading to increased H_2S removal. The pH of biochar was also found to be an important parameter influencing H_2S adsorption. With the increase in carbonization temperature, biochar pH was found to increase due to the formation of alkaline species. Further, lowest H/C ratio in the biochar prepared at 400 °C resulted in low hydrophilicity due to which an increase in H_2S adsorption was observed. Kanjanrong et al. [59], applied biochar produced from woodchips and AD residue for ex-situ elimination of H_2S from biogas. An efficiency of >90% removal of H_2S from biogas was reported, which the authors attributed to the alkaline nature of biochar and high humidity of inlet H_2S gas from the reactor. Fourier Transform Infrared (FTIR) spectroscopy provided evidence for the existence of carboxylic and hydroxide radical groups on biochar surface which were probably responsible for the adsorption of H_2S. The authors also suggested that this sulfur-laden biochar can be used as an amendment to soils deficient in sulfur.

3.3. Role of biochar in biological hydrogen production

Hydrogen is considered as the future fuel due to its high energy density and wide availability. The gravimetric energy of hydrogen (120) is 2.70 times higher than gasoline (44.5 MJ/kg) [69]. Hydrogen can also be produced from biomass and organic waste through microbial photosynthesis and AD. During fermentation (AD), biomass and organic matter undergo microbial decomposition and result in hydrogen production. The role of biochar in biological hydrogen production is significant in terms of energy and environment. The addition of biochar in organic matter prevents ammonia inhibition, acid formation and acts as a pH buffer which enriches microorganism biofilm formation (Fig. 2) [65,68]. The biofilm formation in AD has a positive correlation with hydrogen production. Biochar reduces the lag time in AD by maintaining the stability of the medium via buffering capacity and results in higher hydrogen production as compared to the organic matter without biochar amendment [48].

The addition of organic biochar (12.5 g/L) produced from woody biomass at a pyrolysis temperature of 400–500 °C to municipal solid waste reduced the lag phase from 12.5 ± 0.6 h to 8.1 ± 0.5 h and resulted in 44.59–76.65% higher hydrogen production over control (Table 1). Sunyoto et al. [48] also observed that addition of biochar shortened the lag phase of AD and improved hydrogen production by 31–36% as compared to the control. Hydrogen production from grass fermentation got enhanced by 89.8% with the addition of biochar (600 mg/L) combined with zero-valent iron nanoparticles (400 mg/L) [65] (Table 1). Biochar with zero-valent iron nanoparticles shortened the lag time and enhanced the microbial population of *Clostridium* species which efficiently degraded the biomass and resulted in higher hydrogen production [65]. The role of iron with biochar in boosting hydrogen production in AD has also been reported by Zhang et al. [67]. It was reported that biochar with ferrous iron in a 3:1 ratio has synergistic effects on hydrogen production (Table 1). Recently, Li et al. [62] studied the effect of adding different concentrations of biochar on ethanol and butyrate-type fermentation. The hydrogen production in ethanol and butyrate-type fermentation with biochar addition at 0, 3, 6, 9, and 12 g/L concentrations was 57.64, 125.87, 122.62, 122.69, and 117.54 mL, respectively [62]. The biochar dosage of 3 g/L was observed to be most favorable for both butyrate and ethanol fermentative hydrogen productions. The highest increase in hydrogen production in butyrate and ethanol fermentation was 79.6% and 118.4%, respectively (Table 1) due to buffering and continuous nutrient releasing capacity of biochar.

Wang et al. [66] explored different biochar types, produced from four different feedstocks namely sawdust, sewage sludge, peanut shell, and wheat bran at three different pyrolysis temperatures (300 °C, 500 °C, and 700 °C), for the biological hydrogen production using the same substrate of dewatered activated sludge and food waste (4:1 ratio) (Table 1). The authors reported that the hydrogen production from control was 39.8 mL/day. With the addition of 10 g/L biochar, the hydrogen production increased by 27.89–110.05%, 60.80–109.80%, 18.59–70.35%, and 31.41–64.32% over control by adding biochar obtained from sawdust, sewage sludge, peanut shell, and wheat bran, respectively (Table 1). The biochar produced from sewage sludge although had low surface area and high ash content but promoted the H_2 production by maintaining pH through buffering capacity potential [66].

Biochar leaching reduced the mineral content (Fe, Ca, and K) of biochar with no significant change in hydrogen, carbon, and nitrogen content. Sugiarto et al. [63] investigated the effect of the leached biochar and unleached biochar on hydrogen production in mesophilic AD and observed that the addition of unleached biochar significantly increased the hydrogen production rate up to 54% over control (Table 1). The addition of leached biochar in AD resulted in lower hydrogen production in comparison to unleached biochar treatment which indicates that the leached fraction constitue the mineral content in biochar and plays a crucial role in promoting hydrogen production [63]. Addition of biochar d from cornstalk residue after pretreatment and hydrolysis at the rate of 15 g/L to cow dung feedstock in AD enhanced biological hydrogen production from 2264 mL/L to 3990 mL/L (Table 1). Zhao et al. [70] reported that the residue of the AD system can also be pyrolyzed to biochar and biological hydrogen can be produced from this biochar. Mineral content such as Fe, Ca, Na, K, etc., present in biochar makes it an ideal catalyst for biological hydrogen production and biochar production cost make it economically viable [63,71,72]. Therefore, it can be concluded that biochar can play a significant role in the biological hydrogen production process and will have an unprecedented impact in the area of green energy.

3.4. Role of biochar in microbial fuel cells

Microbial fuel cells (MFCs) are an emerging technology that deals with the bioremediation of inorganic, organic contaminations, nutrients, heavy metals, etc. along with bioenergy generation through the action of exoelectrogenic microorganisms [73–75]. The rate of biodegradation of contaminants and bioenergy is affected by several factors such as MFCs architecture (anode, cathode, proton exchange membrane), and operating conditions, etc. Generally, MFCs consist of electrodes (cathode and anode) separated by a proton exchange membrane (Fig. 3). In MFCs the bioenergy generated is harnessed by connecting an external load between anode and cathodes. The biodegradation of organic contaminants/nutrients liberates electrons and protons and the transfer of these electrons from anode to cathode in MFCs generates bioenergy. The terminal electron acceptor, such as hexacyanoferrate or oxygen consumes electrons and protons at the cathode by reduction.

Electrodes affect the MFCs in term of performances (energy generation/biodegradation) as well as economics (fabrication/production cost). Huggins et al. [76] quoted only electrode material can contribute up to 20–50% of the total fabrication cost of MFCs. To have optimum

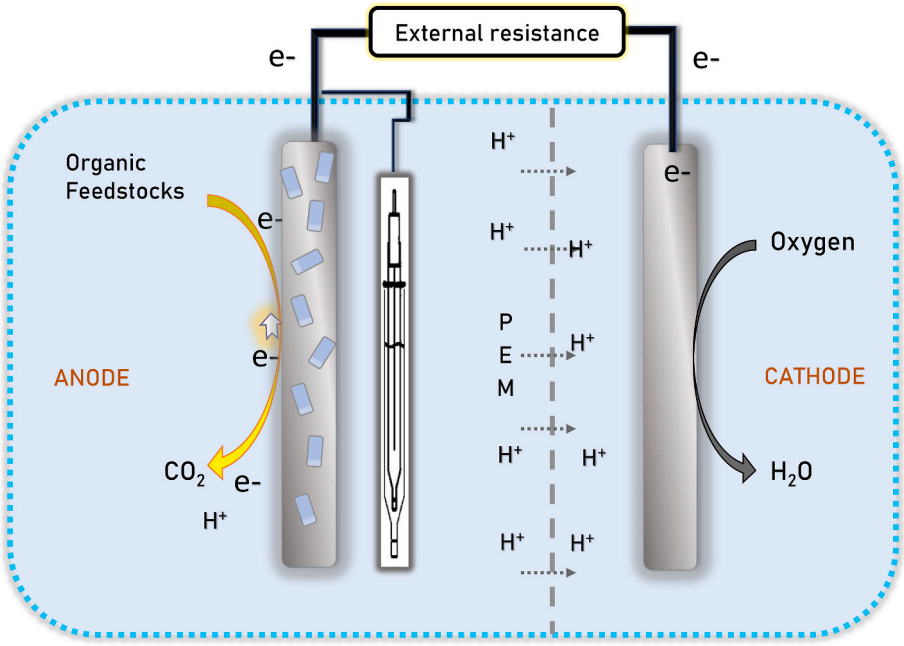

Fig. 3. Schematic illustration of a dual-chamber microbial fuel cell.

performance an ideal electrode should have a higher surface area, stability, biocompatibility, and conductivity [76]. Both in terms of cost and performance, the application of biochar as electrodes in MFCs has abundant scope.

Huggins et al. [76] experimentally investigated the role of wood-based biochar as electrodes in MFCs. Two types of biochar were produced from compressed milling residue, and forestry residue feedstocks that showed power outputs of 457 mWm^{-2}, and 532 mWm^{-2}, respectively [76]. Biochar has also been employed for the fabrication of air cathode in MFCs as reported by Chang et al. [77]. It was observed that air cathode fabricated from Balsa wood chip at 800 °C successfully achieved power density up to 200 mW/m^2 in single-chamber MFCs. The porous nature and high oxygen reduction reaction enhanced the power density of the biochar air cathode [77]. The thickness of biochar cathode also significantly affected the power density of the soil MFCs. Chang et al. [77] observed a power density of 72 mW/m^2 with 3.5 mm biochar which was 45% higher than the power density obtained with the common carbon felt floating anode used in soil MFCs. Huggins et al. [78] firstly reported that biochar can be potentially used as anode and cathode material in open circuit MFCs and they found peak power density of 6 W/m^3. Biochar produced from water hyacinth (*Eichhornia crassipes*) at 900 °C pyrolysis temperature was reported to have high oxygen reduction catalytic activity and therefore it is suggested to be used as an inexpensive electro-catalyst in place of Pt/C catalyst [79]. Allam et al. [79] observed a maximum power density of 12.3 mW/m^2 and 24.7 mW/m^2 with water hyacinth biochar and Pt/C catalyst respectively, in air cathode single-chamber MFCs. Although, the power generation from water hyacinth biochar air cathode was approximately half as compared to the power generation from Pt/C catalyst in single-chamber MFCs, this finding opens the way for replacing metal-based catalysts such as Pt/C with an economic and environmentally friendly catalyst such as water hyacinth biochar [79]. Li et al. [80] also found that biochar produced from corncob can also be used as catalysts in air cathode MFCs.

The biochar produced from corncob feedstock at 650 °C consisting of 655.89 m^2/g electrochemical active area achieved 458.85 mW/m^3 and 0.221 V of maximum power density and output voltage respectively, in air cathode MFCs [80]. Recently, Zhang et al. [81] reported that N doping in biochar extensively improved the oxygen reduction catalyst role of biochar by increasing specific surface area (by 5 times), porosity, and electrical conductivity. The maximum power density of 907.2 mW/m^2 was achieved with N-doped biochar in MFCs which was slightly lower than the power density (1022.9 mW/m^2) of expensive Pt/C catalyst [81]. Biochar can also improve the power generation in sediment MFCs effectively. In a laboratory scale experiment in sediment-MFCs, Chen et al. [82] added coconut biochar at the rate of 10% of the dry weight of sediment and found a 2 to 10 times increase in power generation over no biochar experimental setup. Based on the above discussion, it can be concluded that biochar application as anode, cathode, and catalyst has a significant effect on bio-energy generation and cost-reducing in MFC technology.

3.5. Role of biochar in lithium-sodium ions batteries

The depletion rate of oil, gas, coal, and other non-renewable resources is upsurging with the human population explosion. The majority of non-renewable energy resources are used in industrial activity and vehicles. Currently, the application of power-storing devices such as lithium/sodium batteries in many types of vehicles and portable devices has gained global desirability. Rechargeable ions (sodium/lithium) batteries have higher power, energy density, and higher energy efficiency storage options with long service life [83,84]. In this battery, ions move from anode to cathode through an electrolyte during discharging cycle and vice-verse flow during the charging cycle. The efficiency of electrodes plays a significant role in the overall performance of the ion batteries. A larger surface is not considered appropriate for ion (lithium/sodium/silicon) batteries due to safety purposes. Biochar is an economically feasible and sustainable material with a high specific capacity which enhances its application as an electrode in ion batteries [85].

Activation via KOH/annealing process led to enhanced electronic conductivity and increased microspores structure of the biochar [85]. Application of such activated biochar as cathode in lithium-sulfur battery resulted in high retention capacity (1295 mA h/g) with more than 95% coulombic efficiency [85]. Rios et al. [86], elucidated the feasibility of using biochar obtained from different woody feedstocks such as resinous wood (pine), deciduous wood (ash wood), wheat straw, and miscanthus as anode in sodium-ion batteries. The coulombic efficiency

of Pine, Ashwood, wheat straw, and miscanthus biochar based electrodes in sodium-ion batteries were 85%, 79%, 65%, and 80%, respectively [86]. The lowest coulombic efficiency with wheat straw biochar was related to its high surface area as compared to others [86]. High surface area promotes the consumption of electrolyte species in form of solid electrolyte interphase due to degradation of electrolyte which results in lower coulombic efficiency [86]. Biochar doped with iron further improves its carbon content and the utilization of magnetic biochar as an electrode in lithium-ion batteries showed higher initial specific discharge capacity over unmagnified biochar electrodes [87]. Based on the above discussion, it can be summarized that biochar application as electrodes in ion-based batteries has great feasibility due to its sustainable and cost-effective production method.

4. Role of biochar in GHGs mitigation from agricultural soils

CH_4, N_2O, and CO_2 are the three main GHGs emitted from agricultural soils. Biochar has a great potential in the mitigation of GHGs emissions from agricultural soils and thereby in mitigating global warming [88]. Several strategies such as management of nitrogenous fertilizers, irrigation water management, management of organic matter, tillage management, and cultivar selection were commonly adopted for the mitigation of GHGs from soils. Recently, the potential of biochar to mitigate GHG emissions from agricultural soils was also studied. The CH_4 and N_2O emission mitigation from biochar amended soils are discussed herewith.

4.1. Methane mitigation

CH_4 contributes 16% to the total anthropogenic global warming [89]. Agricultural soils contribute around 15–30% of total CH_4 emission and the majority, i.e. 12% of it, occurs from paddy cultivation [90,91]. Rice cultivation is 2nd most significant source of CH_4 emission after livestock. Therefore, most of the CH_4 mitigation strategies have been focused on mitigation from the paddy fields. These strategies are water management (alternate wetting and drying, midseason drying, system of rice intensification), direct-seeded rice, and use of *Azolla-based* biofertilizers, etc. [92,93]. In the rice ecosystem, flooded water generates anaerobic environment, which stimulates the growth of methanogenic microbes. These methanogens consume soil organic carbon (SOC) and emit CH_4 gas as a byproduct during the methanogenesis process [94,95]. Usually, the organic matter added to the rice soils significantly enhances CH_4 emission [96,97]. However, soil amended with biochar as organic matter shows a negative correlation with CH_4 emission and mitigates the overall concentration [98–100].

CH_4 emission from any soil is a resultant of two processes viz. methanogenesis (anaerobic condition) and methanotrophy (aerobic condition). CH_4 mitigation can be carried out either by enhanced activity of methanotrophic bacteria or inhibition of methanogenic activity. Biochar stimulates the growth of type-I and type-II methanotrophs and thereby enhances the CH_4 consumption and reduces the net CH_4 emissions [101,102]. Soil may act as a source or sink depending upon the biotic and abiotic factors. Application of biochar in soil also reduces NH_4^+ content by adsorption. NH_4^+ inhibition in turn enhances CH_4 oxidation consequently resulting in lower CH_4 flux from soil (Fig. 4). Moreover, higher NH_4^+ content in soil suppresses the activity of methane monooxygenase (MMO) enzyme. MMO is the first enzyme required for CH_4 oxidation in the methanotrophic pathway. On the other hand, biochar addition to soil reduces soil density, enhanced aeration, and acts as soil buffer which likely suppresses methanogens and stimulates methanotrophic bacteria [102]. Ameding the soil with 2% and 4% (w/w soil) rice husk biochar resulted in a significant reduction of 45.2 and 54.9% in CH_4 emission [103]. This CH_4 emission reduction under biochar amended soils was attributed to increased activity of methanotrophic bacteria controlled by the methanotrophic pmoA gene [104]. Ly et al. [105], investigated the influence of rice straw and biochar on CH_4 emission in rice and reported 29% lower CH_4 emission from the soil amended with biochar as compared to rice straw. This higher CH_4 emission from rice straw amended soil was mainly due to higher labile carbon content [105]. Sriphirom et al. [99] studied the effect of mangrove (*Rhizophora apiculata*) biochar alone and with compost application on CH_4 emission and found that CH_4 emission was reduced by 40.57% and 29.5%, respectively in comparison to the respective control (Table 2).

Wu et al. [106] studied the impact of biochar in a six-year field experiment with rice-wheat and recommended that biochar incorporation at the rate of 20 and 40 Mg ha^{-1} with 250 kg N ha^{-1} significantly reduced the CH_4 emission by 11.19%, and 17.45%, respectively over the

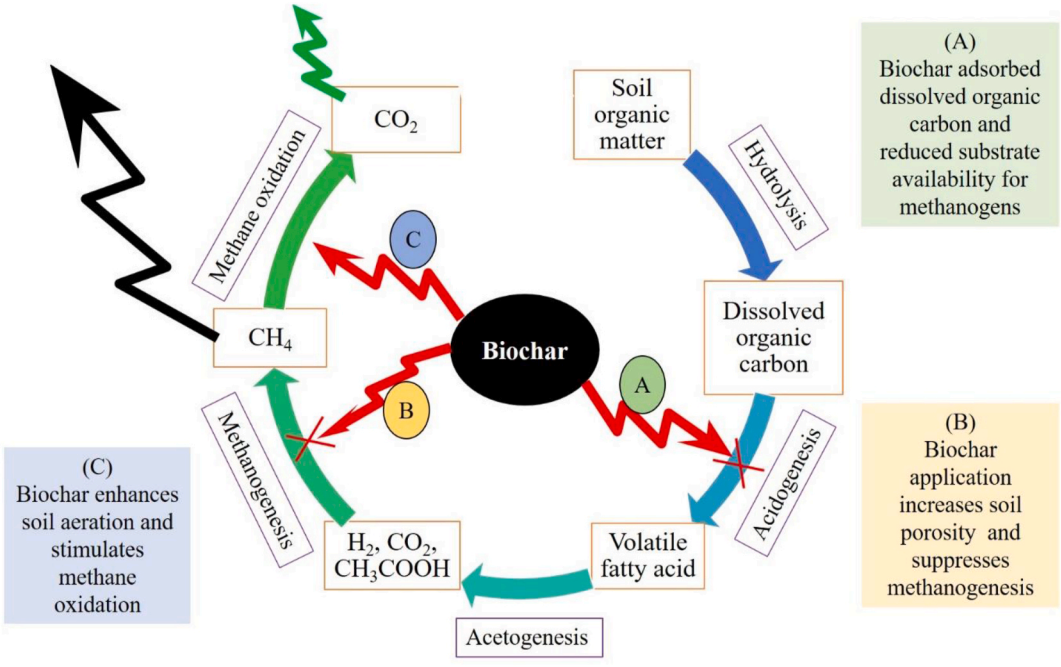

Fig. 4. Mechanism involved in methane mitigation in terrestrial/agricultural soils under biochar amendment.

Table 2
Influence of biochar addition to agricultural soil on methane and nitrous oxide emission.

Reference & study location	Treatments details (Mg ha^{-1})	CH_4 emission kg ha^{-1} (% mitigation)	N_2O emission kg ha^{-1} (% mitigation)	CO_2 emission kg h^{-1} (% mitigation)	Remarks
Rice					
Sriphirom et al. [99], Thailand	Biochar (0)	244 (control)	–	–	Biochar was produced from mangrove (*Rhizophora apiculata*) feedstock through slow pyrolysis.
	Biochar (10)	145 (40.57)	–	–	
	Biochar (10) + Compost (1.5)	172 (29.51)	–	–	
Yang et al. [2], China	Biochar (0)	114.8 (control)	4.84 (control)	–	Biochar was produced from rice straw through pyrolysis at 600 °C temperature.
	Biochar (20)	80.55 (29.83)	5.27 (−8.89)	–	
	Biochar (40)	100.4 (12.54)	3.58 (26.06)	–	
Shao et al. [112], China	Control (0)	16.28 (control)	5.86 (control)	–	*USS is unpyrolyzed municipal sewage sludge. Biochar was produced from dry municipal sewage sludge at 800 °C.
	USS* (20)	149.73 (−820)	3.76 (36.27)	–	
	Biochar (20)	12.63 (22.44)	4.90 (16.80)	–	
Xiao et al. [90], China	Biochar (0)	154.2 (control)	–	–	Biochar was obtained from rice-straw through pyrolysis at 600 °C temperature.
	Biochar (20)	108.4 (32.94)	–	–	
	Biochar (40)	130.1 (15.63)	–	–	
Wang et al. [109], China	Biochar (0% w/w of soil)	58.2** (control)	57.9** (control)	–	Biochar300, biochar500, and Biochar700 were produced at 300, 500, and 700 °C, respectively, from rice straw. **Note: Unit of CH_4 and N_2O is mg kg^{-1} soil.
	Biochar300 (3% w/w of soil)	93.4 (−60.48)	17.9 (69.08)	–	
	Biochar500 (3% w/w of soil)	62.6 (−7.56)	1.28 (97.79)	–	
	Biochar700 (3% w/w of soil)	63.4 (−8.93)	0.59 (98.98)	–	
Kowshika et al. [113], India	Control (150 kg N ha^{-1})	54.9 (control)	–	–	SSB-Silica solubilizing bacteria.
	Biochar (10)	46.9 (14.57)	–	–	
	Biochar (10) + SSB (12.5 kg ha^{-1})	46.0 (16.21)	–	–	
Pandey et al. [114], Vietnam	AWD-FYM (10)	105 (control)	0.97 (control)	–	Biochar was produced from rice straw at 500 °C temp. (AWD-alternate wetting and drying and PF-permanent flooding, FYM-farmyard manure)
	AWD-biochar (6.67)	46 (56.19)	0.67 (30.93)	–	
	PF-FYM (10)	353 (Control)	0.44 (control)	–	
	PF-biochar(6.67)	140 (60.34)	0.27 (38.64)	–	
Singla and Inubushi et al. [115], Japan	Ammonium sulphate (AS) (160 mg pot^{-1})	169 (control)	0.2 (control)	–	Biochar was produced from biogas digester solid slurry at 330 °C temperature.
	AS + biochar (790 mg C pot^{-1})	347 (−105)	−0.4 (100)	–	
Wheat					
Shao et al. [112], China	Control (0)	0.026 (control)	1.95 (control)	–	USS is unpyrolyzed municipal sewage sludge. Biochar was produced from dry municipal sewage sludge at 800 °C.
	USS (20)	0.026 (at par with control)	2.09 (−7.26)	–	
	Biochar (20)	−0.026 (200)	1.32 (32.26)	–	
Wu et al. [106], China	N (250 kg N ha^{-1}) + biochar (0)	62.45 (control)	5.55 (control)	–	Biochar was produced from wheat straw at 500 °C. Six years average result of a field experiment conducted with rice-wheat rotation.
	N + biochar (20)	55.45 (11.19)	4.46 (19.55)	–	
	N + biochar (40)	51.55 (17.45)	4.09 (26.35)	–	
He et al. [116], China	ON (125 kg N ha^{-1})	–	3.93 (control)	–	Wheat straw biochar produced at 450 °C is used. ON-Optimal N dose; ONI-optional N dose + nitrification inhibitor (DCD, 5% by w/w) and urease inhibitor (hydroquinone, 0.3% by w/w)
	ON + biochar1 (7.5)	–	2.73 (−9.43)	–	
	ON + biochar2 (15)	–	3.38 (−35.22)	–	
	ONI (125 kg N ha^{-1})	–	2.22 (control)	–	
	ONI + biochar1(7.5)	–	1.26 kg N ha^{-1} (43.26)	–	
	ONI + biochar2 (15)	–	1.26 kg N ha^{-1} (43.26)	–	
Niu et al. [117], China	Biochar (0)	–	0.35 (control)	–	BC was produced from maize straw feedstock through pyrolysis at approximately 450 °C.
	Biochar3 (3)	–	0.41 (−18.18)	–	
	Biochar6 (6)	–	0.40 (−13.64)	–	
	Biochar12 (12)	–	0.44 (−27.27)	–	
	N (200 kg N ha^{-1}) + biochar (0)	–	0.94 (control)	–	
	N + biochar3 (3)	–	0.88 (6.67)	–	
	N + biochar6 (6)	–	0.84 (10)	–	
	N + biochar12 (12)	–	0.93 (1.67)	–	
Xiang et al. [118], China	ON (225 kg N ha^{-1})	0.196 (control)	6.38 (control)	–	Wheat-derived biochar was used in this study. ON-optimal nitrogen fertilizer dose
	ON + biochar (3.75)	0.132 (32.65)	6.32 (0.99)	–	
	ON + biochar (7.50)	0.145 (25.85)	5.97 (6.40)	–	
Maize					
Yang et al. [119], China	Biochar (0)	−0.299 (control)	0.319 kg ha^{-1} (control)	5142 (control)	Biochar was made from corn straw feedstock ta 400–500 °C. Negative sign indicates CH_4 consumption in soil.
	Biochar15 (15)	−0.559 (−87.27)	0.134 (58.15)	4007 (22.08)	
	Biochar30 (30)	−0.606 (−103)	0.067 (79.15)	4035 (21.53)	
	Biochar45 (45)	−0.076 (74.54)	0.185 (76.49)	3550 (30.97)	
Niu et al. [120], China	N (120 kg N ha^{-1})	–	1.57 (control)	–	Biochar was produced from maize straw at 450 °C pyrolysis temperature.
	N + biochar (3)	–	1.32 (16)	–	
	N + biochar (6)	–	1.35 (15)	–	

(*continued on next page*)

Table 2 (*continued*)

Reference & study location	Treatments details (Mg ha^{-1})	CH_4 emission kg ha^{-1} (% mitigation)	N_2O emission kg ha^{-1} (% mitigation)	CO_2 emission kg h^{-1} (% mitigation)	Remarks
	N + biochar (12)	–	1.27 (19)	–	
Niu et al. [117], China	Control (0)	–	0.90 (control)	–	Biochar was produced from maize straw feedstock through pyrolysis heating at approximately 450 °C.
	Biochar3 (3)	–	1.38 (−54.39)	–	
	Biochar6 (6)	–	1.46 (−63.16)	–	
	Biochar12 (12)	–	1.73 (−92.98)	–	
	N (200 kg N ha^{-1}) + biochar (0)	–	5.19 (control)	–	
	N + biochar3 (3)	–	3.11 (40.0)	–	
	N + biochar6 (6)	–	3.55 (31.52)	–	
	N + biochar12 (12)	–	3.38 (34.85)	–	
Zhang et al. [121], China	CF (239 kg N ha^{-1})	−0.42	3.08 (control)	5837 (control)	Biochar was produced from wheat straw at 450 °C temperature.
	CF + biochar (20)	−0.42	2.09 (32.14)	6171 (−5.72)*	
	CF + biochar (40)	−0.54	2.00 (35.20)	6259 (−7.26)*	CF-conventional fertilizer; BF-Balanced fertilizer.
	BF (217 kg N ha^{-1})	−0.60	0.99 (control)	5966 (control)	*Negative sign indicates consumption of CH_4 in soil.
	BF + biochar (20)	−0.73	0.93 (5.60)	6109 (−2.43)*	
	BF + biochar (40)	−0.74	0.94 (4.76)	6714 (−12.57)*	
Hüppi et al. [122], Switzerland	Control	–	5.55 (control)	–	Green waste mostly obtained from tree pruning was utilized for biochar production.
	Biochar (20)	–	2.67 (51.84)	–	

control (i.e. application of 250 kg N ha^{-1} alone). Feng et al. [98] studied the effect of three types of biochar prepared at different temperatures i.e. 300 °C, 400 °C, and 500 °C on CH_4 emissions from rice soil in a field experiment. Cai et al. [107] also studied the CH_4 mitigation potential of three biochar prepared at 300 °C, 500 °C, and 700 °C temperature in an incubation experiment using paddy soils. Feng et al. [98] and Cai et al. [107] both reported a significantly lower CH_4 reduction in the biochar prepared at higher temperature as compared to biochar prepared at a lower temperature. Therefore, it was concluded that biochar produced at higher temperature has more CH_4 reduction potential [107]. In an anaerobic environment such as paddy fields and natural wetlands, the application of biochar enhanced the anaerobic oxidation of methane (AOM). In agricultural and other terrestrial soil, sometimes the AOM process is coupled with the denitrification process and the process is known as denitrifying anaerobic methane oxidation (DAMO) [102]. DAMO process consumes CH_4 as electron donor and NO_3^- as electron acceptors. Biochar in soil stimulates the DAMO process as it acts as an extra electron acceptor. Nan et al. [108] reported that biochar adsorbs the soil organic carbon on its surface and limits its availability for methanogens resulting in lower production of CH_4 gas (Fig. 4). Biochar is porous and alkaline, and its addition in soil enhances the porosity of rhizospheric zone and stimulates CH_4 oxidation (Fig. 4).

Contrastingly, some studies have also concluded that biochar amendments stimulate the CH_4 emissions from rice soil. Wang et al. [109] investigated the influence of biochar produced from rice straw feedstock on CH_4 emissions (Table 2). They reported that the CH_4 emission from biochar treated soils prepared at 300, 500, and 700 °C was 60.48%, 7.56%, and 8.93% higher than control (Table 2). The authors concluded that the increase in CH_4 emission was mainly because of increased soil dissolved organic carbon content of biochar amended soils. They further argued that biochar prepared at 500 °C (68.1 m^{-2} g^{-1}) and 700 °C (161 m^{-2} g^{-1}) have a larger surface area than biochar prepared at 300 °C (4.40 m^{-2} g^{-1}). The larger surface area enhanced the population of iron-reducing bacteria in soil, which competes with CH_4 producing bacteria and therefore resulted in lower CH_4 emission. Qi et al. [110] also reported similar findings at the field level in biochar amended rice soils in Chongqing, China (Table 2). They concluded that biochar application at the rate of 10 Mg ha^{-1} increased the dissolved organic carbon content of the soil which resulted in 264.79% higher CH_4 emission over control (0 Mg biochar ha^{-1}). Thus, based on the above discussions, it can be concluded that biochar can play a significant role in CH_4 mitigation from rice soils. However, the mitigation potential of biochar varies with the feedstock, amount of biochar added, pyrolysis temperature, water management, agronomic management, and interactions of biochar with other organic matter and chemical fertilizers [98,101,111].

4.2. Nitrous oxide mitigation

N_2O is a potent GHG having an atmospheric lifetime of 114 years GWP 265 which contributes 5% to the total anthropogenic global warming [123]. Its concentration has increased from 285 ppb in the pre-industrial era (1750) to 350 ppb at a rate of 0.73 ppb per year during the last thirty years [89]. Agronomic soils are the largest source of N_2O emissions contributing 67% of total anthropogenic N_2O emission [89]. Globally, the N_2O emissions from agricultural soils have increased from 1.44 Tg in 1960 to 4.25 Tg in 2010 [124]. N_2O emissions from Indian agriculture has increased from 0.14 (1960) to 0.71 (2014) [123]. The mitigation of N_2O emissions from agricultural soils is of global concern. There are several options for N_2O mitigation from the agricultural soils such as the use of neem oil coated urea (NOCU), nitrification inhibitors (NIs), *Azolla* biofertilizers, etc. [91,93,125,126]. Recently, it has been concluded that the incorporation of biochar to agricultural soil also mitigates the N_2O emission with a very high efficiency.

The potential of biochar for N_2O mitigation from the major cereal crops is presented in Table 2. Wu et al. [106] conducted a six years field experiment in a rice-wheat system and observed that biochar application at the rate of 20 and 40 Mg ha^{-1} significantly reduced N_2O emission by 19.55% and 26.35%, respectively over control. In rice crops, Yang et al. [2] reported 8.89% higher N_2O emission over control with a lower dose of biochar (20 Mg ha^{-1}), while increasing biochar dose from 20 Mg ha^{-1} to 40 Mg ha^{-1} resulted in 26.06% lower N_2O emission (Table 2). Yang et al. [119] applied four concentrations of biochar (0, 15, 30, and 30 Mg ha^{-1}) and reported the highest mitigation of N_2O emission (79.15%) in 30 Mg ha^{-1} treatment over control. Further increasing biochar concentration from 30 to 45 Mg ha^{-1} reduced N_2O emission by 76.5%, which indicates that application of an optimum dose of biochar is very much essential for achieving highest N_2O mitigation.

Wang et al. [109] conducted an *ex-situ* study with biochar prepared at 300, 500, and 700 °C temperature i.e. biochar300, biochar500, and biochar700, respectively. They applied biochar by 3% of soil weight basis and reported 98.98%, 97.79%, and 69.08% N_2O mitigation in biochar700, biochar500, and biochar300, respectively, over control (no biochar). The biochar produced at higher pyrolysis temperature had larger pore size which enhanced the soil pH and subsequently suppressed the activity of nitrate reductase enzyme responsible for conversion of nitrate/nitrite to N_2O which therefore resulted in higher N_2O mitigation [109]. Niu et al. [117] investigated the effect of biochar application alone and with inorganic fertilizers on N_2O emission in maize crop. Biochar application alone at the rate of 3, 6, and 12 Mg ha^{-1} increased N_2O emission by 54.39%, 63.16%, and 92.98%, respectively over control (0 Mg biochar ha^{-1}). However, biochar application with urea at the rate 3, 6, and 12 Mg ha^{-1} reduced N_2O emission by 40%,

31.52%, and 34.85%, respectively. They concluded that on application with inorganic N fertilizers biochar adsorbs NH_4^+ on its surface which suppresses the ammonification and nitrification process and thereby net N_2O emission [117].

Recently, a metadata analysis of published studies about biochar potential for N_2O mitigation were done. Cayuela et al. [127] meta-analyzed the global data and found that biochar amended soils mitigate almost 50% of N_2O emissions. Verhofstad et al. [128] reported average reductions of 9–12% in N_2O emission from biochar amended soils. Lately, a global meta-analysis by Borchard et al. [129] reported a 38% average reduction of N_2O emissions from biochar amended soils as compared to control. On the other hand, a few investigations indicated enhancement in the N_2O emission from agricultural soils after biochar amendment. Qi et al. [110] reported that biochar application (10 Mg ha^{-1}) to rice soil increased N_2O emission by 98.17% over control soil lacking biochar amendment. Shokoor et al. [130] conducted a global meta-analysis for comparing the effect of biochar and animal manure on N_2O emission from agricultural soils. Direct application of animal manure improved soil organics, soil microbial population, soil fertility, etc., but it also resulted in higher N_2O emission having a negative impact and enhanced global warming (Fig. 5). The authors observed that the application of organic matter in the form of biochar reduced cumulative N_2O emission by 19.7% over non-biochar soil, and the application of animal manure emitted 17.7% higher N_2O over control [130].

Shakoor et al. [130] found that N_2O emission factor for biochar and animal manure application in soil were −0.08% and 0.46% respectively, which indicated the application of organic matter in the form of biochar play a significant role in N_2O emission mitigation. Organic compost and animal manure have a high content of readily available nitrogen, phosphorus, carbon, and other nutrients, and its application increased substrate (nitrogen and carbon) for nitrification and denitrification processes and enhanced the N_2O flux (Fig. 5). Biochar also has high nutrient content but they are not readily available for microbial processes [130]. Higher oxygen content in biochar applied soil inhibits denitrification process and result in lower N_2O emission over animal manure or compost (Fig. 5).

The N_2O mitigation from agricultural soils mainly depends on the biochar properties and interaction between soil and biochar. Many biochar properties such as acidic and basic functional groups, pH, porosity, redox properties, and its specific surface area vary with the pyrolysis temperature and feedstock used for biochar preparation [127,131]. The biochar temperature, dose of application, and its application with inorganic N greatly influence its N_2O mitigation potential. Biochar produced at higher pyrolysis temperature mitigates N_2O emission more efficiently due to its larger specific surface area [109]. The dose of biochar incorporation also plays a crucial role in the mitigation of N_2O emissions from soils. At a lower rate of application, biochar enhances the N_2O emission, while, at higher doses, it reduces the N_2O emission [2,119]. The performance of biochar for N_2O mitigation gets enhanced with inorganic N fertilizers due to adsorption of NH_4^+ and reduction of NH_4^+ and NO_3^- for nitrification and denitrification processes, respectively which restricts N_2O emissions [117]. Once biochar is applied to soils, it can modify the soil pH, microbial symphony and ultimately reduces the N_2O efflux [132,133]. Biochar application to soil enhances the soil pH, which suppresses the activity of the nitrate reductase enzyme and results in N_2O emission reduction [109]. The application of biochar to agricultural soils neutralized the soil pH, thereby reducing the population of nitrifying bacteria and consequently N_2O emissions [109]. Besides this, it may increase the pH of the soil and N_2O reductase which escorts conversion of N_2O into N_2 and thus decreases N_2O emissions [133].

5. Carbon sequestration and soil health management

Biochar plays a significant role in combating climate change by carbon sequestration in agricultural soils. Biochar is a promising option for long-term soil carbon sequestration. The preliminary estimates of Jacquot et al. [134] suggested that, if biochar is produced from agricultural wastes generated in 2.5% of earth's agricultural land and applied to soil then the pre-industrial (1752) level of atmospheric CO_2 might be achieved by 2050. Lehmann et al. [135] estimated that, if Jhum cultivation (slash-and-burn) is replaced by the slash-and-char (biochar agriculture) then 12% of total anthropogenic emission from the land-use changes can be offset. This huge potential of biochar for carbon sequestration can be attributed to its very stable and high carbon content. Biochar is resistant to carbon degradation and can persist for a longer time in the soil as compared to other sources of carbon such as compost, farmyard manure, and other organic carbon forms of soil biota [136,137].

The stability of biochar is substantially affected by feedstock and production procedures. Generally, the biochar produced at a higher temperature is more stable than biochar produced at a lower temperature [138,139]. Singh et al. [139] reported that 0.5–8.9% of biochar carbon was mineralized over five years period. Biochar produced from the manure-based feedstocks showed faster carbon mineralization than feedstocks based on plants [139]. Thus, it can be wrapped up that biochar produced at higher temperature from plants-based feedstock have more carbon sequestration potential than the biochar produced at lower temperature from the manure-based feedstock. The 50% of the feedstock

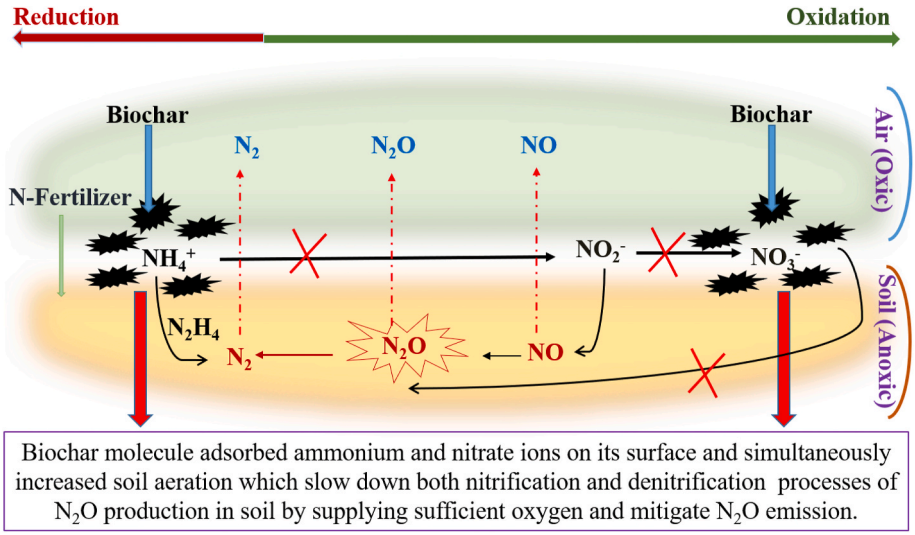

Fig. 5. Mechanism involved in nitrous oxide mitigation from soil under biochar amendent

carbon can be sequestered through biochar in comparison to carbon hold after biomass burning (3%) and decomposition through biological pathways (10–20% after 5–10 years) [135]. Therefore, the biochar itself is a source of carbon stock that persists in soil for a longer duration. Besides this, it can also act together with the indigenous soil organic matter and can either reduce or enhance the rate of microbial decomposition of soil native carbon [140]. Yang et al. [119] found that the application of corn residue biochar at the rate of 30 t ha^{-1} enhanced soil carbon sequestration by 16% in a sandy loam soil of China. Zhang et al. [141] applied wheat straw biochar to soil at the rate of 40 t ha^{-1} and reported that soil organic carbon content was increased by 76.29% in 5 years of application.

The carbon sequestration rate in soils is affected by several biotic (microbial numbers, macro fauna, and plant species) and abiotic (soil texture, pH, moisture, temperature, biochar carbon content, O/C ratio, H/C ratio, etc.) factors [138,142]. El-Naggar et al. [143] reported that carbon sequestration is significantly affected by soil texture and it was higher in sandy soil than sandy loam soil. They reported that soil carbon sequestration through biochar application is negatively correlated with temperature. The carbon mineralization rate at 40 °C soil temperature was higher (0.97–2.71% of total biochar carbon application) than 20 °C soil temperature (0.30–1.14%) [144]. The carbon sequestration process is generally higher in alkaline soil as compared to acidic soils [145]. The drastic negative priming effect in alkaline soil (pH 7.81) controls the biochar degradation in alkaline soil, however, in acidic (pH 5.19) soils, higher degradation of biochar results in lower carbon sequestration and higher CO_2 emissions [145].

Biochar application improves soil health through increasing cation-exchange capacity, neutralizing soil acidity, enhancing water retention capacity, increased microbial diversity, improved nutrient status, reverse soil degradation, discourage deforestation along with reducing N_2 leaching, N_2O emission, and increasing carbon in soils [146–148]. Wang et al. [149] confirmed that biochar-C significantly contributes towards soil aggregate stability. Liu et al. [150] observed enhanced soil water-stable aggregate with the application of wheat straw biochar. Wang et al. [149] reported improvement in soil aggregates of a fine-textured soil (silty loam) with the addition of the softwood biochar. In the case of N_2, the manure-based feedstock for biochar is generally preferable. N_2 in biochar is present on the surface in the form of C–N heterocyclic structure having low bioavailability [147]. The available phosphorous from the biochar is in the range of 0.4–34% [151]. However, potassium, calcium, and magnesium can be bioavailable in the range of 55–65% [151]. Berek et al. [152] observed that most of the potassium present in biochar is available in the water-soluble form if biochar is prepared through slow pyrolysis.

Berek and Hue [153] observed that calcium and magnesium are present mostly in carbonate, phosphate, and/or oxide compounds of calcium and magnesium. The biochar can be used to minimize the soil bulk density [154,155]. The higher porosity of biochar minimizes the bulk density and enhances the water holding capacity of the biochar treated soil [156–158]. Due to porous structure, higher internal surface area, and water retention capacity of biochar, it contributes towards favorable microbial (bacteria and fungi) habitats [159,160]. Bhaduri et al. [161] emphasized the strong interaction between extracellular enzymes and biochar. Demisie et al. [162] observed enhanced activity of β-glucosidase, dehydrogenase and urease enzymes in a red soil amended with an oakwood/bamboo biochar. Luo et al. [163] observed abundance of actinobacteria, gram-negative, gram-positive bacteria, and fungi in biochar amended soil. Gomez et al. [164] observed that biochar addition increased the microbial activity in soils and can alter the community composition as biochar serve as a C source for microbial activity to varying degree [165]. Thus, based on the above discussion, it can be concluded that BC can play a significant role in maintaining/improving soil health by changing the soil biological, physical, and chemical properties.

6. Remediation of contaminated wastewater

Biochar can be potentially used for the removal of pesticides [166–168], heavy metals [169], dyes [9], antibiotics [7], nutrient load, and other contaminants from water/wastewater. In the subsequent section, the applications of biochar for the remediation of wastewater have been discussed.

6.1. Pesticides removal through biochar

Pesticides are the chemicals used for enhancing agricultural production by controlling pests. However, due to lack of accurate application protocol and outbreak of new diseases, they are extensively used, resulting in the contamination of water, soil, and air [170,171]. Water resources are highly fragile and adversely affected by pesticide contamination and therefore need to be removed for sustaining water ecosystems. The role of biochar in the removal of pesticides from water resources has been documented in several scientific studies (Table 3). The adsorption efficacy for pesticides of biochar can be enhanced by doping phosphorus into feedstock. Suo et al. [172] observed 79.6 mg/g of atrazine adsorption capacity with biochar produced from corn straw doped with phosphorus (Table 3). The pore size of biochar (3.18 nm) is generally higher than the atrazine diameter (7.2–7.8 Å) and consequently, atrazine gets arrested on the meso and micropores existing on the surface of biochar [172]. The adsorption capacity of biochar produced is directly affected by temperature [6].

Biochar produced at a lower temperature (300 °C) shows lower adsorption capacity (chlorpyrifos-4.32 mg/g, and chlorpyrifos-methyl-15 mg/g) as compared to biochar produced at higher (600 °C) temperature (chlorpyrifos-14.8 mg/g, and chlorpyrifos-methyl-50.5 mg/g) [6].

Table 3
Removal of pesticides from wastewater through biochar amendments.

References	Name of pesticides	Removal rate	Remarks
Chan et al. [176]	Atrazine Naphthalene Phenanthrene Anthracene	37–97% 49–93% ~100% ~100%	Biochar produced at 450 °C pyrolysis temperature from mixed feedstock (pine, fir woodchip, and spruce).
Okoya et al. [177]	Chlorpyrifos	93.7	Rice husk was used as feedstock for biochar production in this study.
Suo et al. [172]	Atrazine	79.6 mg/g	The phosphorus-doped biochar show maximum adsorption (79.6 mg/g) at 25 °C.
Zheng et al. [6]	Chlorpyrifos Chlorpyrifos-methyl	4.32–14.8 mg/g 15.0–50.5 mg/g	Biochar synthesis at lower temperature (300 °C) show lower adsorption capacity (chlorpyifos-4.32 mg/g, chlorpyifos-methyl-15 mg/g) as compared to biochar produced at higher (600 °C) temperature capacity (chlorpyifos-14.8 mg/g, and chlorpyifos-methyl-50.5 mg/g).
Mandal et al. [173]	Atrazine Imidacloprid	12.3–89.8% 5.9–89.5%	In this study, different Agri-waste biochar (eucalyptus bark, corn cob, rice husk, rice straw, bamboo chips, and acid-treated rice straw) sorption potential were explored.
Wang et al. [174]	Chlorpyrifos	16 mg/g	The maximum adsorption was recorded with biochar synthesis from wheat straw feedstock at 750 °C pyrolysis temperature.
Zheng et al. [168]	Atrazine Simazine	451–1158 mg/kg 243–1066 mg/kg	Green-waste feedstock is used for the synthesis of biochar and pyrolysis temperature for the production was 450 °C.

Mandal et al. [173] used different agri-feedstocks (corn cob, eucalyptus bark, rice husk, rice straw, bamboo chips, and acid-treated rice straw) for biochar production for the sorption of atrazine and imidacloprid (Table 3). The removal efficiency for atrazine and imidacloprid ranged from 12.3 to 89.8% and 5.9–89.5% respectively, and best removal performances were observed in biochar produced with phosphoric acid treated rice straw [173]. Biochar's pH, polarity, pore diameter, and aromaticity affect adsorption [173]. Chlorpyrifos removal through wheat straw biochar was reported by Wang et al. [174]. The highest adsorption (16 mg/g) was observed with straw-derived biochar at 750 °C (Table 3). In chlorpyrifos pesticides, the π···π stack was formed among the aromatic rings and these aromatic rings of chlorpyrifos were adsorbed on the surface of biochar which resulted in their removal from wastewater [174]. Tan et al. [175], produced KOH modified corn straw biochar, and Na_2S modified corn straw biochar and studied their role in the sorption of atrazine pesticides from aqueous solution. The sorption capacity for atrazine with KOH modified corn straw biochar, and Na_2S modified corn straw biochar was 46.39% and 38.66% times higher than the corn straw biochar [175]. The higher surface area and presence of higher porous and aromatic structures in modified corn straw biochar were the significant parameters that boosted the sorption capacity for the atrazine [175].

The sorption of pesticides by biochar is affected by several parameters such as solid/solution ratio, contact time, particle size, and solution pH [168]. Zheng et al. [168] attempted to explore the optimum removal parameters for pesticides (simazine and atrazine) from agricultural wastewater. Pesticides removal efficiency with small particle size biochar was higher than the larger particle sized biochar [168]. Zheng et al. [168] observed that removal efficiency of biochar is inversely proportional to solid/solution ratio. The sorption efficacy for atrazine and simazine increased by 156.76% (451–1158 mg/kg) and 338.68% (243–1066 mg/kg) respectively, when solid/solution ratio was decreased by 20 times (from 1:50 to 1:1000) [168].

6.2. Heavy metals removal through biochar

The contamination of heavy metals (HM) is a common issue in surface water [178], groundwater [179,180], and wastewater [181]. Both natural and anthropogenic sources are responsible for the contamination of various water resources. The consumption of such contaminated water may pose a health risk and need to be remediated for the welfare of the human population. Biochar has the potential to play a significant role in mitigating HM contamination (Table 4). The removal mechanism such as complexation, chemisorption (electrostatic interaction), ion exchange, precipitation, and sorption may play an imperative role in controlling the HM concentration in an aqueous solution [181,182]. Recently, Li et al. [183] used the magnetite-based biochar produced from watermelon rinds for the removal of thallium from wastewater (Table 3). The adsorption capacity of up to 1123 mg/g for thallium was recorded with magnetite-based biochar (Table 4). Mostly mono-metal removal is targeted through biochar applications. Magnetic loofah sponges biochar with chitosan was used for the removal of Cr (VI) from aqueous solution. The adsorption capacity of 30.14 mg/g was recorded (Table 4) with magnetic loofah sponges biochar combined with chitosan and it was 40% higher over pristine biochar.

The role of iron doping in feedstock was also reported by Son et al. [8]. Doping of iron in algal feedstock enhanced adsorption capacity by many folds for Cd, Cu, and Zn [8]. Son et al. [8] found that magnetite biochar (iron-doped biochar) derived from macro-algal biomass showed adsorption capacity varying from 19.40 to 23.16 mg/g, 47.75–55.86 mg/g, and 19.13–22.22 mg/g for Cd, Cu, and Zn, respectively (Table 4). Park et al. [184] conducted a study using sesame straw biochar for the adsorption of mono-metal and multi-metals (Table 4). The adsorption capacity for each HM (Cr-65 mg/g, Pb-102 mg/g, Cd-86 mg/g, Cu-55 mg/g, and Zn-34 mg/g) was found to be higher in mono-metal experiment than the adsorption capacity for HM (Cr-21 mg/g, Pb-88 mg/g, Cd-5 mg/g, Cu-40 mg/g, and Zn-7 mg/g) in multi-metals experiment under similar conditions (Table 4). The reduction in adsorption capacity for HM in the multi-metals experiment is due to high interference created by competition between ions adsorbed which affected adsorption of all HM [184]. Pretreatment of feedstock with $KMnO_4$ before pyrolysis improved the sorption potential of biochar for the HM [185]. $KMnO_4$ pretreatment enhanced the amount of oxygen-containing functional group on biochar surface which results in better sorption of HM (Table 4). Biochar produced from different feedstocks has dissimilar adsorption capacity and it varied due to physical (moisture, ash, volatile matter, carbon, etc.) properties of feedstock [186]. Role of different biomass as adsorbent for the HM from wastewater has been investigated [187,188]. Ahuwlaia et al. [187] reported that plant biomass adsorption capacity ranged from 5 to 641 mg/g mainly for Zn, Ni, Pb, Cd, and Cr. Biomass adsorption capacity can be enhanced by treatment [188]. Renu et al. [188] quoted that ozone treatment rice husk biomass adsorbent capacity ranged from 8.7 to 13.1 mg/g. Ambaye et al. [189] reviewed the adsorption capacity of biochar produced different biomass for the removal of HM and report that biochar adsorption capacity up to 133 mg/g which was comparatively higher over treated biomass.

Agrafioti et al. [186] used three types of biochar produced from different feedstocks (rice husk, sewage sludge, and waste solid) and observed that the As (53%) and Cr (89%) removal was highest with biochar produced from sewage sludge (Table 4). The biochar produced from sewage sludge has Fe_2O_3 on the matrix of biochar which result in higher removal of As and Cr (Table 3). Mohan et al. [190] used the magnetic oak wood and oak bark biochar for remediation of Cd and Pb (Table 4). The adsorption capacity with magnetic oak wood biochar (Cd-7.4 mg/g and Pb-30.2 mg/g) was comparatively higher than the adsorption capacity with magnetic oak bark biochar (Cd-2.87 mg/g and Pb-10.13 mg/g) (Table 3). Kiliç et al. [191] used the almond shell feedstock biochar for the removal of Ni and Co from aqueous solution. The adsorption capacity of the almond shell biochar for Ni and Co was found to be 22.22 mg/g and 28.09 mg/g respectively (Table 4), at pH 7 with adsorbed dose of 7 g/L of solution (concentration of Ni/Co was 100 ppm).

6.3. Antibiotic removal through biochar

The production and use of pharmaceutical products have increased with human population growth. The occurrence of antibiotics such as tetracycline (TCs), fluoroquinolone (FQs), sulfamethoxazole, chloramphenicol, moxifloxacin (MOX), ciprofloxacin (CIP), and others in waste/wastewater is of high concern for human health and environment. Biochar due to its high sorption capacity is extensively used for the adsorption of antibiotics from water/wastewater, drinking water, and other water sources [7,195,205]. Cheng et al. [195] found that a KOH-activated biochar produced from Pomela peel efficiently removed TCs (476.19 mg/g), chlortetracycline (555.56 mg/g), and oxytetracycline (407.5 mg/g) from swine wastewater (Table 3). Pore filling, adsorbate, π–π interactions between the adsorbent, and electrostatic interaction are the main mechanism involved in the adsorption of antibiotics from wastewater [195]. Huang et al. [196] used the biochar derived from hickory chips, bamboo, and bagasse for the sorption of sulfapyridine and sulfamethoxazole from aqueous solution (Table 4). Ball milled biochar produced from hickory chips at 450 °C showed best removal efficiency for antibiotic sulfapyridine (89.6%, with adsorption capacity of 58.6 mg/g), and sulfamethoxazole (83.3%, with adsorption capacity of 25.7 mg/g) (Table 4).

The efficiency of biochar synthesized at lower carbonization temperature (200–500 °C) showed higher adsorption capacity (246.3 mg/g) for tetracycline (trade name Oxytetracycline) antibiotic at 30 °C operating temperature [197]. Biochar prepared at low carbonization temperature has a uniform and regular pore similar to honeycombs which results in higher adsorption capacity for antibiotics [197]. At higher carbonization temperature (>400 °C), the wall micro pores get melted

Table 4
Role of biochar in heavy metals and antibiotics removal from water/wastewater.

Reference	Biochar feedstock	Metal/antibiotic	Adsorption capacity (mg/g)	Mechanisms involved	Remarks
Heavy metals					
Li et al. [183]	Watermelon rinds	Thallium (Ti)	1123	Surface complexation and oxidative precipitation	In this study, magnetite-based biochar coupled with hypochlorite oxidation was used.
Ni et al. [192]	Anaerobically digested sludge	Pb Cd	0.61 mmol/g 0.44 mmol/g	Adsorption	Biochar produced from anaerobically digested sludge has high adsorption capacity.
Xiao et al. [169]	Loofah sponges	Cr (VI)	30.14	Adsorption, precipitation, surface complexation & ion exchange	Magnified loofah sponges biochar combined with chitosan was used in this study.
Son et al. [8]	Kelp	Cd Cu Zn	23.16 55.86 22.22	Adsorption and magnetic separation	The macro-algae (kelp) was doped with iron and the modified biochar was used for the adsorption of the Cu, Cd, and Zn from aqueous solution.
Son et al. [8]	Hijikia	Cd Cu Zn	19.40 47.75 19.13	Adsorption and magnetic separation	The macro-algae (Hijikia) was doped with iron and the modified biochar was used for the sorption of the Zn, Cd, and Cu from aqueous solution.
Tan et al. [193]	Rice straw	Cd	49.261	Adsorption	In this study, magnetic rice straw biochar was prepared and used for the remediation of Cd.
Park et al. [184]	Sesame straw	Cr Pb Cd Cu Zn	65 102 86 55 34	Sorption and magnetic separation	Result of mono metals experiment. The adsorption capacity of each HM was higher than in multi-metal experiments
Park et al. [184]	Sesame straw	Cr Pb Cd Cu Zn	21 88 5 40 7	Sorption	Result of multi-metal experiment. Comparatively the adsorption capacity for HM was reduced in multi-metal experiments
Trakal et al. [194]	Nut Shield	Cd	50.60	Sorption	Magnetic nut shield biochar was used for the sorption of Cd.
Wang et al. [185]	Hickory wood treated with $KMnO_4$	Pb Cu Cd	153.1 34.2 28.1	Surface adsorption	Pretreatments of feedstock with $KMnO_4$ increased the amount of oxygen containing surface functional group of biochar which resulted in better sorption.
Agrafioti et al. [186]	Rice husk	As Cr (VI)	25% 18%	Adsorption via precipitation and electrostatic interaction	The higher removal with sewage sludge biochar was due to higher content Fe_2O_3 content in its ash.
Agrafioti et al. [186]	Sewage sludge	As Cr (VI)	53% 89%		
Agrafioti et al. [186]	Solid wastes	As Cr (VI)	55% 44%		
Mohan et al. [190]	Oakwood	Pb Cd	30.2 7.4	Sorption	Magnetic oak wood was used as feedstock material for biochar production.
Mohan et al. [190]	Oak bark	Pb Cd	10.13 2.87	Sorption	Magnetic oak bark was used as feedstock material for biochar production.
Kiliç et al. [191]	Almond shell	Ni Co	22.22 28.09	Adsorption	Almond shell biochar was effective and low-cost adsorbent for the adsorption of HM.
Antibiotics					
Cheng et al. [195]	Pomela peel	Tetracycline Oxytetracycline Chlortetracycline	476.19 407.5 555.56	Pore filling, electrostatic interaction, and π–π interactions between the adsorbent	In this study, the cost-effective removal of tetracycline was explored.
Huang et al. [196]	Hickory chips	Sulfamethoxazole Sulfapyridine	25.7 58.6	π–π interaction, hydrophobic interaction, electrostatic interaction, and hydrogen bonding	The ball mining significantly enhanced the adsorption capacity of biochar.
Zhang et al. [197]	Corn stover	Oxytetracycline	246.3	Sorption due to high surface pore	Biochar prepared at 500 °C showed the highest sorption capacity at 30 °C.
Wei et al. [198]	Sewage sludge	Tetracycline Doxycycline	104.86 128.98	Hydrogen bonds and π–π interaction	The role of iron-doped biochar for the removal of antibiotics was explored.
Suo et al. [172]	Corn straw	Triazine	79.6	Pore filling, hydrogen bonding, and electrostatic interaction	The P doping increased the meta-phosphate and carboxyl on the biochar surface which boosted adsorption capacity.
Li et al. [199]	Potato stem and leaves	Norfloxacin Ciprofloxacin Enrofloxacin	6.94 8.37 7.19	Adsorption	The removal efficiency with manganese oxide biochar was more than pristine biochar.
Oladipo and Ifebajo [200]	Chicken bone	Tetracycline	98.89	Sorption, Pore filling	Magnetic chicken bone biochar removed tetracycline efficiently.
Kong et al. [201]	*Astragalus membranaceus* residue	Ciprofloxacin	68.9	Sorption, and π–π interaction	Iron doped herbal medicine waste biochar increased the adsorption capacity for the antibiotic.
Shang et al. [202]	*Astragalus mongholicus* residue	Ciprofloxacin	42.9	π–π interactions electrostatic, hydrophobic hydrogen bond	In this study, Chinese herbal medicine *Astragalus mongholicus* residue was used for the biochar preparation.
Wang et al. [203]	Bamboo	Enrofloxacin Ofloxacin	19.91 13.31	Sorption	Salinity had a negative effect on the adsorption capacity of biochar
Rajapaksha et al. [204]	Burcucumber plant	Sulfamethazine	37.7	Sorption, hydrogen bond, and π–π interactions	The impact of steam activation of biochar on sulfamethazine adsorption was demonstrated in this study.

and burnt which may result in lower sorption for biochar prepared at high temperatures [197]. The adsorption capacity of biochar can be enriched by doping of iron [198], zinc [206], nitrogen [207], phosphorus [172], etc., during the process of biochar production. Wei et al. [198] found that the iron-doped biochar has larger functional groups of carboxyl, hydroxyl, and aromatic rings on biochar surface which result in higher adsorption capacity for tetracycline (104.86 mg/g) and doxycycline (128.98 mg/g) (Table 4). The doping of biochar with iron increased the π–π complexation and electrostatic interactions along with hydrogen bonding which results in higher adsorption capacity [198]. Phosphorus (P) doped corn straw biochar showed higher adsorption capacity (79.6 mg/g) than pristine biochar (Table 4) for triazine antibiotic from wastewater due to the presence of additional meta-phosphate and carboxyl groups on biochar surface which boosts adsorption capacity via more pore filling, hydrogen bonding, and electrostatic mechanism [172]. Kong et al. [201] prepared magnetic biochar from *Astragalus membranaceus* residue (herbal medicine waste) and used it for the removal of ciprofloxacin from aqueous solution. The highest adsorption capacity (68.9 mg/g) for the ciprofloxacin was found at pH 6 with herbal magnetic biochar produced from *A. membranaceus* residue (Table 4).

The pore volume and surface area of manganese oxide biochar produced from potato stem and leaves feedstock at 500 °C are higher than raw biochar produced from potato stem and leaves feedstock [199]. The removal of norfloxacin, ciprofloxacin, and enrofloxacin from water with magnetic biochar was 1.2, 1.5, and 1.6 times higher as compared to non-magnetic biochar [199] due to more pore volume and higher surface area. Wang et al. [203] found that the adsorption capacity of biochar for ofloxacin, and enrofloxacin, decreased by 32.85% (from 19.82 mg/g to 13.31 mg/g), and 28.18% (from 19.91 mg/g to 14.30 mg/g) respectively, after increasing the NaCl dose from 0 to 3 g/L. Based on the findings of Wang et al. [203] it can be concluded that the salinity of aqueous solution has a negative impact on biochar adsorption capacity. Oladipo and Ifebajo [200] found that magnetic biochar prepared from chicken bone feedstock led to the removal of tetracycline efficiently with the highest adsorption capacity of 98.89 mg/g from aqueous solution. Rajapaksha et al. [204] studied the effect of steam activation on biochar sorption capacity for the removal of sulfamethazine from aqueous solution. The adsorption capacity for sulfamethazine antibiotic under similar operating condition was enhanced by 55% due to steam activation of biochar and highest sorption capacity up to 37.7 mg/g was recorded with steam-activated biochar.

6.4. Dyes removal through biochar

Textile industry wastewater is the major source of the dyes in water bodies. The removal of dyes from wastewater is of global concern and biochar has tremendous potential in this area [208,209]. Ionic-based sorption, π-π stacking, hydrophobic interaction, and hydrogen bonding between dyes and biochar are the major mechanism involved in the removal of the dye from wastewater [209]. Biochar's physical properties such as surface area, and pore size also play a significant role in dye removal [209]. Physical properties of biochar are affected by nature of the feedstock, pyrolysis temperature, heating rate, etc. Chen et al. [210] studied the adsorption capacity of microalgal biochar produced at 400 °C, 600 °C, and 800 °C and found highest adsorption of malachite green dye (5306.2 mg/g) with biochar produced at 800 °C temperature. This behaviour was attributed to the highest surface area and higher pH which enhanced dye adsorption [208]. Biochar generally has a negatively charged surface area which favors the physical adsorption of positively charged dyes from aqueous solution [208,211].

Abd-Elhamid et al. reported an adsorption capacity of 44.64 mg/g and 90.91 mg/g for the crystal violet and methylene blue dyes, respectively through rice straw biochar [212]. Biochar produced from Litchi peel due to its high pore volume (0.588 cm^3/g) and surface area (1006 m^2/g) was able to adsorb 2468 mg/g and 404.4 mg/g of malachite green and congo red dyes, respectively through pore filling, hydrogen bonding, π-π interactions, and electrostatic interactions [213]. Recently, the adsorption potential of magnetic biochar produced from an edible seaweed named wakame has been reported for methylene blue dye [214]. Yao et al. [214] observed a maximum adsorption capacity of 479.49 mg/g for the methylene blue dye through magnetic wakame biochar produced at 800 °C temperature. The adsorption capacity of biochar synthesized from cow dung, rice husk, and domestic sludge at 500 °C pyrolysis temperature for methylene blue dye was investigated by Ahmad et al. [215]. The highest adsorption capacity (99.0%) was observed for biochar obtained from cow dung.

7. Future prospects

Further research on the biochar applicability especially its use in modern areas for energy storage, remediation process, to enhance the agriculture sustainability needs to be prioritized so as to achieve sustainable development goals. The importance of biochar is evident in its potential for global warming mitigation, utilization in ion batters, as well ass wastewater remediation. The protocols for these applications need to be developed fully so as to maximize the benefits and scale-up these to field-scale in near future. For example, industrial wastewater generation and its discharge into the freshwater bodies without or with partial treatment is still a big challenge even in the presence of strong legislation. Industries need an easy, low-cost, regenerative and effective solution for multiple problems. Biochar is having the potential to serve as a single solution for many problems at various scales. However, to achieve this, many gaps need to be bridged with a clear-cut standardization and our understanding of the processes. Further research needs to be carried out in the following areas:

- Effective utilization of biochar as amendment in anaerobic digestion needs further focus especially for the optimization of biogas recover, y sludge reduction, sludge nutrient enhancement, and functioning as a pH buffer.
- Production, application, and promotion of sulfur-laden biochar in sulfur deficient soil and its effect on the bioavailability of other nutrients needs to be goal-oriented.
- More focused research is needed on the utilization of biochar on its pH buffering potential in hydrogen production [66].
- Biochar is having all the characteristics such as high surface area, high stability, high conductivity, biocompatibility, low cost, and high performance to be utilized as electrodes (anode, cathode, and catalyst) in microbial fuel cells (MFCs) technology [76]. Thus more research and policy support is needed to exploit its full potential for the large-scale application.
- The utilization of magnetic biochar as an electrode in lithium-ion batteries is also a promising area to solve the issues related to secondary pollution and prime energy support [87].
- Optimization of mixed biochar synthesis and operating parameters to remove various types of contaminants from the wastewater is the need of the hour. The purification efficiency needs optimizing especially for the removal of persistent multi-chemicals in a sequential or step-wise manner. This will improve the wastewater discharge quality and reduce the cost of wastewater treatment, and finally reduce the cost of the end product of various industries.
- Policy formulation for the micro as well as macro-level entrepreneur development to utilize biochar at the highest levels needs immediate attention for judicious use of agricultural waste/organic waste, sustainable employment generation, and development.

8. Conclusions

The available findings of biochar research strongly justify the potentials of environmental benefits and limitations of biochar for expanding its use in renewable energy production, GHG mitigation from

agro-ecosystem, and remediation of contaminated wastewater. Biochar has enormous potential for renewable energy production and its application potentially enhances the methane and hydrogen production during anaerobic digestion. It can be a cheap and potential alternative for microbial fuel cell electrode and can significantly reduce the cost of ion-based batteries. It can be potentially utilized for the removal of pollutants such as pesticides, antibiotics, heavy metals, dyes, etc. from contaminated wastewater. The application of biochar in the agro-ecosystem boosts the soil carbon sequestration and mitigates the CH_4 and N_2O emissions. Therefore, the appropriate application of biochar can be recommended for tackling environmental issues in the atmosphere, hydrosphere, and lithosphere. To utilize the full potential of biochar to achieve the goal of renewable energy, wastewater remediation, and GHG mitigation, it is necessary that these sectors need to be integrated properly. Although the use of biochar is not a complete solution for all the environmental problems, it is indeed a potential candidate that requires serious attention in the environmental sustainability for energy-water-agroecosystem nexus. The availability of feedstocks for biochar and environmental problems varies with region to region. Therefore, region specific and target specific biochar needs to be developed for better utilization of various waste materials. The incessant research activities in this area would boost the refinement of biochar for solution to various environmental problems which can enhance the environmental sustainability in various regions.

Declaration of competing interest

All authors do not have any conflict of interest in this MS. All are agreed for the submission of this MS.

Acknowledgments

Sandeep K. Malyan and Rajesh Singh are thankful to the National Institute of Hydrology, Roorkee for providing all the facilities required in this study. Smita S Kumar acknowledges JC Bose University of Science & Technology, YMCA for facilitating this work. Ram Kishor Fagodiya, acknowledges ICAR-Central Soil Salinity Research Institute-Karna, Pooja Ghosh acknowledges Indian Institute of Technology Delhi, Amit Kumar acknowleadges Central Silk Board Jorhat, Assam, and Lakhveer Singh acknowleadges SRM University, for facilitating this work. The authors express their sincere gratitude to the anonymous editors and reviewers for helping to improve the standard of the manuscript.

References

[1] A. K Gupta DK, Gupta CK, Dubey R, Fagodiya RK, Sharma G, et al. Role of biochar in carbon sequestration and greenhouse gas mitigation. Biochar Appl. Agric. Environ. Manag. 2020:141–65. https://doi.org/10.1007/978-3-030-40997-5_7.

[2] Yang S, Xiao Y, Sun X, Ding J, Jiang Z, Xu J. Biochar improved rice yield and mitigated CH4 and N2O emissions from paddy field under controlled irrigation in the Taihu Lake Region of China. Atmos Environ 2019;200:69–77. https://doi.org/10.1016/j.atmosenv.2018.12.003.

[3] Glaser B, Parr M, Baran C, Kopolo G. Biochar is carbon negative. Nat Geosci 2009; 2. https://doi.org/10.1038/ngeo395. 2–2.

[4] Kuzyakov Y, Subbotina I, Chen H, Bogomolova I, Xu X. Black carbon decomposition and incorporation into soil microbial biomass estimated by 14C labeling. Soil Biol Biochem 2009;41:210–9. https://doi.org/10.1016/j.soilbio.2008.10.016.

[5] Sharma GK, Jena RK, Hota S, Kumar A, Ray P, Fagodiya RK, et al. Recent development in bioremediation of soil pollutants through biochar for environmental sustainability. Biochar Appl. Agric. Environ. Manag. 2020: 123–40. https://doi.org/10.1007/978-3-030-40997-5_6.

[6] Zheng H, Zhang Q, Liu G, Luo X, Li F, Zhang Y, et al. Characteristics and mechanisms of chlorpyrifos and chlorpyrifos-methyl adsorption onto biochars: influence of deashing and low molecular weight organic acid (LMWOA) aging and co-existence. Sci Total Environ 2019;657:953–62. https://doi.org/10.1016/j.scitotenv.2018.12.018.

[7] Yang J, Ji G, Gao Y, Fu W, Irfan M, Mu L, et al. High-yield and high-performance porous biochar produced from pyrolysis of peanut shell with low-dose ammonium polyphosphate for chloramphenicol adsorption. J Clean Prod 2020; 264:121516. https://doi.org/10.1016/j.jclepro.2020.121516.

[8] Son EB, Poo KM, Chang JS, Chae KJ. Heavy metal removal from aqueous solutions using engineered magnetic biochars derived from waste marine macroalgal biomass. Sci Total Environ 2018;615:161–8. https://doi.org/10.1016/j.scitotenv.2017.09.171.

[9] Rangabhashiyam S, Balasubramanian P. The potential of lignocellulosic biomass precursors for biochar production: performance, mechanism and wastewater application—a review. Ind Crop Prod 2019;128:405–23. https://doi.org/10.1016/j.indcrop.2018.11.041.

[10] Zhang C, Zeng G, Huang D, Lai C, Chen M, Cheng M, et al. Biochar for environmental management: mitigating greenhouse gas emissions, contaminant treatment, and potential negative impacts. Chem Eng J 2019;373:902–22. https://doi.org/10.1016/j.cej.2019.05.139.

[11] Qambrani NA, Rahman MM, Won S, Shim S, Ra C. Biochar properties and eco-friendly applications for climate change mitigation, waste management, and wastewater treatment: a review. Renew Sustain Energy Rev 2017;79:255–73. https://doi.org/10.1016/j.rser.2017.05.057.

[12] Roy P, Dias G. Prospects for pyrolysis technologies in the bioenergy sector: a review. Renew Sustain Energy Rev 2017;77:59–69. https://doi.org/10.1016/j.rser.2017.03.136.

[13] Al-Wabel MI, Al-Omran A, El-Naggar AH, Nadeem M, Usman AR. Pyrolysis temperature induced changes. Bioresour Technol 2013;131:374–9.

[14] Angin D. Effect of pyrolysis temperature and heating rate on biochar obtained from pyrolysis of safflower seed press cake. Bioresour Technol 2013;128:593–7. https://doi.org/10.1016/j.biortech.2012.10.150.

[15] Hossain MK, Strezov Vladimir V, Chan KY, Ziolkowski A, Nelson PF. Influence of pyrolysis temperature on production and nutrient properties of wastewater sludge biochar. J Environ Manag 2011;92:223–8. https://doi.org/10.1016/j.jenvman.2010.09.008.

[16] Yu KL, Lau BF, Show PL, Ong HC, Ling TC, Chen WH, et al. Recent developments on algal biochar production and characterization. Bioresour Technol 2017;246: 2–11. https://doi.org/10.1016/j.biortech.2017.08.009.

[17] Tripathi M, Sahu JN, Ganesan P. Effect of process parameters on production of biochar from biomass waste through pyrolysis: a review. Renew Sustain Energy Rev 2016;55:467–81. https://doi.org/10.1016/j.rser.2015.10.122.

[18] Kebelmann K, Hornung A, Karsten U, Griffiths G. Intermediate pyrolysis and product identification by TGA and Py-GC/MS of green microalgae and their extracted protein and lipid components. Biomass Bioenergy 2013;49:38–48. https://doi.org/10.1016/j.biombioe.2012.12.006.

[19] Ahmed A, Abu MS, Azad AK, Sukri RS. Intermediate pyrolysis of Acacia cincinnata and Acacia holosericea species for bio-oil and biochar production. Energy Convers Manag 2018;176:393–408. https://doi.org/10.1016/j.enconman.2018.09.041.

[20] Tinwala F, Mohanty P, Parmar S, Patel A, Pant KK. Intermediate pyrolysis of agro-industrial biomasses in bench-scale pyrolyser : product yields and its characterization. Bioresour Technol 2015;188:258–64. https://doi.org/10.1016/j.biortech.2015.02.006.

[21] Yakub I, Abdalla Y, Yusup S, Kabir F. Valorization of Napier grass via intermediate pyrolysis : optimization using response surface methodology and pyrolysis products characterization. J Clean Prod 2017;142:1848–66. https://doi.org/10.1016/j.jclepro.2016.11.099.

[22] Manyà JJ. Pyrolysis for biochar purposes: a review to establish current knowledge gaps and research needs. Environ Sci Technol 2012;46:7939–54. https://doi.org/10.1021/es301029g.

[23] Bridgwater AV, Czernik S, Piskorz J. An overview of fast pyrolysis. Prog Thermochem Biomass Convers 2008;30:977–97. https://doi.org/10.1002/9780470694954.ch80.

[24] Yang C, Li R, Zhang B, Qiu Q, Wang B, Yang H, et al. Pyrolysis of microalgae: a critical review. Fuel Process Technol 2019;186:53–72. https://doi.org/10.1016/j.fuproc.2018.12.012.

[25] Pourkarimi S, Hallajisani A, Alizadehdakhel A, Nouralishahi A. Biofuel production through micro- and macroalgae pyrolysis – a review of pyrolysis methods and process parameters. J Anal Appl Pyrolysis 2019;142:104599. https://doi.org/10.1016/j.jaap.2019.04.015.

[26] Hameed Z, Aslam M, Khan Z, Maqsood K, Atabani E, Ghauri M, et al. Gasification of municipal solid waste blends with biomass for energy production and resources recovery : current status , hybrid technologies and innovative prospects. Renew Sustain Energy Rev 2021;136:110375. https://doi.org/10.1016/j.rser.2020.110375.

[27] Bouraoui Z, Dupont C, Jeguirim M, Limousy L, Gadiou R. CO2 gasification of woody biomass chars: the influence of K and Si on char reactivity. Compt Rendus Chem 2016;19:457–65. https://doi.org/10.1016/j.crci.2015.08.012.

[28] Limousy L, Jeguirim M, Labaki M. Energy applications of coffee processing by-products. In: Handb. Coffee process. By-products sustain. Appl. Elsevier Inc.; 2017. p. 323–67. https://doi.org/10.1016/B978-0-12-811290-8.00011-6.

[29] Fokaides PA. Energy recovery alternatives for the sustainable management of olive oil industry. Elsevier Inc.; 2017. https://doi.org/10.1016/B978-0-12-805314-0.00004-2.

[30] Rodriguez Alonso E, Dupont C, Heux L, Da Silva Perez D, Commandre JM, Gourdon C. Study of solid chemical evolution in torrefaction of different biomasses through solid-state 13C cross-polarization/magic angle spinning NMR (nuclear magnetic resonance) and TGA (thermogravimetric analysis). Energy 2016;97:381–90. https://doi.org/10.1016/j.energy.2015.12.120.

[31] van der Stelt MJC, Gerhauser H, Kiel JHA, Ptasinski KJ. Biomass upgrading by torrefaction for the production of biofuels: a review. Biomass Bioenergy 2011;35: 3748–62. https://doi.org/10.1016/j.biombioe.2011.06.023.

[32] Bridgeman TG, Jones JM, Shield I, Williams PT. Torrefaction of reed canary grass, wheat straw and willow to enhance solid fuel qualities and combustion properties. Fuel 2008;87:844–56. https://doi.org/10.1016/j.fuel.2007.05.041.

[33] Mumme J, Srocke F, Heeg K, Werner M. Use of biochars in anaerobic digestion. Bioresour Technol 2014;164:189–97. https://doi.org/10.1016/j.biortech.2014.05.008.

[34] Shen Y, Forrester S, Koval J, Urgun-Demirtas M. Yearlong semi-continuous operation of thermophilic two-stage anaerobic digesters amended with biochar for enhanced biomethane production. J Clean Prod 2017;167:863–74. https://doi.org/10.1016/j.jclepro.2017.05.135.

[35] Sahota S, Shah G, Ghosh P, Kapoor R, Sengupta S, Singh P, et al. Review of trends in biogas upgradation technologies and future perspectives. Bioresour Technol Rep 2018;1:79–88. https://doi.org/10.1016/j.biteb.2018.01.002.

[36] Song J, Wang Y, Zhang S, Song Y, Xue S, Liu L, et al. Coupling biochar with anaerobic digestion in a circular economy perspective: a promising way to promote sustainable energy, environment and agriculture development in China. Renew Sustain Energy Rev 2021;144:110973. https://doi.org/10.1016/j.rser.2021.110973.

[37] Ghosh P, Sengupta S, Singh L, Sahay A. Life cycle assessment of waste-to-bioenergy processes: a review. Bioreactors, INC; 2020. p. 105–22. https://doi.org/10.1016/b978-0-12-821264-6.00008-5.

[38] Ghosh P, Shah G, Sahota S, Singh L, Vijay VK. Biogas production from waste: technical overview, progress, and challenges. Bioreactors, INC; 2020. p. 89–104. https://doi.org/10.1016/b978-0-12-821264-6.00007-3.

[39] Kapoor R, Ghosh P, Tyagi B, Vijay VK, Vijay V, Thakur IS, et al. Advances in biogas valorization and utilization systems: a comprehensive review. J Clean Prod 2020:123052. https://doi.org/10.1016/j.jclepro.2020.123052.

[40] Cáceres KT, Rincón A, Cajigas ÁA, Cerón A, Cáceres KT. Influence of pH and the C/N ratio on the biogas production of wastewater. RevFacIngUniv Antioquia 2019:88–95. https://doi.org/10.17533/udea.redin.20190627.

[41] Kumar M, Dutta S, You S, Luo G, Zhang S, Show PL, et al. A critical review on biochar for enhancing biogas production from anaerobic digestion of food waste and sludge. J Clean Prod 2021;305:127143. https://doi.org/10.1016/j.jclepro.2021.127143.

[42] Zhao Q, Arhin SG, Yang Z, Liu H, Li Z, Anwar N, et al. pH regulation of the first phase could enhance the energy recovery from two-phase anaerobic digestion of food waste. Water Environ Res 2021:1–11. https://doi.org/10.1002/wer.1527.

[43] Li Y, Chen Y, Wu J. Enhancement of methane production in anaerobic digestion process : a review. Appl Energy 2019;240:120–37. https://doi.org/10.1016/j.apenergy.2019.01.243.

[44] Sharma B, Suthar S. Enriched biogas and biofertilizer production from Eichhornia weed biomass in cow dung biochar-amended anaerobic digestion system. Environ Technol Innov 2021;21:101201. https://doi.org/10.1016/j.eti.2020.101201.

[45] Wei W, Guo W, Ngo HH, Mannina G, Wang D, Chen X, et al. Enhanced high-quality biomethane production from anaerobic digestion of primary sludge by corn stover biochar. Bioresour Technol 2020;306:123159. https://doi.org/10.1016/j.biortech.2020.123159.

[46] Giwa AS, Xu H, Chang F, Wu J, Li Y, Ali N, et al. Effect of biochar on reactor performance and methane generation during the anaerobic digestion of food waste treatment at long-run operations. J Environ Chem Eng 2019;7:103067. https://doi.org/10.1016/j.jece.2019.103067.

[47] Pan J, Ma J, Liu X, Zhai L, Ouyang X, Liu H. Effects of different types of biochar on the anaerobic digestion of chicken manure. Bioresour Technol 2019;275:258–65. https://doi.org/10.1016/j.biortech.2018.12.068.

[48] Sunyoto NMS, Zhu M, Zhang Z, Zhang D. Effect of biochar addition on hydrogen and methane production in two-phase anaerobic digestion of aqueous carbohydrates food waste. Bioresour Technol 2016;219:29–36. https://doi.org/10.1016/j.biortech.2016.07.089.

[49] Qin Y, Yin X, Xu X, Yan X, Bi F, Wu W. Specific surface area and electron donating capacity determine biochar's role in methane production during anaerobic digestion. Bioresour Technol 2020;303:122919. https://doi.org/10.1016/j.biortech.2020.122919.

[50] Wang G, Li Q, Gao X, Wang XC. Synergetic promotion of syntrophic methane production from anaerobic digestion of complex organic wastes by biochar: performance and associated mechanisms. Bioresour Technol 2018;250:812–20. https://doi.org/10.1016/j.biortech.2017.12.004.

[51] Gebregiorgis T, Rene ER, Nizami A, Dupont C, Vaccari M, Hullebusch ED Van. Beneficial role of biochar addition on the anaerobic digestion of food waste : a systematic and critical review of the operational parameters and mechanisms. J Environ Manag 2021;290:112537. https://doi.org/10.1016/j.jenvman.2021.112537.

[52] Wang C, Liu Y, Wang C, Xing B, Zhu S, Huang J, et al. Biochar facilitates rapid restoration of methanogenesis by enhancing direct interspecies electron transfer after high organic loading shock. Bioresour Technol 2021;320:124360. https://doi.org/10.1016/j.biortech.2020.124360.

[53] Masebinu SO, Akinlabi ET, Muzenda E, Aboyade AO. A review of biochar properties and their roles in mitigating challenges with anaerobic digestion. Renew Sustain Energy Rev 2019;103:291–307. https://doi.org/10.1016/j.rser.2018.12.048.

[54] Kapoor R, Ghosh P, Kumar M, Vijay VK. Evaluation of biogas upgrading technologies and future perspectives: a review. Environmental Science and Pollution Research; 2019. https://doi.org/10.1007/s11356-019-04767-1.

[55] Pan J, Ma J, Zhai L, Luo T, Mei Z, Liu H. Achievements of biochar application for enhanced anaerobic digestion: a review. Bioresour Technol 2019;292:122058. https://doi.org/10.1016/j.biortech.2019.122058.

[56] Shen Y, Linville JL, Urgun-Demirtas M, Schoene RP, Snyder SW. Producing pipeline-quality biomethane via anaerobic digestion of sludge amended with corn stover biochar with in-situ CO2 removal. Appl Energy 2015;158:300–9. https://doi.org/10.1016/j.apenergy.2015.08.016.

[57] Linville JL, Shen Y, Ignacio-de Leon PA, Schoene RP, Urgun-Demirtas M. In-situ biogas upgrading during anaerobic digestion of food waste amended with walnut shell biochar at bench scale. Waste Manag Res 2017;35:669–79. https://doi.org/10.1177/0734242X17704716.

[58] Sahota S, Vijay VK, Subbarao PMV, Chandra R, Ghosh P, Shah G, et al. Characterization of leaf waste based biochar for cost effective hydrogen sulphide removal from biogas. Bioresour Technol 2018;250:635–41. https://doi.org/10.1016/j.biortech.2017.11.093.

[59] Kanjanarong J, Giri BS, Jaisi DP, Oliveira FR, Boonsawang P, Chaiprapat S, et al. Removal of hydrogen sulfide generated during anaerobic treatment of sulfate-laden wastewater using biochar: evaluation of efficiency and mechanisms. Bioresour Technol 2017;234:115–21. https://doi.org/10.1016/j.biortech.2017.03.009.

[60] Sánchez E, Herrmann C, Maja W, Borja R. Effect of organic loading rate on the anaerobic digestion of swine waste with biochar addition. Environ Sci Pollut Res 2021. https://doi.org/10.1007/s11356-021-13428-1.

[61] Sugiarto Y, Mayang N, Sunyoto S, Zhu M, Jones I. Effect of biochar addition on microbial community and methane production during anaerobic digestion of food wastes : the role of minerals in biochar. Bioresour Technol 2021;323:124585. https://doi.org/10.1016/j.biortech.2020.124585.

[62] Li W, He L, Cheng C, Cao G, Ren N. Effects of biochar on ethanol-type and butyrate-type fermentative hydrogen productions. Bioresour Technol 2020;306:123088. https://doi.org/10.1016/j.biortech.2020.123088.

[63] Sugiarto Y, Sunyoto NMS, Zhu M, Jones I, Zhang D. Effect of biochar in enhancing hydrogen production by mesophilic anaerobic digestion of food wastes: the role of minerals. Int J Hydrogen Energy 2021;46:3695–703. https://doi.org/10.1016/j.ijhydene.2020.10.256.

[64] Zhao L, Chen C, Ren HY, Wu JT, Meng J, Nan J, et al. Feasibility of enhancing hydrogen production from cornstalk hydrolysate anaerobic fermentation by RCPH-biochar. Bioresour Technol 2020;297:122505. https://doi.org/10.1016/j.biortech.2019.122505.

[65] Yang G, Wang J. Synergistic enhancement of biohydrogen production from grass fermentation using biochar combined with zero-valent iron nanoparticles. Fuel 2019;251:420–7. https://doi.org/10.1016/j.fuel.2019.04.059.

[66] Wang G, Li Q, Dzakpasu M, Gao X, Yuwen C, Wang XC. Impacts of different biochar types on hydrogen production promotion during fermentative co-digestion of food wastes and dewatered sewage sludge. Waste Manag 2018;80:73–80. https://doi.org/10.1016/j.wasman.2018.08.042.

[67] Zhang J, Fan C, Zang L. Improvement of hydrogen production from glucose by ferrous iron and biochar. Bioresour Technol 2017;245:98–105. https://doi.org/10.1016/j.biortech.2017.08.198.

[68] Sharma P, Melkania U. Biochar-enhanced hydrogen production from organic fraction of municipal solid waste using co-culture of Enterobacter aerogenes and E. coli. Int J Hydrogen Energy 2017;42:18865–74. https://doi.org/10.1016/j.ijhydene.2017.06.171.

[69] Liu WJ, Jiang H, Yu HQ. Emerging applications of biochar-based materials for energy storage and conversion. Energy Environ Sci 2019;12:1751–79. https://doi.org/10.1039/c9ee00206e.

[70] Zhao L, Wu KK, Chen C, Ren HY, Wang ZH, Nan J, et al. Role of residue cornstalk derived biochar for the enhanced bio-hydrogen production via simultaneous saccharification and fermentation of cornstalk. Bioresour Technol 2021;330:125006. https://doi.org/10.1016/j.biortech.2021.125006.

[71] Chi NTL, Anto S, Ahamed TS, Kumar SS, Shanmugam S, Samuel MS, et al. A review on biochar production techniques and biochar based catalyst for biofuel production from algae. Fuel 2021;287:119411. https://doi.org/10.1016/j.fuel.2020.119411.

[72] Waqas M, Aburiazaiza AS, Miandad R, Rehan M, Barakat MA, Nizami AS. Development of biochar as fuel and catalyst in energy recovery technologies. J Clean Prod 2018;188:477–88. https://doi.org/10.1016/j.jclepro.2018.04.017.

[73] Kumar SS, Malyan SK, Bishnoi NR. Performance of buffered ferric chloride as terminal electron acceptor in dual chamber microbial fuel cell. J Environ Chem Eng 2017;5:1238–43. https://doi.org/10.1016/j.jece.2017.02.010.

[74] Kumar SS, Kumar V, Malyan SK, Sharma J, Mathimani T, Maskarenj MS, et al. Microbial fuel cells (MFCs) for bioelectrochemical treatment of different wastewater streams. Fuel 2019;254. https://doi.org/10.1016/j.fuel.2019.05.109.

[75] Kumar SS, Kumar V, Kumar R, Malyan SK, Bishnoi NR. Ferrous sulfate as an in-situ anodic coagulant for enhanced bioelectricity generation and COD removal from landfill leachate. Energy 2019;176:570–81. https://doi.org/10.1016/j.energy.2019.04.014.

[76] Huggins T, Wang H, Kearns J, Jenkins P, Ren ZJ. Biochar as a sustainable electrode material for electricity production in microbial fuel cells. Bioresour Technol 2014;157:114–9. https://doi.org/10.1016/j.biortech.2014.01.058.

[77] Chang HC, Gustave W, Yuan ZF, Xiao Y, Chen Z. One-step fabrication of binder-free air cathode for microbial fuel cells by using balsa wood biochar. Environ Technol Innov 2020;18:100615. https://doi.org/10.1016/j.eti.2020.100615.

[78] Huggins TM, Latorre A, Biffinger JC, Ren ZJ. Biochar based microbial fuel cell for enhanced wastewater treatment and nutrient recovery. Sustain 2016;8:1–10. https://doi.org/10.3390/su8020169.

[79] Allam F, Elnouby M, El-Khatib KM, El-Badan DE, Sabry SA. Water hyacinth (Eichhornia crassipes) biochar as an alternative cathode electrocatalyst in an air-cathode single chamber microbial fuel cell. Int J Hydrogen Energy 2020;45:5911–27. https://doi.org/10.1016/j.ijhydene.2019.09.164.

[80] Li M, Zhang H, Xiao T, Wang S, Zhang B, Chen D, et al. Low-cost biochar derived from corncob as oxygen reduction catalyst in air cathode microbial fuel cells. Electrochim Acta 2018;283:780–8. https://doi.org/10.1016/j.electacta.2018.07.010.
[81] Zhang Y, Deng L, Hu H, Qiao Y, Yuan H, Chen D, et al. Pomelo peel-derived, N-doped biochar microspheres as an efficient and durable metal-free ORR catalyst in microbial fuel cells. Sustain Energy Fuels 2020;4:1642–53. https://doi.org/10.1039/c9se00834a.
[82] Chen S, Tang J, Fu L, Yuan Y, Zhou S. Biochar improves sediment microbial fuel cell performance in low conductivity freshwater sediment. J Soils Sediments 2016;16:2326–34. https://doi.org/10.1007/s11368-016-1452-z.
[83] Lu L, Han X, Li J, Hua J, Ouyang M. A review on the key issues for lithium-ion battery management in electric vehicles. J Power Sources 2013;226:272–88. https://doi.org/10.1016/j.jpowsour.2012.10.060.
[84] Wen Y, He K, Zhu Y, Han F, Xu Y, Matsuda I, et al. Expanded graphite as superior anode for sodium-ion batteries. Nat Commun 2014;5:1–10. https://doi.org/10.1038/ncomms5033.
[85] Gu X, Wang Y, Lai C, Qiu J, Li S, Hou Y, et al. Microporous bamboo biochar for lithium-sulfur batteries. Nano Res 2014;8:129–39. https://doi.org/10.1007/s12274-014-0601-1.
[86] Saavedra Rios C del M, Simone V, Simonin L, Martinet S, Dupont C. Biochars from various biomass types as precursors for hard carbon anodes in sodium-ion batteries. Biomass Bioenergy 2018;117:32–7. https://doi.org/10.1016/j.biombioe.2018.07.001.
[87] Salimi P, Norouzi O, Pourhoseini SEM, Bartocci P, Tavasoli A, Di Maria F, et al. Magnetic biochar obtained through catalytic pyrolysis of macroalgae: a promising anode material for Li-ion batteries. Renew Energy 2019;140:704–14. https://doi.org/10.1016/j.renene.2019.03.077.
[88] Waqas M, Asam Z, Rehan M, Anwar MN, Khattak RA, Ismail IMI, et al. Development of biomass-derived biochar for agronomic and environmental remediation applications. Biomass Convers Biorefinery 2021;11:339–61. https://doi.org/10.1007/s13399-020-00936-2.
[89] IPPC., IPCC. (Intergorvernmental panel on climate change). 2014. Synthesis Report 5.
[90] Xiao Y, Yang S, Xu J, Ding J, Sun X, Jiang Z. Effect of biochar amendment on methane emissions from paddy field under water-saving irrigation. Sustain Times 2018;10. https://doi.org/10.3390/su10051371.
[91] Malyan SK, Bhatia A, Kumar A, Gupta DK, Singh R, Kumar SS, et al. Methane production, oxidation and mitigation: a mechanistic understanding and comprehensive evaluation of influencing factors. Sci Total Environ 2016;572:874–96. https://doi.org/10.1016/j.scitotenv.2016.07.182.
[92] Gupta DK, Bhatia A, Kumar A, Das TK, Jain N, Tomer R, et al. Mitigation of greenhouse gas emission from rice-wheat system of the Indo-Gangetic plains: through tillage, irrigation and fertilizer management. Agric Ecosyst Environ 2016;230:1–9. https://doi.org/10.1016/j.agee.2016.05.023.
[93] Malyan SK, Bhatia A, Kumar SS, Fagodiya RK, Pugazhendhi A, Duc PA. Mitigation of greenhouse gas intensity by supplementing with Azolla and moderating the dose of nitrogen fertilizer. Biocatal Agric Biotechnol 2019;20:101266. https://doi.org/10.1016/j.bcab.2019.101266.
[94] Malyan SK. Reducing methane emission from rice soil through microbial interventions. New Delhi: ICAR-Indian Agricultural Research Institute; 2017, 110012. India.
[95] Kumar SS, Kumar A, Singh S, Malyan SK, Baram S, Sharma J, et al. Industrial wastes: fly ash, steel slag and phosphogypsum- potential candidates to mitigate greenhouse gas emissions from paddy fields. Chemosphere 2020;241:124824. https://doi.org/10.1016/j.chemosphere.2019.124824.
[96] Dubey SK. Microbial ecology of methane emission in rice agroecosystem: a review. Appl Ecol Environ Res 2005. https://doi.org/10.15666/aeer/0302_001027.
[97] Le Mer J, Roger P. Production, oxidation, emission and consumption of methane by soils: a review. Eur J Soil Biol 2001;37:25–50. https://doi.org/10.1016/S1164-5563(01)01067-6.
[98] Feng Y, Xu Y, Yu Y, Xie Z, Lin X. Mechanisms of biochar decreasing methane emission from Chinese paddy soils. Soil Biol Biochem 2012;46:80–8. https://doi.org/10.1016/j.soilbio.2011.11.016.
[99] Sriphirom P, Chidthaisong A, Yagi K, Tripetchkul S, Towprayoon S. Evaluation of biochar applications combined with alternate wetting and drying (AWD) water management in rice field as a methane mitigation option for farmers' adoption. Soil Sci Plant Nutr 2020;66:235–46. https://doi.org/10.1080/00380768.2019.1706431.
[100] Mona S, Malyan SK, Saini N, Deepak B, Pugazhendhi A, Kumar SS. Towards sustainable agriculture with carbon sequestration, and greenhouse gas mitigation using algal biochar. Chemosphere 2021;275:129856. https://doi.org/10.1016/j.chemosphere.2021.129856.
[101] Wu Z, Song Y, Shen H, Jiang X, Li B, Xiong Z. Biochar can mitigate methane emissions by improving methanotrophs for prolonged period in fertilized paddy soils. Environ Pollut 2019;253:1038–46. https://doi.org/10.1016/j.envpol.2019.07.073.
[102] Zhao Q, Wang Y, Xu Z, Yu Z. How does biochar amendment affect soil methane oxidation? A review. J Soils Sediments 2021. https://doi.org/10.1007/s11368-021-02889-z.
[103] Pratiwi EPA, Shinogi Y. Rice husk biochar application to paddy soil and its effects on soil physical properties, plant growth, and methane emission. Paddy Water Environ 2016;14:521–32. https://doi.org/10.1007/s10333-015-0521-z.
[104] Han X, Sun X, Wang C, Wu M, Dong D, Zhong T, et al. Mitigating methane emission from paddy soil with rice-straw biochar amendment under projected climate change. Sci Rep 2016;6:1–10. https://doi.org/10.1038/srep24731.
[105] Ly P, Duong Vu Q, Jensen LS, Pandey A, de Neergaard A. Effects of rice straw, biochar and mineral fertiliser on methane (CH4) and nitrous oxide (N2O) emissions from rice (Oryza sativa L.) grown in a rain-fed lowland rice soil of Cambodia: a pot experiment. Paddy Water Environ 2015;13:465–75. https://doi.org/10.1007/s10333-014-0464-9.
[106] Wu Z, Zhang X, Dong Y, Li B, Xiong Z. Biochar amendment reduced greenhouse gas intensities in the rice-wheat rotation system: six-year field observation and meta-analysis. Agric For Meteorol 2019;278. https://doi.org/10.1016/j.agrformet.2019.107625.
[107] Cai F, Feng Z, Zhu L. Effects of biochar on CH4 emission with straw application on paddy soil. J Soils Sediments 2018;18:599–609. https://doi.org/10.1007/s11368-017-1761-x.
[108] Nan Q, Xin L, Qin Y, Waqas M, Wu W. Exploring long-term effects of biochar on mitigating methane emissions from paddy soil: a review. Biochar 2021. https://doi.org/10.1007/s42773-021-00096-0.
[109] Wang N, Chang ZZ, Chang ZZ, Xue XM, Yu JG, Shi XX, et al. Biochar decreases nitrogen oxide and enhances methane emissions via altering microbial community composition of anaerobic paddy soil. Sci Total Environ 2017;581–582:689–96. https://doi.org/10.1016/j.scitotenv.2016.12.181.
[110] Qi L, Pokharel P, Chang SX, Zhou P, Niu H, He X, et al. Biochar application increased methane emission, soil carbon storage and net ecosystem carbon budget in a 2-year vegetable–rice rotation. Agric Ecosyst Environ 2020;292. https://doi.org/10.1016/j.agee.2020.106831.
[111] Zhang A, Cui L, Pan G, Li L, Hussain Q, Zhang X, et al. Effect of biochar amendment on yield and methane and nitrous oxide emissions from a rice paddy from Tai Lake plain, China. Agric Ecosyst Environ 2010;139:469–75. https://doi.org/10.1016/j.agee.2010.09.003.
[112] Shao Q, Ju Y, Guo W, Xia X, Bian R, Li L, et al. Pyrolyzed municipal sewage sludge ensured safe grain production while reduced C emissions in a paddy soil under rice and wheat rotation. Environ Sci Pollut Res 2019;26:9244–56. https://doi.org/10.1007/s11356-019-04417-6.
[113] Kowshika N, Maragatham N, Geethalaksmi V, Maheswari M, Panneerselvam S. Impact of soil amendments on methane emission from rice field. J Agrometerorology 2017;19:256–8.
[114] Pandey A, Mai VT, Vu DQ, Bui TPL, Mai TLA, Jensen LS, et al. Organic matter and water management strategies to reduce methane and nitrous oxide emissions from rice paddies in Vietnam. Agric Ecosyst Environ 2014;196:137–46. https://doi.org/10.1016/j.agee.2014.06.010.
[115] Singla A, Inubushi K. Effect of biochar on CH4 and N2O emission from soils vegetated with paddy. Paddy Water Environ 2014;12:239–43. https://doi.org/10.1007/s10333-013-0357-3.
[116] He T, Liu D, Yuan J, Luo J, Lindsey S, Bolan N, et al. Effects of application of inhibitors and biochar to fertilizer on gaseous nitrogen emissions from an intensively managed wheat field. Sci Total Environ 2018;628–629:121–30. https://doi.org/10.1016/j.scitotenv.2018.02.048.
[117] Niu Y, Chen Z, Müller C, Zaman MM, Kim D, Yu H, et al. Yield-scaled N2O emissions were effectively reduced by biochar amendment of sandy loam soil under maize - wheat rotation in the North China Plain. Atmos Environ 2017;170:58–70. https://doi.org/10.1016/j.atmosenv.2017.09.050.
[118] Xiang J, Liu D, Ding W, Yuan J, Lin Y. Effects of biochar on nitrous oxide and nitric oxide emissions from paddy field during the wheat growth season. J Clean Prod 2015;104:52–8. https://doi.org/10.1016/j.jclepro.2014.12.038.
[119] Yang W, Feng G, Miles D, Gao L, Jia Y, Li C, et al. Impact of biochar on greenhouse gas emissions and soil carbon sequestration in corn grown under drip irrigation with mulching. Sci Total Environ 2020;729:138752. https://doi.org/10.1016/j.scitotenv.2020.138752.
[120] Niu Y, Luo J, Liu D, Müller C, Zaman M, Lindsey S, et al. Effect of biochar and nitrapyrin on nitrous oxide and nitric oxide emissions from a sandy loam soil cropped to maize. Biol Fertil Soils 2018;54:645–58. https://doi.org/10.1007/s00374-018-1289-2.
[121] Zhang D, Pan G, Wu G, Kibue GW, Li L, Zhang X, et al. Biochar helps enhance maize productivity and reduce greenhouse gas emissions under balanced fertilization in a rainfed low fertility inceptisol. Chemosphere 2016;142:106–13. https://doi.org/10.1016/j.chemosphere.2015.04.088.
[122] Hüppi R, Felber R, Neftel A, Six J, Leifeld J. Effect of biochar and liming on soil nitrous oxide emissions from a temperate maize cropping system. Soil 2015;1:707–17. https://doi.org/10.5194/soil-1-707-2015.
[123] Fagodiya RK, Pathak H, Bhatia A, Jain N, Kumar A, Malyan SK. Global warming impacts of nitrogen use in agriculture: an assessment for India since 1960. Carbon Manag 2020;11:291–301. https://doi.org/10.1080/17583004.2020.1752061.
[124] Fagodiya RK, Pathak H, Kumar A, Bhatia A, Jain N. Global temperature change potential of nitrogen use in agriculture: a 50-year assessment. Sci Rep 2017;7:1–8. https://doi.org/10.1038/srep44928.
[125] Fagodiya RK, Pathak H, Bhatia A, Jain N, Gupta DK, Kumar A, et al. Nitrous oxide emission and mitigation from maize–wheat rotation in the upper Indo-Gangetic Plains. Carbon Manag 2019;10:489–99. https://doi.org/10.1080/17583004.2019.1650579.
[126] Malyan SK, Bhatia A, Tomer R, Harit RC, Jain N, Bhowmik A, et al. Mitigation of yield-scaled greenhouse gas emissions from irrigated rice through Azolla, Blue-green algae, and plant growth–promoting bacteria. Environ Sci Pollut Res 2021. https://doi.org/10.1007/s11356-021-14210-z.
[127] Cayuela ML, van Zwieten L, Singh BP, Jeffery S, Roig A, Sánchez-Monedero MA. Biochar's role in mitigating soil nitrous oxide emissions: a review and meta-

analysis. Agric Ecosyst Environ 2014;191:5–16. https://doi.org/10.1016/j.agee.2013.10.009.
[128] Verhofstad MJJM, Poelen MDM, van Kempen MML, Bakker ES, Smolders AJP. Finding the harvesting frequency to maximize nutrient removal in a constructed wetland dominated by submerged aquatic plants. Ecol Eng 2017;106:423–30. https://doi.org/10.1016/j.ecoleng.2017.06.012.
[129] Borchard N, Schirrmann M, Cayuela ML, Kammann C, Wrage-Mönnig N, Estavillo JM, et al. Biochar, soil and land-use interactions that reduce nitrate leaching and N2O emissions: a meta-analysis. Sci Total Environ 2019;651:2354–64. https://doi.org/10.1016/j.scitotenv.2018.10.060.
[130] Shakoor A, Shahzad SM, Chatterjee N, Arif MS, Farooq TH, Altaf MM, et al. Nitrous oxide emission from agricultural soils: application of animal manure or biochar? A global meta-analysis. J Environ Manag 2021;285:112170. https://doi.org/10.1016/j.jenvman.2021.112170.
[131] Grutzmacher P, Puga AP, Bibar MPS, Coscione AR, Packer AP, de Andrade CA. Carbon stability and mitigation of fertilizer induced N2O emissions in soil amended with biochar. Sci Total Environ 2018;625:1459–66. https://doi.org/10.1016/j.scitotenv.2017.12.196.
[132] Gardiner CA, Clough TJ, Cameron KC, Di HJ, Edwards GR, de Klein CAM. Potential inhibition of urine patch nitrous oxide emissions by Plantago lanceolata and its metabolite aucubin. New Zeal J Agric Res 2018;61:495–503. https://doi.org/10.1080/00288233.2017.1411953.
[133] Harter J, Krause HM, Schuettler S, Ruser R, Fromme M, Scholten T, et al. Linking N2O emissions from biochar-amended soil to the structure and function of the N-cycling microbial community. ISME J 2014;8:660–74. https://doi.org/10.1038/ismej.2013.160.
[134] Jacquot J. Can a kind of ancient charcoal put the brakes on global warming. Popular Mech 2009.
[135] Lehmann J, Gaunt J, Rondon M. Bio-char sequestration in terrestrial ecosystems - a review. Mitig Adapt Strategies Glob Change 2006;11:403–27. https://doi.org/10.1007/s11027-005-9006-5.
[136] Purakayastha TJ, Bera T, Bhaduri D, Sarkar B, Mandal S, Wade P, et al. A review on biochar modulated soil condition improvements and nutrient dynamics concerning crop yields: pathways to climate change mitigation and global food security. Chemosphere 2019;227:345–65. https://doi.org/10.1016/j.chemosphere.2019.03.170.
[137] Wiesmeier M, Urbanski L, Hobley E, Lang B, von Lützow M, Marin-Spiotta E, et al. Soil organic carbon storage as a key function of soils - a review of drivers and indicators at various scales. Geoderma 2019;333:149–62. https://doi.org/10.1016/j.geoderma.2018.07.026.
[138] Leng L, Huang H, Li H, Li J, Zhou W. Biochar stability assessment methods: a review. Sci Total Environ 2019;647:210–22. https://doi.org/10.1016/j.scitotenv.2018.07.402.
[139] Singh BP, Cowie AL, Smernik RJ. Biochar carbon stability in a clayey soil as a function of feedstock and pyrolysis temperature. Environ Sci Technol 2012;46:11770–8. https://doi.org/10.1021/es302545b.
[140] Paustian K, Larson E, Kent J, Marx E, Swan A. Soil C sequestration as a biological negative emission strategy. Front Clim 2019;1:1–11. https://doi.org/10.3389/fclim.2019.00008.
[141] Zhang X, Chen C, Chen X, Tao P, Jin Z, Han Z. Persistent effects of biochar on soil organic carbon mineralization and resistant carbon pool in upland red soil, China. Environ Earth Sci 2018;77:1–8. https://doi.org/10.1007/s12665-018-7359-9.
[142] Malyan SK, Kumar A, Baram S, Kumar J, Singh S, Kumar SS, et al. Role of fungi in climate change abatement through carbon sequestration. Recent Adv. White Biotechnol. Through Fungi 2019:283–95. https://doi.org/10.1007/978-3-030-25506-0_11.
[143] El-Naggar A, Lee SS, Awad YM, Yang X, Ryu C, Rizwan M, et al. Influence of soil properties and feedstocks on biochar potential for carbon mineralization and improvement of infertile soils. Geoderma 2018;332:100–8. https://doi.org/10.1016/j.geoderma.2018.06.017.
[144] Fang Y, Singh B, Singh BP, Krull E. Biochar carbon stability in four contrasting soils. Eur J Soil Sci 2014;65:60–71. https://doi.org/10.1111/ejss.12094.
[145] Sheng Y, Zhu L. Biochar alters microbial community and carbon sequestration potential across different soil pH. Sci Total Environ 2018;622–623:1391–9. https://doi.org/10.1016/j.scitotenv.2017.11.337.
[146] Biswas B, Nirola R, Biswas JK, Pereg L, Willett IR, Naidu R. Environmental microbial health under changing climates: state, implication and initiatives for high-performance soils. 2019. https://doi.org/10.1007/978-3-030-26265-5_1.
[147] Chen W, Meng J, Han X, Lan Y, Zhang W. Past, present, and future of biochar. Biochar 2019;1:75–87. https://doi.org/10.1007/s42773-019-00008-3.
[148] Abbas F, Hammad HM, Anwar F, Farooque AA, Jawad R, Bakhat HF, et al. Transforming a valuable bioresource to biochar, its environmental importance, and potential applications in boosting circular bioeconomy while promoting sustainable agriculture. Sustain Times 2021;13:1–16. https://doi.org/10.3390/su13052599.
[149] Wang D, Fonte SJ, Parikh SJ, Six J, Scow KM. Biochar additions can enhance soil structure and the physical stabilization of C in aggregates. Geoderma 2017;303:110–7. https://doi.org/10.1016/j.geoderma.2017.05.027.
[150] Liu Z, Chen X, Jing Y, Li Q, Zhang J, Huang Q. Effects of biochar amendment on rapeseed and sweet potato yields and water stable aggregate in upland red soil. Catena 2014. https://doi.org/10.1016/j.catena.2014.07.005.
[151] Ippolito J, Spokas K, Novak F, Lentz R, Cantrell K. Biochar elemental composition and factors infl uencing nutrient retention. Biochar Environ Manag 2015:1–2. https://doi.org/10.4324/9780203762264-14.
[152] Berek AK, Hue NV, Radovich TJK, Ahmad AA. Biochars improve nutrient phyto-availability of hawai⇔i⇔s highly weathered soils. Agronomy 2018;8:1–18. https://doi.org/10.3390/agronomy8100203.
[153] Berek AK, Hue NV. Characterization of biochars and their use as an amendment to acid soils. Soil Sci 2016;181:412–26. https://doi.org/10.1097/SS.0000000000000177.
[154] Obia A, Mulder J, Martinsen V, Cornelissen G, Børresen T. In situ effects of biochar on aggregation, water retention and porosity in light-textured tropical soils. Soil Tillage Res 2016;155:35–44. https://doi.org/10.1016/j.still.2015.08.002.
[155] Verheijen FGA, Zhuravel A, Silva FC, Amaro A, Ben-Hur M, Keizer JJ. The influence of biochar particle size and concentration on bulk density and maximum water holding capacity of sandy vs sandy loam soil in a column experiment. Geoderma 2019;347:194–202. https://doi.org/10.1016/j.geoderma.2019.03.044.
[156] Hue N. Biochar for maintaining soil health. Soil Heal.; 2020. p. 21–46. https://doi.org/10.1007/978-3-030-44364-1_2.
[157] Fischer BMC, Manzoni S, Morillas L, Garcia M, Johnson MS, Lyon SW. Improving agricultural water use efficiency with biochar – a synthesis of biochar effects on water storage and fluxes across scales. Sci Total Environ 2019;657:853–62. https://doi.org/10.1016/j.scitotenv.2018.11.312.
[158] Thuy Duong V, Minh Khanh N, Thi Hanh Nguyen N, Ngoc Phi N, Tan DUCN, Hoa Kho D. Impact of biochar on the water holding capacity and moisture of basalt and grey soil. J Sci 2019:36. 0.
[159] Jaafar NM, Clode PL, Abbott LK. Soil microbial responses to biochars varying in particle size, surface and pore properties. Pedosphere 2015;25:770–80. https://doi.org/10.1016/S1002-0160(15)30058-8.
[160] Palansooriya KN, Wong JTF, Hashimoto Y, Huang L, Rinklebe J, Chang SX, et al. Response of microbial communities to biochar-amended soils: a critical review. Biochar 2019;1:3–22. https://doi.org/10.1007/s42773-019-00009-2.
[161] Bhaduri D, Saha A, Desai D, Meena HN. Restoration of carbon and microbial activity in salt-induced soil by application of peanut shell biochar during short-term incubation study. Chemosphere 2016;148:86–98. https://doi.org/10.1016/j.chemosphere.2015.12.130.
[162] Demisie W, Liu Z, Zhang M. Effect of biochar on carbon fractions and enzyme activity of red soil. Catena 2014;121:214–21. https://doi.org/10.1016/j.catena.2014.05.020.
[163] Luo Y, Dungait JAJ, Zhao X, Brookes PC, Durenkamp M, Li G, et al. Pyrolysis temperature during biochar production alters its subsequent utilization by microorganisms in an acid arable soil. Land Degrad Dev 2018;29:2183–8. https://doi.org/10.1002/ldr.2846.
[164] Gomez JD, Denef K, Stewart CE, Zheng J, Cotrufo MF. Biochar addition rate influences soil microbial abundance and activity in temperate soils. Eur J Soil Sci 2014;65:28–39. https://doi.org/10.1111/ejss.12097.
[165] Palanisamy G, Jung HY, Sadhasivam T, Kurkuri MD, Kim SC, Roh SH. A comprehensive review on microbial fuel cell technologies: processes, utilization, and advanced developments in electrodes and membranes. J Clean Prod 2019;221:598–621. https://doi.org/10.1016/j.jclepro.2019.02.172.
[166] Do Minh T, Song J, Deb A, Cha L, Srivastava V, Sillanpää M. Biochar based catalysts for the abatement of emerging pollutants: a review. Chem Eng J 2020;394:124856. https://doi.org/10.1016/j.cej.2020.124856.
[167] Ponnam V, Katari NK, Mandapati RN, Nannapaneni S, Tondepu S, Jonnalagadda SB. Efficacy of biochar in removal of organic pesticide, Bentazone from watershed systems. J Environ Sci Health Part B Pestic Food Contam Agric Wastes 2020;55:396–405. https://doi.org/10.1080/03601234.2019.1707008.
[168] Zheng W, Guo M, Chow T, Bennett DN, Rajagopalan N. Sorption properties of greenwaste biochar for two triazine pesticides. J Hazard Mater 2010;181:121–6. https://doi.org/10.1016/j.jhazmat.2010.04.103.
[169] Xiao F, Cheng J, Cao W, Yang C, Chen J, Luo Z. Removal of heavy metals from aqueous solution using chitosan-combined magnetic biochars. J Colloid Interface Sci 2019;540:579–84. https://doi.org/10.1016/j.jcis.2019.01.068.
[170] Yadav IC, Devi NL, Syed JH, Cheng Z, Li J, Zhang G, et al. Current status of persistent organic pesticides residues in air, water, and soil, and their possible effect on neighboring countries: a comprehensive review of India. Sci Total Environ 2015;511:123–37. https://doi.org/10.1016/j.scitotenv.2014.12.041.
[171] Kumar SS, Ghosh P, Malyan SK, Sharma J, Kumar V. A comprehensive review on enzymatic degradation of the organophosphate pesticide malathion in the environment. J Environ Sci Heal Part C 2019;37. Press.
[172] Suo F, You X, Ma Y, Li Y. Rapid removal of triazine pesticides by P doped biochar and the adsorption mechanism. Chemosphere 2019;235:918–25. https://doi.org/10.1016/j.chemosphere.2019.06.158.
[173] Mandal A, Singh N, Purakayastha TJ. Characterization of pesticide sorption behaviour of slow pyrolysis biochars as low cost adsorbent for atrazine and imidacloprid removal. Sci Total Environ 2017;577:376–85. https://doi.org/10.1016/j.scitotenv.2016.10.204.
[174] Wang P, Yin Y, Guo Y, Wang C. Removal of chlorpyrifos from waste water by wheat straw-derived biochar synthesized through oxygen-limited method. RSC Adv 2015;5:72572–8. https://doi.org/10.1039/c5ra10487d.
[175] Tan G, Sun W, Xu Y, Wang H, Xu N. Sorption of mercury (II) and atrazine by biochar, modified biochars and biochar based activated carbon in aqueous solution. Bioresour Technol 2016;211:727–35. https://doi.org/10.1016/j.biortech.2016.03.147.
[176] Chan CCV, Lari K, Soulsbury K. An intermittently operated biochar filter to remove chemical contaminants from drinking water. Int J Environ Sci Technol 2020;17:3119–30. https://doi.org/10.1007/s13762-019-02615-w.

[177] Okoya AA, Adegbaju OS, Akinola OE, Akinyele AB, Amuda OS. Comparative assessment of the efficiency of rice husk biochar and conventional water treatment method to remove chlorpyrifos from pesticide polluted water. Curr J Appl Sci Technol 2020;39:1–11. https://doi.org/10.9734/cjast/2020/v39i230491.
[178] Srinivasa Gowd S, Govil PK. Distribution of heavy metals in surface water of Ranipet industrial area in Tamil Nadu, India. Environ Monit Assess 2008;136:197–207. https://doi.org/10.1007/s10661-007-9675-5.
[179] Kumar A, Bharti, Malyan SK, Kumar SS, Dutt D, Kumar V. An assessment of trace element contamination in groundwater aquifers of Saharanpur, Western Uttar Pradesh, India. Biocatal Agric Biotechnol 2019;20:101213. https://doi.org/10.1016/j.bcab.2019.101213.
[180] Malyan SK, Singh R, Rawat M, Kumar M, Pugazhendhi A, Kumar A, et al. An overview of carcinogenic pollutants in groundwater of India. Biocatal Agric Biotechnol 2019;21:101288. https://doi.org/10.1016/j.bcab.2019.101288.
[181] Inyang MI, Gao B, Yao Y, Xue Y, Zimmerman A, Mosa A, et al. A review of biochar as a low-cost adsorbent for aqueous heavy metal removal. Crit Rev Environ Sci Technol 2016;46:406–33. https://doi.org/10.1080/10643389.2015.1096880.
[182] Kumar A, Joshi H, Kumar A. Remediation of arsenic by metal/metal oxide based nanocomposites/nanohybrids: contamination scenario in groundwater, practical challenges, and future perspectives. Separ Purif Rev 2020:1–32. https://doi.org/10.1080/15422119.2020.1744649. 00.
[183] Li H, Xiong J, Zhang G, Liang A, Long J, Xiao T, et al. Enhanced thallium(I) removal from wastewater using hypochlorite oxidation coupled with magnetite-based biochar adsorption. Sci Total Environ 2020;698:134166. https://doi.org/10.1016/j.scitotenv.2019.134166.
[184] Park JH, Ok YS, Kim SH, Cho JS, Heo JS, Delaune RD, et al. Competitive adsorption of heavy metals onto sesame straw biochar in aqueous solutions. Chemosphere 2016;142:77–83. https://doi.org/10.1016/j.chemosphere.2015.05.093.
[185] Wang H, Gao B, Wang S, Fang J, Xue Y, Yang K. Removal of Pb(II), Cu(II), and Cd (II) from aqueous solutions by biochar derived from KMnO4 treated hickory wood. Bioresour Technol 2015;197:356–62. https://doi.org/10.1016/j.biortech.2015.08.132.
[186] Agrafioti E, Kalderis D, Diamadopoulos E. Arsenic and chromium removal from water using biochars derived from rice husk, organic solid wastes and sewage sludge. J Environ Manag 2014;133:309–14. https://doi.org/10.1016/j.jenvman.2013.12.007.
[187] Ahluwalia SS, Goyal D. Microbial and plant derived biomass for removal of heavy metals from wastewater. Bioresour Technol 2007;98:2243–57. https://doi.org/10.1016/j.biortech.2005.12.006.
[188] Renu, Agarwal M, Singh K. Heavy metal removal from wastewater using various adsorbents: a review. J Water Reuse Desalin 2017;7:387–419. https://doi.org/10.2166/wrd.2016.104.
[189] Ambaye TG, Vaccari M, van Hullebusch ED, Amrane A, Rtimi S. Mechanisms and adsorption capacities of biochar for the removal of organic and inorganic pollutants from industrial wastewater. Int J Environ Sci Technol 2020. https://doi.org/10.1007/s13762-020-03060-w.
[190] Mohan D, Kumar H, Sarswat A, Alexandre-Franco M, Pittman CU. Cadmium and lead remediation using magnetic oak wood and oak bark fast pyrolysis bio-chars. Chem Eng J 2014;236:513–28. https://doi.org/10.1016/j.cej.2013.09.057.
[191] Kiliç M, Kirbiyik Ç, Çepelioğullar Ö, Pütün AE. Adsorption of heavy metal ions from aqueous solutions by bio-char, a by-product of pyrolysis. Appl Surf Sci 2013;283:856–62. https://doi.org/10.1016/j.apsusc.2013.07.033.
[192] Ni BJ, Huang QS, Wang C, Ni TY, Sun J, Wei W. Competitive adsorption of heavy metals in aqueous solution onto biochar derived from anaerobically digested sludge. Chemosphere 2019;219:351–7. https://doi.org/10.1016/j.chemosphere.2018.12.053.
[193] Tan Z, Wang Y, Kasiulienė A, Huang C, Ai P. Cadmium removal potential by rice straw-derived magnetic biochar. Clean Technol Environ Policy 2017;19:761–74. https://doi.org/10.1007/s10098-016-1264-2.
[194] Trakal L, Veselská V, Šafařík I, Vítková M, Číhalová S, Komárek M. Lead and cadmium sorption mechanisms on magnetically modified biochars. Bioresour Technol 2016;203:318–24. https://doi.org/10.1016/j.biortech.2015.12.056.
[195] Cheng D, Ngo HH, Guo W, Chang SW, Nguyen DD, Zhang X, et al. Feasibility study on a new pomelo peel derived biochar for tetracycline antibiotics removal in swine wastewater. Sci Total Environ 2020;720:137662. https://doi.org/10.1016/j.scitotenv.2020.137662.
[196] Huang J, Zimmerman AR, Chen H, Gao B. Ball milled biochar effectively removes sulfamethoxazole and sulfapyridine antibiotics from water and wastewater. Environ Pollut 2020;258:113809. https://doi.org/10.1016/j.envpol.2019.113809.
[197] Zhang M, Meng J, Liu Q, Gu S, Zhao L, Dong M, et al. Corn stover-derived biochar for efficient adsorption of oxytetracycline from wastewater. J Mater Res 2019;34:3050–60. https://doi.org/10.1557/jmr.2019.198.
[198] Wei J, Liu Y, Li J, Zhu Y, Yu H, Peng Y. Adsorption and co-adsorption of tetracycline and doxycycline by one-step synthesized iron loaded sludge biochar. Chemosphere 2019;236:124254. https://doi.org/10.1016/j.chemosphere.2019.06.224.
[199] Li R, Wang Z, Zhao X, Li X, Xie X. Magnetic biochar-based manganese oxide composite for enhanced fluoroquinolone antibiotic removal from water. Environ Sci Pollut Res 2018;25:31136–48. https://doi.org/10.1007/s11356-018-3064-1.
[200] Oladipo AA, Ifebajo AO. Highly efficient magnetic chicken bone biochar for removal of tetracycline and fluorescent dye from wastewater: two-stage adsorber analysis. J Environ Manag 2018;209:9–16. https://doi.org/10.1016/j.jenvman.2017.12.030.
[201] Kong X, Liu Y, Pi J, Li W, Liao QJ, Shang J. Low-cost magnetic herbal biochar: characterization and application for antibiotic removal. Environ Sci Pollut Res 2017;24:6679–87. https://doi.org/10.1007/s11356-017-8376-z.
[202] Shang JG, Kong XR, He LL, Li WH, Liao QJH. Low-cost biochar derived from herbal residue: characterization and application for ciprofloxacin adsorption. Int J Environ Sci Technol 2016;13:2449–58. https://doi.org/10.1007/s13762-016-1075-3.
[203] Wang Y, Lu J, Wu J, Liu Q, Zhang H, Jin S. Adsorptive removal of fluoroquinolone antibiotics using bamboo biochar. Sustain Times 2015;7:12947–57. https://doi.org/10.3390/su70912947.
[204] Rajapaksha AU, Vithanage M, Ahmad M, Seo DC, Cho JS, Lee SE, et al. Enhanced sulfamethazine removal by steam-activated invasive plant-derived biochar. J Hazard Mater 2015;290:43–50. https://doi.org/10.1016/j.jhazmat.2015.02.046.
[205] Peiris C, Gunatilake SR, Mlsna TE, Mohan D, Vithanage M. Biochar based removal of antibiotic sulfonamides and tetracyclines in aquatic environments: a critical review. Bioresour Technol 2017;246:150–9. https://doi.org/10.1016/j.biortech.2017.07.150.
[206] Zhou Y, Liu X, Xiang Y, Wang P, Zhang J, Zhang F, et al. Modification of biochar derived from sawdust and its application in removal of tetracycline and copper from aqueous solution: adsorption mechanism and modelling. Bioresour Technol 2017;245:266–73. https://doi.org/10.1016/j.biortech.2017.08.178.
[207] Zhu S, Huang X, Ma F, Wang L, Duan X, Wang S. Catalytic removal of aqueous contaminants on N-doped graphitic biochars: inherent roles of adsorption and nonradical mechanisms. Environ Sci Technol 2018;52:8649–58. https://doi.org/10.1021/acs.est.8b01817.
[208] Chen Y di, Lin YC, Ho SH, Zhou Y, Ren N qi. Highly efficient adsorption of dyes by biochar derived from pigments-extracted macroalgae pyrolyzed at different temperature. Bioresour Technol 2018;259:104–10. https://doi.org/10.1016/j.biortech.2018.02.094.
[209] Li W, Mu B, Yang Y. Feasibility of industrial-scale treatment of dye wastewater via bio-adsorption technology. Bioresour Technol 2019;277:157–70. https://doi.org/10.1016/j.biortech.2019.01.002.
[210] Yu KL, Show PL, Ong HC, Ling TC, Chen WH, Salleh MAM. Biochar production from microalgae cultivation through pyrolysis as a sustainable carbon sequestration and biorefinery approach. Clean Technol Environ Policy 2018;20. https://doi.org/10.1007/s10098-018-1521-7. 2047–55.
[211] Sewu DD, Boakye P, Woo SH. Highly efficient adsorption of cationic dye by biochar produced with Korean cabbage waste. Bioresour Technol 2017;224:206–13. https://doi.org/10.1016/j.biortech.2016.11.009.
[212] Abd-Elhamid AI, Emran M, El-Sadek MH, El-Shanshory AA, Soliman HMA, Akl MA, et al. Enhanced removal of cationic dye by eco-friendly activated biochar derived from rice straw. Appl Water Sci 2020;10:1–11. https://doi.org/10.1007/s13201-019-1128-0.
[213] Wu J, Yang J, Feng P, Huang G, Xu C, Lin B. High-efficiency removal of dyes from wastewater by fully recycling litchi peel biochar. Chemosphere 2020;246:125734. https://doi.org/10.1016/j.chemosphere.2019.125734.
[214] Yao X, Ji L, Guo J, Ge S, Lu W, Cai L, et al. Magnetic activated biochar nanocomposites derived from wakame and its application in methylene blue adsorption. Bioresour Technol 2020;302:122842. https://doi.org/10.1016/j.biortech.2020.122842.
[215] Ahmad A, Khan N, Giri BS, Chowdhary P, Chaturvedi P. Removal of methylene blue dye using rice husk, cow dung and sludge biochar: characterization, application, and kinetic studies. Bioresour Technol 2020;306:123202. https://doi.org/10.1016/j.biortech.2020.123202.

TITLE/ AUTHOR	Nano-sized mesoporous biochar derived from biomass pyrolysis as electrochemical energy storage supercapacitor / Husain, Z., Shakeelur Raheman, A.R., Ansari, K.B., (...), Qyyum, M.A., Lam, S.S.
SOURCE	Materials Science for Energy Technologies Volume 5, January 2022, Pages 99-109 https://doi.org/10.1016/j.mset.2021.12.003 (Database : Science Direct)

Materials Science for Energy Technologies 5 (2022) 99–109

Contents lists available at ScienceDirect

Materials Science for Energy Technologies

journal homepage: www.keaipublishing.com/en/journals/materials-science-for-energy-technologies

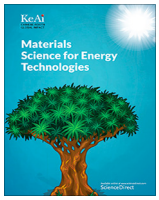

Nano-sized mesoporous biochar derived from biomass pyrolysis as electrochemical energy storage supercapacitor

Zakir Husain [a,b,1], Shakeelur Raheman A.R. [c,1], Khursheed B. Ansari [d,*], Aniruddha B. Pandit [a,*], Mohd Shariq Khan [e], Muhammad Abdul Qyyum [f], Su Shiung Lam [g,h]

[a] Department of Chemical Engineering, Institute of Chemical Technology, Mumbai, Maharashtra 400019, India
[b] Department of Civil Engineering, Indian Institute of Technology, Gandhinagar, Gujarat 382355, India
[c] Department of Applied Science, Shri Vile Parle Kelavani Mandal's Institute of Technology, Dhule, Maharashtra 424001, India
[d] Department of Chemical Engineering, Zakir Husain College of Engineering and Technology, Aligarh Muslim University, Aligarh, Uttar Pradesh 202001, India
[e] Department of Chemical Engineering, College of Engineering, Dhofar University, Salalah 211, Sultanate of Oman
[f] Department of Petroleum & Chemical Engineering, Sultan Qaboos University, Muscat, Oman
[g] Higher Institution Centre of Excellence (HICoE), Institute of Tropical Aquaculture and Fisheries (AKUATROP), Universiti Malaysia Terengganu, Kuala Nerus, Terengganu 21030, Malaysia
[h] Henan Province Forest Resources Sustainable Development and High-value Utilization Engineering Research Center, School of Forestry, Henan Agricultural University, Zhengzhou 450002, China

ARTICLE INFO

Article history:
Received 26 October 2021
Revised 12 December 2021
Accepted 16 December 2021
Available online 22 December 2021

Keywords:
Biomass pellets
Pyrolysis
Nano-sized biochar
Characterization
Pseudo capacitance
Electrochemical performance

ABSTRACT

Energy storage is essential to conserve and deliver energy to end-user with continuity and durability. A sustainable energy supply with minimal process losses requires cost-effective and environmentally friendly energy storage material. In this study, self-co-dopes N (3.65 %) and O (6.44 %) porous biochar were produced from pyrolysis of biomass pellets (made from garden wastes) and examined for energy storage application. The presence of co-doped-heteroatoms within the carbon matrix of biochar resulted in enhanced surface wettability, fast charge transfers, increased electrical conductivity, and low internal resistance. Biochar produced at 800 ℃ (i.e. biochar-800) showed desirable pseudocapacitive nature induced by self-co-doped heteroatoms. Two-electrode measurements in aqueous 1 M H_2SO_4 revealed that biochar-800 possessed 228F g^{-1} of specific capacitance at a current density of 1 Ag^{-1} Additionally, biochar-800 exhibited a high energy density of 7.91 Wh kg^{-1} in aqueous electrolyte and promising cycling stability with 88% capacitance retention after 5000 cycles at 10 A g^{-1}. Enhanced capacitive performance of biochar-800 was assigned to the presence of self-co-doped heteroatom, the high specific surface area of 312 m^2g^{-1}, and self-formed mesopores (pore size around 15.2 nm). This study demonstrates the great promise of porous biochar derived from biomass pellets as a low-cost electrode material for high-performance energy storage devices.

1. Introduction

The growing population and industrial energy demand, depleting traditional fossil fuels, and deteriorating environment have prompted efforts to look for sustainable energy and storage [1]. Nowadays, batteries and supercapacitors are widely used as energy storage devices. Large amounts of energy can be stored in metal-air [2], sodium-sulfur [3], and lithium-ion batteries [4], which can later be utilized when needed. Most batteries, however, work on the electrochemical cycle and hence depend on the electrode and electrolyte materials for their efficiency. Compared to the electrochemical cycle-based batteries, the supercapacitor is electrostatically controlled and shows promising features in operation and sustainability [5,6]. In the context of performance, supercapacitor holds several advantages over batteries, such as high power capacity, fast charging/discharging from several thousand to millions of cycles, but it has the constraint of low energy density [7]. Several nanostructured materials such as graphene [8,9], carbon nanotubes (CNT) [8,10], carbon nanosheets [11], graphene quantum dots (GQDs) [12], porous and mesoporous carbon [13], 3-D graphene sponge, and foam [14] are explored to increase the efficiency of supercapacitor. Notably, it is easy to produce and characterize the nano-materials mentioned above on the laboratory scale; how-

* Corresponding authors.
E-mail addresses: akabadruddin@myamu.ac.in (K.B. Ansari), ab.pandit@ictmumbai.edu.in (A.B. Pandit).
[1] Zakir Husain and Shakeelur Rahman A.R have contributed equally to this work.

https://doi.org/10.1016/j.mset.2021.12.003
2589-2991/

ever, due to the high price of precursor and related tedious synthesis process, nano-material production at a large scale remains challenging. Also, the manufacturing cost of nano-materials is reported to be high (≈ $150 – $200 per kg) [15]. As an alternative, a potentially cheaper biomass-based nano-sized biochar would be more attractive in this scenario (i.e., coconut shell-derived biochar as supercapacitor material, $5 – $40 per kg) [15]. Similarly, metal oxide and conducting polymer-based supercapacitor possess an advantage over biochar-based supercapacitors due to high specific capacitance and pseudocapacitive nature. However, metal oxide suffers in electrical conductivity while conducting polymers experience a gradual loss of capacitive performance [16–18]. It is a known fact that the most critical component for the supercapacitor is the electrode material, which determines its performance. Therefore, the emerging field of supercapacitor research is manufacturing cost-effective and high-performance materials using an easy synthesis method applicable on a large scale [7,19].

A detailed literature review reveals that biomass-derived biochar can be an electrode material for charge storage applications [7,20–22]. Moreover, biomass-derived products can be utilized for energy generation and storage [7,23,24]. The different biomass-based precursors, viz. cellulose, orange peel, coconut-shell, corncob, peanut shells, carbon stalk, have been investigated for their conversion into supercapacitor material (or biochar) because of their abundant availability, cost-effectiveness, and renewable nature [19,25–29]. Moreover, the biochar showed a unique microstructure, good electrical conductivity, high specific surface area (800–3012 m^2g^{-1}), and the chemical composition comprising natural self-doped heteroatoms [7,30–32]. The naturally embedded heteroatoms in the biochar structure, i.e., nitrogen (N), sulfur (S), phosphorus (P), calcium (Ca), play an essential role as an electron donor, maintaining surface hydrophilicity and excellent cyclic stability [33–38]. Further, the hetero-atoms improve carbon wettability, electron conductivity, and basic strength, inducing pseudo-capacitive behavior [7]. The synergistic effect of the pore structure, which is due to unique feedstock (biomass) microstructure and rich heteroatoms, makes the self-doped biochar a potential candidate for the energy storage device [39].

Xu et al. performed the carbonization of gelatin (an animal derivative) under an inert atmosphere to make self-doped biocarbon (specific surface area ≈ 3012 m^2g^{-1}) and test for supercapacitor application [40]. The nitrogen on the carbon surface remained the most common mono-heteroatom, which was further classified into four standard forms, such as pyridine-N (N-6), pyrrolic/pyridine-N (N-5), quaternary- N (N-Q), and oxidized pyridine-N (N-X) [41]. Consequently, in multiple heteroatom co-doping, carbon materials comprised O-N-S heteroatoms [41]. Numerous research has shown the potential of O-N-S co-doped hierarchical porous carbon for use as supercapacitor electrodes (summarize in Chen et al., 2019) [2,42,43]. Compared to mono-heteroatom doping, carbon with multi-heteroatom doping showed a higher specific capacity [43].

The literature suggests that biochar prepared from the pyrolysis of biomass precursors (e.g., agricultural waste, wood residue, and manure) hold a hierarchical porous structure and remain promising for supercapacitor applications [44,45]. Wang et al. demonstrated that Ni-loaded biochar prepared from dairy manure and sewage sludge pyrolysis could be a good supercapacitor material with 123 Fg^{-1} specific capacitance [46]. The specific capacitance of biochar was reduced by only 2% after 1000 charge-discharge cycles. In another report, the biochar prepared from the carbonization of southern yellow pine sawdust was utilized as an anode electrode material in the supercapacitor [47]. The capacitor exhibited the specific capacitance of 21 Fg^{-1} at 5 mV s^{-1} along with no decay in performance after 1000 cycles. The Bamboo fibers were prepared using two-step carbonization (viz. hydrothermal treatment at 180 °C in acidic media followed by pyrolysis at 800 °C under Argon atmosphere indicated a high specific capacitance of 510 Fg^{-1} at 0.4 A g^{-1} [45]. Further, it showed excellent charge storage stability over 5000 charge-discharge cycles. Furthermore, following gamma radiation, the biomass-derived biochar demonstrated enhanced supercapacitor performance [48]. After gamma irradiation (dose of 100 kGy), the biochar showed higher specific capacitance (246.2 Fg^{-1}) than the untreated biochar (115.3 Fg^{-1}). Additionally, the biochar depicted around 96% capacity retention for 10,000 cycles at 2 Ag^{-1} because of its particle size and enhanced porosity (after irradiation). The hollow tubular-like porous carbon (HT-PC) was prepared from the biomass (or waste feather finger grass flower) carbonization (via pyrolysis at 550 °C followed by acid wash and drying) [49]. HT-PC indicated the highest specific capacitance of 315 Fg^{-1} at 1 Ag^{-1} and retained 96% of its capacitance after 50,000 cycles. The supercapacitor features of the biochar remained strongly dependant on the biomass sources and the preparation methods. The reports on nano-sized biochar prepared from garden waste biomasses are rarely available in the literature to the best of our knowledge. Therefore, the current research is aimed to produce nano-sized biochar (from the waste garden biomass material or biomass pellet) equipped with a high energy density for supercapacitor applications. This work explicitly utilized biochar (one of the byproducts of the biomass pyrolysis process) and demonstrated its potential for use as an energy storage material for supercapacitors. The biochar containing heteroatoms were prepared at 600 ℃ and 800 ℃ and named biochar-600 and biochar-800, respectively. The ability of the biochar as a supercapacitor was evaluated by extensive characterization such as X-ray diffraction (XRD), Raman spectroscopy, energy-dispersive X-ray (EDX), transmission electron microscopy (TEM), BET surface area analysis, and X-ray photon spectroscopy. Additionally, the biochar's cyclic voltammetry and specific capacitance measurements were performed at various current densities to evaluate its capacitance, cyclic stability, and energy storage capacity.

2. Experimental section

The preparation of biomass pellets from garden biomass waste and biomass-derived biochar formation is shown in Fig. 1[A] and discussed below.

2.1. Preparation of biomass pellet

The following steps were involved in the preparation and production of biomass pellets from garden waste:

(i) Collection of biomass such as wood straw, chips, grass, and garden waste (ii) Size reduction of biomass in a crusher/shredder to achieve it in the form of powder (particle size ≈ 1 – 4 mm) (iii) Addition of water to the shredded biomass for the process of lignin melting that served as a binder (iv) Transformation of biomass powder into pellets (dia. 8 – 10 mm and length 15 – 35 mm) in a Pellet Maker PM-125 machines (Fig. 1[A]). The biomass pellet density and moisture content were estimated at 1100–1300 kg^{-1} m^3 and 7 – 10 wt%, respectively.

2.2. Production of biochar

The dried biomass pellets (i.e., 10gm) with an initial moisture content of 7 wt% was placed in the quartz boat for the pyrolysis process. The pyrolysis of biomass pellets was conducted in a tubular quartz reactor at 600 ℃ and 800 ℃ at constant heating rate 5 °C/min to convert it into biochar (Fig. 1[B]) During the pyrolysis process nitrogen (N) gas at a 100 ml/min flow rate was supplied to maintain the inert atmosphere. Pyrolysis vapors were released by

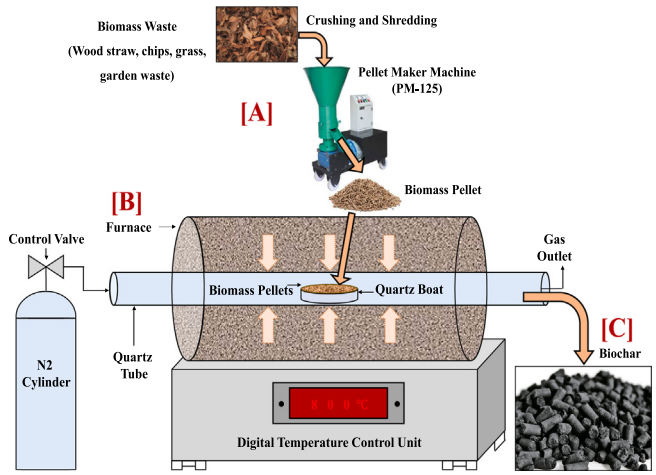

Fig. 1. [A] Preparation of biomass pellets [B] Preparation of biomass-derived biochar [C] Camera image of biomass-derived biochar (biochar-800).

the thermal decomposition of biomass pellets, which instantly left the reactor system because of the constant sweeping by the inert nitrogen gas, leaving behind carbonaceous biochar as the final product. The product samples (i.e., biochar-600 and biochar-800) were collected from the reactor at the end of the operation. Finally, to obtain the nano-sized carbon sheet within biochar, the collected biochar-600 and biochar-800 were crushed in mortar-pestle, dispersed in an ethanol solution, and kept for 6 h in an ultrasonic bath. The biochar-800 image is shown in Fig. 1[C]. The biochar samples were then employed to fabricate a coin cell for the two-electrode system, which is discussed in the next section.

2.3. Fabrication of cell for two-electrode measurement

The two-electrode coin cell used to fabricate the supercapacitor is depicted in Fig. S1 (supporting information). The electrode material was prepared by adding 90 wt% of biochar (in powder form), 5 wt% acetylene black, and 5 wt% polyvinylidene fluoride (PVDF) into the 2 ml N-Methyl-2-pyrrolidone (NMP) followed by bath sonication to form the uniform slurry. The current collector (i.e., conducting carbon sheet) was weighed before and after the material deposition to control the electrode material's mass loading. Besides the two conducting carbon sheets, the slurry of the electrode material was spin-coated evenly, followed by drying at 60 °C in the vacuum oven. Mass loading of 1.5 mg was uniformly deposited on each electrode with a surface area of 0.9 cm^2. An electrolyte-soaked glass fiber separator (Whatman) was placed between these two electrodes, and the supercapacitor cell was assembled in the CR2032 type coin cell. All electrochemical measurements were conducted on the CHI-302 N electrochemical workstation. In 1 M H_2SO_4, cyclic voltammetry (CV) measurements were performed in the range of 0 V to 1 V by varying the scan rate in 5 mVs^{-1} to 150 mVs^{-1}. The H_2SO_4 was selected as an electrolyte over KOH (potassium hydroxide) or KNO_3 (potassium nitrite) electrolytes because of its smaller ions size, which readily enters into the electrode pores and thus helps in enhancing the electrochemical energy storage performance. Further, the galvanostatic charge–discharge (GCD) measurement was conducted in the range of 1 Ag^{-1} to 10 Ag^{-1} and over a voltage range of 0 V to 1 V. Further, the electrochemical impedance spectroscopy test was conducted with an A.C. amplitude of 10 mV in the frequency range of 10 kHz to 10 mHz.

For quantitative purposes, in the two-electrode symmetric cell, the specific capacitance (C_S) of the electrode was measured from the charge–discharge curve value using the equation (1) [50].

$$C_s = \frac{2 \times I\Delta t}{m\Delta v} \quad (1)$$

$C_s$denotes the specific capacitance of electrode in (F g^{-1}); I (A) represents the constant discharge current, 'm' indicates the mass of active material loaded on one of the electrodes, and Δv signifies the potential change in (V) within the discharge time Δt (in second). The energy density of the supercapacitor was calculated by using equation (2).

$$E = \frac{1}{2} C_s V^2 \quad (2)$$

2.4. Characterization of biochar

The detailed characterization of biochar for its potential as a supercapacitor is discussed below.

- ***The crystallinity of biochar:*** Using the powder X-Ray diffraction technique (XRD), the prepared biochar's crystalline nature was determined, and the patterns were reported using CuKα radiation (a = 1.54 Å) in BRUKER D8 ADVANCE.
- ***Surface morphology of biochar:*** The surface morphology and structures of biochar samples were characterized using higher-resolution transmission electron microscopy (HR-TEM). JEM 2100F by JEOL instrument was used to measure particle size and dispersion of biochar with an operating voltage of 200 kV.
- ***Surface area and pore structure analysis of biochar:*** Brunauer-Emmett-Teller (BET) technique was used for the specific surface area measurement of biochar samples in a SMART SORM 93 instrument. The pore size distributions were calculated using the Barrett-Joyner-Halenda (BJH) method. Moreover, BRUKER RFS 27 Standalone FT-Raman Spectrometer was used to understand the scattering center of a porous structure of biochar samples with a spectral range of 4000–50 cm^{-1} using Nd: YAG 1064 nm LASER source.
- ***Surface chemical composition of biochar:*** The surface composition of biochar samples was determined through X-ray photoelectron spectroscopy (XPS) on a PHI 5000 Versa Probe III (by physical electronics) with a monochromatic, micro-focused, scanning x-ray source.

3. Result and discussion

3.1. X-ray diffraction analysis of biochar

The results on X-ray diffraction (XRD) analysis of biochar-600 and biochar-800 samples are shown in Fig. 2[A]. The 2θ values of XRD measurement are found in the range of 10° to 60° at 0.02^0 steps with a count time of 0.2 s. The diffraction peak intensity at angle 2θ values of 25.8° and 43.7° are assigned to (002) well-

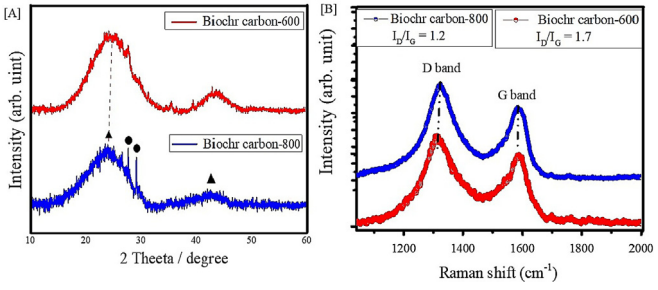

Fig. 2. Characterization of biochar via [A] X-Ray Diffraction and [B] Raman spectroscopy.

developed graphitic stacking and (100) reflection of the disordered carbon layer, respectively. With an increase in the pyrolysis temperature, the intensity of peaks (002) and (100) of biochar-800 sample decreased, referring to the graphitic structure of amorphous carbon [51]. Furthermore, the diffraction peak intensity at 43.7° of biochar-800 is reduced at a higher temperature, confirming pore formation within the material [52]. In the case of biochar-800, the diffraction peak intensity at 28.1° was due to inorganic components (SiO_2) within the biomass collected from the garden. The diffraction peak intensity at 29.4° revealed $CaCO_3$ due to the presence of the minerals in natural biomass [53].

3.2. Raman spectroscopy analysis of biochar

Raman spectroscopy was performed to analyze the defects and nature of the disorder within the biochar materials. In Fig. 2[B], the spectra for biochar-600 and biochar-800 show the peaks at nearly 1317 $cm^{-1}$and 1327 cm^{-1} are assigned to the D band (disorder sp^2 hybridized carbon atoms of graphite and defect site). The peaks located at 1581 cm^{-1} and 1583 cm^{-1} are G band which corresponds to the phonon mode in-plane vibration of sp^2 bonded carbon atom and serve as graphitic carbon fingerprints. The D and G bands' intensity ratio (I_D/I_G) reflects the degree of disorder in the carbon material [54]. Herein biochar-800 shows the comparatively lower I_D/I_G ratio of 1.2 than biochar-600 (I_D/I_G ratio of 1.7), which is assigned to the high density of disorder and defects in biochar-600 [55]. As a result, the biochar-800 has low sp^3 amorphous carbon rather than nanocrystalline graphite, which is consistent with the XRD results [56].

3.3. Surface area analysis of biochar

The surface area and porosity are the essential properties of biochar to assess its capacitive performance. Fig. 3[A] shows the N_2 adsorption/desorption isotherm analysis of biochar samples at various temperatures, which demonstrates a type I and type II pattern for relative pressure P/P_0 and high P/P_0 with an appropriate H_4 hysteresis loop [57,58]. The biochar samples showed a certain amount of N_2 adsorption below the relative pressure P/P_0 (less than 0.1), suggesting the presence of a mesoporous structure. The increase in relative pressure beyond $P/P_0 > 0.9$ reflected the integral porosity in biochar samples, caused by the interspace between the carbon layer, which provided the sufficient mesopores channel to access the electrolyte [58]. The biochar sample obtained at the higher temperature, i.e., biochar-800, exhibited an enhanced porous structure than the biochar-600, which was also revealed by the TEM image in Fig. S2. Further, the BET surface area of the biochar-800 showed a higher value of 312 m^2g^{-1} than the biochar-600 (99.1 m^2g^{-1}). Thus, an increase in activation temperature contributed to an increase in the capacity to generate narrow mesopores as well as pre-existing mesopores. As a consequence, the porosity of biochar samples increased, which is attributed to the increased surface area and pore volume of the biochar-800, as seen in Fig. 3B [59]. Table 1 reports the values of surface area, total and mesopores volume, and average pore diameter for different biochar samples. The higher surface area of biochar-800 is likely to improve the electrochemical charge storage performance of the supercapacitor by enhancing the capacitance, although the increased porosity could facilitate the transport of electrolyte ions within the pores of the supercapacitor during the operation.

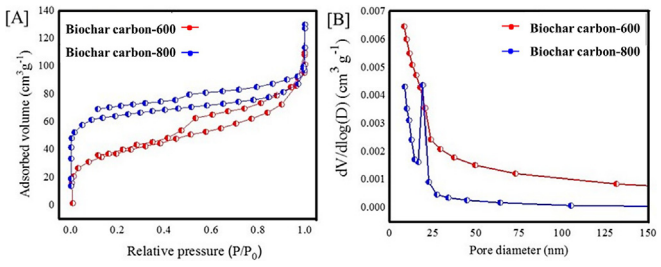

Fig. 3. [A] N_2 adsorption isotherm of biochar samples [B] Pore diameter and volume of biochar's.

3.4. Characterization of surface morphology and heteroatoms of biochar

To prepare the sample for TEM examination, 1 mg of biochar-800 powder was mixed with 1 ml of ethanol solution and sonicated for 15 min to obtain a homogeneous suspension. Later, 5 μl of the suspension was dropped on a 3.05 mm diameter Cu grid followed by drying under the I.R. lamp. The established porous structural features of biochar-800 were verified by TEM and high-resolution TEM analysis. The TEM analysis of biochar-800 revealed a hierarchical microporous feature of carbon, which facilitated the electrolyte ion transfer and decreased the resistance to ion diffusion (*cf.* Fig. 4[A] to [C]). The biochar-800 was identified as a composite of graphitic carbon rings assigned to the interlayer spacing of the (002) plan. Besides, the scanning transmission electron microscope-high-angle annular dark-field (STEM-HAADF) and its corresponding Energy-dispersive X-ray spectroscopy (EDS) elemental mapping images revealed the presence of heteroatoms and metal elements (Fig. 4[D] to [J]). The elemental mapping images exhibited the homogeneous distribution of C, N, O, effectively incorporated into the carbon structure and uniformly distributed in biochar-800 at the nanoscale. The presence of Ca, Fe, and Si elements was likely due to the dust particles attached to the biomass during the collection and palletization process, which interestingly enhanced the electrical conductivity of the biochar-800. The corresponding selected area electron diffraction (SAED) pattern exhibited the blurred diffraction ring, and it is assigned to the disorder or defected carbon structure, which could provide more adsorption sites to improve the capacitance performance (*cf.* Fig. 4[K]).

3.5. Characterization of surface composition of biochar

The XPS analysis revealed the chemical composition and chemical interaction/binding energy of the surface functional groups of biochar-800. The biochar-800 survey spectrum showed the presence of carbon (C), nitrogen (N), and oxygen (O) elements, indicating the self-doping heteroatoms within the biochar structure, as shown in Fig. 5[A]. The high-resolution spectra of C 1s are deconvoluted into four different binding energies viz. 284.7 eV, 285.4 eV, 287.1 eV, and 289 eV corresponding to C–C, C–N, C–O, and C = O species, respectively (*cf.* Fig. 5[B]). The C–C bond at 284.7 eV indicated that most of the sp^2 carbon atoms in biochar-800 are arranged in a conjugated honeycomb lattice. It was observed that binding energy acquired by C–C remained higher than the rest of the bond in the C 1s spectrum [60].

Further, the high-resolution spectrum of N 1s was divided into three constituent peaks: 399.8 eV, 400.5 eV, and 401.19 eV, assigned to the pyridine N (N-6), pyrrolic N (N-5), and quaternary N (N-Q), making a contribution of lone pair of the electron to the conjugated carbon, as depicted in Fig. 5[C] [61,62]. N-Q exhibited the ability of the electron donor and promoted the electron transfer kinetics. However, N-5 and N-6 were considered to contribute pseudo capacitance because it was situated at the edge of the C site [63,64]. Therefore, increased N-content, particularly N-5 and N-6 peak intensity, remained an effective strategy to enhance hydrophilicity and capacitance of the carbon-based electrode

Table 1. S
Surface area, pore volumes, and average pore diameter of biochar samples

Sample name	S_{BET} (m^2 g^{-1})	Total pore volume (V_{tot}) cm^3 g^{-1}	Mesopores volume cm^3 g^{-1}	Average pore size (nm)
Biochar-600	199.1	28.18	0.0613	23.45
Biochar-800	312	43.95	0.143	15.12

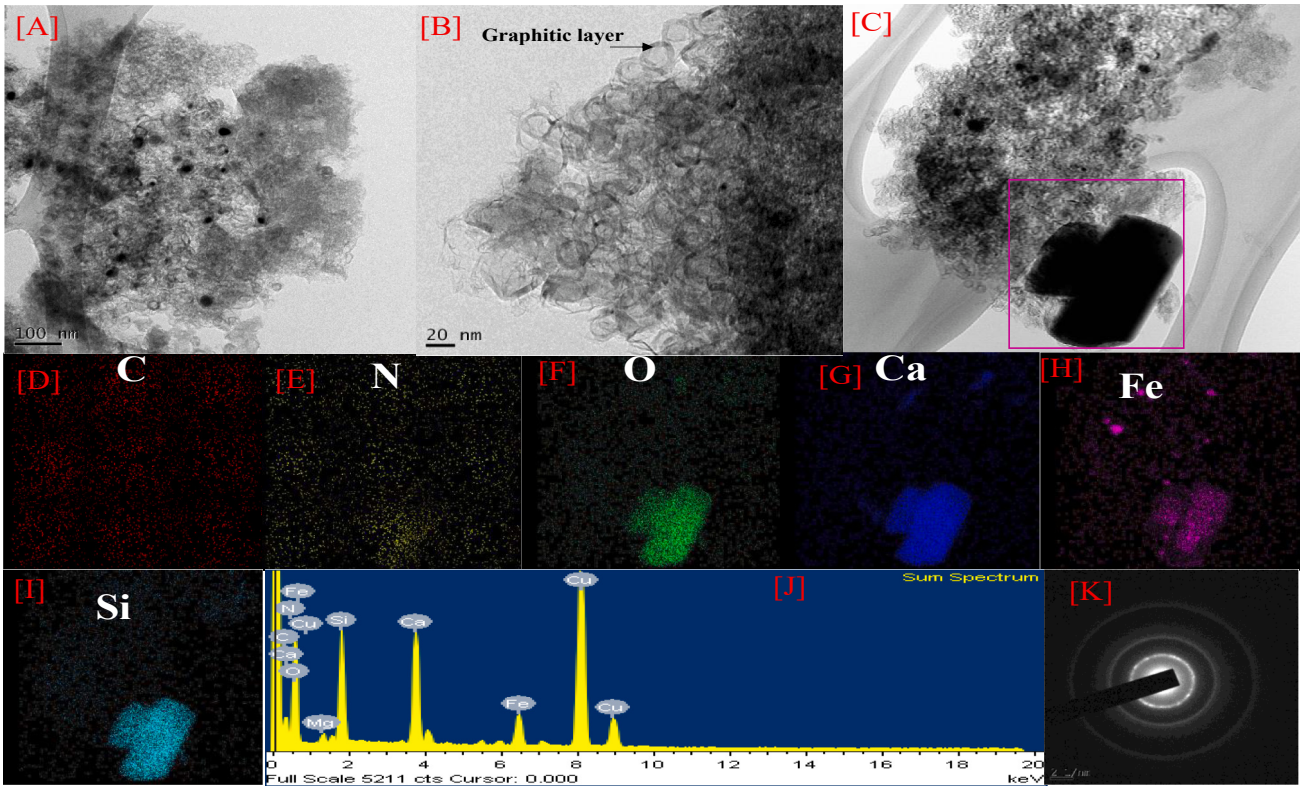

Fig. 4. [A] to [C] HR-TEM images of biochar-800 [D to J] STEM image and corresponding EDX elemental mapping of biochar-800 [K] SAED pattern of biochar-800.

[65,66]. It is worth noting that the nitrogen in the graphitic carbon matrix of biochar possesses higher binding energy (401.19 eV) and active nature than the rest of the nitrogen (Fig. 5[D]). Moreover, the deconvoluted O 1s spectrum showed the binding energy as 533.4 eV and 536.3 eV, which corresponded to the single-bond of oxygen with carbon (i.e., C–O and C–O.H. groups, O-II), while double-bound of oxygen with carbon (i.e., C = O group, O-I) was observed at 532.2 eV. Further, the peak intensity observed at 536.3 eV can be attributed to carboxylic or chemisorbed oxygen or water (i.e., O = C–O group, O-III) [67,68]. The presence of oxygen-containing functional groups promoted the electrolyte ion's penetration into the biochar nanopores and enhanced the surface wettability. The surface composition analysis of the biochar samples via XPS thus revealed several key species responsible for supercapacitor performance. The schematic representation of the N and O co-doped carbon matrix, which played a crucial role in deciding electrochemical behavior, is represented in Fig. 5[E].

4. Electrochemical performance of biochar

4.1. Specific capacitance and galvanostatic charging-discharging (GCD) behavior of biochar

The supercapacitor study of the heteroatom-rich biochar was examined using a two-electrode system in 1 M H_2SO_4. The CV measurement of biochar-600 and biochar-800 was performed at a scan rate of 50 mVs^{-1} to evaluate the electrochemical kinetics of the electrode (*cf.* Fig. 6[A]). A couple of very well-defined redox peaks between 100 mV and 300 mV were distinctly seen from the CV curves of biochar-600 and biochar-800, which emerged primarily from the reversible faradic redox reaction associated with the presence of heteroatoms in the carbon structure of biochar. These heteroatoms remained electrochemically active, and the CV curve showed assertive pseudocapacitive behavior [69,70]. Even at a higher scan rate of 50 mVs^{-1}, the biochar-800 showed an excellent redox peak and its large enclosure area relative to the biochar-600, which suggests that at the higher temperature, the prepared material could possess a comparatively greater specific surface and hence higher specific capacitance.

Furthermore, the comparative galvanostatic charging-discharging (GCD) performance of the biochar-600 and biochar-800 as shown in Fig. 6[B]. The specific capacitance calculated from the discharging curve of biochar-600 and biochar-800 was 206F g^{-1} and 228F g^{-1}, respectively, which can be assigned to an increased specific surface area at a higher temperature and the slightly distorted triangular shape of the GCD curve, which confirm the pseudocapacitance nature of the biochar. In addition, using equation (2), the measured energy density at 1 A g^{-1} for biochar-600 and biochar-800 was determined as 7.27 Wh kg^{-1} and 7.91 Wh kg^{-1}, respectively. In two-electrode measurements, biochar-800 exhibited higher or comparable specific capacitance to the previously mentioned biomass-derived nanostructured biochar summarized in Table 2. No activation reagent is required in the

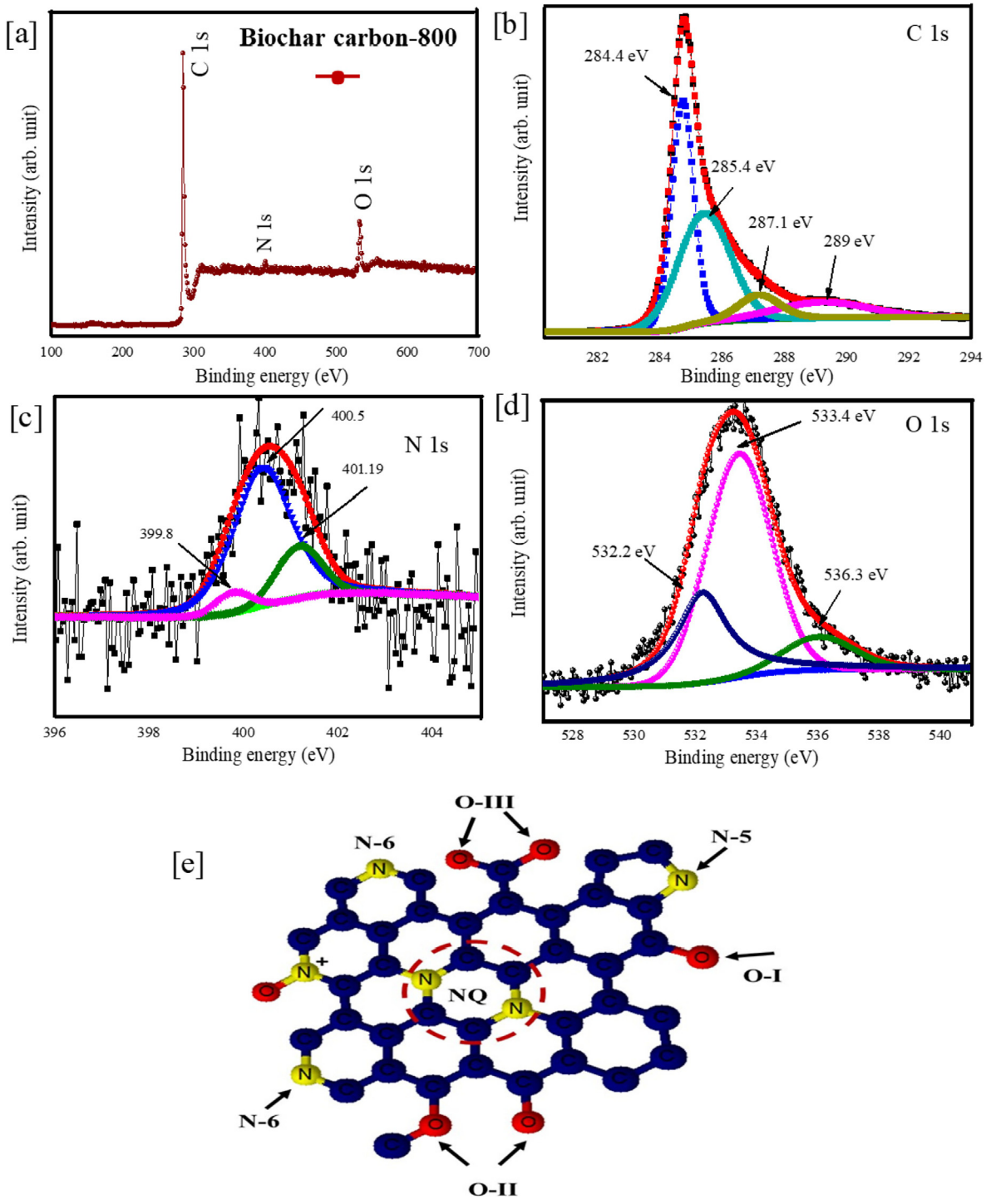

Fig. 5. [A] XPS survey scan spectra of the biochar-800 and high-resolution scan of [B-D] C 1s, N 1s, and O 1s [E] Schematic representation of different N and O functionalities.

synthesis of biochar-800 to increase the surface area of the material, which gives it an edge over other materials and lowers the processing cost of the biochar-800.

The electrochemical impedance spectroscopy (EIS) measurement was carried out in a 0.01 Hz to 0.1 GHz frequency window to evaluate the electrode/electrolyte interface, which triggered the overall impedance of the supercapacitor. In a Nyquist plot Fig. 6[C], the point where the plot intersects the real axis (x-axis) refers to equivalent series resistance (ESR), also known as the solution resistance (R_s), which was found as 3.4 Ω and 3.49 Ω, respectively, for biochar-600 and biochar-800 samples. The slight increase in the ESR value of biochar-800 is assigned to the increased pyrolysis temperature, making the biochar surface more hydrophobic and reducing the contact area at the electrode-electrolyte interface. This electrode also exhibited a nearly vertical line in the low-frequency region, suggesting a good capacitive performance. Extrapolating the vertical portion (low-frequency area) to the real axis yields the total cell resistance (R_{cell}). Notably, the biochar-800 showed lower R_{cell} (4.9 Ω) compared to the biochar-600 (6.9 Ω), due to its lower charge transfer resistance (R_{CT}). The

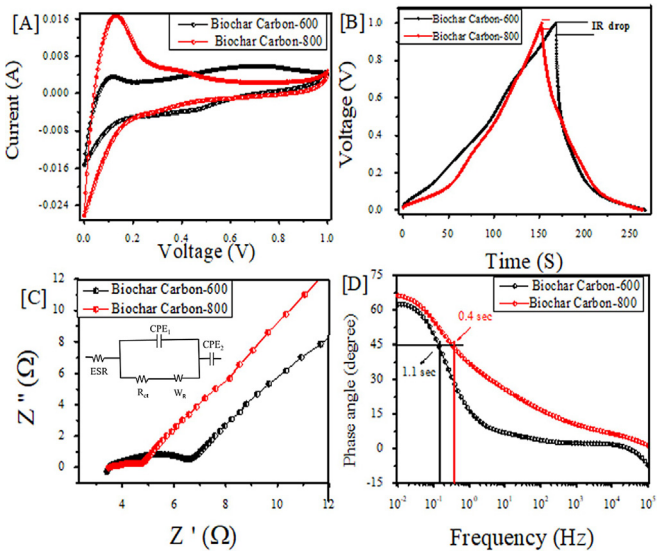

Fig. 6. [A] Cyclic voltammogram of biochar-600 and biochar-800 at a scan rate of 50 mVs^{-1} in 1M H_2SO_4, [B] GCD curve of biochar-600 and biochar-800 at a current density of 1 A g^{-1}, [C] Nyquist plot of biochar-600 and biochar-800 samples (inset shows the electrochemical equivalent circuit), [D] Bode plots of biochar-600 and biochar-800 samples

semicircle region of Fig. 6[C] revealed electrochemical reaction impedance of the electrode, while the smaller diameter of the semicircle denoted lower R_{CT}. Nyquist plot suggested that the biochar-800 had a smaller arc radius than biochar-600, confirming the fast electric response with the lowest R_{CT} value of 1.3 Ω compared to biochar-600 (3.24 Ω), which suggested the promotion of charge transfer in the case of biochar-800. The Warburg resistance (W_R) is estimated by subtracting R_{CT} and ESR from the R_{cell} value, and it remained as 0.27 Ω and 0.12 Ω for biochar-600 and biochar-800, respectively. Thus, the smaller R_{CT} and W_R values of biochar-800 indicated better charge transfer and ion penetration, resulting in excellent rate performance.

Fig. 6[D] demonstrates the Bode phase plots of the impedance phase angle vs. frequency obtained from the EIS plot. Since the capacitive and resistive impedances are identical at a phase angle of − 45°, the relaxation time constant (τ) can be calculated by $\tau = \frac{1}{f}$ at the particular phase. The relaxation time shows how fast the stored energy of the electrode can effectively be distributed. The phase angles are close to − 90° at low frequencies, suggesting ideal capacitive behavior. The biochar-800 showing the maximum phase angle of − 66° at the low-frequency region can be assigned to the capacitive behavior; the phase angle remained less than that of an ideal capacitive nature − 90°, demonstrating the pseudocapacitive nature of the electrode material [71]. The characteristic frequencies (f) for a phase angle of − 45° are 0.186 Hz and 0.48 Hz, corresponding to the relaxation time constant of 5.3 s and 2.0 s for biochar-600 and biochar-800, respectively. As the pyrolysis temperature increased, the diffusion coefficient of electrolyte in biochar-800 increased due to the high specific surface area, electrical conductivity, and mesopores structure. The mass transfer process and electrochemical reversibility of the biochar-800 were also improved with more prominent capacitive characteristics.

4.2. CV characteristic, internal resistance, and cycling stability of biochar

The CV measurement of the biochar-600 and biochar-800 samples at different scan rates from 10 mVs^{-1} to 150 mVs^{-1} and between 0.0 V and 1.0 V is demonstrated in Fig. 7[A] and [B]. Fig. 7[A] and [B] show that as the scan rate increased, the oxidation and reduction peaks of biochar-600 and biochar-800 shifted towards more positive and then negative values, primarily due to polarization and ohm resistance during the faradic processes. Similarly, as pyrolysis temperature increased (or from biochar-600 to biochar-800), slight improvements in the shape of the CV curves of biochar-800 were observed, such as the increase in the CV curve area and current density, which resulted in superior capacitance value. Dunn's power law equation was adapted to define the energy storage mechanism of biochar-600 and biochar-800, respectively, where the relationship between measured current (i) and scan rate (v) dependent equation is given as [81].

$$i = a.v^b \tag{3}$$

Where 'b' represents the adjustable parameter, which can be obtained from the slope of the plot of log (i) vs. log (v) at particular potential, as shown in Fig. 7[C] and [D]. A value of b = 0.5 is related to the diffusion-controlled Faradic process, while b = 1 implies to the capacitive (i.e., non –faradic) process. Futher, a value of b between 0.5 and 1 suggests an integrated process (i.e., faradic and non-faradic process). Fig. 7[C] and [D] exhibit that the 'b' value for biochar-600 and biochar-800 for anodic and cathodic peaks remained at 0.53, 0.63, and 0.51, 0.87, respectively, suggesting that the energy storage is a combination of diffusion-controlled and charge storage process which conformed the pseudocapacitive contribution[82]. Fig. 7[E] and [F] show the GCD curve at the different current density from 1 A $g^{-1}$to the 5 A g^{-1}. As current density increased, the internal resistance (I.R.) drop increased sharply due to the electrolyte's enhanced ionic motion velocity over a short period which posed difficulty for the electrolyte ions to penetrate within the pores of the biochar material. At 1 A g^{-1}, the biochar-600 showed an increased I.R. drop of 0.007 V compared to the biochar-800 (0.003 V). At a current density of 1 A g^{-1}, the biochar-800 exhibited a specific capacitance of 228F g^{-1} in a

Table 2
Two electrode-specific capacitance measurements of electrode prepared by using various biomass-derived biochar

Biomass	Activation agent	S_{BET} (m^2g^{-1})	Electrolyte	Specific capacitance (F g^{-1})	Current density (A g^{-1})	Ref.
Phonex tree leaves	K_2FeO_4	2208	6 M KOH	254	0.5 A g^{-1}	[72]
Silkworm Cocoon	KOH	3386	6 M KOH	155.1	5 A g^{-1}	[73]
Tea waste	KOH	911.9	6 M KOH	167	1 A g^{-1}	[74]
Cotton	KOH	2307	6 M KOH	193	0.1–50 A g^{-1}	[75]
Lecithin	KOH	1803	1 M H_2SO_4	178	0.5 A g^{-1}	[76]
Soybean root	KOH	2143	6 M KOH	276	0.5 A g^{-1}	[77]
Dried Fungus	KOH	2959	6 M KOH	235	1 A g^{-1}	[78]
Bean dregs	KOH	2876	1 M H_2SO_4	210.2	1 A g^{-1}	[79]
Bagasse	KOH	1260	1 M H_2SO_4	225	1 A g^{-1}	[80]
Biochar-600	No-Activation	199.1	1 M H_2SO_4	206	1 A g^{-1}	Presentwork
Biochar-800	No-Activation	312	1 M H_2SO_4	228	1 A g^{-1}	Present work

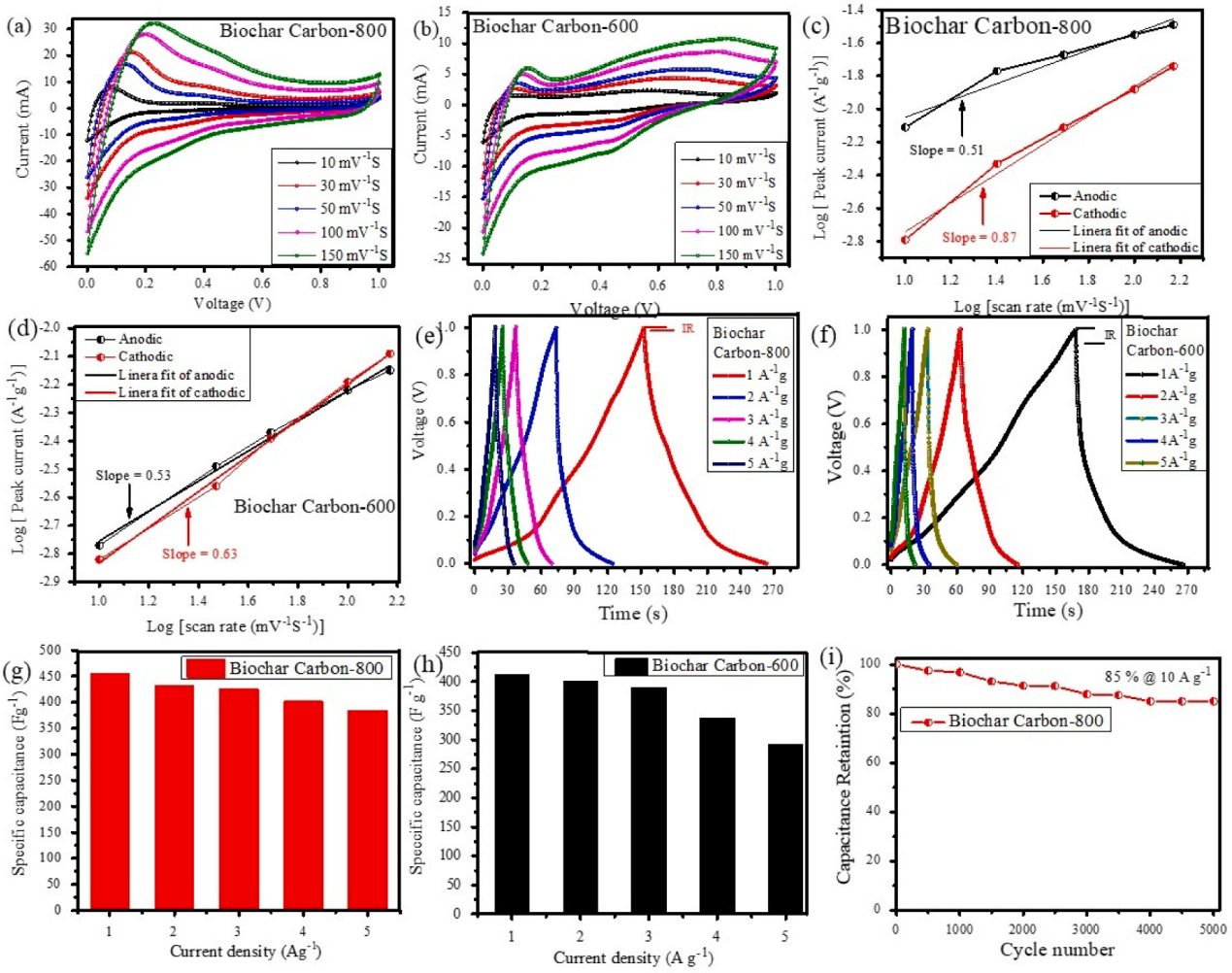

Fig. 7. [A – B] CV curve of biochar-600 and biochar-800 in a two-electrode system [C – D] log (i) vs log (v) plot at different scan rate [E – F], Galvanostatic charge-discharge curve of biochar-600 and biochar-800 [G – H] Specific capacitance at different current densities [I] Cyclic stability of biochar-800 at a constant current density of 10 $A^{-1}g$ up to 5000 cycles

two-electrode cell. However, for an increase in the current density up to 5 A g^{-1}, the specific capacitance of biochar-800 retained up to 84 % as compared to biochar-600 (~70 %), as shown in Fig. 7[G] and [H]. The high specific capacitance retention % of biochar-800 can be attributed to the reduced internal charge transfer resistance, increased specific surface area, and mesopores at higher temperatures. The cycling stability of biochar-800 was examined by the GCD of the electrode between 0 V and 1 V. Fig. 7[I] shows that after 5000 charge–discharge cycles and at a high current density of 10 A g^{-1}, the capacitance retention % of biochar-800 remained near 88%, possibly due to the heteroatoms and porous carbon structures of biochar-800 which enabled access of electrolyte ions, and led to long-term cycling life and excellent reversibility of the biochar-800 electrode [83–85].

4.3. Application of biochar-800 as a coin cell supercapacitor

Fig. 8[A] shows a schematic of the coin cell device supercapacitor developed from biochar-800, as it showed the best electrochemical performance. The coin cell supercapacitor was constructed by spin coating 14 mg of biochar-800 slurry on conducting carbon paper containing 90 wt% of biochar-800, 5 wt% carbon black, and 5 wt% PVDF. The separator was placed between the electrodes after being immersed in 1-ethyl-3mthylimdazolium

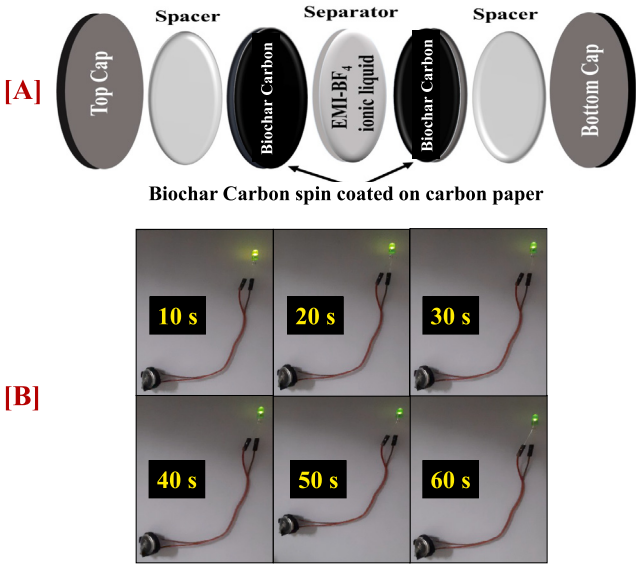

Fig. 8. [A] Schematic illustration of biochar-800-coin cell configuration, [B] Demonstration of working biochar-800-coin cell device glowing LED after the 30 s charging

tetrafluoroborate (EMI-BF_4) ionic liquid as the electrolyte for a non-aqueous solution. The coin cell was pressed in a hydraulic coin cell crimping machine. The coin cell device was charged for the 30 s by applying 3 V; consequently, it glows 3 V LEDs for up to 60 s without any external power source Fig. 8[B]. The working of the coin cell device via video is demonstrated in the supporting information.

5. Conclusion

In summary, an electrode material was proposed and developed for symmetric pseudocapacitors with high specific capacitance and long cycling stability at higher current density. The prepared biochar exhibited N and O co-doped heteroatoms in the hierarchical porous carbon structure with a high micropore volume of 0.143 cm^3/gm. The biochar produced at 800 °C showed a specific capacitance of 228F g^{-1} at 1 A g^{-1} in 1 M H_2SO_4 and a rate capability of ~ 84.1% when current density increased up to 5 A g^{-1} (191.9F g^{-1}). Remarkably, the biochar-800 also showed an excellent energy density of 7.91 Wh kg^{-1} in 1 M H_2SO_4 electrolyte and improved cycling stability 88% capacitance retention after 5000 cycles at a high current density of 10 A g^{-1}. The increased specific capacitance is assigned to the existence of N and O co-doped heteroatoms within the graphitic carbon matrix of biochar, which enhanced the electrical conductivity, and ion adsorption on the surface, at ambient temperature. Furthermore, the low relaxation time constant, drop in the internal resistance, high specific surface area, and the presence of micropores played a crucial role in enhancing the electrochemical performance of biochar-800. Thus, the current study demonstrates that the low-cost co-doped heteroatoms rich hierarchical porous biochar material derived from the biomass pellets pyrolysis would be an excellent choice for a high-performance pseudocapacitive energy conversion device.

CRediT authorship contribution statement

Zakir Husain: Original work, methodology, data creation, and initial drafting. **A.R. Shakeelur Raheman:** Original work, methodology, data creation, and initial drafting. **Khursheed B. Ansari:** Conceptualization, mentoring and proofreading. **Aniruddha B. Pandit:** Supervision, project administration, funding acquisition. **Mohd Shariq Khan:** Critical comments and proofreading. **Muhammad Abdul Qyyum:** Critical comments and proofreading. **Su Shiung Lam:** Comments on supercapacitor.

Declaration of competing interest

The authors declare that they have no known competing financial interests or personal relationships that could have appeared to influence the work reported in this paper.

Acknowledgments

Zakir Husain and Shakeelur Rahman A. R. gratefully acknowledge the financial support from J.B. Joshi Research Foundation, MANF UGC ((F1-17.1/2013-14/MANF-2013-14-MUS-MAH-27907) , BRNS (2013/20/34/1/BRNS), and Nanomission (SR/NM/NS-1110/2012) Government of India. The authors would also like to thank Universiti Malaysia Terengganu under International Partnership Research Grant (UMT/CRIM/2-2/2/23 (23), Vot 55302), and the Ministry of Higher Education, Malaysia under the Higher Institution Centre of Excellence (HICoE), Institute of Tropical Aquaculture and Fisheries (AKUATROP) program (Vot. No. 63933 & Vot. No. 56051, UMT/CRIM/2-2/5 Jilid 2 (10)) for supporting Prof Lam to perform this joint project. The author would like to thank Dr. Sameer Patel (Department of Civil Engineering, Indian Institute of Technology, Gandhinagar, Gujarat, 382355, India) for his valuable suggestions on the manuscript.

Appendix A. Supplementary data

Supplementary data to this article can be found online at https://doi.org/10.1016/j.mset.2021.12.003.

References

[1] C. Zou, Q. Zhao, G. Zhang, B. Xiong, Energy revolution: From a fossil energy era to a new energy era, Natural Gas Industry B 3 (2016) 1–11.
[2] H.-F. Wang, Q. Xu, Materials Design for Rechargeable Metal-Air Batteries, Matter 1 (2019) 565–595.
[3] H. Iwahara, Conducting Materials: Solid-ionic and Super-ionic, in: K.H.J. Buschow, R.W. Cahn, M.C. Flemings, B. Ilschner, E.J. Kramer, S. Mahajan, P. Veyssière (Eds.), Encyclopedia of Materials: Science and Technology, Elsevier, Oxford, 2001, pp. 1482–1496.
[4] O.L. Li, T. Ishizaki, Chapter 4 – Development, Challenges, and Prospects of Carbon-Based Electrode for Lithium-Air Batteries, in: K.Y. Cheong, G. Impellizzeri, M.A. Fraga (Eds.), Emerging Materials for Energy Conversion and Storage, Elsevier, 2018, pp. 115–152.
[5] H. Yuan, H. Shimotani, J. Ye, S. Yoon, H. Aliah, A. Tsukazaki, M. Kawasaki, Y. Iwasa, Electrostatic and Electrochemical Nature of Liquid-Gated Electric-Double-Layer Transistors Based on Oxide Semiconductors, Journal of the American Chemical Society 132 (2010) 18402–18407.
[6] J. Walter, H. Wang, B. Luo, C.D. Frisbie, C. Leighton, Electrostatic versus Electrochemical Doping and Control of Ferromagnetism in Ion-Gel-Gated Ultrathin La0.5Sr0.5CoO3−δ, ACS Nano 10 (2016) 7799–7810.
[7] A. Gopalakrishnan, S. Badhulika, Effect of self-doped heteroatoms on the performance of biomass-derived carbon for supercapacitor applications, Journal of Power Sources 480 (2020) 228830.
[8] F. Zhao, A. Vicenzo, M. Hashempour, M. Bestetti, Supercapacitor electrodes by direct growth of multi-walled carbon nanotubes on Al: a study of performance versus layer growth evolution, Electrochimica Acta 150 (2014) 35–45.
[9] W. Ni, L. Shi, Review Article: Layer-structured carbonaceous materials for advanced Li-ion and Na-ion batteries: Beyond graphene, Journal of Vacuum Science & Technology A 37 (2019) 040803.
[10] A. Izadi-Najafabadi, S. Yasuda, K. Kobashi, T. Yamada, D.N. Futaba, H. Hatori, M. Yumura, S. Iijima, K. Hata, Extracting the Full Potential of Single-Walled Carbon Nanotubes as Durable Supercapacitor Electrodes Operable at 4 V with High Power and Energy Density, Advanced Materials 22 (2010) E235–E241.
[11] H. Zhang, X. He, J. Gu, Y. Xie, H. Shui, X. Zhang, N. Xiao, J. Qiu, Wrinkled porous carbon nanosheets from methylnaphthalene oil for high-performance supercapacitors, Fuel Processing Technology 175 (2018) 10–16.
[12] S. Zhang, L. Sui, H. Dong, W. He, L. Dong, L. Yu, High-Performance Supercapacitor of Graphene Quantum Dots with Uniform Sizes, ACS Applied Materials & Interfaces 10 (2018) 12983–12991.
[13] A. Castro-Muñiz, S. Lorenzo-Fierro, A. Martínez-Alonso, J.M.D. Tascón, V. Fierro, F. Suárez-García, J.I. Paredes, Ordered mesoporous carbons obtained from low-value coal tar products for electrochemical energy storage and water remediation, Fuel Processing Technology 196 (2019) 106152.
[14] C. Zhou, Y. Zhang, Y. Li, J. Liu, Construction of High-Capacitance 3D CoO@Polypyrrole Nanowire Array Electrode for Aqueous Asymmetric Supercapacitor, Nano Letters 13 (2013) 2078–2085.
[15] M. Zhi, F. Yang, F. Meng, M. Li, A. Manivannan, N. Wu, Effects of Pore Structure on Performance of An Activated-Carbon Supercapacitor Electrode Recycled from Scrap Waste Tires, ACS Sustainable Chemistry & Engineering 2 (2014) 1592–1598.
[16] H. Jiang, J. Ma, C. Li, Mesoporous Carbon Incorporated Metal Oxide Nanomaterials as Supercapacitor Electrodes, Advanced Materials 24 (2012) 4197–4202.
[17] R.R. Salunkhe, Y.V. Kaneti, Y. Yamauchi, Metal-Organic Framework-Derived Nanoporous Metal Oxides toward Supercapacitor Applications: Progress and Prospects, ACS Nano 11 (2017) 5293–5308.
[18] G.A. Snook, P. Kao, A.S. Best, Conducting-polymer-based supercapacitor devices and electrodes, Journal of Power Sources 196 (2011) 1–12.
[19] Y.-P. Gao, Z.-B. Zhai, K.-J. Huang, Y.-Y. Zhang, Energy storage applications of biomass-derived carbon materials: batteries and supercapacitors, New Journal of Chemistry 41 (2017) 11456–11470.
[20] Z. Hu, X. Li, Z. Tu, Y. Wang, O.D. Dacres, Y. Sun, M. Sun, H. Yao, "Thermal dissolution carbon enrichment" treatment of biomass wastes: Supercapacitor electrode preparation using the residue, Fuel Processing Technology 205 (2020) 106430.
[21] M. Khalid, A.M.B. Honorato, A.A. Pasa, H. Varela, A sugar derived carbon-red phosphorus composite for oxygen evolution reaction and supercapacitor activities, Materials Science for Energy Technologies 3 (2020) 508–514.
[22] P. Konnerth, D. Jung, J.W. Straten, K. Raffelt, A. Kruse, Metal oxide-doped activated carbons from bakery waste and coffee grounds for application in supercapacitors, Materials Science for Energy Technologies 4 (2021) 69–80.

[23] J.R. Miller, A.F. Burke, Electrochemical Capacitors: Challenges and Opportunities for Real-World Applications, The Electrochemical Society interface 17 (2008) 53–57.
[24] R. Farma, M. Deraman, A. Awitdrus, I.A. Talib, E. Taer, N.H. Basri, J.G. Manjunatha, M.M. Ishak, B.N.M. Dollah, S.A. Hashmi, Preparation of highly porous binderless activated carbon electrodes from fibres of oil palm empty fruit bunches for application in supercapacitors, Bioresource Technology 132 (2013) 254–261.
[25] M.M. Pérez-Madrigal, M.G. Edo, C. Alemán, Powering the future: application of cellulose-based materials for supercapacitors, Green Chemistry 18 (2016) 5930–5956.
[26] K. Subramani, N. Sudhan, M. Karnan, M. Sathish, Orange Peel Derived Activated Carbon for Fabrication of High-Energy and High-Rate Supercapacitors, ChemistrySelect 2 (2017) 11384–11392.
[27] L. Sun, C. Tian, M. Li, X. Meng, L. Wang, R. Wang, J. Yin, H. Fu, From coconut shell to porous graphene-like nanosheets for high-power supercapacitors, Journal of Materials Chemistry A 1 (2013) 6462–6470.
[28] J.-Q.-Q. Guo Pei-Zhi, Z.H.A.N.G. Li-Li, Z.H.A.O. Shan-Yu, Z.H.A.O. Xiu-Song, Preparation and Characterization of Peanut Shell-Based Microporous Carbons as Electrode Materials for Supercapacitors, Acta Phys. -Chim. Sin. 27 (2011) 2836–2840.
[29] M. Chen, X. Kang, T. Wumaier, J. Dou, B. Gao, Y. Han, G. Xu, Z. Liu, L. Zhang, Preparation of activated carbon from cotton stalk and its application in supercapacitor, Journal of Solid State Electrochemistry 17 (2013) 1005–1012.
[30] H. Wang, Z. Li, D. Mitlin, Tailoring Biomass-Derived Carbon Nanoarchitectures for High-Performance Supercapacitors, ChemElectroChem 1 (2014) 332–337.
[31] Y. Liu, J. Chen, B. Cui, P. Yin, C. Zhang, Design and Preparation of Biomass-Derived Carbon Materials for Supercapacitors: A Review, C 4 (2018) 53.
[32] H. Yang, S. Ye, J. Zhou, T. Liang, Biomass-Derived Porous Carbon Materials for Supercapacitor, Frontiers in Chemistry 7 (2019).
[33] G. Kandasamy, Recent Advancements in Doped/Co-Doped Carbon Quantum Dots for Multi-Potential Applications, C 5 (2019) 24.
[34] Y. Zhu, S. Murali, M.D. Stoller, K.J. Ganesh, W. Cai, P.J. Ferreira, A. Pirkle, R.M. Wallace, K.A. Cychosz, M. Thommes, D. Su, E.A. Stach, R.S. Ruoff, Carbon-Based Supercapacitors Produced by Activation of Graphene, Science 332 (2011) 1537–1541.
[35] D. Hulicova-Jurcakova, M. Seredych, G.Q. Lu, T.J. Bandosz, Combined Effect of Nitrogen- and Oxygen-Containing Functional Groups of Microporous Activated Carbon on its Electrochemical Performance in Supercapacitors, Advanced Functional Materials 19 (2009) 438–447.
[36] M. Seredych, D. Hulicova-Jurcakova, G.Q. Lu, T.J. Bandosz, Surface functional groups of carbons and the effects of their chemical character, density and accessibility to ions on electrochemical performance, Carbon 46 (2008) 1475–1488.
[37] Y. Zhao, M. Liu, X. Deng, L. Miao, P.K. Tripathi, X. Ma, D. Zhu, Z. Xu, Z. Hao, L. Gan, Nitrogen-functionalized microporous carbon nanoparticles for high performance supercapacitor electrode, Electrochimica Acta 153 (2015) 448–455.
[38] Z.R. Ismagilov, A.E. Shalagina, O.Y. Podyacheva, A.V. Ischenko, L.S. Kibis, A.I. Boronin, Y.A. Chesalov, D.I. Kochubey, A.I. Romanenko, O.B. Anikeeva, T.I. Buryakov, E.N. Tkachev, Structure and electrical conductivity of nitrogen-doped carbon nanofibers, Carbon 47 (2009) 1922–1929.
[39] D.-W. Wang, F. Li, H.-M. Cheng, Hierarchical porous nickel oxide and carbon as electrode materials for asymmetric supercapacitor, Journal of Power Sources 185 (2008) 1563–1568.
[40] B. Xu, S. Hou, G. Cao, F. Wu, Y. Yang, Sustainable nitrogen-doped porous carbon with high surface areas prepared from gelatin for supercapacitors, Journal of Materials Chemistry 22 (2012) 19088–19093.
[41] M. Yang, Z. Zhou, Recent Breakthroughs in Supercapacitors Boosted by Nitrogen-Rich Porous Carbon Materials, Advanced Science 4 (2017) 1600408.
[42] W. Qian, F. Sun, Y. Xu, L. Qiu, C. Liu, S. Wang, F. Yan, Human hair-derived carbon flakes for electrochemical supercapacitors, Energy & Environmental Science 7 (2014) 379–386.
[43] J. Lee, J. Oh, Y. Jeon, Y. Piao, Multi-Heteroatom-Doped Hollow Carbon Attached on Graphene Using LiFePO4 Nanoparticles as Hard Templates for High-Performance Lithium-Sulfur Batteries, ACS Applied Materials & Interfaces 10 (2018) 26485–26493.
[44] L. Zhang, J. Jiang, N. Holm, F. Chen, Mini-chunk biochar supercapacitors, Journal of Applied Electrochemistry 44 (2014) 1145–1151.
[45] C. Zequine, C.K. Ranaweera, Z. Wang, S. Singh, P. Tripathi, O.N. Srivastava, B.K. Gupta, K. Ramasamy, P.K. Kahol, P.R. Dvornic, R.K. Gupta, High Per formance and Flexible Supercapacitors based on Carbonized Bamboo Fibers for Wide Temperature Applications, Scientific Reports 6 (2016) 31704.
[46] Y. Wang, Y. Zhang, L. Pei, D. Ying, X. Xu, L. Zhao, J. Jia, X. Cao, Converting Ni-loaded biochars into supercapacitors: Implication on the reuse of exhausted carbonaceous sorbents, Scientific Reports 7 (2017) 41523.
[47] J. Jiang, High Temperature Monolithic Biochar Supercapacitor Using Ionic Liquid Electrolyte, Journal of The Electrochemical Society 164 (2017) H5043–H5048.
[48] E. Adhamash, R. Pathak, Q. Qiao, Y. Zhou, R. McTaggart, Gamma-radiated biochar carbon for improved supercapacitor performance, RSC Advances 10 (2020) 29910–29917.
[49] R.A. Senthil, V. Yang, J. Pan, Y. Sun, A green and economical approach to derive biomass porous carbon from freely available feather finger grass flower for advanced symmetric supercapacitors, Journal of Energy Storage 35 (2021) 102287.
[50] H. Wang, H. Yi, X. Chen, X. Wang, Asymmetric supercapacitors based on nano-architectured nickel oxide/graphene foam and hierarchical porous nitrogen-doped carbon nanotubes with ultrahigh-rate performance, Journal of Materials Chemistry A 2 (2014) 3223–3230.
[51] A. Ariharan, B. Viswanathan, V. Nandhakumar, Nitrogen-incorporated carbon nanotube derived from polystyrene and polypyrrole as hydrogen storage material, International Journal of Hydrogen Energy 43 (2018) 5077–5088.
[52] S.R. Mangisetti, M. Kamaraj, R. Sundara, Green Approach for Synthesizing Three Different Carbon Microstructures from a Single Biowaste Bombax malabaricum for Fully Biocompatible Flexible Supercapacitors and Their Performance in Various Electrolytes, ACS Omega 4 (2019) 6399–6410.
[53] T. Li, X. Bai, Y.-X. Qi, N. Lun, Y.-J. Bai, Fe3O4 nanoparticles decorated on the biochar derived from pomelo pericarp as excellent anode materials for Li-ion batteries, Electrochimica Acta 222 (2016) 1562–1568.
[54] L. Wang, C. Yang, S. Dou, S. Wang, J. Zhang, X. Gao, J. Ma, Y. Yu, Nitrogen-doped hierarchically porous carbon networks: synthesis and applications in lithium-ion battery, sodium-ion battery and zinc-air battery, Electrochimica Acta 219 (2016) 592–603.
[55] W. Qian, J. Zhu, Y. Zhang, X. Wu, F. Yan, Condiment-Derived 3D Architecture Porous Carbon for Electrochemical Supercapacitors, Small 11 (2015) 4959–4969.
[56] Y. Wang, Y. Song, Y. Wang, X. Chen, Y. Xia, Z. Shao, Graphene/silk fibroin based carbon nanocomposites for high performance supercapacitors, Journal of Materials Chemistry A 3 (2015) 773–781.
[57] M. Kruk, M. Jaroniec, Gas Adsorption Characterization of Ordered Organic–Inorganic Nanocomposite Materials, Chemistry of Materials 13 (2001) 3169–3183.
[58] G. Pognon, T. Brousse, D. Bélanger, Effect of molecular grafting on the pore size distribution and the double layer capacitance of activated carbon for electrochemical double layer capacitors, Carbon 49 (2011) 1340–1348.
[59] S. Gao, K. Geng, H. Liu, X. Wei, M. Zhang, P. Wang, J. Wang, Transforming organic-rich amaranthus waste into nitrogen-doped carbon with superior performance of the oxygen reduction reaction, Energy & Environmental Science 8 (2015) 221–229.
[60] C. Zhan, X. Yu, Q. Liang, W. Liu, Y. Wang, R. Lv, Z.-H. Huang, F. Kang, Flour food waste derived activated carbon for high-performance supercapacitors, RSC Advances 6 (2016) 89391–89396.
[61] C. Zhu, J. Zhai, S. Dong, Bifunctional fluorescent carbon nanodots: green synthesis via soy milk and application as metal-free electrocatalysts for oxygen reduction, Chemical Communications 48 (2012) 9367–9369.
[62] Z.-Y. Sui, Y. Cui, J.-H. Zhu, B.-H. Han, Preparation of Three-Dimensional Graphene Oxide-Polyethylenimine Porous Materials as Dye and Gas Adsorbents, ACS Applied Materials & Interfaces 5 (2013) 9172–9179.
[63] T. Lin, I.W. Chen, F. Liu, C. Yang, H. Bi, F. Xu, F. Huang, Nitrogen-doped mesoporous carbon of extraordinary capacitance for electrochemical energy storage, Science 350 (2015) 1508–1513.
[64] L. Zhang, T. You, T. Zhou, X. Zhou, F. Xu, Interconnected Hierarchical Porous Carbon from Lignin-Derived Byproducts of Bioethanol Production for Ultra-High Performance Supercapacitors, ACS Applied Materials & Interfaces 8 (2016) 13918–13925.
[65] W. Luo, B. Wang, C.G. Heron, M.J. Allen, J. Morre, C.S. Maier, W.F. Stickle, X. Ji, Pyrolysis of Cellulose under Ammonia Leads to Nitrogen-Doped Nanoporous Carbon Generated through Methane Formation, Nano Letters 14 (2014) 2225–2229.
[66] T. Liu, T. Kou, D. Bulmahn, C. Ortuno-Quintana, G. Liu, J.Q. Lu, Y. Li, Tuning the Electrochemical Properties of Nitrogen-Doped Carbon Aerogels in a Blend of Ammonia and Nitrogen Gases, ACS Applied Energy Materials 1 (2018) 5043–5053.
[67] M. Demir, B. Ashourirad, J.H. Mugumya, S.K. Saraswat, H.M. El-Kaderi, R.B. Gupta, Nitrogen and oxygen dual-doped porous carbons prepared from pea protein as electrode materials for high performance supercapacitors, International Journal of Hydrogen Energy 43 (2018) 18549–18558.
[68] S. Hu, Y. Tan, C. Feng, S. Wang, Z. Sun, H. Wu, G. Zhang, Improving biomass-derived carbon with cobalt/cobalt oxide doping for oxygen reduction reaction, Journal of Solid State Electrochemistry 23 (2019) 2291–2299.
[69] D.-D. Zhou, W.-Y. Li, X.-L. Dong, Y.-G. Wang, C.-X. Wang, Y.-Y. Xia, A nitrogen-doped ordered mesoporous carbon nanofiber array for supercapacitors, Journal of Materials Chemistry A 1 (2013) 8488–8496.
[70] E. Frackowiak, Carbon materials for supercapacitor application, Physical Chemistry Chemical Physics 9 (2007) 1774–1785.
[71] G.K. Veerasubramani, K. Krishnamoorthy, P. Pazhamalai, S.J. Kim, Enhanced electrochemical performances of graphene based solid-state flexible cable type supercapacitor using redox mediated polymer gel electrolyte, Carbon 105 (2016) 638–648.
[72] J. He, D. Zhang, Y. Wang, J. Zhang, B. Yang, H. Shi, K. Wang, Y. Wang, Biomass-derived porous carbons with tailored graphitization degree and pore size distribution for supercapacitors with ultra-high rate capability, Applied Surface Science 515 (2020) 146020.
[73] J. Sun, J. Niu, M. Liu, J. Ji, M. Dou, F. Wang, Biomass-derived nitrogen-doped porous carbons with tailored hierarchical porosity and high specific surface area for high energy and power density supercapacitors, Applied Surface Science 427 (2018) 807–813.
[74] X. Song, X. Ma, Y. Li, L. Ding, R. Jiang, Tea waste derived microporous active carbon with enhanced double-layer supercapacitor behaviors, Applied Surface Science 487 (2019) 189–197.

[75] P. Cheng, T. Li, H. Yu, L. Zhi, Z. Liu, Z. Lei, Biomass-Derived Carbon Fiber Aerogel as a Binder-Free Electrode for High-Rate Supercapacitors, The Journal of Physical Chemistry C 120 (2016) 2079–2086.
[76] M. Demir, S.K. Saraswat, R.B. Gupta, Hierarchical nitrogen-doped porous carbon derived from lecithin for high-performance supercapacitors, RSC Advances 7 (2017) 42430–42442.
[77] N. Guo, M. Li, Y. Wang, X. Sun, F. Wang, R. Yang, Soybean Root-Derived Hierarchical Porous Carbon as Electrode Material for High-Performance Supercapacitors in Ionic Liquids, ACS Applied Materials & Interfaces 8 (2016) 33626–33634.
[78] K. Wang, M. Xu, Z. Gu, P. Ahrenkiel, J. Lee, W. Gibbons, J. Croat, Q. Fan, Pyrrole modified biomass derived hierarchical porous carbon as high performance symmetrical supercapacitor electrodes, International Journal of Hydrogen Energy 41 (2016) 13109–13115.
[79] C. Ruan, K. Ai, L. Lu, Biomass-derived carbon materials for high-performance supercapacitor electrodes, RSC Advances 4 (2014) 30887–30895.
[80] M. Wahid, D. Puthusseri, D. Phase, S. Ogale, Enhanced Capacitance Retention in a Supercapacitor Made of Carbon from Sugarcane Bagasse by Hydrothermal Pretreatment, Energy & Fuels 28 (2014) 4233–4240.
[81] W. Sun, G. Gao, Y. Du, K. Zhang, G. Wu, A facile strategy for fabricating hierarchical nanocomposites of V2O5 nanowire arrays on a three-dimensional N-doped graphene aerogel with a synergistic effect for supercapacitors, Journal of Materials Chemistry A 6 (2018) 9938–9947.
[82] H.B. Li, M.H. Yu, F.X. Wang, P. Liu, Y. Liang, J. Xiao, C.X. Wang, Y.X. Tong, G.W. Yang, Amorphous nickel hydroxide nanospheres with ultrahigh capacitance and energy density as electrochemical pseudocapacitor materials, Nature Communications 4 (2013) 1894.
[83] L. Cao, H. Li, Z. Xu, H. Zhang, L. Ding, S. Wang, G. Zhang, H. Hou, W. Xu, F. Yang, S. Jiang, Comparison of the heteroatoms-doped biomass-derived carbon prepared by one-step nitrogen-containing activator for high performance supercapacitor, Diamond and Related Materials 114 (2021) 108316.
[84] J. Wang, Y. Xu, M. Yan, B. Ren, X. Dong, J. Miao, L. Zhang, X. Zhao, Z. Liu, Preparation and application of biomass-based porous carbon with S, N, Zn, and Fe heteroatoms loading for use in supercapacitors, Biomass and Bioenergy 156 (2022) 106301.
[85] H. Quan, X. Fan, W. Wang, W. Gao, Y. Dong, D. Chen, Hierarchically porous carbon derived from biomass: Effect of mesopore and heteroatom-doping on electrochemical performance, Applied Surface Science 460 (2018) 8–16.

TITLE/ AUTHOR	**Strategic hazard mitigation of waste furniture boards via pyrolysis: Pyrolysis behavior, mechanisms, and value-added products / Foong, S.Y., Liew, R.K., Lee, C.L., (...), Tsang, Y.F., Lam, S.S.**
SOURCE	**Journal of Hazardous Materials Volume 421, 5 January 2022, 126774 https://doi.org/10.1016/j.jhazmat.2021.126774 (Database : Science Direct)**

Journal of Hazardous Materials 421 (2022) 126774

Contents lists available at ScienceDirect

Journal of Hazardous Materials

journal homepage: www.elsevier.com/locate/jhazmat

Strategic hazard mitigation of waste furniture boards via pyrolysis: Pyrolysis behavior, mechanisms, and value-added products

Shin Ying Foong [a,b,1], Rock Keey Liew [b,c,d,1], Chern Leing Lee [e], Wei Peng Tan [f], Wanxi Peng [a], Christian Sonne [g,a], Yiu Fai Tsang [h,**], Su Shiung Lam [b,a,*]

[a] Henan Province Engineering Research Center for Biomass Value-added Products, School of Forestry, Henan Agricultural University, Zhengzhou 450002, China
[b] Higher Institution Centre of Excellence (HICoE), Institute of Tropical Aquaculture and Fisheries (AKUATROP), Universiti Malaysia Terengganu, 21030 Kuala Nerus, Terengganu, Malaysia
[c] NV WESTERN PLT, No. 208B, Second floor, Jalan Macalister, Georgetown, Pulau Pinang 10400, Malaysia
[d] Eco-Innovation Research Interest Group, Faculty of Science and Marine Environment, Universiti Malaysia Terengganu, 21030 Kuala Nerus, Terengganu, Malaysia
[e] School of Engineering, Chemical Engineering Discipline, Monash University Malaysia, Jalan Lagoon Selatan, Bandar Sunway, Selangor 47500, Malaysia
[f] School of Pharmacy, International Medical University, 126, Jalan Jalil Perkasa 19, Bukit Jalil, 57000 Kuala Lumpur, Malaysia
[g] Aarhus University, Department of Bioscience, Arctic Research Centre (ARC), Frederiksborgvej 399, PO Box 358, Roskilde, DK-4000 Denmark
[h] Department of Science and Environmental Studies, The Education University of Hong Kong, Tai Po, New Territories, Hong Kong

ARTICLE INFO

Keywords:
Fiberboard
Plywood
Particleboard
Hazard mitigation
Waste valorization

ABSTRACT

Waste furniture boards (WFBs) contain hazardous formaldehyde and volatile organic compounds when left unmanaged or improperly disposed through landfilling and open burning. In this study, pyrolysis was examined as a disposal and recovery approach to convert three types of WFBs (i.e., particleboard, plywood, and fiberboard) into value-added chemicals using thermogravimetric analysis coupled with Fourier-transform infrared spectrometry (TG-FTIR) and pyrolysis coupled with gas chromatography/mass spectrometry (Py-GC/MS). TG-FTIR analysis shows that pyrolysis performed at an optimum temperature of 250–550 °C produced volatile products mainly consisting of carbon dioxide, carbon monoxide, and light hydrocarbons, such as methane. Py-GC/MS shows that pyrolysis at different final temperatures and heating rates recovered mainly phenols (25.9–54.7%) for potential use as additives in gasoline, colorants, and food. The calorific value of WFBs ranged from 16 to 18 MJ/kg but the WFBs showed high H/C (1.7–1.8) and O/C (0.8–1.0) ratios that provide low chemical energy during combustion. This result indicates that WFBs are not recommended to be burned directly as fuel, however, they can be pyrolyzed and converted into solid pyrolytic products such as biochar with improved properties for fuel application. Hazardous components, such as cyclopropylmethanol, were removed and converted into value-added compounds, such as 1,4:3,6-dianhydro-D-glucopyranose, for use in pharmaceuticals. These results show that the pyrolysis of WFBs at high temperature and low heating rate is a promising feature to produce value-added chemicals and reduce the formation of harmful chemical species. Thus, the release of hazardous formaldehyde and greenhouse gases into the environment is redirected.

1. Introduction

According to a report by the United States Environmental Protection Agency (USEPA), the production of wood waste, such as waste furniture boards (WFBs), reached 18.0 million tons in 2018. Of these, 3.1 million tons were recycled, 2.8 million tons were combusted for energy recovery, and 12.1 million tons (2/3) ended up in landfills (Karidis, 2021). This high waste volume could be attributed to the demand for new furniture and the undesirable approach (e.g., landfill) currently used to dispose this type of waste. Moreover, when companies are relocated or face closure, unused furniture may be discarded as waste, thus adding to the waste volume (Ikiz et al., 2021). The disposal of WFBs

* Correspondence to: Henan Province Forest Resources Sustainable Development and High-value Utilization Engineering Research Center, School of Forestry, Henan Agricultural University, Zhengzhou 450002, China.
** Corresponding author.
E-mail addresses: tsangyf@eduhk.hk (Y.F. Tsang), lam@umt.edu.my (S.S. Lam).
[1] These authors contributed equally to this work and act as co-first authors.

https://doi.org/10.1016/j.jhazmat.2021.126774
Received 10 June 2021; Received in revised form 18 July 2021; Accepted 27 July 2021
Available online 29 July 2021

is problematic due to its bulky size, making it difficult to be transferred, recycled and, sold; moreover, it contains hazardous materials, such as binders, waxes, flame retardants, paints, and coating, all being difficult to dispose safely thereby having environmental impacts (Rodgers et al., 2021).

Plywood (PW), particleboard (PB), and medium-density fiberboard (MDF), containing adhesives such as urea-formaldehyde (UF-resin) and phenol-formaldehyde, are commonly used in furniture manufacturing due to their low fabrication cost, fast curing rate, light color, and non-combustibility (Khan et al., 2020; van den Broek et al., 2020). Other adhesives, such as phenolic, melamine, and isocyanates, are also used but their costs are higher than UF-resin (USEPA, 2002). These additives are carcinogenic and thus toxic to human health, causing irritation of nose, eyes, skin, and throat and even cancers (Zhao et al., 2019). Moreover, these boards are further processed to become water-resistant through the application of waxes and paints containing a complex mixture of pigments, additives, and binders. In addition, flame retardants are also added to the boards for fire protection and these chemicals are associated with adverse health effects, including neurotoxicity, cancer, and reproductive toxicity (Rodgers et al., 2021; Wi et al., 2021). Therefore, these chemicals make it difficult to dispose WFBs through conventional approaches, such as landfilling.

WFBs mostly end up in landfills or are combusted either by incineration or open burning, which causes considerable air and soil pollution. The combustion of WFBs emit hazardous air pollutants (HAPs) including formaldehyde due to the presence of binding resin, releases volatile organic compounds (VOCs) such as toluene, xylene, and benzene due to the presence of waxes and paints, and generates CO_2, SO_2, CO, and NO_x. HAPs and VOCs are hazardous gases that cause not only mild effects on human health (e.g., irritations, headaches, and nausea) but also major harmful effects, including liver lesions, central nervous system and kidney failure, and cancer (USEPA, 2020, 2021). Landfills often generate methane, which is one of the chemicals listed as an HAP component causing global warming among other (USEPA, 2020). In addition to emitting pollutants, wood waste poses low biodegradability while landfills produce leachate that seeps into the surrounding aquatic environments and thereby pollutes the ground water that in turn threatens drinking water security and safety (Kapelewska et al., 2019).

Thus, landfilling and combustion cause long-term and undesirable hazardous effects to the environment; in view of this, thermochemical conversion methods, such as pyrolysis, are introduced as a promising technology for the disposal of WFBs (Chen et al., 2020; Ren et al., 2020). Pyrolysis is a thermochemical process to decompose biomass/waste material into pyrolytic products (e.g., biochar, bio-oil, and biogas) in an inert or oxygen-limited environment (Foong et al., 2021). This simultaneous reduction of waste and production of bioenergy via thermochemical technologies, such as pyrolysis, has been attracting increased attention due to the depletion of reserved fossil fuels. Pyrolysis usually occurs in enclosed systems, thus it limits the emission of HAPs, VOCs, and gases such as CO_2, NO_x and SO_2 into the atmospheric environment. The overproduction of WFBs and the abundance of lignocellulosic content in WFBs make it suitable as feedstock in pyrolysis for the recovery of value-added products (Undri et al., 2015). Among pyrolytic products, biochar is used as a bio-fertilizer, dye absorbent, and catalyst (Lam et al., 2018b; Liew et al., 2018b; Nam et al., 2018; Yek et al., 2019). The bio-oil produced may be upgraded into biofuel or used as chemical additives, whereas the biogas can potentially replace fossil fuel and supply electricity (Ge et al., 2021; González-Arias et al., 2020). This provides motivation for developing countries to pyrolyze wastes and then utilize the recovered pyrolytic products for industrial and domestic applications (González-Arias et al., 2020), considering that developed countries, such as the US and the UK, have also developed pyrolysis plants for fuel recovery from plastic waste (Honus et al., 2016; Riedewald et al., 2021).

Thermogravimetric analysis coupled with Fourier-transform infrared spectrometry (TG-FTIR) is used to determine the gaseous products emitted from the pyrolysis process. These instruments enable identification of the major gaseous products emitted at a temperature ranging from room temperature to 800 °C (Liang et al., 2018). However, TG-FTIR only operates at low heating rates (< 50 °C/min) due to limited heat conduction, and only compounds with a small size and low boiling point are detected, making it less applicable for pyrolysis studies (Qiao et al., 2019). Therefore, pyrolysis coupled with gas chromatography/-mass spectrometry (Py-GC/MS) is introduced to improve the specificity of the gaseous components produced from the pyrolysis process. Py-GC/MS is used to study pyrolysis reaction during varied heating rates and final pyrolysis temperatures and enables the real-time detection of volatiles released as they enter the chromatography column directly, thereby minimizing the occurrence of secondary reactions (Zhang et al., 2019). However, Py-GC/MS has a limitation on the detection of light gases (e.g., CO_2, CH_4, H_2, and CO) released during pyrolysis, whereas TG-FTIR enables the detection of light gases according to temperature changes. As such, Py-GC/MS and TG-FTIR provide precise measurement and detection of the gaseous components emitted, and is an important method to study the pyrolysis behavior of selected components (Liang et al., 2018).

The pyrolysis behavior and gaseous products of various wastes, including municipal solid waste (Ma et al., 2019; Xu et al., 2018), biomass (Lee et al., 2021; Liu et al., 2019; Wang et al., 2019), and food waste (Cai et al., 2019; Ming et al., 2020), have been analyzed using TG-FTIR and Py-GC/MS. Most of the research examined the volatiles emitted at specific pyrolysis temperatures, activation energy or kinetic pyrolysis models, and the product distribution of emitted gases. For instance, Aslan et al. (2018) studied the kinetics and the gaseous products emitted from the pyrolysis of MDF using TG-FTIR and Py-GC/MS, showing that the gas components detected at the maximum decomposition temperature (i.e., 800 °C) included alkenes, ketones, phenols, and cyclic compounds. Han et al. (2015) analyzed the pyrolysis properties of MDF and PB with TGA and Py-GC/MS, showing that the majority of the oil products were obtained at 500 °C. Xu et al. (2019) studied the pyrolysis behavior of oak timber with TGA and Py-GC/MS, reporting that the gaseous product being ketones, phenols, furans, esters, alcohols, and acids, with acids (37–43%) being the dominant components. Other studies showed that pyrolysis of poplar wood gave slightly different composition in the gaseous products including furans, carbonyls, and ketones, with phenols being the dominant (36%) (Wang et al., 2017). The difference in the component of the gaseous products could be attributed to the composition and content of lignocellulosic compounds in the wood, where the high content of lignin favored the formation of phenols, whereas the high content of hemicellulose favored the formation of acids (Staš et al., 2020).

Although previous studies have provided valuable information on the kinetics and gaseous components produced from the pyrolysis, limited research has been performed on the evaluation of gases emitted from WFBs pyrolysis using TG-FTIR and Py-GC/MS (Moreno and Font, 2015; Plis et al., 2016). Therefore, this study aims to explore the potential of using pyrolysis for an efficient and environmentally friendly approach to dispose harmful WFBs while converting the material into value-added chemicals. To the best of the author's knowledge, no study has so far combined TG-FTIR and Py-GC/MS analyses to perform an in-depth investigation of pyrolysis behavior and gases emitted from WFBs pyrolysis. The first step investigates pyrolysis behavior and the characteristics of gaseous products emitted from WFBs via TG-FTIR, whereas the second varies the final pyrolysis temperatures and heating rates via Py-GC/MS to study the composition and product distribution of gases emitted by WFBs pyrolysis. These results provide a fundamental understanding of WFBs pyrolysis and propose a new approach to waste reduction, hazard mitigation (e.g., limiting the emission of HAPs and VOCs), and recovery of biochemicals (e.g., phenols) from WFBs.

2. Materials and methods

2.1. Preparation of WFBs

Three types of WFBs, namely PW, PB, and MDF, were collected from a furniture manufacturing factory in Zhengzhou (Henan), China. The samples had a size of 80 mm × 150 mm × 15 mm (Fig. 1a). They were dried in an oven at 105 °C for 12 h to remove moisture. These boards were crushed into 20–30 mm using a lopping shear (Fiskars 32-inch PowerGear Bypass Lopper) and further ground into powder form using a laboratory blender (7010S, Waring). The powder was sieved to a particle size of < 125 μm as shown in Fig. 1b and stored in a sealed bag before being subjected to analysis.

2.2. Chemical properties of WFBs

The elemental contents of carbon (C), hydrogen (H), nitrogen (N), and sulfur (S) of the WFBs were analyzed using a CHNS elemental analyzer (FlashEA 1112, Thermo Electron Corporation, USA). The powder was dried in an oven at 105 °C for 1 h to remove the remaining moisture before analysis. Approximately 3 mg of WFBs powder were filled into a tin capsule and subjected into the autosampler of the elemental analyzer for analysis. The sample was combusted at 1000 °C to produce gaseous products such as water, SO_2, and CO_2 in order to detect C, H, and S via an infrared absorption detector. A thermal conductivity detector was used to detect N content. The oxygen (O) content was calculated from the mass difference as shown in Eq. 1 (Liew et al., 2018c).

$$Oxygen\ (O) = 100\ wt.\% - Carbon\ (C) - Hydrogen\ (H) - Nitrogen\ (N) - Sulfur\ (S) \quad (1)$$

The proximate analysis of WFBs were determined via a thermogravimetric analyser (STA-8000, PerkinElmer, country) with a constant argon flow of 50 mL/min to determine the volatile matter (VM), moisture content, ash content, and fixed carbon. Approximately 10 mg of sample was heated from ambient temperature to 900°C at a constant heating rate of 20°C/min. Moisture content and VM were determined from the weight loss of the sample at ≤150°C and 150–550°C, respectively. Ash content was obtained from the analysis of the lignocellulosic component. Fixed carbon content was calculated by the mass difference as shown in Eq. (2) (Lam et al., 2018a).

$$Fixed\ carbon\ (wt.\%) = 100\ wt.\% - moisture - volatile\ matter - ash \quad (2)$$

The lignocellulosic components (i.e., biochemical contents) of the WFBs were determined by the Van Soest method using a fiber analyzer (ANKOM 2000, Macedon, USA) as the digestion device (Ma et al., 2019; Van Soest et al., 1991). The neutral detergent fiber (NDF), acid detergent fiber (ADF), and acid detergent lignin (ADL) contents were determined from this test. Approximately 0.5 g of WFBs powder was weighed and sealed in a filter bag (ANKOM F57, Macedon, USA). The sample bag (i.e., filter bag) was digested in the fiber analyzer using 1.3 L of neutral detergent solution (ANKOM FND20C, Macedon, USA) at 100 °C for 75 min, followed by washing with 100 °C deionized water for three times (3–5 min each time) to remove the excess neutral detergent solution. Next, the bag was immersed in acetone (Sigma-Aldrich) for 3–5 min for extraction of non-lignocellulosic components. The bag was then air-dried and oven-dried at 105 °C for 4 h to remove the remaining moisture. Lastly, the dried sample was cooled to room temperature and weighed to obtain NDF content. ADF content was measured in a similar procedure as NDF, with the neutral detergent solution replaced by 1 N sulfuric acid (H_2SO_4) (ANKOM FAD20C, Macedon, USA), and WFBs powder replaced by the remaining NDF. ADL content was measured by hydrolyzing ADF with 72% (w/w) H_2SO_4 solution (Fisher scientific) at room temperature for 3 h. The residue was filtered and dried in an oven at 105 °C for 4 h. ADL content was obtained after the dried sample was cooled to room temperature and weighed. ADL was combusted in a muffle furnace at 550 °C for 2 h to identify the ash content. The contents of hemicellulose, cellulose, and lignin were quantified from Eqs. (3)–(5) (Adjalle et al., 2017; Liu et al., 2021; Patowary and Baruah, 2018).

$$Hemicellulose\ (wt.\%) = NDF\ (wt.\%) - ADF\ (wt.avb\%) \quad (3)$$

$$Cellulose\ (wt.\%) = ADF\ (wt.\%) - ADL\ (wt.\%) \quad (4)$$

$$Lignin\ (wt.\%) = ADL\ (wt.\%) - ash\ (wt.\%) \quad (5)$$

2.3. Energy properties of WFBs

The energy properties of the WFBs were assessed with indicators such as higher heating value (HHV), molar ratios of O/C and H/C, and fuel ratio (FR) to identify the energy content of the WFBs. HHV (i.e., calorific value) refers to the maximum amount of heat produced by a material when completely burnt (Perea-Moreno et al., 2016), while the molar ratios of O/C and H/C were used to determine the energy contents according to the oxygen-carbon and hydrogen-carbon bonds contained in a material (Hidayat et al., 2018b), and FR was used to determine the quality of material as solid fuel. A low FR often leads to less char combustion, quick burnout, and more flaming combustion, which is not preferable (Adeleke et al., 2020). These indicators were calculated according to Eqs. (6)–(9). The changes in elemental ratio are also illustrated in detail via the van Krevelen diagram, a graphical plot commonly used to investigate fuel properties according to different chemical compositions.

$$HHV\ (MJ/kg) = -1.3675 + 0.3137C + 0.7009H + 0.0318O \quad (6)$$

$$O/C = (O_{WFB}/MW\ \ of\ \ O) \div (C_{WFB}/MW\ \ of\ \ C) \quad (7)$$

$$H/C = (H_{WFB}/MW\ \ of\ \ H) \div (C_{WFB}/MW\ \ of\ \ C) \quad (8)$$

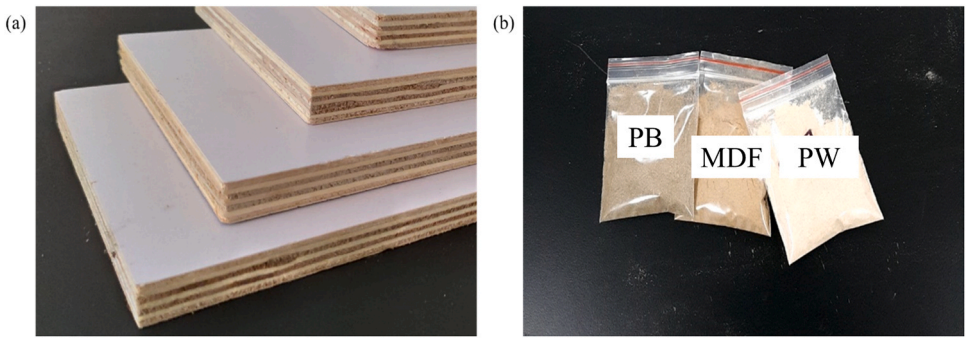

Fig. 1. (a) WFBs from a furniture manufacturing factory; (b) WFBs powder of PW, PB, and MDF.

$$FR = Fixed\ carbon_{WFB}/Volatile\ matter_{WFB} \quad (9)$$

2.4. TG-FTIR analysis

Pyrolysis behavior and gaseous product distribution can be investigated via a thermogravimetric (TG) analyzer (STA-8000, PerkinElmer, USA) combined with an online FTIR. The heating rate of the WFBs in the TG analyzer was set at 20 °C/min to ensure the pyrolysis of WFBs were under kinetic-controlled regime. In this work, approximately 10 mg of the sample was heated from room temperature to 900 °C with argon flow at 50 mL/min. The mass of the sample loaded for each run was less than 15 mg to ensure the kinetic control of the process and possible temperature gradient in the sample (Gu et al., 2013). The evolved gases entered the FTIR via a transfer line, in which the temperature was maintained at 200 °C to avoid possible gas condensation and secondary reactions. The FTIR spectrum was collected at a resolution of 4 cm^{-1} in a wavenumber ranging from 400 cm^{-1} to 4000 cm^{-1}, with a scan frequency of 16 scans/min. The National Institute of Standards and Technology (NIST) spectrum database was used to interpret the FTIR spectra of the WFBs. Some homo-diatomic gases, such as H_2 and N_2, were not detected by FTIR due to the limitation of the analyzer.

2.5. Py-GC/MS analysis

Py-GC/MS analysis was conducted using a vertical type pyrolyzer (5977B, Agilent, USA) coupled with a gas chromatography/mass spectrometry (7890B, Agilent, USA). Py-GC/MS is frequently used to determine the fast pyrolytic product distribution of samples at isothermal temperature conditions. Approximately 1 mg of sample was placed into a quartz capillary column. The probe consisted of a quartz column surrounded by platinum wire, whereas the probe provided different heating conditions during the pyrolysis process. Different final pyrolysis temperatures (i.e., 500, 600, and 700 °C) and heating rates (i.e., 30, 60, and 90 °C/min) were selected to investigate the effect of the selected conditions toward the pyrolytic product distributions. A heating rate of 50 °C/min and a pyrolysis time of 10 s were set for various final pyrolysis temperatures, whereas a final temperature of 600 °C and pyrolysis time of 10 s were set for various heating rates. The injection valve and pyrolytic product transfer line temperature was set to 300 °C to avoid possible gas condensation. The GC separation of pyrolysis vapor was performed using a TR-5MS column (30 m × 0.25 mm × 0.25 μm). The carrier gas selected was highly purified helium. Shunt mode was used, with a split ratio of 50:1 and a shunt rate of 50 mL/min. The GC program began at an initial temperature of 40 °C, which was maintained for 2 min, increased to 200 °C at a heating rate of 5 °C/min, and then increased to 280 °C at 10 °C/min and maintained at 280 °C for 15 min. Ion source temperatures were set at 230 °C with an ionizing voltage of 70 eV and an ionization current of 150 μA for electron ionization; the scanning quality range was 28–500 amu. The components obtained were identified by comparing with the NIST mass spectral library using similar indices of > 70%, and the quantification of components was obtained by calculating the percentage areas of each component from pyrolysis volatiles. The calculated data were used to interpret the experimental results. The solid residue of the pyrolysis was not measured because the focus of this study is to examine the pyrolysis vapor comprising majority of the components of the WFBs. The analysis was performed for at least three times to obtain the mean value for the data and to ensure the reproducibility of the experiment.

3. Results and discussion

3.1. Thermogravimetric analysis

Fig. 2 shows the thermogravimetry (TGA) and derivative thermogravimetry (DTG) curves for PW, PB, and MDF at a heating rate of 20 °C/min. PB showed a lower weight loss than PW and MDF within a decomposition temperature range of 250 °C to 550 °C. In addition, PB showed a smaller peak compared to PW and MDF at its maximum decomposition temperature (i.e., 366 °C) in the DTG curve; this result is consistent with the lower mass loss representing the volatile content detected in PB (64.4 wt%) compared to PW (69.1 wt%) and MDF (67.8 wt%).

Interestingly, PW showed two peaks in the DTG curve, indicating two different decomposition stages at a temperature ranging from 250 °C to 550 °C. This phenomenon is due to the possible decomposition of binding resin (e.g., urea-formaldehyde) at lower temperatures (Lai et al., 2018). The thermal degradation of urea-formaldehyde (UF-resin) that occurred at temperatures ranging from 177 °C to 457 °C likely decomposed ahead of lignocellulose component because UF-resin consists of thermally unstable methylene, carbonyl, and imino group network structures (Zhan et al., 2019). The cellulose and lignin of the lignocellulose component started to decompose at 280 °C and 430 °C,

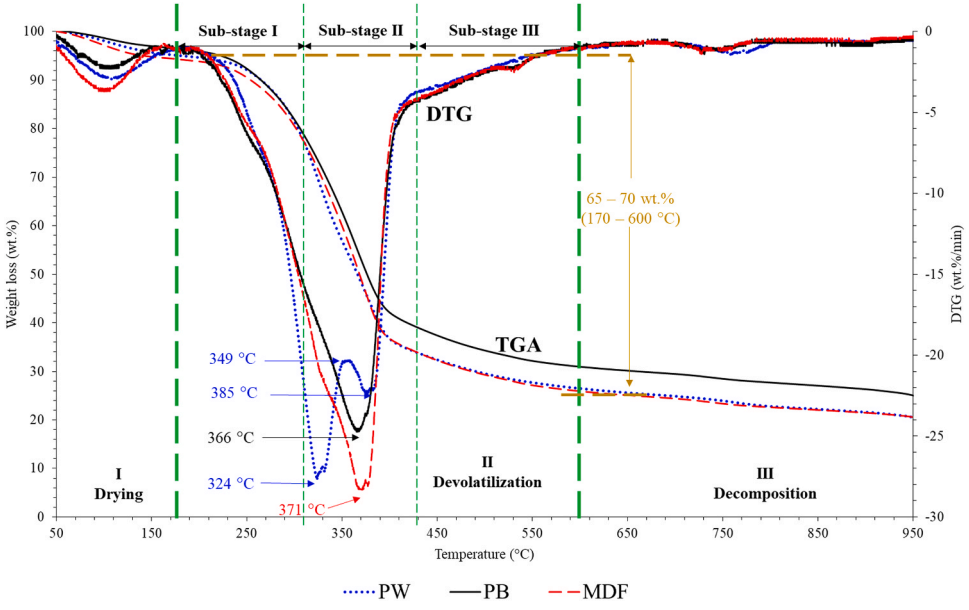

Fig. 2. Degradation stage during pyrolysis of WFBs at a heating rate of 50 °C/min.

respectively, resulting in an overlap of the UF-resin and lignocellulose decomposition stages. The formation of two peaks in the PW DTG curve is probably due to the inhibition of cellulose decomposition at 349 °C. During pyrolysis, the end of the hydroxymethyl group split from the UF-resin to produce formaldehyde, followed by a C–N bond cleavage to produce N-containing volatiles. The N-containing volatiles are reactive and unstable at high temperatures, thus tend to react with cellulose in the lignocellulose components, resulting in accelerated bond cleavage as observed from the first peak of the DTG curve of PW (324 °C). However, a lower mass loss was observed at 349 °C, which could be due to an inhibition of cellulose decomposition. At this temperature, an inhibition of cellulose decomposition may occur due to the produced free radicals, which likely react with lignin instead of cellulose to produce thermally unstable intermediates. As a result, the rate of cellulose decomposition was reduced, leading to a lower mass loss. The unstable intermediate was likely converted into oxycarbides and N-containing components that react and decompose with lignin as observed from the second peak at 385 °C (Zhan et al., 2019).

The thermal decomposition stages, including drying (<170 °C), devolatilization (170 °C to 600 °C), and decomposition stages (>600 °C) during WFBs pyrolysis are shown in Fig. 2. First, weight loss was observed at the drying stage during which the WFBs underwent devolatilization where most of the VM was released at temperatures ranging from 170 °C to 600 °C. Around 70 wt% of the weight loss was then observed at the devolatilization stage, revealing that most volatiles were released due to the decomposition of lignocellulosic components. Lignocellulosic components mainly comprise hemicellulose, cellulose, and lignin, which decompose at different temperature ranges due to their various chemical structures as illustrated in Fig. 2 (Cai et al., 2019).

The devolatilization stage can be further divided into three sub-stages. Sub-stage I represents the devolatilization of the hemicellulose. Hemicellulose comprises mannose, galactose, xylose, arabinose, and glucose (light component), which have the lowest thermal stability among other lignocellulosic components; thus, it decomposes at lower temperatures (i.e., 170–310 °C) (Ma et al., 2015). Sub-stage II occurs at 310–430 °C, corresponding to cellulose devolatilization. Cellulose has slightly higher thermal stability than hemicellulose due to the presence of linear and unbranched structures that decompose at higher temperatures (i.e., 280–400 °C) (Fateh et al., 2013). Sub-stage III (i.e., 430–600 °C) corresponds to the devolatilization stage of lignin having the highest thermal stability and decomposing at temperatures higher than 430 °C due to its complex polymer network containing phenoxy and phenyl groups. The presence of aromatic rings in lignin requires higher energy for bond cleavage compared with C–C and C–O bonds in cellulose and hemicellulose. These results are in agreement with previous research on devolatilization of lignocellulosic materials, where thermal degradation starts at 200 °C and the highest mass loss is observed at temperatures ranging from 200 °C to 600 °C (Lam et al., 2016b; Ming et al., 2020; Xu et al., 2018).

The final WFBs pyrolysis stage is the decomposition stage, where most of the volatiles are released and the remaining non-volatile carbon undergoes carbonization to produce biochar (Lam et al., 2016a). Overall, the optimum WFBs pyrolysis temperature is 200–550 °C as most VM releases and converts into potentially useful liquid and gaseous products. Pyrolysis temperatures above 600 °C represent the carbonization stage where char forms.

3.2. Chemical properties of WFBs

The chemical properties of WFBs are shown in Table 1. The major elements in PW, PB, and MDF were carbon (C) and oxygen (O), followed by small amounts of hydrogen (H) and nitrogen (N), whereas no sulfur (S) was detected. The presence of high contents of C and O in WFBs are mostly due to lignocellulosic components containing hydrocarbon and phenolic components (Ma et al., 2019). PW had the highest VM and cellulose content and the lowest FC and C contents among the three

Table 1
Chemical properties of WFBs in the present study.

Proximate analysis (wt%)	PW	PB	MDF
Moisture[a]	4.5	4.1	5.2
Volatile matter[a] (VM)	69.1	64.4	67.8
Fixed carbon[a,c](FC)	23.3	27.5	23.7
Ash[a]	3.1	4.0	3.3
Elemental analysis (wt%)			
Carbon[a](C)	38.0	41.8	41.2
Hydrogen[a](H)	5.5	6.4	6.3
Nitrogen[a](N)	7.7	5.2	5.2
Sulphur[a](S)	–	–	–
Oxygen[a,c] (O)	48.8	46.7	47.3
O/C[b]	0.963	0.838	0.861
H/C[b]	1.737	1.837	1.835
Biochemical composition (wt%)			
Hemicellulose[a]	14.0	12.7	14.9
Cellulose[a]	46.0	35.1	35.6
Lignin[a]	36.9	48.2	46.2
HHV[a] (MJ/kg)	15.96	17.72	17.48
Fuel ratio (FR)	0.337	0.427	0.350

"-" refers to not detected.
[a] Based on a dry basis.
[b] Molar ratio.
[c] By difference.

WFBs. Lignin comprises complex carbon structures and thus having high thermal stability. During the heating process, the remaining non-volatile carbon is known as FC and was likely to be derived mainly from lignin, whereas hemicellulose and cellulose with lower thermal stability easily volatilized during heating, thus contributing to the VM content (Liew et al., 2018a). This phenomenon explains the high cellulose and low lignin content of PW, which result in high VM and low FC. A small amount of ash detected in WFBs (3.1–4.0 wt%) may comprise Na, Al, Mn, Fe and K and could act as an inorganic catalyst that increases cracking processes and thereby increases the yield of VM (Liew et al., 2018c).

MDF showed a different biochemical composition despite having nearly the same elemental contents compared to PW. This result could be due to the differences in wood type used in the furniture boards. MDF has a higher hemicellulose content (14.9 wt%), which decomposed into organic volatiles at a similar pyrolysis condition as PW (14.0 wt%) (Table 1), thus contributing to higher VM content. This result is consistent with the research carried out by Zhao et al. (2017), showing that hemicellulose is rich in random, branches and amorphous structures that can easily be decomposed to form volatiles at low temperature. As a result, MDF with a higher content of hemicellulose produced larger amounts of VM than PW with a lower hemicellulose content. PW consisted of the highest N content (7.6 wt%) compared to PB and MDF probably due to the higher amount of N-containing bind resin used in its manufacturing (Zhan et al., 2019). Combustion of materials with a high amount of N would produce NO_x (i.e., NO, NO_2, and N_2O), and these gases lead to acid rain. Moreover, S was not detected in the WFBs, probably due to the low content of S to be detected by the elemental analyzer. Thus, the formation of SO_2 (a major component contributing to acid rain) is likely to be negligible from WFBs pyrolysis and combustion (Cruz et al., 2020). However, direct burning of WFBs is not encouraged because it produces NO_x causing air pollution.

3.3. Energy properties of WFBs

The high heating value (HHV) of WFBs range from 16 MJ/kg to 18 MJ/kg with PW showing the lowest HHV, whereas PB and MDF having similar HHVs (Table 1). However, WFBs consisted of high O content (i.e., 46.7–48.8 wt%) and could result in the production of liquid oil with high O content from the pyrolysis of WFBs, causing unstable liquid oil products during storage. As a result, the liquefaction process of fuel was hindered, thereby reducing its calorific value.

C–O bonds have a higher bond dissociation energy than C–C bonds. During combustion, less heat energy is produced from components with C–O bonds (305 kJ/mol) compared to components with C–C bonds (411 kJ/mol), thus reducing the performance of fuel including its calorific value (Cruz et al., 2020; Kaufman, 1993). Therefore, PW had the lowest HHV (16.0 MJ/kg) due to the high O content (48.8 wt%). Fig. 3 shows the van Krevelen plot for the WFBs compared to the conventional solid fuel lignite and the biochar derived from PW, PB, and MDF; the results on the biochar were obtained from the pyrolysis of PW, PB, and MDF in a lab scale pyrolysis unit from previous studies (Haeldermans et al., 2019; Liu and Balasubramanian, 2013; Mitchell et al., 2013). The biochar had lower H/C and O/C ratios compared to WFBs and lignite, indicating a higher energy potential in the biochar (Ayiania et al., 2019).

The low O/C ratio in biochar reflects fewer C–O bonds and more C–C bonds. Hence, a higher chemical energy was obtained from biochar with low O/C ratio as lesser energy is required to break the C–C bond having a lower bond dissociation energy (607 kJ/mol) compared to the C–O (1077 kJ/mol); as a result, the HHV of biochar increased (Lee et al., 2019; Speight, 2017). Moreover, solid fuels (e.g., biochar) with low H/C and O/C ratios are recognized as clean fuels since they produce less water vapor and smoke during combustion (Lee et al., 2019). Therefore, given its higher H/C and O/C ratios, WFBs could be converted into biochar with improved fuel properties. The FR of PW, PB, and MDF was within the range of 0.34–0.43, which is lower than lignite (0.84) (Liu and Balasubramanian, 2013), whereas the lower FR indicates poor combustion performance and increased emission of air pollutants. Thus, burning these boards is not recommended for energy recovery; instead, they should be converted into liquid or gaseous fuels due to their high VM contents.

3.4. TG-FTIR analysis

The time evolution of the FTIR spectra for all three types of boards showed similar behavior in the released gases. Fig. 4 displays the FTIR spectra of the WFBs at different time intervals and temperatures. For the pyrolysis of PW, almost no gaseous substances were detected at temperatures below 60 °C. The FTIR spectra started to show weak peaks of water vapor after 2 min at a temperature around 70 °C, whereas multiple FTIR peaks were detected within the ranges of 3500–4000 cm^{-1} and 1300–2000 cm^{-1}, indicating the presence of water vapor. On top of the water vapor peaks, weak peaks were detected at 2350 cm^{-1} and ~700 cm^{-1}, suggesting the presence of CO_2 in the gas mixture. The released gaseous product became predominantly CO_2 after 8 min at 200 °C, where prominent peaks were found at 2400 cm^{-1} and 700 cm^{-1} along with weaker peaks of water vapor. In addition, multiple peaks were detected at ~3300 cm^{-1} and 950 cm^{-1}, suggesting the presence of NH_3 at this temperature. It should be noted that as the temperature of the experiment progressed to a higher temperature (approximately 300 °C), the CH_4 peaks at 2800–3100 cm^{-1} and 1200–1350 cm^{-1} became more prominent. After 20 min, the presence of CO became more prominent as evidenced by 2100 cm^{-1} and 2200 cm^{-1} peaks at 430 °C in the FTIR spectra. This finding is consistent with that of Fateh et al. (2013), showing that CO_2 peaks were found at a temperature higher than 280 °C. The result was further supported by the FTIR of PW at 12 min and 270 °C, where no CO peak was found in the spectra. The presence of new peaks at 500–700 cm^{-1} and 1500–1800 cm^{-1} at a later stage was likely due to the presence of volatile aromatic hydrocarbons, such as benzene and toluene. At this point, inferring the composition of the gas mixture became difficult as the FTIR spectra became heavily convoluted.

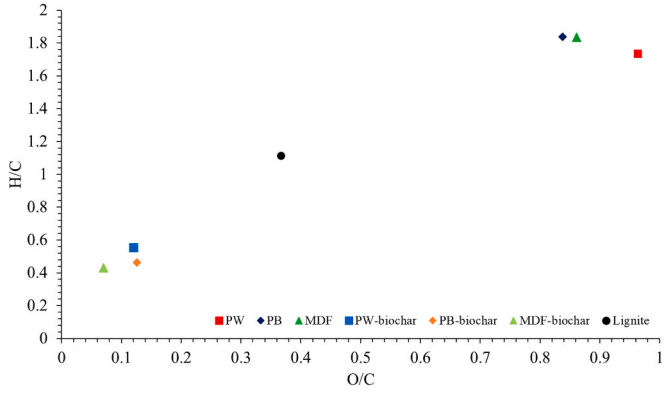

Fig. 3. Van Krevelen plot for WFBs, including PW, PB, MDF, PW-biochar, PB-biochar, MDF-biochar, and lignite.

The FTIR spectrum of PB pyrolysis did not exhibit any significant release of gaseous components before 70 °C. A weak CO_2 peak at around 2400 cm^{-1} was detected at approximately 70 °C. The CO_2 peak became more prominent as the experiment progressed to 4 min, where a sharp peak was detected at around 2400 cm^{-1} and a weaker peak was observed at around 500 cm^{-1} in the FTIR spectra. Multiple peaks after 8 min at 2500–3700 cm^{-1} and 1300–1800 cm^{-1} bands indicated the presence of water vapor. The water vapor peaks were presumably the absorbed water in the wood composites. The absorbed water required a higher temperature (>100 °C) to reach the boiling point. The water molecule collided with the wood composites, thus creating pressure. This pressure was transmitted throughout the absorbed water molecule causing the water molecule hard to form bubbles and escape as gas molecules (start boiling); thus, a higher temperature was required to boil the absorbed water. At around 12–16 min (>300 °C), more absorbance peaks started to register on the FTIR spectrum, indicating the presence of multiple components in the vapor phase. At this point, it is difficult to deconvolute the FTIR spectrum and identify the exact composition of the gas mixture. However, we could still deduce that CO_2 (dominant peak at 2400 cm^{-1}) remains to be the main component of the mixture. The new peaks at around 2900–3000 cm^{-1} and 1200–1400 cm^{-1} suggested the presence of volatile alkane gases, such as methane. This finding is similar to the FTIR spectra of wood lignin where the peak appears around 2900–3000 cm^{-1} and 1200–1400 cm^{-1}, indicating the presence of C–H stretching and C–H bending vibrations of the methyl group, respectively (Zhao et al., 2014). The presence of new peaks at around 1500–1800 cm^{-1} was likely due to volatile aromatic hydrocarbons, such as benzene and toluene, which were by-products of pyrolysis. After 20 min, the volatile alkane and aromatic hydrocarbon became less prominent as the experiment progressed to 30 min. It is noteworthy that at the later pyrolysis stage around 24–30 min, the IR spectra of CO at 2100 cm^{-1} and 2200 cm^{-1} peaks became more prominent, indicating that CO is released at a higher temperature.

The FTIR spectra of MDF below 70 °C showed no release of volatile components, whereas water peaks started to appear at 3500–4000 cm^{-1}, 1400–1900 cm^{-1}, and 500–700 cm^{-1}, where the sample temperature reached 70 °C, indicating the release of retained water. When the experiment progressed to 4 min at around 110 °C, extra peaks started to emerge at 600–800 cm^{-1} and 2300–2400 cm^{-1} along with the water vapor peaks detected earlier, indicating the release of CO_2 possibly due to the side chain C-C bond breakage in lignin (Liu et al., 2008). As pyrolysis progressed to a higher temperature (~200 °C), the CO_2 concentration of the vapor phase increased, and the pyrolysis became so convoluted that an exact breakdown of the gas phase composition became impossible (without further processing). However, new peaks were registered in the FTIR spectrum at the 1500–1800 cm^{-1} and 2900–3100 cm^{-1} bands, suggesting the presence of volatile alkanes (e.g., CH_4) or aromatic hydrocarbons (e.g., toluene or benzene) in the gas phase. The FTIR spectra of the gas phase remained the same until the reaction progressed to 20 min, where the release of CO_2 became significantly weaker, whereas the release of CO (at the 2100 and 2200 cm^{-1} peaks) increased at the later stage of pyrolysis.

Overall, the main components released from WFBs were CO_2, CH_4,

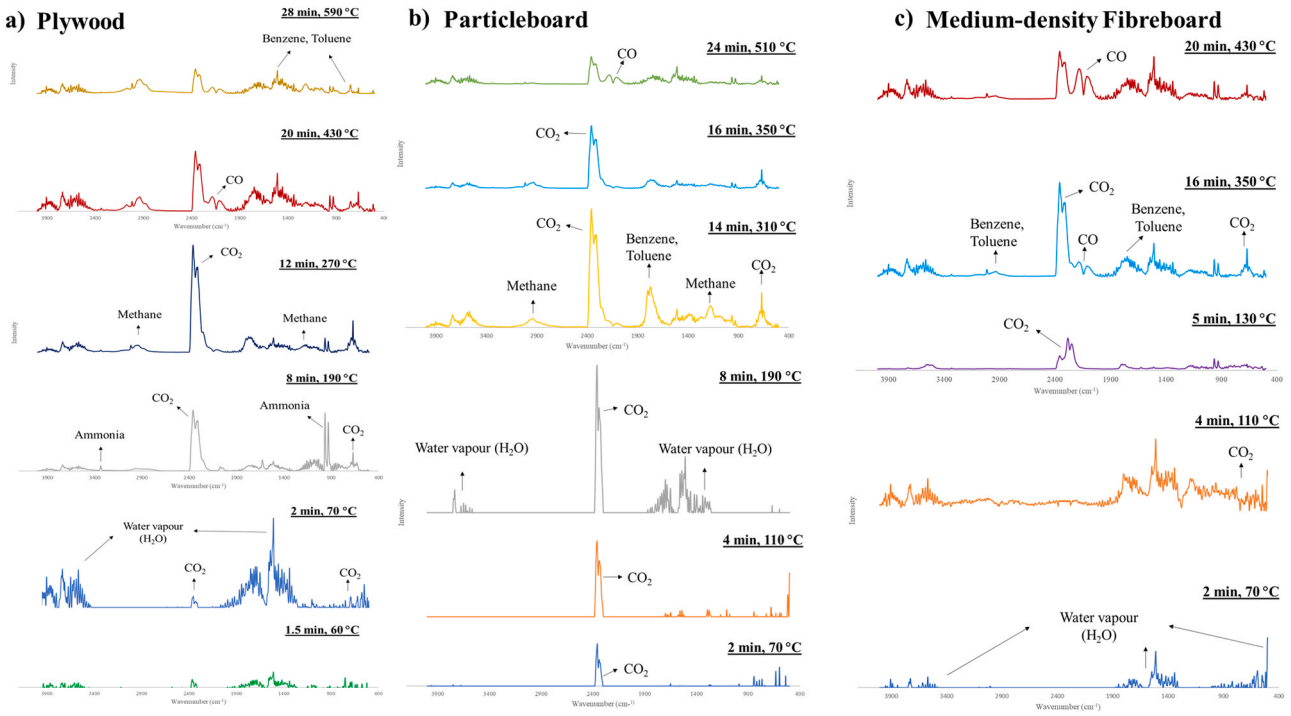

Fig. 4. FTIR spectra of (a) PW, (b) PB, and (c) MDF at different time intervals and temperatures.

CO, H_2O, and aromatic compounds, such as toluene and benzene. Combustible gases, such as CO, H_2, and CH_4, are fuel sources; thus, the use of pyrolysis provides an alternative to transform the hazardous components (e.g., benzene and toluene) in WFBs into biofuel (Chen et al., 2021). The release of CO_2, CH_4, and CO was due to the cleavage of functional groups, such as carbonyl, ether, carboxyl, and methoxyl, as well as the secondary cracking of phenolic compounds (Chen et al., 2019a). CO was observed at higher temperatures (>700 °C) due to the Boudouard reaction between char and CO_2 (Ong et al., 2020; Yang et al., 2021). The FTIR spectrum of the WFBs also shows that the organic components in WFBs undergo thermal degradation at sub-stage II of pyrolysis to produce light molecular weight compounds, such as benzene and toluene. These components can be added to gasoline to improve the octane rating and provide an alternative to recover useful chemicals from WFBs and divert the waste from combustion and landfills that burden the environment.

3.5. Py-GC/MS analysis

The chemical components detected and obtained from WFBs pyrolysis can be classified into phenols, carbonyls, alcohols, hydrocarbon, nitrogenous, and other oxygenates. Among them, compounds, such as aldehyde, ketone, ester, and carboxylic acids, are grouped into "carbonyls", whereas compounds, such as silicone and oxygenates other than carbonyl, are grouped into "other oxygenates". Amines and amides are grouped into "nitrogenous" compounds. The pyrolytic products are also classified according to carbon number ranges: C_1–C_5, C_6–C_{10}, C_{11}–C_{15}, C_{16}–C_{20}, and $C_{>20}$. Lower molecular weight compounds, such as CO, CH_4, and H_2, were not detected due to the detection limit of GC/MS.

3.5.1. Effect of final pyrolysis temperature

Final pyrolysis temperature refers to the highest temperature achieved and recorded during the pyrolysis process, representing one of the key factors affecting the product distribution of pyrolytic products. The extent of chemical reactions that occurred during pyrolysis is influenced by different final pyrolysis temperatures. For example, a high final pyrolysis temperature improves the degree of decarbonylation and secondary reactions such as addition, aromatization, and saturation reactions (Qiao et al., 2019). Fig. 5 shows the distribution of pyrolytic products at different final pyrolysis temperatures according to product series and carbon number range for WFBs with a standard error of 5%. Different types of WFBs showed different products during pyrolysis; this variation could be attributed to the use of different types of wood and the addition of different components, such as adhesives, paints, coatings, and additives, during the manufacturing process. Woods, such as poplar, oak, larch, cherry, and maple, with different compositions of lignocellulosic component would result in varied final product distributions. During pyrolysis, hemicellulose and cellulose are converted into carbonyls through cracking, whereas lignin is converted into phenols via dehydration, depolymerization, and decarboxylation (Wang et al., 2017).

As shown in Fig. 5a, the phenol group in PW decreased by 23.5% and the oxygenates increased by 20.6% when the final temperature increased from 500 °C to 700 °C. These changes are likely due to the reaction between PW and UF-resin at a high temperature (700 °C). When heating was provided, the UF-resin decomposed to form a thermally unstable N-containing intermediate. This intermediate could react with lignin in PW and thus improve the decomposition of lignin. Phenol is one of the products produced from lignin decomposition. As the temperature increased, recondensation, hydration, and polymerization reactions between phenols and other volatiles (e.g., oxygenated components released during pyrolysis) were promoted, reducing the production of phenols and promoting the formation of other oxygenates at high temperature (Zhan et al., 2019).

The pyrolysis of MDF produced the highest percentage of phenols (45.6–49.8%). The heat received by the MDF (compressed wood sawdust/powder) could be inhibited due to the compactness and smaller particle size of the wood powder in MDF as compared to PB (compressed wood chips) and PW (glued wood pieces). Additional heat energy was required to initiate the decomposition of MDF as the heat was transmitted from the outer core into the inner core of particles during pyrolysis. This result is in agreement with that reported by Suriapparao and Vinu (2018), indicating that a decrease in particle size would

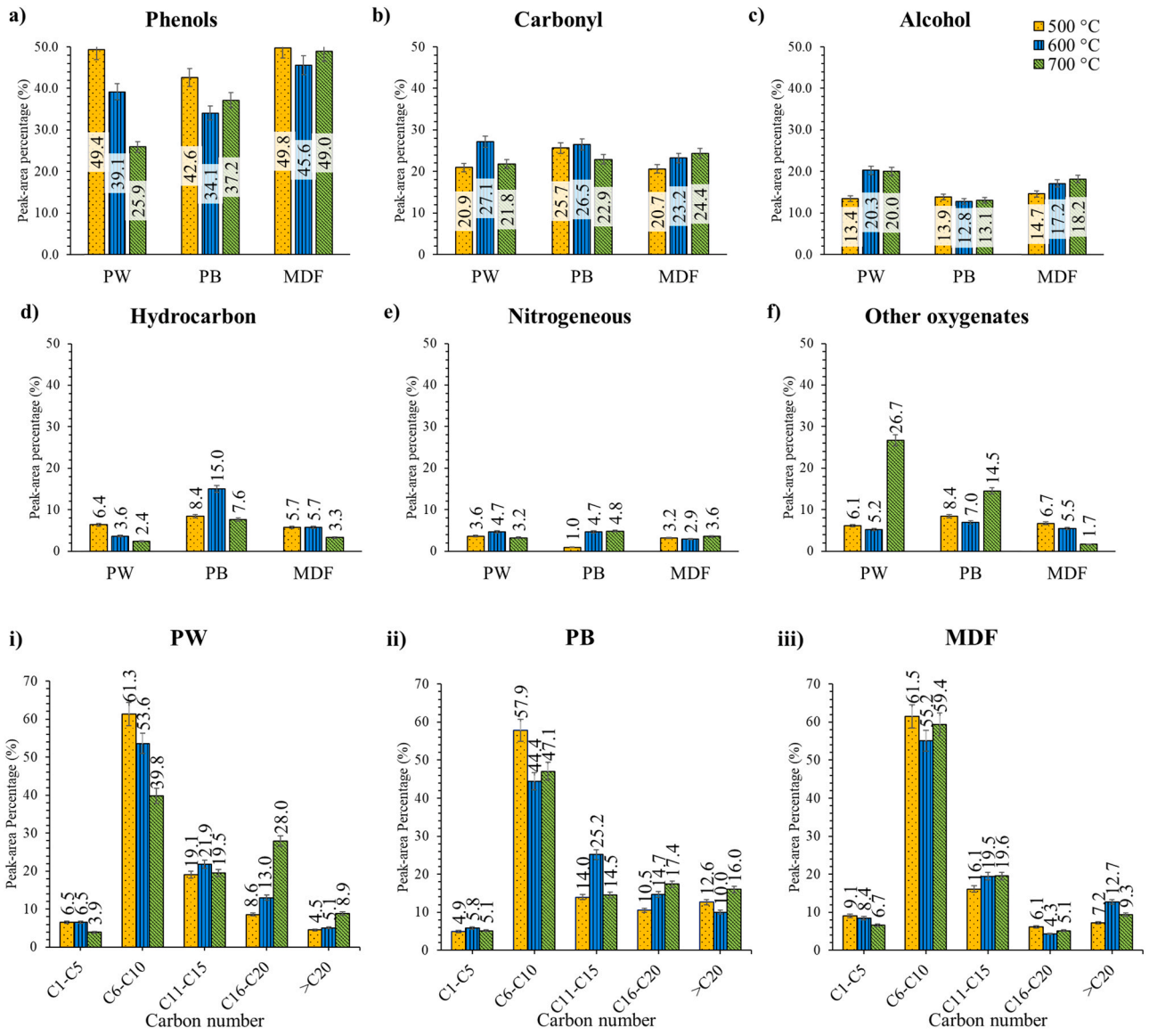

Fig. 5. Distribution of pyrolytic products from WFBs at different final temperatures according to product series (a-f) and carbon number (i-iii). These components are grouped into (a) phenols, (b) carbonyls, (c) alcohols, (d) hydrocarbons, (e) nitrogenous, and (f) other oxygenates.

increase the activation energy. As a result, additional heat energy is required for the pyrolysis decomposition of feedstock with small particle size.

Carbonyls and alcohols are other main products from WFBs pyrolysis, suggesting that the lignocellulosic components fragmented into smaller molecules, such as ester, carboxylic acid, aldehyde, and ketones, through dehydration, cracking, scission, decarbonylation, and cyclization (Yu et al., 2021). Moreover, oxygenates, such as ketones and carboxylic acid, were produced from hemicellulose decomposition and aldehydes and phenols from lignin degradation (Taghizadeh-Alisaraei et al., 2017). Interestingly, products from PB pyrolysis show the highest content of hydrocarbons (up to 15%) compared to that observed from PW and MDF pyrolysis. High final pyrolysis temperature promotes decarboxylation by removing carboxyl groups from carbonyl compounds, resulting in the production of hydrocarbons and CO_2 (Mishra et al., 2020). However, the hydrocarbon content decreased around 700 °C, probably due to re-condensation of hydrocarbons with moisture or other volatiles, forming additional phenol and other oxygenates (Fig. 5a, f). Table 2 shows the main components produced from the pyrolysis of WFBs at different final pyrolysis temperatures.

The pyrolysis of PW produced components with a higher carbon number range of C_{16}-C_{20} and lower carbon number range of C_6-C_{10} when the temperature increased. This result was possibly due to the reactions, such as recondensation, hydration, and polymerization, which occurred more frequently between PW, UF-resin, and light molecular weight components (compounds with C_6-C_{10}) at higher temperatures. Light molecules received a higher amount of energy at higher final temperatures and hence reacted more frequently with volatiles (e.g., phenol) released during pyrolysis via reactions, such as re-condensation and polymerization, resulting in the production of higher molecular weight components (Jiang et al., 2019). The C–N bond in UF-resin was likely to be cracked at a high temperature, producing thermally unstable N-containing compounds (e.g., amines and amides), which could react more frequently with the light hydrocarbons to produce complex carbon components, thus increasing the amount of components with high carbon number at 700 °C (Zhan et al., 2019).

In addition, an increase in temperature resulted in increased sinapyl alcohol and decreased 4-ethylsyringol for PW pyrolysis. As the temperature increased, 4-ethylsyringol was likely to react with methanol (cracking of hydroxymethyl attached to cycloalkane rings or aromatic

Table 2
Main components produced (%) at different final pyrolysis temperatures and heating rates for PW, PB, and MDF.

No.	Compounds	PW					PB					MDF				
		500 °C	600 °C	700 °C	30 °C/min	60 °C/min	90 °C/min	500 °C	600 °C	700 °C	30 °C/min	60 °C/min	90 °C/min	500 °C	600 °C	700 °C	30 °C/min	60 °C/min	90 °C/min
21	Cyclopentanedione	1.3	0.7	0.2	–	–	–	0.9	0.7	0.8	–	–	–	1.6	0.9	1.0	–	–	–
20	Cyclopropylmethanol	3.8	5.2	2.6	2.6	5.6	5.3	4.0	4.3	3.6	4.3	5.3	5.5	6.9	6.6	5.6	4.6	5.7	7.1
18	1,4:3,6-Dianhydro-D-glucopyranose	3.9	2.8	1.9	6.1	4.4	4.2	0.7	0.9	0.8	1.3	1.4	1.4	1.2	1.0	1.0	1.7	0.6	0.9
19	3-Ethyl-2-hydroxy-2-cyclopenten-1-one	0.2	0.4	0.1	–	–	–	0.8	0.3	0.7	–	–	–	0.5	0.4	0.3	–	–	–
5	4-vinylguaiacol	4.8	3.5	2.1	4.9	4.9	4.3	6.2	5.2	5.8	6.5	7.3	7.1	6.1	6.0	5.8	6.1	7.1	6.1
17	3,5-Dimethoxy-4-hydroxytoluene	3.9	3.1	2.0	3.3	3.3	3.0	3.2	2.5	2.6	3.3	0.3	2.7	3.5	3.1	3.1	3.0	3.4	3.1
7	Acetosyringone	1.0	1.0	0.7	1.1	0.9	1.0	0.8	0.1	0.7	0.9	0.8	0.7	0.9	1.0	1.0	0.7	1.0	0.8
6	Syringol	7.9	7.4	3.5	7.4	7.6	7.9	7.2	5.0	5.9	6.4	6.8	7.4	7.4	6.8	7.1	6.4	9.6	7.1
2	Guaiacol	0.3	0.2	0.1	–	–	–	0.7	0.3	0.5	–	–	–	0.3	0.3	0.3	–	–	–
10	4-ethylsyringol	17.4	9.8	6.3	–	–	–	7.7	7.0	7.4	–	–	–	9.9	9.3	9.4	–	–	–
4	Isoeugenol	3.0	1.9	1.2	3.5	2.8	3.3	4.8	3.3	4.3	4.1	5.1	5.8	5.3	5.0	3.8	3.8	5.0	5.3
12	4-Propenyl-2,6-dimethoxyphenol	8.1	7.0	4.3	9.4	9.0	8.6	6.7	6.3	6.2	7.5	7.5	7.0	9.5	9.3	9.6	7.8	8.8	9.8
16	Syringylacetone	1.7	1.8	1.3	3.0	3.1	2.5	1.4	1.2	1.3	2.8	2.2	1.9	2.3	2.2	2.2	1.8	2.9	3.0
11	Sinapylalcohol	1.4	7.8	10.1	1.3	1.0	2.7	2.5	4.2	3.4	2.6	2.1	1.8	1.0	3.1	3.6	1.7	0.6	0.7
22	Hexadecanoic acid	2.5	2.0	1.6	2.6	2.5	2.5	1.9	1.8	2.4	2.6	1.9	2.0	1.4	1.5	1.6	0.7	1.3	1.3
/	Paromomycin	1.4	0.6	1.5	2.0	1.8	2.3	1.4	0.6	2.3	0.3	2.0	0.6	1.5	1.5	1.1	0.6	0.9	1.4
/	Ethyl cholate	1.3	1.2	1.7	1.9	1.5	1.3	4.2	1.9	4.4	1.8	1.2	1.2	2.9	2.5	2.4	1.7	0.5	1.3

"-" refers to not detected.
"/" refers to not assigned.

rings), followed by dehydrogenation to form sinapyl alcohol (Xu et al., 2018). The increased amount of sinapyl alcohol could be contributed by 4-propyl-2,6-dimethoxyphenol and syringol via reaction with the hydroxyl radical and butene-3-ol, respectively. Paromomycin decreased and cyclopropylmethanol increased with increased temperature from 500 °C to 600 °C but showed an opposite trend at 700 °C. The cracking of paromomycin at a lower temperature could produce cyclopropylmethanol and N-containing structures, but these structures were likely to recondense to produce paromomycin when receiving higher heat energy during pyrolysis, thus explaining the fluctuating trend for paromomycin and cyclopropylmethanol (Zhan et al., 2019).

The pyrolysis of PB showed a slightly different trend from the pyrolysis of PW, where pyrolysis at a final temperature of 600 °C produced less C_6–C_{10} components but more C_{11}–C_{15} components. Interestingly, the hydrocarbon content of PB at 600 °C increased, suggesting that the pyrolysis of PB at 600 °C favored the formation of C_{11}–C_{15} hydrocarbons. Components with carbon number $C_{>20}$ and C_5–C_{10} decreased at 600 °C but increased at 700 °C; by contract, $C_{4–6}$ showed the opposite trend. This result can be explained as when the temperature increased, the decomposition of $C_{>20}$ components improved due to the higher heat energy provided at a higher temperature, resulting in the production of a high amount of component with carbon number $C_{4–6}$ and a low amount of component with carbon number $C_{>20}$. When the temperature increased further (700 °C), additional heat energy became available, resulting in increased reactions, such as hydration, polymerization, and re-condensation of $C_{4–6}$ compounds with $C_{>20}$ and C_6–C_{10} compounds.

For the pyrolysis of MDF, the trend in carbon number and product series were nearly similar at different final pyrolysis temperatures, suggesting that the amount of heat energy supplied during the pyrolysis had less influence on the product distribution. Thus, final pyrolysis temperature was not the main factor that altered the chemical composition in VM from MDF pyrolysis. Therefore, 500 °C is suggested to be the optimum temperature for pyrolysis of MDF to obtain components with low carbon numbers and high phenol contents. Overall, the final pyrolysis temperature showed an obvious effect on the pyrolysis of PW and PB but less effect on the pyrolysis of MDF. In general, the pyrolysis of WFBs at 500 °C produced the highest amount of 4-ethylsyringol, which can be used as food additives, but the pyrolysis at 700 °C produced the highest amount of sinapyl alcohol, which may cause skin, eye, or respiratory irritation. Value-added chemicals, such as paromomycin (used as an antimicrobial for parasitic infections) and 3,5-dimethoxy-4-hydroxytoluene (pharmaceutical formulation for spasmolytic or antispasmodic agent), can also be recovered from WFBs pyrolysis. The pyrolysis at 700 °C reduced the formation of cyclopropylmethanol, a danger component that is flammable, corrosive, and irritating, and is a health hazard. Moreover, the pyrolysis of WFBs produced a high amount of phenols, which can be used as gasoline additives, food additives, colorants, pesticides, and antioxidants, as well as intermediates for the pharmaceutical industry. This result suggests that WFBs can be a suitable raw material for the recovery of phenol via pyrolysis.

3.5.2. *Effect of pyrolysis heating rate*

Heating rate is also an important factor that affects the pyrolysis process. An increase in heating rate indicates that the feedstock receives higher energy per unit of time. Thus, pyrolysis with a higher heating rate could improve the breaking of chemical bonds and promote the conversion of feedstock into pyrolytic products. The increase in heating rate also favors the breaking of higher bond dissociation energy chemical bonds due to the huge amount of energy gained in one time. However, when the heating rate is too high, heat transfer may become a rate-control step for the pyrolysis process, resulting in an incomplete decomposition of the feedstock (Qiao et al., 2019). During the pyrolysis process at high heating rates, the volatiles released from biomass are immediately fragmented upon gaining a high amount of heat energy. The hot volatile then exits the reactor immediately, resulting in a shorter reaction time to obtain the desired products (Qiao et al., 2019). Fig. 6

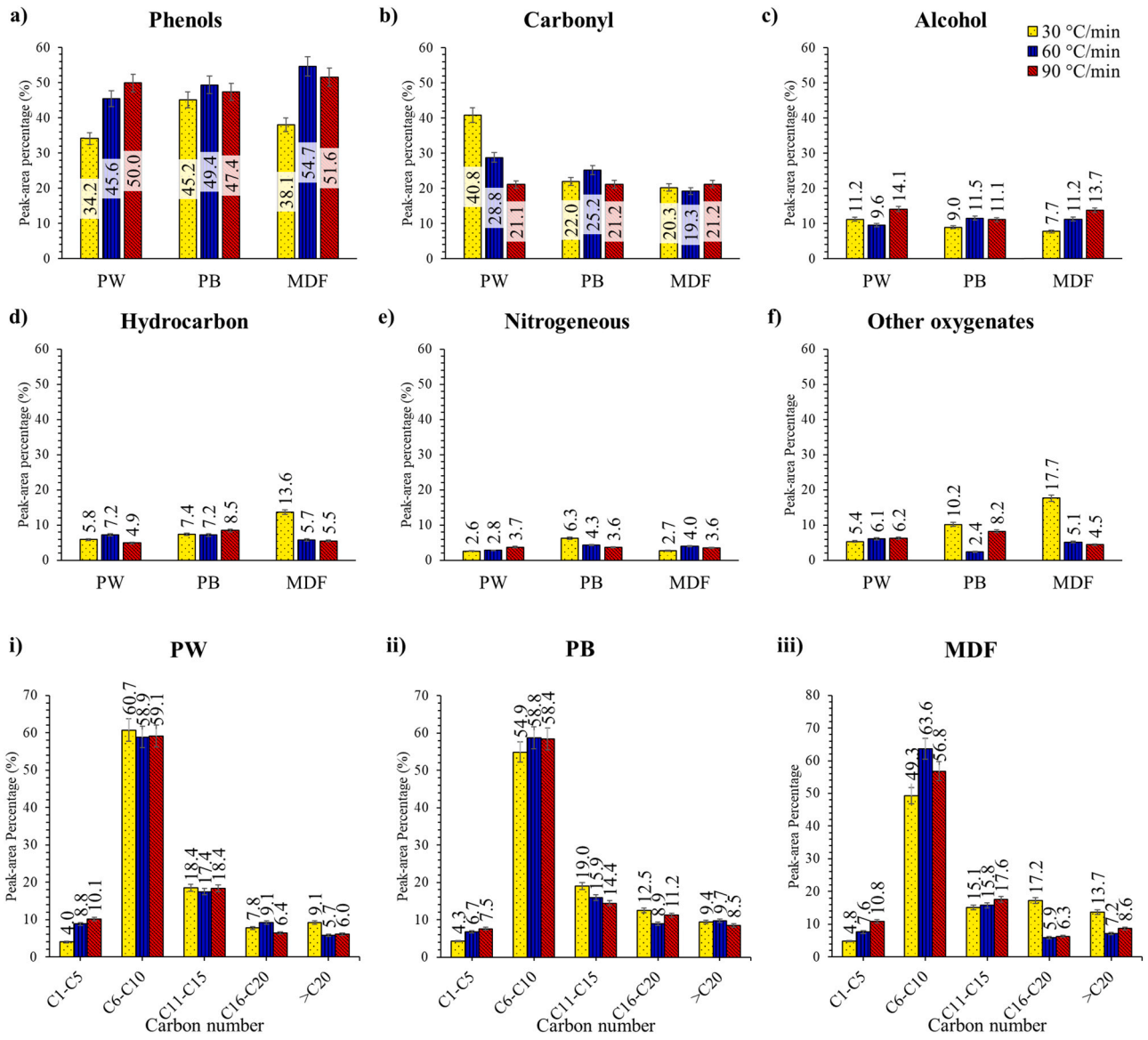

Fig. 6. Distribution of pyrolytic products from WFBs at different heating rates according to product series (a-f) and carbon number (i-iii). These components are grouped into (a) phenols, (b) carbonyls, (c) alcohols, (d) hydrocarbons, (e) nitrogenous, and (f) other oxygenates.

shows the distribution of pyrolytic products from WFBs at different heating rates according to product series and carbon number with a standard error of 5%.

Pyrolysis of WFBs produced the highest amount of phenols, followed by carbonyls and alcohols (Fig. 6). For PW pyrolysis, the high heating rate improved the heat energy transferred to PW, resulting in the improved thermal cracking of different components in PW. However, the lignin in PW required higher bond dissociation energy for decomposition to form phenols due to its complex structure with high thermal stability. As aforementioned, a high heating rate favors the breaking of higher bond dissociation energy chemical bonds. Therefore, the increase in heating rate promoted the decomposition of lignin into phenol, thus increasing phenol production. By contrast, a lower heating rate limited the heat transfer in PW; thus, components, such as cellulose and hemicellulose, with lower thermal stability were decomposed to produce carbonyl and alcohol.

For the PB pyrolysis, a high content of oxygenates was observed from the pyrolysis at 30 °C/min and 90 °C/min (Fig. 6f). The optimum pyrolysis heating rate for PB is 60 °C/min that provided sufficient heat energy to decompose PB and produce phenols and carbonyls. When the heating rate was increased to 90 °C/min, additional energy was supplied to PB, resulting in the formation of additional radical fragments. These fragments can recombine with oxygen-containing volatiles generated in the reaction region and in turn increase the proportion of "other oxygenates". This result concurs with the result obtained by Xiong et al. (2020), claiming that a fast heating rate (50 °C/s) in the pyrolysis of lignocellulosic biomass promoted the formation of oxygen-containing components.

The pyrolysis of MDF was highly affected by the heating rate (Fig. 6). The amount of $C_{>16}$ compounds obtained at 30 °C/min was much higher than that obtained at 60 °C/min and 90 °C/min due to the decomposition of low-thermal stable cellulose and hemicellulose, which in turn increased the hydrocarbon content. However, the limited heat received by MDF at a low heating rate probably led to the incomplete decomposition of the lignin component in the MDF. In addition, reactions, such as decarboxylation and decarbonylation of lignin, required a high amount of heat energy to produce CO and CO_2 (Akhtar and Saidina Amin, 2012). Therefore, the lignin in MDF received insufficient heat energy to eliminate the oxygen molecule, resulting in the increased formation of other oxygenates. By contrast, a high heating rate provided

a high amount of heat energy to lignin in MDF, thus promoting the decomposition of lignin to produce phenols and alcohol.

According to Table 2, the pyrolysis of PW produced a lower amount (2.6 wt%) of cyclopropylmethanol (hazardous carbohydrate-derived products) at 30 °C/min. The increased amount of 1,4:3,6-dianhydro-D-glucopyranose was due to the re-condensation of cyclopropylmethanol (Chen et al., 2017) when the heating rate was increased. At a low heating rate, the heat energy that transferred to the cellulose in PW decreased, thus reducing the extent of PW cellulose decomposition. However, the energy is still sufficient for cellulose to decompose into lighter molecules, such as cyclopropylmethanol owing to its low thermal stability properties. Meanwhile, it could re-condense with the volatiles retained in the reaction region to produce a high molecular weight component as 1,4:3,6-dianhydro-D-glucopyranose; 1,4:3,6-dianhydro-D-glucopyranose was reported to show beneficial biological activity in phobic disorder treatment (Ragupathi et al., 2018). The results demonstrate that pyrolysis is a potential approach to convert hazardous components, such as cyclopropylmethanol (flammable, irritating, and corrosive) into value-added pharmaceutical chemicals.

The pyrolysis of PB showed a similar product distribution trend with PW with respect to the carbon number at increasing heating rate, where most of the compound was having the carbon number ranging from C_6 to C_{15}. However, a fluctuation in the carbon number distribution of PB was observed (Table 2). Paromomycin increased at 60 °C/min but decreased at 90 °C/min. The heating rate at 90 °C/min promoted the decomposition of paromomycin due to the high heat energy gained. However, a low amount of paromomycin was obtained at 30 °C/min, probably due to insufficient heat energy for the decomposition of complex components with a high bond dissociation energy in PB to produce paromomycin. This result explains the different amounts of paromomycin produced at different heating rates. Therefore, 60 °C/min is an optimum heating rate for the production of paromomycin that can be refined for use as an antimicrobial for parasitic infections (Kempf et al., 2013).

For the pyrolysis of MDF, an obvious increase in the production of lower molecular weight components ($C_{<12}$) such as 4-propenyl-2,6-dimethoxyphenol, cyclopropylmethanol, isoeugenol, and syringylacetone was observed, demonstrating that the high heating rate promoted the decomposition of MDF. The limited recombination of light compounds was due to the immediate removal of volatiles in the reaction region at high heating rates. The syringol content showed a similar trend with the paromomycin in PB pyrolysis, where 60 °C/min is the optimum heating rate for the maximum production of syringol.

Overall, the pyrolysis heating rate showed a noticeable effect on the pyrolysis of MDF but less effect on the pyrolysis of PW and PB. The MDF is composed of compressed wood powder, whereas PW and PB are made up of wood pieces and woodchips, respectively. Wood powder has a smaller particle size than wood pieces and wood chips, and the particles in MDF could easily receive the heat energy and decompose to produce pyrolytic products (Foong et al., 2020). The MDF in powder form (present in smaller particle sizes) has a higher surface area than wood chips and pieces, thus having a larger surface area to receive heat energy and subject to decomposition. In addition, the smaller particle size in MDF suggests that it would take a shorter distance and less time for heat to transfer from the outer surface to the core of the particle, thus improving the decomposition of MDF during pyrolysis. By contrast, wood chips and pieces have larger particle sizes, which require a longer time to heat up. As a result, a more significant effect was observed by varying the heating rate for MDF pyrolysis compared to the pyrolysis of PW and PB.

Phenols were the main component obtained from WFBs pyrolysis. The optimum pyrolysis heating rate for WFBs were suggested to be 60 °C/min to obtain a pyrolytic product with a lower carbon number while ensuring complete decomposition and avoiding undesired secondary reaction among the volatile released during pyrolysis. Cyclopropylmethanol, a harmful chemical, was less produced via the pyrolysis of WFBs at a heating rate of 30 °C/min. 4-vinylguaiacol, a flavoring agent for peanut, spicy, wine-like or apple flavors, can be obtained from the pyrolysis of WFBs at a heating rate of 60 °C/min. Optimum pyrolysis conditions for WFBs should be examined and selected by minimizing the production of hazardous compounds and maximizing the production of value-added chemicals.

3.6. Pyrolysis pathway for WFBs involving the reaction mechanism, product distribution, and conversion of hazardous components

The proposed pyrolytic reaction mechanisms for WFBs using thermogravimetric analysis, FTIR and Py-GC/MS are shown in Fig. 7. The hemicellulose, cellulose, and lignin components in wood decompose at different temperature ranges (Moreno and Font, 2015). Hemicellulose and cellulose consist mainly of sugar units, whereas lignin consists of phenyl propane monomers (p-hydroxyphenyl propane, guaiacyl propane and syringyl propane) linked together with different bonds, such as β–β, β–1, β–5, 5–5, β–O–4 and α–O–4 (Mei et al., 2019; Song et al., 2016). Reaction pathways for WFBs pyrolysis vary at different final pyrolysis temperatures and heating rates. It is worth noting that some of the components produced from WFBs pyrolysis at different final temperatures are not observed from the product from WFBs pyrolysis at different heating rates. For example, cyclopentane-1,2-dione (**21**), 3-ethyl-2-hydroxy-2-cyclopentene-1-one (**19**), guaiacol (**2**), and 4-ethylsyringol (**10**) were not observed at different pyrolysis heating rates likely due to bond cleavage of lignocellulosic components (Kumar et al., 2020).

The lignin structure (Fig. 7) reveals that the homolytic cleavage of the C_α–O bond in lignin (**a**) of WFBs produces radical **1,** followed by hydrogenation to produce guaiacol (**2**). Another pathway of producing guaiacol (**2**) is the direct cleavage of compound **a** with lower energy (186.5 kJ/mol) compared with the reaction with free radical in the intermediate state (340.7 kJ/mol) (Huang and He, 2015). The homolytic cleavage of the C_α–C_β bond in lignin (**a**) is unlikely to occur during pyrolysis as radical **1** favors the production of 2-hydroxybenzaldehyde instead of guaiacol (**2**), according to the research by Huang and He (2015). Variation in heating rate does not produce guaiacol (**2**) probably because the dissociation of chemical bonds in lignin favors the formation of components with higher bond dissociation energies such as syringol (**6**) (Qiao et al., 2019). C_β–O bond has a lower bond dissociation energy than C_α–C_β in lignin pyrolysis (Huang et al., 2014). The β–O–4 bond exists as the major type of linkage (48–60%) depending on the type of wood (Britt et al., 2000; Ouyang et al., 2013). The C_β–O bond in lignin (**b**) has decomposed into radical **3** and then undergoes hydrogenation to form isoeugenol (**4**). The result is similar with the research by Yu et al. (2021), showing that intermediate radicals formed from C_α–O and C_β–O bonds often react with H radicals to achieve a stable state. In addition, some of the isoeugenol (**4**) undergo ethenolysis to produce 4-vinylguaiacol (**5**) (Baader et al., 2013). This reaction was not affected by final pyrolysis temperature and heating rate as it formed exothermically in pyrolysis which required lower energy compared to endothermic reaction.

Syringol-derivatives were also a major product from WFBs pyrolysis at different final pyrolysis temperatures and heating rates. Up to 9.5% of syringol (**6**) was produced and predicted from the cleavage from the C–C bond in the lignin structure. Approximately 3% of 3,5-dimethoxy-4-hydroxytoluene (**17**) was produced via the cleavage of the C–C and C–O bonds. Thus, the formation of syringol (**6**) is preferable as there is only one type of bond cleavage, thus requiring lower bond dissociation energy. Syringol (**6**) can react with the acetic acid to produce acetosyringone (**7**), where acetic acid could be a product from the pyrolysis process. Chen et al. (2019b) showed that the pyrolysis of hemicellulose caused the O-acetyl and pentose units to degrade thermally into furfural and acetic acid. Therefore, the result further supports the formation of acetosyringone (**7**) as a product from WFBs pyrolysis. Furthermore, syringol (**6**) can undergo demethylation to produce syringaldehyde (**14**) and then further reacts with acetone to produce 4-(4-hydroxy-3,5-dimethoxyphenyl)-3-buten-2-one (**15**), followed by hydrogenation to

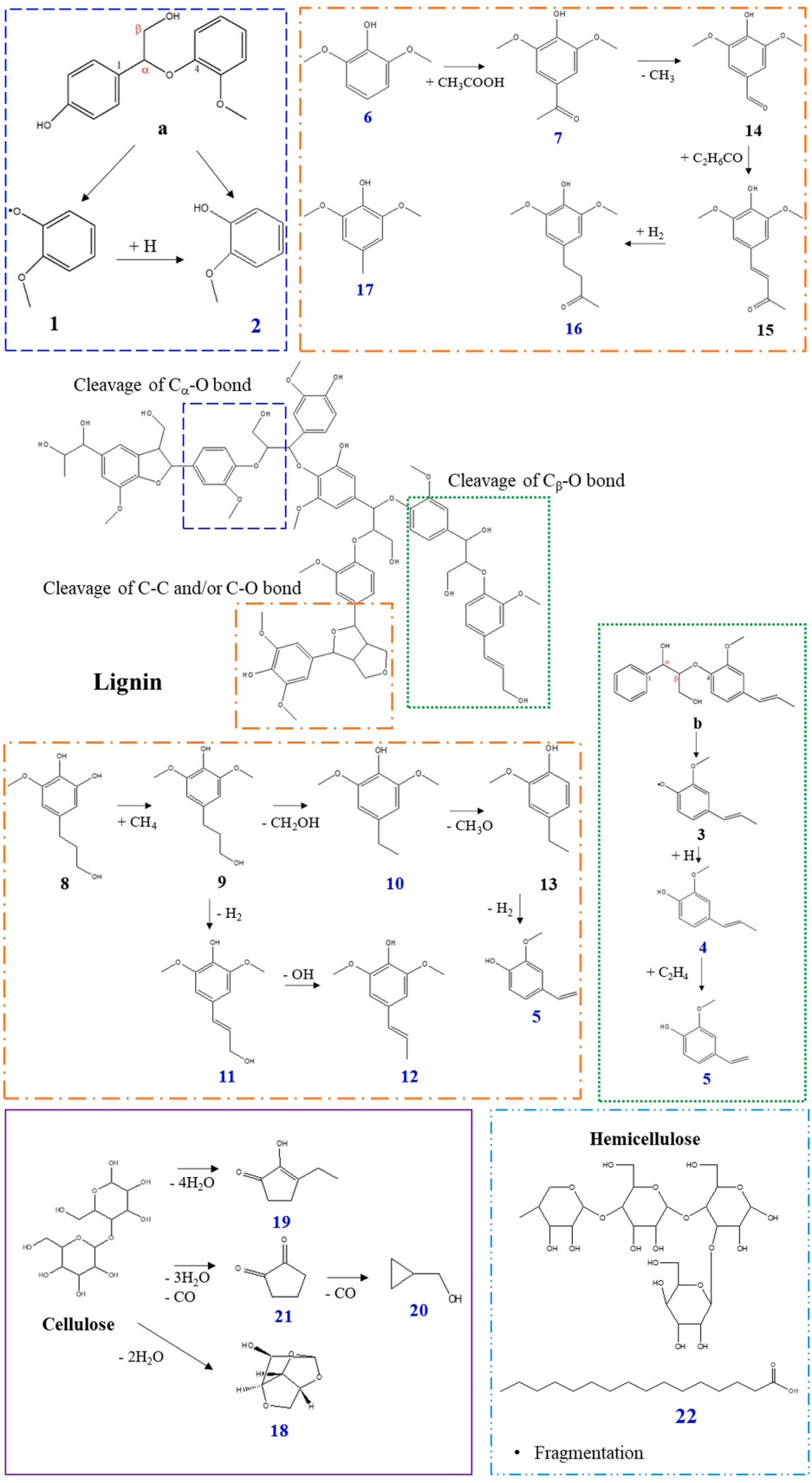

Fig. 7. Proposed reaction mechanism for lignin and possible reactions for cellulose and hemicellulose during the pyrolysis of WFBs.

produce syringylacetone (**16**). This compound was patented as a preservative for cosmetic composition, showing that the pyrolysis of WFBs have the potential to contribute to the cosmetic field by providing chemical additives needed in cosmetic production.

On the other hand, 5-(3-hydroxypropyl)-3-methoxy-1,2-benzenediol (**8**) was produced from the cleavage of the C–O bond in the lignin, followed by the hydrogenation process. Next, it was predicted to undergo methylation to produce compound **9**. Compound **9** then underewent dehydroxymethylation to form 4-ethylsyringol (**10**). The 4-ethylsyringol (**10**) can also react with methanol produced by the cracking of hydroxymethyl attached to cycloalkane rings or aromatic rings, followed by dehydrogenation to form sinapylalcohol (**11**). The 4-ethylsyringol (**10**) can also undergo demethoxylation followed by dehydrogenation to produce 4-vinylguaiacol (**5**). Interestingly, the formation of 4-ethylsyringol (**10**) was not observed in pyrolysis at different heating rates but it was produced in different final pyrolysis temperatures of PW (Table S1). Therefore, the pyrolysis of PW at different heating rates prefers the formation of higher dissociation energy compounds, such as 4-propenyl-2,6-dimethoxyphenol (**12**). Moreover, the formation of 4-vinylguaiacol (**5**) in PW was proposed via the ethenolysis of isoeugenol (**4**) that occurs exothermically during pyrolysis. Compound **9** can undergo dehydrogenation to produce sinapyl alcohol (**11**) followed by dehydroxylation to produce 4-propenyl-2,6-dimethoxyphenol (**12**).

Apart from the specific fragmentation of lignin components in WFBs pyrolysis, some general fragmentations of lignocellulosic components of WFBs were observed. Cellulose is formed by a repeating unit of six-carbon ring known as pyranose. The pyranose rings are linked by the β–1,4–glycoside bond. During pyrolysis, cellulose undergoes dehydration, open-ring, and transglycosylation reactions when receiving heat energy, thus forming compounds, such as cyclopentane-1,2-dione (**21**), cyclopropylmethanol (**20**), 1,4:3,6-dianhydro-D-glucopyranose (**18**), and 3-ethyl-2-hydroxy-2-cyclopentene-1-one (**19**) (Quan et al., 2016). This result is aligned with the research performed by Dai et al. (2019) on cellulose pyrolysis, further supporting that 1,4:3,6-dianhydro-D-glucopyranose (**18**) is a cleavage from cellulose via double dehydration reaction of glucopyranose. Acids produced from WFBs pyrolysis are mainly from the fragmentation of the hemicellulose component (Zong et al., 2020). The amount of hexadecenoic acid produced from WFBs are in the range of 0.7–2.6%, showing that most of the acids undergoes decarboxylation during pyrolysis to produce light molecular weight components.

As mentioned in Section 3.5, cyclopropylmethanol (**20**) is classified as a "dangerous" chemical with properties, such as corrosive, flammable, and irritating. The formation of this chemical increases with the decrease of final pyrolysis temperature and the increase in heating rate. Several chemical pathways lead to the production of cyclopropylmethanol (**20**), including the cracking of paromomycin, 1,4:3,6-dianhydro-D-glucopyranose (**18**), and cyclopentanedione (**21**). According to the mechanism proposed by Ragupathi et al. (2018), cyclopentanoses (compound **19** and **21**) can be produced from cellulose decomposition at low pyrolysis temperature via dehydration and decarbonylation. Therefore, high pyrolysis temperature could provide additional heat energy to decompose the cellulose in WFBs, in turn enhancing the secondary reaction (e.g., recondensation and polymerization) between cyclopropylmethanol (**20**), cyclopentanedione (**21**), and 3-ethyl-2-hydroxy-2-cyclopenten-1-one (**19**) in forming high molecular weight components, such as paromomycin and 1,4:3,6-dianhydro-D-glucopyranose (**18**), resulting in the low yield of these compounds. Increasing the heating rate also resulted in an increased yield of cyclopropylmethanol (**20**). This result was obtained probably because the high heating rate eliminated the possible occurrence of a secondary reaction. At a high heating rate, components, such as 1,4:3,6-dianhydro-D-glucopyranose (**18**), receive high amounts of heat energy, resulting in complete decomposition to produce cyclopropylmethanol (**20**). The produced cyclopropylmethanol (**20**) then left the reaction region immediately and was not subjected to secondary reactions with other volatiles in the reaction region. As a result, additional cyclopropylmethanol (**20**) were produced with the increase in heating rate. As previously mentioned, cyclopropylmethanol (**20**) can be eliminated via the secondary reaction during the pyrolysis process. Therefore, low heating rate and high final pyrolysis temperature are proposed for the pyrolysis of WFBs to reduce the formation of the hazardous cyclopropylmethanol (**20**) component. It is worth noting that the reactions shown in Fig. 7 are the possible chemical pathways inferred from the Py-GC/MS and TG-FTIR analysis of WFBs; thus, it may not be the only pathway for WFBs pyrolysis to reduce the hazardous components and produce value-added components in the pyrolytic products.

Table 3 shows the end-products from the pyrolysis of a number of selected feedstocks. Compared to the information in Table 3, pyrolysis of wood-based feedstock in this study produced mainly phenols. This result could be attributed to the high contents of lignocellulosic component (lignin) yielding high amounts of phenols. By contrast, the paperboard is rich in cellulose and hemicellulose with glucose structural units bonded with the β–O–4 glycosidic bond, showing a low degree of polymerization and thermal stability. Therefore, these thermally unstable components are easily decomposed to produce higher carbonyl compounds such as levoglucosan, acetic acid, and acetaldehyde (Kumar et al., 2020). The pyrolysis of sawdust yielded high amounts of acids via the chemical reactions, such as depolymerization and pyran ring cleavage. Pyrolytic products with high carbonyl contents (e.g., aldehydes and ketones) are undesirable due to their highly reactive properties that react easily to form undesirable components, such as oxygenates (Ma et al., 2019). Therefore, pyrolysis of MDF is suitable as a feedstock for production of products with less carbonyl components. Compared to the above mentioned studies, pyrolysis of waste dahlia flower led to formation of hydrocarbons used as a fuel source for combustion (Mishra et al., 2020). However, the WFBs produced low amounts of hydrocarbon from pyrolysis, indicating that it is not suitable for recovery into renewable liquid fuel using pyrolysis.

3.7. Comparison between pyrolysis, landfill, and combustion of waste materials with respect to hazard mitigation and waste recovery

Pyrolysis and combustion (incineration) are waste-to-energy recovery technologies that can reduce greenhouse gas emission by up to 68% (Dong et al., 2019). According to the life cycle assessment (LCA) by Dong et al. (2018), pyrolysis recovered higher energy amounts and lower emission of harmful gases, such as NO_x and SO_2, in comparison with combustion. A similar study by Hu et al. (2020) on oily sludge reported that pyrolysis achieved only 7% of ecotoxicity impact of combustion, which has lower adverse effects on soils and groundwater. The normalized life cycle environmental impacts showed that pyrolysis registered the lowest total normalized score value (47.3 impacts per person per year), followed by landfill (586 impacts per person per year) and combustion (701 impacts per person per year). Thus, pyrolysis is considered a promising approach for low-impact refinery oil sludge treatment.

Combustion accounts for majority of the impact in different categories, including global warming potential, ecotoxicity, fossil fuel depletion, and photochemical smog formation. For instance, the combustion of 1000 kg of oil sludge released 12,000 kg of CO_2-eq, 32 kg of N-eq, and 49 kg of SO_2-eq into the atmosphere (Hu et al., 2020). A research performed by Fernandez-Lopez et al. (2015) revealed that pyrolysis yielded lower amounts of greenhouse gases and did not emit pollutants, such as NO_x and SO_2. By contrast, Dong et al. (2018) reported that pyrolysis reduced up to 34% direct emission of pollutants as compared to combustion due to the homogeneous gas-gas reaction and lower amount of flue gas released from syngas combustion in the pyrolysis plant.

Landfilling is associated with the most significant effects in terms of global warming potential (GWP) and ecotoxicity. The GWP impact was

Table 3
Product distribution of selected feedstock under different pyrolysis conditions.

Feedstock	Operation condition	Pyrolytic products (%)						Ref.
		Phenols	Carbonyl	Alcohol	Hydrocarbon	Nitrogeneous	Other oxygenates	
Plywood	Final temperature: 500, 600, 700 °C	25.9–49.4	20.9–27.1	13.4–20.3	2.4–6.4	3.2–4.7	5.2–26.7	Current research
Particleboard	Final temperature: 500, 600, 700 °C	34.1–42.6	22.9–26.5	12.8–13.9	7.6–15.0	1.0–4.8	2.9–3.6	Current research
Medium density fiberboard	Final temperature: 500, 600, 700 °C	45.6–49.8	20.7–24.4	14.7–18.2	3.3–5.7	2.9–3.6	1.7–6.7	Current research
Plywood	Heating rate: 30, 60, 90 °C/min	34.2–50.0	21.1–40.8	9.6–14.1	4.9–7.2	2.6–3.7	5.4–6.2	Current research
Particleboard	Heating rate: 30, 60, 90 °C/min	45.2–49.4	21.2–25.2	9.0–11.5	7.2–8.5	3.6–6.3	2.4–10.2	Current research
Medium density fiberboard	Heating rate: 30, 60, 90 °C/min	38.1–54.7	19.3–21.2	7.7–13.7	5.5–13.6	2.7–4.0	4.5–17.7	Current research
Paperboard	Temperature: 500 °C	2.0	36.8	5.74	33.1	3.8	6.8	(Ma et al., 2019)
Sawdust	Temperature: 500 °C	17.5	48.62	8.1	4.15	19.7	11.8	(Ma et al., 2019)
Waste tea	Temperature: 600 °C	4.0	54.4	3.23	10.4	4.0	–	(Cai et al., 2019)
Waste dahlia flower	Temperature: 600 °C	8.8	21.1	1.8	51.2	2.5	7.9	(Mishra et al., 2020)
Imperata cylindrica	Temperature: 500 °C	57.8	26.1	6.8	11.9	–	–	(Hidayat et al., 2018a)
Imperata cylindrica	Temperature: 600 °C	51.0	29.8	6.3	15.8	–	–	(Hidayat et al., 2018a)
Jerusalem artichoke stalk	Heating rate: 100 °C/s	21.8	53.8	–	–	–	24.4	(Wang et al., 2019)
Jerusalem artichoke stalk	Heating rate: 1000 °C/s	21.5	56.7	–	–	–	21.9	(Wang et al., 2019)

"-" refers to not detected.

mainly due to CO_2 (23%) and methane (77%) emissions, which contributed to 93% of to the total GWP impact as reported by Hu et al. (2020). The ecotoxicity effect (4.02×10^4 CTUe) was contributed by the anaerobic and aerobic biodegradation of petroleum hydrocarbon, which could potentially contaminate ground water and soil by leachate (containing heavy metals and polycyclic aromatic hydrocarbon) (Hu et al., 2020). Demetrious and Crossin (2019) reported that compared with pyrolysis, landfilling increased the emission of biogenic CH_4 and nitrate, thus resulting in more severe air and water pollutions.

Previous research has revealed that landfilling and combustion need to be avoided because they will increase the emission of greenhouse gases and pollutants, such as NO_x, SO_2, and leachate. Therefore, these two approaches are becoming increasingly impracticable for the disposal of WFBs as it will emit harmful gases and pollutants into the environment. Pyrolysis can potentially be used to treat and recover WFBs as it can be operated in an enclosed system, whereas the release of volatiles can be condensed into biofuel or subjected into further recovery or treatment process in the pyrolysis plant. Thus, these harmful gases and leachate are not released to the environment and endanger the living organism. Moreover, pyrolytic products can be upgraded into biofuel or solid fuel as an alternative to mitigate the depletion of fossil fuel.

3.8. Future perspectives and challenge for scale-up

The present research proposes a pyrolysis approach that converts WFBs into value-added chemicals at low heating rate and high final pyrolysis temperatures. It is envisaged that future studies could be performed to investigate the feasibility and scalability of this approach by optimizing the key process parameters including process temperature, heating rate, carrier gas flow rate, and feedstock size as these are important for optimizing the types, yield, and properties of the desired pyrolytic products such as biochar, bio-oil, and syngas. For instance, pyrolysis at a higher heating rate and temperature favored the formation of bio-oil or gaseous product, whereas a lower heating rate favored the formation of biochar (Liew et al., 2018c). The use of feedstock with different particle sizes may be influenced by pyrolysis temperature which affects the product yield (Deng et al., 2021). The current understandings of the reaction mechanism during WFBs pyrolysis at different reaction conditions does not allow an accurate estimation of the pyrolytic products.

Scaling up the pyrolysis of WFBs is challenging as it is a complex mixture comprising different types of materials, including wood, binders, waxes, flame retardants, coatings, and paints. These components can be further classified according to their types, such as different wood species (varies lignocellulosic content) and formaldehyde binder (phenol and urea). Each of these components having different chemical composition could show different pyrolysis behavior. For instance, Hu et al. (2019) reported that the pyrolysis of poplar produced more char and less tar, but the pyrolysis of pine produced less char with more gas and tar. This result was attributed to the C/H ratio as well as the lignocellulosic content of the wood species. However, research on the pyrolysis of complex furniture waste, such as the WFBs, is limited. Thus, the reaction mechanism and the synergistic effects between these components should be further investigated to improve the scalability of this approach.

Heating source is important for upscaling of pyrolysis as it is required to heat and increase the feedstock temperature to reach the desired high temperature for pyrolytic decomposition. The current set up for the pyrolysis of WFBs utilized electric heating as energy source, which may result in low energy efficiency due to the heating mechanism of electric furnace. The heat energy was transferred from the surface to the core of the feedstock for the decomposition to occur. Excess electricity was required to heat up the reactor, and heat was lost during heating of the feedstock, thus lowering the energy efficiency. Microwave pyrolysis can be used to improve the heat transfer by utilizing microwave radiation as the heat source to provide a uniform and rapid feedstock heating (Foong et al., 2021). As a result, the energy input and duration needed for pyrolysis process could be reduced while the consistent heating helps to treat larger feedstock volumes and thereby facilitate upscaling (Tagade et al., 2021).

Previous research has also demonstrated that the optimum pyrolysis conditions obtained from the bench scale experiments are not suitable for direct application in the pilot scale operation. Upgrading the

pyrolysis from bench scale to pilot scale affects the yield of pyrolytic products. For instance, Soni and Karmee (2020) investigated the pyrolysis of sawdust in the bench and pilot scale systems and the results showed that the pilot scale system produced higher bio-oil yield but lower biochar yield. During the bench scale, the biochar trapped the generated volatiles and underwent secondary tar cracking, thus increasing the yield of biochar. By contrast, the biochar in the pilot scale experiment was continuously removed from the reactor, thereby decreasing the secondary cracking of tar to form solid char and producing less biochar. Therefore, further research is required to optimize the process parameters of WFBs pyrolysis to make it more suitable for pilot and full-scale rectors.

In addition to the above, it is important to perform life cycle (LCA) and energy efficiency (EEA) assessments for the recovery of WFBs using pyrolysis. LCA is important to measure the environmental impacts, where EEA is applied to compare the energy conversion rate of WFBs pyrolysis. Techno-economic analysis also helps to examine the economic feasibility of WFBs pyrolysis. However, no study is reported on the LCA and techno-economic analysis for the pyrolysis of WFBs so far. Therefore, these analyses are suggested to estimate the effects of the process to the environment, net present value (an economic indicator used to evaluate the profitability), and energy efficiency of WFBs pyrolysis.

4. Conclusion

WFBs are made up of a complex mixture of potentially hazardous resin, paints, waxes, and coatings, thus causing undesired environmental pollution if improperly disposed by landfilling and open burning. Pyrolysis has potential to reduce the release of hazardous formaldehyde and greenhouse gases into the environment through the conversion of WFBs into value-added chemical additives, such as paromomycin. The possible reactions occurred during pyrolysis of WFBs include depolymerization, cracking, dehydrogenation, decarbonylation, and dehydration. The pyrolysis of WFBs should be performed at high final temperatures and low heating rates to minimize the generation of hazardous chemicals, such as cyclopropylmethanol, by promoting the secondary reaction with volatiles released during the pyrolysis process to form value-added chemicals instead of hazardous compounds. Further research on the effect of other operation conditions, parameters, and modeling in the bench scale or pilot scale is recommended to improve the feasibility for applying this technology to the safe disposal and recovery of WFBs.

CRediT authorship contribution statement

Shin Ying Foong: Conceptualization, Methodology, Investigation, Writing – original draft, **Rock Keey Liew:** Writing – review & editing, Supervision, **Chern Leing Lee:** Data Curation, Formal analysis, **Wei Peng Tan:** Data Curation, Software, **Wanxi Peng:** Funding acquisition, Resources, **Christian Sonne:** Writing – review & editing, **Yiu Fai Tsang:** Writing – review & editing, Funding acquisition, **Su Shiung Lam:** Writing – review & editing, Project administration, Supervision, Resources.

Declaration of Competing Interest

The authors declare that they have no known competing financial interests or personal relationships that could have appeared to influence the work reported in this paper.

Acknowledgements

The authors would like to thank Universiti Malaysia Terengganu under International Matching Grant (UMT/CRIM/2-2/25/Jld. 8 (49), Vot 53376) for supporting this project. This work was also supported by the Ministry of Higher Education, Malaysia under the Higher Institution Centre of Excellence (HICoE), Institute of Tropical Aquaculture and Fisheries (AKUATROP) program (Vot. No. 63933 & Vot. No. 56051, UMT/CRIM/2-2/5 Jilid 2 (10)). The work is also supported by the Program for Innovative Research Team (in Science and Technology) in University of Henan Province (No. 21IRTSTHN020) and Central Plain Scholar Funding Project of Henan Province (No. 212101510005). The authors also acknowledge Henan Agricultural University for the financial and technical support and the use of facilities throughout this research under a Research Collaboration Agreement (RCA) with Universiti Malaysia Terengganu.

Appendix A. Supporting information

Supplementary data associated with this article can be found in the online version at doi:10.1016/j.jhazmat.2021.126774.

References

Adeleke, A.A., Odusote, J.K., Ikubanni, P.P., Lasode, O.A., Malathi, M., Paswan, D., 2020. The ignitability, fuel ratio and ash fusion temperatures of torrefied woody biomass. Heliyon 6. https://doi.org/10.1016/j.heliyon.2020.e03582.

Adjalle, K., Larose, L.-V., Bley, J., Barnabé, S., 2017. The effect of organic nitrogenous compound content and different pretreatments on agricultural lignocellulosic biomass characterization methods. Cellulose 24, 1395–1406. https://doi.org/10.1007/s10570-017-1199-8.

Akhtar, J., Saidina Amin, N., 2012. A review on operating parameters for optimum liquid oil yield in biomass pyrolysis. Renew. Sustain Energy Rev. 16, 5101–5109. https://doi.org/10.1016/j.rser.2012.05.033.

Aslan, D.I., Özoğul, B., Ceylan, S., Geyikçi, F., 2018. Thermokinetic analysis and product characterization of Medium Density Fiberboard pyrolysis. Bioresour. Technol. 258, 105–110. https://doi.org/10.1016/j.biortech.2018.02.126.

Ayiania, M., Terrell, E., Dunsmoor, A., Carbajal-Gamarra, F.M., Garcia-Perez, M., 2019. Characterization of solid and vapor products from thermochemical conversion of municipal solid waste woody fractions. Waste Manag. 84, 277–285. https://doi.org/10.1016/j.wasman.2018.11.042.

Baader, S., Ohlmann, D.M., Gooßen, L.J., 2013. Isomerizing ethenolysis as an efficient strategy for styrene synthesis. Eur. J. Chem. 19, 9807–9810. https://doi.org/10.1002/chem.201301336.

Britt, P.F., Buchanan Iii, A.C., Cooney, M.J., Martineau, D.R., 2000. Flash vacuum pyrolysis of methoxy-substituted lignin model compounds. J. Org. Chem. 65, 1376–1389. https://doi.org/10.1021/jo991479k.

van den Broek, J., Klein Cerrejon, D., Pratsinis, S.E., Güntner, A.T., 2020. Selective formaldehyde detection at ppb in indoor air with a portable sensor. J. Hazard Mater. 399, 123052 https://doi.org/10.1016/j.jhazmat.2020.123052.

Cai, H., Liu, J., Xie, W., Kuo, J., Buyukada, M., Evrendilek, F., 2019. Pyrolytic kinetics, reaction mechanisms and products of waste tea via TG-FTIR and Py-GC/MS. Energ. Convers. Manag. 184, 436–447. https://doi.org/10.1016/j.enconman.2019.01.031.

Chen, H., Xie, Y., Chen, W., Xia, M., Li, K., Chen, Z., Chen, Y., Yang, H., 2019a. Investigation on co-pyrolysis of lignocellulosic biomass and amino acids using TG-FTIR and Py-GC/MS. Energ. Convers. Manag. 196, 320–329. https://doi.org/10.1016/j.enconman.2019.06.010.

Chen, W.H., Wang, C.W., Ong, H.C., Show, P.L., Hsieh, T.H., 2019b. Torrefaction, pyrolysis and two-stage thermodegradation of hemicellulose, cellulose and lignin. Fuel 258. https://doi.org/10.1016/j.fuel.2019.116168.

Chen, X., Yang, H., Chen, Y., Chen, W., Lei, T., Zhang, W., Chen, H., 2017. Catalytic fast pyrolysis of biomass to produce furfural using heterogeneous catalysts. J. Anal. Appl. Pyrolysis 127, 292–298. https://doi.org/10.1016/j.jaap.2017.07.022.

Chen, Y., Du, L., Li, S., Song, W., Jensen, P.A., Lin, W., 2021. Pyrolysis of antibiotic mycelial dreg and characterization of obtained gas, liquid and biochar. J. Hazard Mater. 402. https://doi.org/10.1016/j.jhazmat.2020.123826.

Chen, Y.D., Liu, F., Ren, N.Q., Ho, S.H., 2020. Revolutions in algal biochar for different applications: state-of-the-art techniques and future scenarios. Chin. Chem. Lett. 31, 2591–2602. https://doi.org/10.1016/j.cclet.2020.08.019.

Cruz, G., Rodrigues, A.L.P., da Silva, D.F., Gomes, W.C., 2020. Searches for physics beyond the standard model with the MT2 variable in hadronic final states with and without disappearing tracks in proton-proton collisions at s=13Te. Eur. Phys. J. C Part. Fields 80, 3. https://doi.org/10.1007/s10973-020-09330-6.

Dai, G., Wang, K., Wang, G., Wang, S., 2019. Initial pyrolysis mechanism of cellulose revealed by in-situ DRIFT analysis and theoretical calculation. Combust. Flame 208, 273–280. https://doi.org/10.1016/j.combustflame.2019.07.009.

Demetrious, A., Crossin, E., 2019. Life cycle assessment of paper and plastic packaging waste in landfill, incineration, and gasification-pyrolysis. J. Mater. Cycles Waste Manag. 21, 850–860. https://doi.org/10.1007/s10163-019-00842-4.

Deng, B., Yuan, X., Siemann, E., Wang, S., Fang, H., Wang, B., Gao, Y., Shad, N., Liu, X., Zhang, W., Guo, X., Zhang, L., 2021. Feedstock particle size and pyrolysis temperature regulate effects of biochar on soil nitrous oxide and carbon dioxide emissions. Waste Manag. 120, 33–40. https://doi.org/10.1016/j.wasman.2020.11.015.

Dong, J., Tang, Y., Nzihou, A., Chi, Y., Weiss-Hortala, E., Ni, M., 2018. Life cycle assessment of pyrolysis, gasification and incineration waste-to-energy technologies:

theoretical analysis and case study of commercial plants. Sci. Total Environ. 626, 744–753. https://doi.org/10.1016/j.scitotenv.2018.01.151.
Dong, J., Tang, Y., Nzihou, A., Chi, Y., 2019. Key factors influencing the environmental performance of pyrolysis, gasification and incineration Waste-to-Energy technologies. Energ. Convers. Manag. 196, 497–512. https://doi.org/10.1016/j.enconman.2019.06.016.
Fateh, T., Rogaume, T., Luche, J., Richard, F., Jabouille, F., 2013. Kinetic and mechanism of the thermal degradation of a plywood by using thermogravimetry and Fourier-transformed infrared spectroscopy analysis in nitrogen and air atmosphere. Fire Saf. J. 58, 25–37.
Fernandez-Lopez, M., Puig-Gamero, M., Lopez-Gonzalez, D., Avalos-Ramirez, A., Valverde, J., Sanchez-Silva, L., 2015. Life cycle assessment of swine and dairy manure: pyrolysis and combustion processes. Bioresour. Technol. 182, 184–192. https://doi.org/10.1016/j.biortech.2015.01.140.
Foong, S.Y., Liew, R.K., Yang, Y., Cheng, Y.W., Yek, P.N.Y., Wan Mahari, W.A., Lee, X.Y., Han, C.S., Vo, D.V.N., Van Le, Q., Aghbashlo, M., Tabatabaei, M., Sonne, C., Peng, W., Lam, S.S., 2020. Valorization of biomass waste to engineered activated biochar by microwave pyrolysis: progress, challenges, and future directions. Chem. Eng. J. 389. https://doi.org/10.1016/j.cej.2020.124401.
Foong, S.Y., Chan, Y.H., Cheah, W.Y., Kamaludin, N.H., Tengku Ibrahim, T.N.B., Sonne, C., Peng, W., Show, P.L., Lam, S.S., 2021. Progress in waste valorization using advanced pyrolysis techniques for hydrogen and gaseous fuel production. Bioresour. Technol. 320. https://doi.org/10.1016/j.biortech.2020.124299.
Ge, S., Yek, P.N.Y., Cheng, Y.W., Xia, C., Wan Mahari, W.A., Liew, R.K., Peng, W., Yuan, T.Q., Tabatabaei, M., Aghbashlo, M., Sonne, C., Lam, S.S., 2021. Progress in microwave pyrolysis conversion of agricultural waste to value-added biofuels: a batch to continuous approach. Renew. Sustain. Energy Rev. 135. https://doi.org/10.1016/j.rser.2020.110148.
González-Arias, J., Gil, M.V., Fernández, R.Á., Martínez, E.J., Fernández, C., Papaharalabos, G., Gómez, X., 2020. Integrating anaerobic digestion and pyrolysis for treating digestates derived from sewage sludge and fat wastes. Environ. Sci. Pollut. 27, 32603–32614. https://doi.org/10.1007/s11356-020-09461-1.
Gu, X., Ma, X., Li, L., Liu, C., Cheng, K., Li, Z., 2013. Pyrolysis of poplar wood sawdust by TG-FTIR and Py-GC/MS. J. Anal. Appl. Pyrolysis 102, 16–23. https://doi.org/10.1016/j.jaap.2013.04.009.
Haeldermans, T., Claesen, J., Maggen, J., Carleer, R., Yperman, J., Adriaensens, P., Samyn, P., Vandamme, D., Cuypers, A., Vanreppelen, K., Schreurs, S., 2019. Microwave assisted and conventional pyrolysis of MDF – Characterization of the produced biochars. J. Anal. Appl. Pyrolysis 138, 218–230. https://doi.org/10.1016/j.jaap.2018.12.027.
Han, T.U., Kim, Y.M., Watanabe, C., Teramae, N., Park, Y.K., Kim, S., Lee, Y., 2015. Analytical pyrolysis properties of waste medium-density fiberboard and particle board. J. Ind. Eng. Chem. 32, 345–352. https://doi.org/10.1016/j.jiec.2015.09.008.
Hidayat, S., Abu Bakar, M.S., Yang, Y., Phusunti, N., Bridgwater, A.V., 2018a. Characterisation and Py-GC/MS analysis of Imperata cylindrica as potential biomass for bio-oil production in Brunei Darussalam. J. Anal. Appl. Pyrolysis 134, 510–519. https://doi.org/10.1016/j.jaap.2018.07.018.
Hidayat, S., Bakar, M.S.A., Yang, Y., Phusunti, N., Bridgwater, A., 2018b. Characterisation and Py-GC/MS analysis of Imperata cylindrica as potential biomass for bio-oil production in Brunei Darussalam. J. Anal. Appl. Pyrolysis 134, 510–519. https://doi.org/10.1016/j.jaap.2018.07.018.
Honus, S., Kumagai, S., Němček, O., Yoshioka, T., 2016. Replacing conventional fuels in USA, Europe, and UK with plastic pyrolysis gases–Part I: experiments and graphical interchangeability methods. Energ. Convers. Manag. 126, 1118–1127. https://doi.org/10.1016/j.enconman.2016.08.055.
Hu, G., Feng, H., He, P., Li, J., Hewage, K., Sadiq, R., 2020. Comparative life-cycle assessment of traditional and emerging oily sludge treatment approaches. J. Clean. Prod. 251. https://doi.org/10.1016/j.jclepro.2019.119594.
Hu, X., Guo, H., Gholizadeh, M., Sattari, B., Liu, Q., 2019. Pyrolysis of different wood species: impacts of C/H ratio in feedstock on distribution of pyrolysis products. Biomass. Bioenerg. 120, 28–39. https://doi.org/10.1016/j.biombioe.2018.10.021.
Huang, J., He, C., 2015. Pyrolysis mechanism of α-O-4 linkage lignin dimer: a theoretical study. J. Anal. Appl. Pyrolysis 113, 655–664. https://doi.org/10.1016/j.jaap.2015.04.012.
Huang, J., Liu, C., Wu, D., Tong, H., Ren, L., 2014. Density functional theory studies on pyrolysis mechanism of β-O-4 type lignin dimer model compound. J. Anal. Appl. Pyrolysis 109, 98–108. https://doi.org/10.1016/j.jaap.2014.07.007.
Ikiz, E., Maclaren, V.W., Alfred, E., Sivanesan, S., 2021. Impact of COVID-19 on household waste flows, diversion and reuse: the case of multi-residential buildings in Toronto, Canada. Resour. Conserv. Recycl. 164. https://doi.org/10.1016/j.resconrec.2020.105111.
Jiang, Y., Zong, P., Tian, B., Xu, F., Tian, Y., Qiao, Y., Zhang, J., 2019. Pyrolysis behaviors and product distribution of Shenmu coal at high heating rate: a study using TG-FTIR and Py-GC/MS. Energ. Convers. Manag. 179, 72–80. https://doi.org/10.1016/j.enconman.2018.10.049.
Kapelewska, J., Kotowska, U., Karpińska, J., Astel, A., Zieliński, P., Suchta, J., Algrzym, K., 2019. Water pollution indicators and chemometric expertise for the assessment of the impact of municipal solid waste landfills on groundwater located in their area. Chem. Eng. J. 359, 790–800. https://doi.org/10.1016/j.cej.2018.11.137.
Karidis, A., 2021. Tackling a Multi-Million-Ton Furniture Waste Problem.⟨https://www.waste360.com/waste/tackling-multi-million-ton-furniture-waste-problem⟩ (accessed 28 May 2021).
Kaufman, G.B., 1993. Inorganic chemistry: principles of structure and reactivity, 4th ed. (Huheey, James E.; Keiter, Ellen A.; Keiter, Richard L.). J. Chem. Educ. 70, A279. https://doi.org/10.1021/ed070pA279.1.
Kempf, I., Le Roux, A., Perrin-Guyomard, A., Mourand, G., Le Devendec, L., Bougeard, S., Richez, P., Le Pottier, G., Eterradossi, N., 2013. Effect of in-feed paromomycin supplementation on antimicrobial resistance of enteric bacteria in turkeys. Vet. J. 198, 398–403. https://doi.org/10.1016/j.tvjl.2013.05.030.
Khan, T.A., Gupta, A., Jamari, S.S., Nasir, M., Jang, S., Kim, H.J., Asim, M., 2020. Synthesis of micro carbonaceous material by pyrolysis of rubber wood and its effect on properties of urea-formaldehyde (UF) resin. Int. J. Adhes. Adhes. 99. https://doi.org/10.1016/j.ijadhadh.2020.102589.
Kumar, R., Strezov, V., Weldekidan, H., He, J., Singh, S., Kan, T., Dastjerdi, B., 2020. Lignocellulose biomass pyrolysis for bio-oil production: a review of biomass pre-treatment methods for production of drop-in fuels. Renew. Sustain. Energy Rev. 123. https://doi.org/10.1016/j.rser.2020.109763.
Lai, Z., Li, S., Zhang, Y., Li, Y., Mu, J., 2018. Influence of urea formaldehyde resin on the pyrolysis of biomass components: cellulose, hemicellulose, and lignin. BioResources 13, 2218–2232. https://doi.org/10.15376/biores.13.2.2218-2232.
Lam, S.S., Liew, R.K., Lim, X.Y., Ani, F.N., Jusoh, A., 2016a. Fruit waste as feedstock for recovery by pyrolysis technique. Int. Biodeter. Biodeg. 113, 325–333.
Lam, S.S., Liew, R.K., Lim, X.Y., Ani, F.N., Jusoh, A., 2016b. Fruit waste as feedstock for recovery by pyrolysis technique. Int. Biodeterior. Biodegrad. 113, 325–333. https://doi.org/10.1016/j.ibiod.2016.02.021.
Lam, S.S., Liew, R.K., Cheng, C.K., Rasit, N., Ooi, C.K., Ma, N.L., Ng, J.-H., Lam, W.H., Chong, C.T., Chase, H.A., 2018a. Pyrolysis production of fruit peel biochar for potential use in treatment of palm oil mill effluent. J. Environ. Manag. 213, 400–408.
Lam, S.S., Liew, R.K., Cheng, C.K., Rasit, N., Ooi, C.K., Ma, N.L., Ng, J.-H., Lam, W.H., Chong, C.T., Chase, H.A., 2018b. Pyrolysis production of fruit peel biochar for potential use in treatment of palm oill mill effluent. J. Environ. Manag. 213, 400–408. https://doi.org/10.1016/j.jenvman.2018.02.092.
Lee, B.H., Jeong, T.Y., Trinh, V.T., Jeon, C.H., 2021. Thermal degradation of kenaf (Hibiscus cannabinus L.): impact of torrefaction on pyrolysis kinetics and thermal behavior. Energy Rep. 7, 951–959. https://doi.org/10.1016/j.egyr.2021.01.012.
Lee, J., Hong, J., Jang, D., Park, K.Y., 2019. Hydrothermal carbonization of waste from leather processing and feasibility of produced hydrochar as an alternative solid fuel. J. Environ. Manag. 247, 115–120. https://doi.org/10.1016/j.jenvman.2019.06.067.
Liang, F., Wang, R., Hongzhong, X., Yang, X., Zhang, T., Hu, W., Mi, B., Liu, Z., 2018. Investigating pyrolysis characteristics of moso bamboo through TG-FTIR and Py-GC/MS. Bioresour. Technol. 256, 53–60. https://doi.org/10.1016/j.biortech.2018.01.140.
Liew, R.K., Azwar, E., Yek, P.N.Y., Lim, X.Y., Cheng, C.K., Ng, J.H., Jusoh, A., Lam, W.H., Ibrahim, M.D., Ma, N.L., Lam, S.S., 2018a. Microwave pyrolysis with KOH/NaOH mixture activation: a new approach to produce micro-mesoporous activated carbon for textile dye adsorption. Bioresour. Technol. 266, 1–10. https://doi.org/10.1016/j.biortech.2018.06.051.
Liew, R.K., Chong, M.Y., Osazuwa, O.U., Nam, W.L., Phang, X.Y., Su, M.H., Cheng, C.K., Chong, C.T., Lam, S.S., 2018b. Production of activated carbon as catalyst support by microwave pyrolysis of palm kernel shell: a comparative study of chemical versus physical activation. Res. Chem. Inter. 44, 3849–3865. https://doi.org/10.1007/s11164-018-3388-y.
Liew, R.K., Nam, W.L., Chong, M.Y., Phang, X.Y., Su, M.H., Yek, P.N.Y., Ma, N.L., Cheng, C.K., Chong, C.T., Lam, S.S., 2018c. Oil palm waste: an abundant and promising feedstock for microwave pyrolysis conversion into good quality biochar with potential multi-applications. Process Saf. Environ. Prot. 115, 57–69.
Liu, C., Duan, X., Chen, Q., Chao, C., Lu, Z., Lai, Q., Megharaj, M., 2019. Investigations on pyrolysis of microalgae Diplosphaera sp. MM1 by TG-FTIR and Py-GC/MS: products and kinetics. Bioresour. Technol. 294. https://doi.org/10.1016/j.biortech.2019.122126.
Liu, J., Jin, S., Bao, C., Sun, Y., Li, W., 2021. Rapid determination of lignocellulose in corn stover based on near-infrared reflectance spectroscopy and chemometrics methods. Bioresour. Technol. 321, 124449 https://doi.org/10.1016/j.biortech.2020.124449.
Liu, Q., Wang, S., Zheng, Y., Luo, Z., Cen, K., 2008. Mechanism study of wood lignin pyrolysis by using TG-FTIR analysis. J. Anal. Appl. Pyrolysis 82, 170–177. https://doi.org/10.1016/j.jaap.2008.03.007.
Liu, Z., Balasubramanian, R., 2013. A comparison of thermal behaviors of raw biomass, pyrolytic biochar and their blends with lignite. Bioresour. Technol. 146, 371–378. https://doi.org/10.1016/j.biortech.2013.07.072.
Ma, W., Rajput, G., Pan, M., Lin, F., Zhong, L., Chen, G., 2019. Pyrolysis of typical MSW components by Py-GC/MS and TG-FTIR. Fuel 251, 693–708. https://doi.org/10.1016/j.fuel.2019.04.069.
Ma, Z., Chen, D., Gu, J., Bao, B., Zhang, Q., 2015. Determination of pyrolysis characteristics and kinetics of palm kernel shell using TGA-FTIR and model-free integral methods. Energ. Convers. Manag. 89, 251–259. https://doi.org/10.1016/j.enconman.2014.09.074.
Mei, Q., Shen, X., Liu, H., Han, B., 2019. Selectively transform lignin into value-added chemicals. Chin. Chem. Lett. 30, 15–24. https://doi.org/10.1016/j.cclet.2018.04.032.
Ming, X., Xu, F., Jiang, Y., Zong, P., Wang, B., Li, J., Qiao, Y., Tian, Y., 2020. Thermal degradation of food waste by TG-FTIR and Py-GC/MS: pyrolysis behaviors, products, kinetic and thermodynamic analysis. J. Clean. Prod. 244. https://doi.org/10.1016/j.jclepro.2019.118713.
Mishra, R.K., Mohanty, K., Wang, X., 2020. Pyrolysis kinetic behavior and Py-GC–MS analysis of waste dahlia flowers into renewable fuel and value-added chemicals. Fuel 260. https://doi.org/10.1016/j.fuel.2019.116338.
Mitchell, P.J., Dalley, T.S.L., Helleur, R.J., 2013. Preliminary laboratory production and characterization of biochars from lignocellulosic municipal waste. J. Anal. Appl. Pyrolysis 99, 71–78. https://doi.org/10.1016/j.jaap.2012.10.025.

Moreno, A.I., Font, R., 2015. Pyrolysis of furniture wood waste: decomposition and gases evolved. J. Anal. Appl. Pyrolysis 113, 464–473. https://doi.org/10.1016/j.jaap.2015.03.008.

Nam, W.L., Phang, X.Y., Su, M.H., Liew, R.K., Ma, N.L., Rosli, M.H.N., Lam, S.S., 2018. Production of bio-fertilizer from microwave vacuum pyrolysis of palm kernel shell for cultivation of Oyster mushroom (*Pleurotus ostreatus*). Sci. Total Environ. 624, 9–16. https://doi.org/10.1016/j.scitotenv.2017.12.108.

Ong, H.C., Chen, W.H., Singh, Y., Gan, Y.Y., Chen, C.Y., Show, P.L., 2020. A state-of-the-art review on thermochemical conversion of biomass for biofuel production: a TG-FTIR approach. Energy Convers. Manag. 209. https://doi.org/10.1016/j.enconman.2020.112634.

Ouyang, X.P., Liu, C.L., Pang, Y.X., Qiu, X.Q., 2013. Synthesis of a trimeric lignin model compound composed of α-O-4 and β-O-4 linkages under microwave irradiation. Chin. Chem. Lett. 24, 1091–1094. https://doi.org/10.1016/j.cclet.2013.09.001.

Patowary, D., Baruah, D., 2018. Effect of combined chemical and thermal pretreatments on biogas production from lignocellulosic biomasses. Ind. Crops Prod. 124, 735–746. https://doi.org/10.1016/j.indcrop.2018.08.055.

Perea-Moreno, A.J., Aguilera-Ureña, M.J., Manzano-Agugliaro, F., 2016. Fuel properties of avocado stone. Fuel 186, 358–364. https://doi.org/10.1016/j.fuel.2016.08.101.

Plis, A., Kotyczka-Morańska, M., Kopczyński, M., Łabojko, G., 2016. Furniture wood waste as a potential renewable energy source: a thermogravimetric and kinetic analysis. J. Therm. Anal. Calor. 125, 1357–1371. https://doi.org/10.1007/s10973-016-5611-7.

Qiao, Y., Wang, B., Zong, P., Tian, Y., Xu, F., Li, D., Li, F., Tian, Y., 2019. Thermal behavior, kinetics and fast pyrolysis characteristics of palm oil: analytical TG-FTIR and Py-GC/MS study. Energ. Convers. Manag. 199. https://doi.org/10.1016/j.enconman.2019.111964.

Quan, C., Gao, N., Song, Q., 2016. Pyrolysis of biomass components in a TGA and a fixed-bed reactor: thermochemical behaviors, kinetics, and product characterization. J. Anal. Appl. Pyrolysis 121, 84–92. https://doi.org/10.1016/j.jaap.2016.07.005.

Ragupathi, V., Stephen, A., Arivoli, D., Kumaresan, S., 2018. Pass-assistd preidiction of biological activity spectra of methanolic extract of gymnopilus junonius, a wild mushroom from southern western ghats India. Eur. J. Pharm. Med. Res. 5, 340–347.

Ren, X., Guo, J., Li, S., Chang, J., 2020. Thermogravimetric analysis-fourier transform infrared spectroscopy study on the effect of extraction pretreatment on the pyrolysis properties of eucalyptus wood waste. ACS Omega 5, 23364–23371. https://doi.org/10.1021/acsomega.0c03271.

Riedewald, F., Patel, Y., Wilson, E., Santos, S., Sousa-Gallagher, M., 2021. Economic assessment of a 40,000 t/y mixed plastic waste pyrolysis plant using direct heat treatment with molten metal: a case study of a plant located in Belgium. Waste Manag. 120, 698–707. https://doi.org/10.1016/j.wasman.2020.10.039.

Rodgers, K.M., Bennett, D., Moran, R., Knox, K., Stoiber, T., Gill, R., Young, T.M., Blum, A., Dodson, R.E., 2021. Do flame retardant concentrations change in dust after older upholstered furniture is replaced? Environ. Int. 153. https://doi.org/10.1016/j.envint.2021.106513.

Song, Y., Wang, Z., Yan, N., Zhang, R., Li, J., 2016. Demethylation of wheat straw alkali lignin for application in phenol formaldehyde adhesives. Polymers 8. https://doi.org/10.3390/polym8060209.

Soni, B., Karmee, S.K., 2020. Towards a continuous pilot scale pyrolysis based biorefinery for production of biooil and biochar from sawdust. Fuel 271. https://doi.org/10.1016/j.fuel.2020.117570.

Speight, J.G., 2017. Lange's Handbook of Chemistry. McGraw-Hill Education.

Staš, M., Auersvald, M., Kejla, L., Vrtiška, D., Kroufek, J., Kubička, D., 2020. Quantitative analysis of pyrolysis bio-oils: a review. Trends Anal. Chem. 126. https://doi.org/10.1016/j.trac.2020.115857.

Suriapparao, D.V., Vinu, R., 2018. Effects of biomass particle size on slow pyrolysis kinetics and fast pyrolysis product distribution. Waste Biomass. Valor 9, 465–477. https://doi.org/10.1007/s12649-016-9815-7.

Tagade, A., Kirti, N., Sawarkar, A.N., 2021. Pyrolysis of agricultural crop residues: an overview of researches by Indian scientific community. Bioresour. Technol. Rep. 15, 100761 https://doi.org/10.1016/j.biteb.2021.100761.

Taghizadeh-Alisaraei, A., Assar, H.A., Ghobadian, B., Motevali, A., 2017. Potential of biofuel production from pistachio waste in Iran. Renew. Sustain Energy Rev. 72, 510–522. https://doi.org/10.1016/j.rser.2017.01.111.

Undri, A., Abou-Zaid, M., Briens, C., Berruti, F., Rosi, L., Bartoli, M., Frediani, M., Frediani, P.J.F., 2015. Bio-oil from pyrolysis of wood pellets using a microwave multimode oven and different microwave absorbers. Fuel 153, 464–482. https://doi.org/10.1016/j.fuel.2015.02.081.

USEPA, 2002. Wood Products Industry: Medium Density Fiberboard Manufacturing. In: Emission Factors & AP 42. EnviroAtlas, pp. 1–27.

USEPA, 2020. Initial List of Hazardous Air Pollutants with Modifications. ⟨https://www.epa.gov/haps/initial-list-hazardous-air-pollutants-modifications⟩ (accessed 29 March 2021).

USEPA, 2021. Volatile Organic Compounds' Impact on Indoor Air Quality. ⟨https://www.epa.gov/indoor-air-quality-iaq/volatile-organic-compounds-impact-indoor-air-quality⟩ (accessed 29 March 2021).

Van Soest, P.J., Robertson, J.B., Lewis, B.A., 1991. Methods for dietary fiber, neutral detergent fiber, and nonstarch polysaccharides in relation to animal nutrition. J. Dairy Sci. 74, 3583–3597. https://doi.org/10.3168/jds.S0022-0302(91)78551-2.

Wang, B., Xu, F., Zong, P., Zhang, J., Tian, Y., Qiao, Y., 2019. Effects of heating rate on fast pyrolysis behavior and product distribution of Jerusalem artichoke stalk by using TG-FTIR and Py-GC/MS. Renew. Energy 132, 486–496. https://doi.org/10.1016/j.renene.2018.08.021.

Wang, T., Zhang, R., Peng, L., Ai, Y., Lu, Q., 2017. Pyrolysis characteristic changes of poplar wood during natural decay. J. Anal. Appl. Pyrolysis 128, 257–260. https://doi.org/10.1016/j.jaap.2017.10.003.

Wi, S., Park, J.H., Kim, Y.U., Kim, S., 2021. Evaluation of environmental impact on the formaldehyde emission and flame-retardant performance of thermal insulation materials. J. Hazard Mater. 402. https://doi.org/10.1016/j.jhazmat.2020.123463.

Xiong, Z., Guo, J., Chaiwat, W., Deng, W., Hu, X., Han, H., Chen, Y., Xu, K., Su, S., Hu, S., Wang, Y., Xiang, J., 2020. Assessing the chemical composition of heavy components in bio-oils from the pyrolysis of cellulose, hemicellulose and lignin at slow and fast heating rates. Fuel Process Technol. 199. https://doi.org/10.1016/j.fuproc.2019.106299.

Xu, F., Wang, B., Yang, D., Ming, X., Jiang, Y., Hao, J., Qiao, Y., Tian, Y., 2018. TG-FTIR and Py-GC/MS study on pyrolysis mechanism and products distribution of waste bicycle tire. Energ. Convers. Manag. 175, 288–297. https://doi.org/10.1016/j.enconman.2018.09.013.

Xu, J., Zhang, Y., Shen, Y., Li, C., Wang, Y., Ma, Z., Sun, W., 2019. New perspective on wood thermal modification: relevance between the evolution of chemical structure and physical-mechanical properties, and online analysis of release of VOCs. Polymers 11. https://doi.org/10.3390/polym11071145.

Yang, Y., Liew, R.K., Tamothran, A.M., Foong, S.Y., Yek, P.N.Y., Chia, P.W., Van Tran, T., Peng, W., Lam, S.S., 2021. Gasification of refuse-derived fuel from municipal solid waste for energy production: a review. Environ. Chem. Lett. 1–14. https://doi.org/10.1007/s10311-020-01177-5.

Yek, P.N.Y., Liew, R.K., Osman, M.S., Lee, C.L., Chuah, J.H., Park, Y.-K., Lam, S.S., 2019. Microwave steam activation, an innovative pyrolysis approach to convert waste palm shell into highly microporous activated carbon. J. Environ. Manag. 236, 245–253. https://doi.org/10.1016/j.jenvman.2019.01.010.

Yu, J., Wang, D., Sun, L., 2021. The pyrolysis of lignin: pathway and interaction studies. Fuel 290. https://doi.org/10.1016/j.fuel.2020.120078.

Zhan, H., Zhuang, X., Song, Y., Liu, J., Li, S., Chang, G., Yin, X., Wu, C., Wang, X., 2019. A review on evolution of nitrogen-containing species during selective pyrolysis of waste wood-based panels. Fuel 253, 1214–1228. https://doi.org/10.1016/j.fuel.2019.05.122.

Zhang, J., Liu, J., Evrendilek, F., Zhang, X., Buyukada, M., 2019. TG-FTIR and Py-GC/MS analyses of pyrolysis behaviors and products of cattle manure in CO_2 and N2 atmospheres: kinetic, thermodynamic, and machine-learning models. Energ. Convers. Manag. 195, 346–359. https://doi.org/10.1016/j.enconman.2019.05.019.

Zhao, C., Jiang, E., Chen, A., 2017. Volatile production from pyrolysis of cellulose, hemicellulose and lignin. J. Energy Inst. 90, 902–913. https://doi.org/10.1016/j.joei.2016.08.004.

Zhao, Z., Sakai, S., Wu, D., Chen, Z., Zhu, N., Huang, C., Sun, S., Zhang, M., Umemura, K., Yong, Q., 2019. Further exploration of sucrose–citric acid adhesive: investigation of optimal hot-pressing conditions for plywood and curing behavior. Polymers 11, 1996. https://doi.org/10.3390/polym11121996.

Zong, P., Jiang, Y., Tian, Y., Li, J., Yuan, M., Ji, Y., Chen, M., Li, D., Qiao, Y., 2020. Pyrolysis behavior and product distributions of biomass six group components: starch, cellulose, hemicellulose, lignin, protein and oil. Energ. Convers. Manag. 216. https://doi.org/10.1016/j.enconman.2020.112777.

TITLE/ AUTHOR	Generating alternative fuel and bioplastics from medical plastic waste and waste frying oil using microwave co-pyrolysis combined with microbial fermentation / Wan Mahari, W.A., Kee, S.H., Foong, S.Y., (...), Lam, S.S., Sonne, C.
SOURCE	Renewable and Sustainable Energy Reviews Volume 153, January 2022, 111790 https://doi.org/10.1016/j.rser.2021.111790 (Database : Science Direct)

Renewable and Sustainable Energy Reviews 153 (2022) 111790

Contents lists available at ScienceDirect

Renewable and Sustainable Energy Reviews

journal homepage: www.elsevier.com/locate/rser

Generating alternative fuel and bioplastics from medical plastic waste and waste frying oil using microwave co-pyrolysis combined with microbial fermentation

Wan Adibah Wan Mahari [a,b,1], Seng Hon Kee [c,1], Shin Ying Foong [b], Tan Suet May Amelia [c], Kesaven Bhubalan [c,d,e,***], Mustafa Man [f], YaFeng Yang [a], Hwai Chyuan Ong [g], Meththika Vithanage [h], Su Shiung Lam [b,a,**], Christian Sonne [i,a,*]

[a] Henan Province Engineering Research Center for Biomass Value-Added Products, School of Forestry, Henan Agricultural University, Zhengzhou, Henan, 450002, China
[b] Pyrolysis Technology Research Group, Higher Institution Centre of Excellence (HICoE), Institute of Tropical Aquaculture and Fisheries, Universiti Malaysia Terengganu, 21030, Kuala Nerus, Terengganu, Malaysia
[c] Ocean Pollution and Ecotoxicology Research Group, Faculty of Science and Marine Environment, Universiti Malaysia Terengganu, 21030, Kuala Nerus, Terengganu, Malaysia
[d] Institute of Marine Biotechnology, Universiti Malaysia Terengganu, 21030, Kuala Nerus, Terengganu, Malaysia
[e] Malaysian Institute of Pharmaceuticals and Nutraceuticals, NIBM, 11700, Pulau Pinang, Malaysia
[f] Faculty of Ocean Engineering Technology and Informatics, Universiti Malaysia Terengganu, 21030, Kuala Nerus, Terengganu, Malaysia
[g] Future Technology Research Center, National Yunlin University of Science and Technology, 123 University Road, Section 3, Douliou, Yunlin 64002, Taiwan
[h] Ecosphere Resilience Research Centre, Faculty of Applied Sciences, University of Sri Jayewardenepura, Nugegoda, 10250, Sri Lanka
[i] Aarhus University, Department of Bioscience, Arctic Research Centre (ARC), Frederiksborgvej 399, PO Box 358, DK, 4000, Roskilde, Denmark

ARTICLE INFO

Keywords:
Pyrolysis
Microwave
Medical waste
Fermentation
Bioplastics

ABSTRACT

In the present study, microwave co-pyrolysis (MCP) was used to simultaneously convert medical plastic waste (MPW) and waste frying oil (WFO) into liquid oil products. The MCP process demonstrated a faster heating rate (24 °C/min) and shorter process time (20 min) compared to conventional pyrolysis techniques converting MPW and WFO into liquid oil (≥80 wt%). The MCP reduced the oxygen content from 25.7 to 9.82 wt% in liquid oil encompassing light aliphatic hydrocarbons ranging from C_{10} to C_{28}, generating a novel sustainable liquid fuel. The liquid having a high carbon content (approximately 77.1 wt%) and low carbon to nitrogen ratio (27.9) is a suitable energy feedstock for polyhydroxyalkanoate (PHA) bioplastic production in the form of poly3-hydroxybutyrate [P(3HB)]. The liquid oil acted as an energy source for the growth of *Bacillus* sp. During microbial fermentation, yielding approximately 11% (w/w) P(3HB). Bioplastics are biodegradable, biocompatible with humans and non-toxic to marine organisms, representing a valuable additive in the production of cosmetics, detergents, and as medical scaffolds for tissue engineering. The results indicate the promising upcycling of waste products by this approach through pyrolytic biorefinery into value-added fuel and bioplastic products, being important for the future sustainable production of renewable resources.

1. Introduction

The global population growth and development of the healthcare industry have increased significantly over the last few decades leading to massive production of medical waste, further aggravated by the recent coronavirus pandemic (COVID-19) [1]. The COVID-19 pandemic has amplified the use of plastic-based personal protective equipment such as

* Corresponding author. Henan Province Engineering Research Center for Biomass Value-Added Products, Henan Agricultural University, Zhengzhou, Henan, 450002, China.
** Corresponding author. Henan Province Engineering Research Center for Biomass Value-Added Products, Henan Agricultural University, Zhengzhou, Henan, 450002, China.
*** Corresponding author. Ocean Pollution and Ecotoxicology Research Group, Faculty of Science and Marine Environment, Universiti Malaysia Terengganu, 21030, Kuala Nerus, Terengganu, Malaysia.
E-mail addresses: kesaven@umt.edu.my (K. Bhubalan), lam@umt.edu.my (S.S. Lam), cs@bios.au.dk (C. Sonne).
[1] These authors contributed equally to the manuscript.

https://doi.org/10.1016/j.rser.2021.111790
Received 16 May 2021; Received in revised form 12 September 2021; Accepted 15 October 2021
Available online 23 October 2021

surgical masks, gloves, medical gowns, feet and surface protectors, leading to a sudden surge in medical waste. In addition, COVID-19 has triggered the utilization of single-use plastic materials such as intravenous drips, saline bottles, and syringes. These practices significantly increase the existing challenges to disposing plastic waste. In fact, approximately 1.6 million tonnes of plastic have been produced daily worldwide since the COVID-19 outbreak, leading to an estimated 3.4 billion pieces of single-use medical plastic being discarded on a daily basis [1].

Several approaches are applied to reduce the amount of medical plastic waste including incineration, landfilling, autoclaving, and chemical disinfection. Landfilling is not a viable option as it requires huge land space and generates leachate that pollutes soil and aquatic environments, including groundwater [2]. Incineration is the most used technique as it reduces the volume of medical plastic waste by approximately 90%, while generating heat and energy for boilers and diverting waste from landfills [2,3]. Despite its benefits, incineration also poses risks to human health and the environment because of the release of hazardous compounds such as polychlorinated dibenzofurans (furans), polychlorinated dibenzo-p-dioxins (dioxins), heavy metals (*i.e.* cadmium and arsenic), and volatile organic compounds (VOCs), all of which are considered carcinogens [2,4].

The limitations of existing waste disposal and recovery of value-added products highlight the potential of microwave pyrolysis in converting plastic waste into energy sources. Pyrolysis is a thermochemical method operating under hypoxic conditions and high operating temperatures of approximately 400–800 °C using microwave radiation, during which waste materials decompose into energy products such as liquid oil and gases [5,6]. Microwave pyrolysis of plastic waste produces liquid oil that comprises aliphatic and aromatic hydrocarbons as potential fuel or chemical additives [7]. Nevertheless, liquid oil obtained from the microwave pyrolysis of plastic waste alone possesses high viscosity and contains waxy paraffinic components due to the unsatisfactory decomposition of long-chain paraffin wax compounds [7].

Owing to this problem, microwave co-pyrolysis may rectify the limitations of conventional microwave pyrolysis, as it involves the processing of two or more feedstock materials to generate a positive synergistic interaction, improving the oil yield and properties [8,9]. Previous studies reported that microwave co-pyrolysis of household cooking oil and waste plastic increased the yield of liquid oil products by 84 wt%, compared to the wastes being pyrolyzed individually [10]. Table 1 shows the current pyrolysis technologies used to convert waste cooking oil and plastic into liquid fuel, including the product yield and limitations. Nevertheless, there are lack of studies investigating the capability of the liquid oil obtained as carbon source in bacterial fermentation for bioplastics production.

Liquid oil produced by microwave co-pyrolysis is an energy and carbon-rich product with potential as energy source in bacterial fermentation for the production of bioplastics, particularly polyhydroxyalkanoate (PHA). These PHAs are polymers produced by microorganisms under nutrient-limited and carbon-enriched conditions owing to their petrochemical plastic properties, biocompatibility, and biodegradability [14]. According to Yustinah et al. [15], poly-3-hydroxybutyrate [P(3HB)] is the most common PHA. Studies have shown that PHA films can naturally biodegrade in the mangrove environment [16], lakes [17] or marine environments [18] within six weeks, making PHA a suitable replacement for common non-degradable petrochemical-based plastics.

In recent studies, PHA has shown tissue biocompatibility in both humans and animals [19]. A review on the *in vivo* degradation of PHA polymers by Bhubalan et al. [20] reported that 3-hydroxybutyric acid and 4-hydroxybutyric acid were present in human and animal blood. Moreover, PHA possesses plastic characteristics, making it a viable replacement for synthetic plastics; however, PHA production is often hampered by the production costs, as the energy feedstock for microbial fermentation is expensive. An alternative, yet inexpensive continuous supply of carbon as an energy source would be suitable for PHA production. Previous studies have revealed that feedstock derived from sweetwater [21], molasses [22], and glycerol [21] are viable for PHA production. Several microorganisms including *Ralstonia eutropha* (presently known as *Cupravidus necator*), *Pseudomonas* sp., *Alcaligenes* sp., *Aeromonas* sp., *Enterococcus* sp., *Brevundimonas* sp., and *Bacillus* sp., enable the synthesis of PHA [23,24]. For example, PHA produced by gram-negative bacteria, *R. eutropha*, possesses an outer layer membrane of lipopolysaccharides (LPS), an endotoxin responsible for inflammatory reactions contaminating the PHA and rendering it unsuitable for use *in vitro* [25]. In contrast, the PHA produced by gram-positive bacteria does not possess the LPS membrane, which gives it a wider application in the

Nomenclatures

Notations

Tc	**Crystallization temperature**
Tg	**Glass transition**
Tm	**Melting temperature**
ΔH_m	**Enthalpy of fusion of the sample**
ΔH_m^0	**Enthalpy fusion of 100% crystalline P(3HB) (142 J g^{-1})**

Abbreviations

ATP	Adenosine triphosphate
C	Carbon
CDW	Cell dry weight
CoASH	Coenzyme A
COVID-19	Coronavirus pandemic
DSC	Differential scanning calorimetry
FTIR	Fourier Transform Infrared Spectroscopy
GC-FID	Gas Chromatography with Flame Ionization Detection
GCMS	Gas Chromatography-Mass Spectrometry
H	Hydrogen
KBr	Potassium bromide
KH_2PO_4	Potassium dihydrogen phosphate
LDPE	Low-density polyethylene
LPS	Lipopolysaccharides
MCP	Microwave co-pyrolysis
MPW	Medical plastic waste
MSM	Minimum salt medium
N	Nitrogen
Na_2HPO_4	Disodium hydrogen phosphate
NH_4Cl	Ammonium chloride
NOx	Nitrogen oxides
NR	Nutrient rich
O	Oxygen
PHA	Polyhydroxyalkanoate
PhaA	(*R*)-3-hydroxybutyryl-CoA by β-ketothiolase
Pha B	NADPH-dependent acetoacetyl-CoA reductase
PhaC	PHA synthase
P(3HB)	Poly3-hydroxybutyrate
S	Sulphur
SDGs	Sustainable Development Goals
TGA	Thermogravimetric analysis
VOCs	Volatile organic compounds
WFO	Waste frying oil

Table 1
Current research in pyrolysis of waste cooking oil and plastic waste.

Feedstock	Pyrolysis system	Main findings	Refs.
Waste cooking oil	Conventional pyrolysis using fixed-bed reactor Waste origin: Borj-Cedria Technopark refectory	Yield of liquid oil: 80 wt% Calorific value: 37 MJ/kg Main composition of liquid oil: alkanes, alkenes, cyclic hydrocarbons, carboxylic acids, aldehydes, ketones, alcohols, and esters Potential application: fuel Drawback: high amount of oxygenated compounds and low calorific value	[11]
Waste cooking oil	Catalytic microwave vacuum pyrolysis Catalysts: HZSM-5 and metal oxide Waste origin: Yihai Kerry Oils and Foodstuffs Co. ltd. (Nanchang, Jiangxi)	Yield of liquid oil: 37.5 wt% Main composition of liquid oil: benzene, toluene, ethylbenzene, and xylene Potential application: industrial chemicals Drawback: Low yield of liquid oil	[12]
Plastic waste	Catalytic microwave pyrolysis Catalysts: ZSM-5 Waste origin: high-density polyethelene	Yield of liquid oil: 42.2 wt% Yield of wax: 17 wt% Main composition of liquid oil: aromatic, alkanes, alkenes Potential application: Fuel Drawback: low yield of liquid oil and high wax production	[13]
Plastic waste	Microwave pyrolysis Waste origin: high-density polyethelene	Yield of liquid oil and wax: 69% Main composition of liquid oil: aromatic, alkanes, alkenes Potential application: Fuel Drawback: high wax production	[7]
Waste cooking oil and plastic waste	Microwave vacuum co-pyrolysis Waste origin: Palm oil and high-density polyethelene	Yield of liquid oil: 84 wt% Main composition of liquid oil: alkanes, alkenes Potential application: Fuel	[10]

medical industry. According to Mohapatra et al. (2017) and Bhubalan et al. (2011), *Bacillus* sp., which are gram-positive, are capable of producing PHA copolymers depending on the carbon and energy source, benefitting the industrial sector, especially in agriculture, biomedicine, automobiles and packaging [19,20,26–28].

The use of biodegradable products from renewable sources represents an alternative resource that helps reduce plastic waste, which suffocates and contaminates the ecosphere. Bioplastics also decrease the carbon footprint, offer energy savings in processing, and does not use non-renewable raw materials during fermentation, while reducing the use of harmful chemicals [29]. In addition, the development of biodegradable bioplastics *via* upcycling of non-biodegradable plastic waste supports the United Nations Sustainable Development Goals (SDGs), especially Goal #12, to ensure sustainable consumption of waste, with the intention of minimising waste generation and maximising the production of value-added products.

To our best knowledge, no studies have reported the production of liquid oil for the synthesis of bioplastics. Previous studies have reported bioplastics production using microbial fermentation [28,30]. In contrast, this study promotes the energy application of liquid oil produced from the microwave co-pyrolysis of waste materials and use this liquid oil as an energy source for microbial fermentation to produce bioplastics. The valorisation of waste materials into value-added products, including fuel, bioplastics, and chemical additives *via* microwave co-pyrolysis technology is a novel ground-breaking method to ensure sustainable consumption and production of renewable materials.

2. Materials and methods

2.1. Preparation of feedstock materials

The feedstock materials used in this study were medical plastic waste (MPW) and waste frying oil (WFO). The MPW consisted of glucose and saline bottles made of low-density polyethylene (LDPE) obtained from KPJ Penang Specialist Hospital, Malaysia. MPW used in this study was non-infectious waste that has no direct contamination from the patients. As a precaution step prior to pyrolysis, the MPW was cleaned with detergents and decon 90 cleaning solution to kill any germ or bacteria from the waste. The MPW was then dried in an oven at 30–40 °C within 1 or 2 h to remove the moisture content. After drying, it was shredded (5–10 mm) in order to fit for insertion into the pyrolysis reactor. The WFO was obtained from restaurants near the Universiti Malaysia Terengganu, Malaysia. Large solid particles and impurities in the WFO were removed using Whatman Filter Paper (grade 40) and vacuum filtration.

2.2. Microwave co-pyrolysis

The co-pyrolysis experiment was conducted in a 800 W microwave oven that has been modified. The co-pyrolysis apparatus was assimilated with several core parts: 1) a quartz reactor (150 × 100 × 100 mm) with two necks was fabricated to pyrolyse the wastes, and the reactor was enfolded within a ceramic fibre blanket to reduce heat loss; 2) a microwave oven was utilised as the source of heating; 3) a condensation system containing a liebig condenser, a vigreux column, cold traps, and liquid oil containers; 4) a temperature controller and a type K thermocouple to monitor the temperature and heating rate during microwave co-pyrolysis; 5) nitrogen was purged into the pyrolysis reactor to eliminate air and maintain an oxygen-free condition. The detailed setup of microwave co-pyrolysis apparatus is reported in our previous work [10].

In this study, various microwave powers (600, 700, and 800 W) were investigated to examine its influence on the production and characteristics of the produced liquid oil. A feedstock ratio of 1:1 (50 g of WFO and 50 g of MPW) was inserted to the pyrolysis reactor. Activated carbon (50 g) was also added to the pyrolysis reactor to act as a microwave absorbent. Both WFO and MPW are poor microwave absorbers, thus activated carbon assists the heating process by absorbing the microwave radiation, efficiently converting it into heat to pyrolyse the feedstocks. The heating rate was determined according to the maximum temperature attained versus the heating time during the experiment. Microwave pyrolysis of MPW and WFOwas also performed separately to compare the performance of co-pyrolysis with the pyrolysis of individual feedstock.

The pyrolysis experiment was terminated after the generation of pyrolytic volatiles discontinued in the reactor. The yield of the liquid oil product was determined by measuring the increased weight of the liquid oil container after the experiment (Eq. (1)). The experiments were performed in triplicate to obtain the average reading for each sample. The yields of char and gases were not the main focus of this study; thus, they were excluded from analysis.

$$Yield\ of\ liquid\ oil\ (wt.\%) = \frac{weight\ of\ liquid\ oil}{weight\ of\ feedstocks} \times 100 \quad (1)$$

2.3. Analytical method to analyse feedstock and liquid oil

The thermal behavior and proximate content of feedstocks, *viz.* WVO, PKS and HPW were determined using a thermogravimetric (TGA) analyser (Mettler-Toledo TGA/SDTA851e, Switzerland). The feedstocks were heated from ambient temperature to 900 °C at a heating rate of 20 °C/min. Argon was used as the carrier gas that vented through the

system at a flow rate of 0.1 L/min. The amount of volatile matters in the feedstock was obtained based on the weight loss occurred between 100 °C and 600 °C [31]. Further weight loss occurred at 600–900 °C indicated the presence of char residue [32]. Fixed carbon content was obtained by subtracting the char residue and volatile matter content and from the dry mass of the feedstock [33].

Elemental analysis of the liquid oil was executed using a Vario MACRO elemental analyser (Elementar Analysemsysteme GmbH, Germany) to determine the elemental composition (*i.e.,* hydrogen, oxygen, nitrogen, carbon, sulphur) in the liquid oil. Gas chromatography-mass spectrometry (GCMS) analysis of the liquid oil was performed using a 6890 GC-MS instrument equipped with a mass spectrometer detector. The column used was 5% phenyl methyl siloxane from HP-5MS (length, 30 mm; diameter, 0.25 mm; film thickness, 0.25 μm). The initial temperature of the oven was 30 °C, with a holding time of 1 min. The temperature of the oven was subsequently set at the rate of 5 °C/min, from 30 °C to 300 °C. The concentration of each compound was calculated as a percentage of the total area of all the peaks in the analysis.

2.4. Bacterial strain isolation and preservation

Bacillus megaterium UMTKB-1 (GenBank accession number: KF991583) was previously isolated from tissue samples of the marine sponge *Callyspongia* sp., obtained from the waters near Langkawi Island, Malaysia [21]. The strain was maintained in a nutrient rich (NR) broth at 30 °C and 200 rpm, and preserved in 40% (v/v) glycerol stock at −80 °C for long-term storage.

2.5. Media and culture conditions

Media preparation and culture conditions were based on Yatim et al. (2017) [21]. The seed culture was prepared using NR medium (10 g/L peptone, 10 g/L meat extract and 2 g/L yeast extract). The PHA production was performed in minimal salt medium (MSM) which comprised 1.5 g/L KH_2PO_4, 3.6 g/L Na_2HPO_4, 0.5 g/L NH_4Cl, and 1 ml/L of MgSO4·$7H_2O$ (0.1 M) supplemented with 1 mL/L of trace element solution. The components of trace elements (Table 2) were dissolved in 0.1 M HCl.

2.6. Biosynthesis of polyhydroxyalkanoate with shake-flask culture

A one-stage shake-flask cultivation technique was implemented to synthesise PHA using the strain *B. megaterium* UMTKB-1, as previously reported by Yatim et al. (2017) [21] with some modifications. The effect of liquid oil produced from microwave co-pyrolysis of MPW and WFO at different microwave power on the PHA production was tested by supplementing 5 g/L of liquid oil with 0.5 g/L of ammonium chloride (NH_4Cl) as the sole supply of nitrogen. The influence of liquid oil produced from microwave pyrolysis and co-pyrolysis on PHA production was determined. The seed culture of *B. megaterium* UMTKB-1 was prepared by adding 1 mL/L of inoculum to NR broth incubated for 14 h at 200 rpm and 30 °C. The inoculum size for biosynthesis was maintained at 3% (v/v) for 48 h.

Table 2
Components of trace element solution.

Constituents	Concentration (g/L)
Cobalt (II) sulfate heptahydrate ($CoSO_4·7H_2O$)	2.81
Manganese (II) chloride tetrahydrate ($MnCl_2·4H_2O$)	1.98
Iron (II) sulfate heptahydrate ($FeSO_4·7H_2O$)	2.78
Calcium chloride dihydrate ($CaCl_2·2H_2O$)	1.67
Zinc sulfate heptahydrate ($ZnSO_4·7H_2O$)	0.29
Copper (II) chloride dihydrate ($CuCl_2·2H_2O$)	0.17

2.7. Polyhydroxyalkanoate content determination

The amount of PHA produced by *B. megaterium* UMTKB-1 was determined using GC 2010 (Shimadzu, Kyoto, Japan). This method was adapted from the work of Yatim et al. (2017) [21]. Freeze-dried bacterial cells (15 mg) were added to sulphuric acid and methanol (15:85, v/v %). The mixture was incubated for 2 h and 20 min at 100 °C to transform PHA monomers into methyl esters. The mixture was left to cool to room temperature, followed by the addition of 1 mL distilled water. The mixture was vortexed to encourage the phase separation. The bottom layer with the reaction product was extracted and dehydrated using anhydrous sodium sulfate. The moisture-free product was analysed by GC-FID with a Supelco SPB™-1 fused silica capillary column of dimensions 30 m × 0.25 mm × 0.25 μm (Sigma Aldrich, USA).

2.8. Polyhydroxyalkanoate characterisation

2.8.1. Fourier Transform Infrared analysis

Approximately 5 mg of PHA and 100 mg of potassium bromide (KBr) were weighed and pounded into a fine powder. The mixture was pelletized using a KBr pellet and inserted into a Fourier Transform Infrared (FTIR) spectrometer IRTracer-100, Shimadzu. The PHA was scanned 50 times to determine the functional groups at a resolution of 4 cm^{-1} and a spectral range of 4000–400 cm^{-1}. This method was adapted from Vigneswari et al. (2015), with some modifications [34].

2.8.2. Differential scanning calorimetry analysis

The thermal properties of the PHA materials were analysed using differential scanning calorimetry (DSC), which was performed using a Diamond PerkinElmer Pyris 1 thermal analyser that was paired with a liquid nitrogen cooling accessory. An estimated 5–8 mg of polymer was encapsulated within an aluminium pan. The sample was heated from −50 to 200 °C at a rate of 10 °C/min under a N_2 flow [35]. The sample was maintained at 200 °C for 2 min and then rapidly quenched to −50 °C for 5 min. The sample was then reheated from −50 to 200 °C at a rate of 10 °C/min. The DSC curve of the second heating was employed for PHA thermal property analysis. The glass transition temperature (T_g) was derived from the heat capacity change midpoint, whereas the melting point (T_m) and enthalpy of fusion (ΔH_m) were derived from the melting endotherm peak. The percentage of crystallinity was calculated based on the study by Gumel et al. (2012) [36] and the formula is as follows (Eq. (2)):

$$Crystallinity\ (\%) = \frac{\Delta H_m}{\Delta H_m^0} \quad (2)$$

ΔH_m: enthalpy fusion of the sample.

ΔH_m^0 : enthalpy fusion of 100% crystalline P(3HB) (142 J g^{-1}).

3. Results and discussion

3.1. Characteristics of waste frying oil and medical plastic waste

Fig. 1 shows the thermogravimetric analysis of WFO and MPW. The first stage of thermal decomposition occurs from ambient temperature (28 °C) to 110 °C, which is also known as the dehydration stage [32]. As illustrated in Fig. 1, both WFO and MPW show negligible mass reduction prior to reaching 110 °C, indicating low moisture content in both samples. Interestingly, MPW and WFO started to decompose at 390 °C and 285 °C, respectively, indicating that MPW has a higher decomposition temperature than the WFO. MPW is composed of long-chain hydrocarbons with a high degree of crystallinity and higher bond strength that require higher energy and temperature to break the bond. In contrast, WFO consists of low molecular-weight hydrocarbons (*e.g.* fatty acid chains) that can be broken down at lower temperature [32].

Most volatile matter was released prior to 600 °C, followed by a

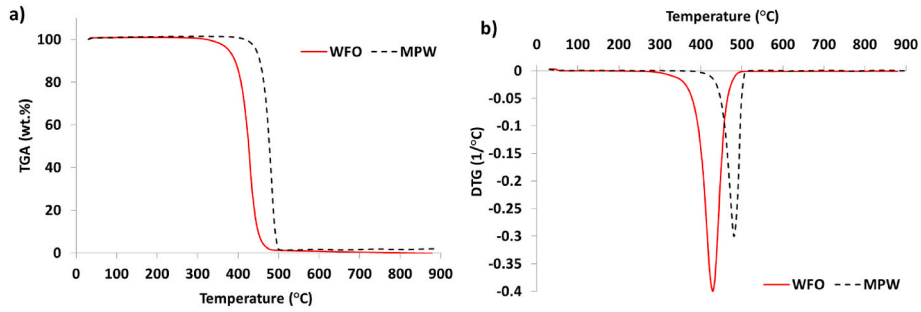

Fig. 1. Thermogravimetric analysis (a) and derivative thermogravimetry (b) of waste frying oil and medical plastic waste.

slight weight reduction observed at 600–900 °C, suggesting that limited charring occurred for WFO and MPW, producing less than 0.5 wt% of fixed carbon in both samples. Approximately 99 wt% of the content are released as volatile matter, hence limiting the char production during the decomposition process. Both MPW and WFO showed high weight loss between 200 and 600 °C, indicating the presence of high volatile matter content (~99 wt%) in both feedstocks. This signifies the desired characteristic of MPW and WFO to decompose and convert into mainly volatiles that condense to form potentially useful liquid oil product for use as fuel [10,37].

As aforementioned, MPW is a polymer consisting of long-chain hydrocarbons that is rich in carbon (86.2 wt%) and hydrogen (13.3 wt%), with a potential to be converted into aliphatic hydrocarbons that can be used as a source of fuel or energy for bacterial growth. Additionally, WFO contains saturated, unsaturated, and short-fatty acid chains composed of carboxylic acid groups, thus containing a high carbon (52.6 wt%), oxygen (26.3 wt%) and hydrogen (17.8 wt%) content [38]. The high carbon content in WFO and MPW demonstrates their potential as energy and carbon sources for the selected bioplastics producing bacteria [39]. The carbon content of feedstocks could act as an energy source in the metabolic activities of bacteria, which influence bacterial growth, redox potential of cell metabolism, composition, and yield of bioplastic polymers [40]. This implies that WFO and MPW are potentially suitable for enhancing bacterial growth and accumulating PHA for use as bioplastics. Moreover, WFO and MPW show low nitrogen content (0.02–0.33 wt%) with no sulphur, which validates their potential as a green feedstock for bioplastics production. This is due to the limited nitrogen content with potential to promote and boost homogeneous bioplastics production [39,41].

Fig. 2 shows the FTIR spectra, functional groups, and classification of components obtained from WFO and MPW. A strong peak was discovered at wavenumbers ranging from 3000 to 2800 cm^{-1} for both samples,

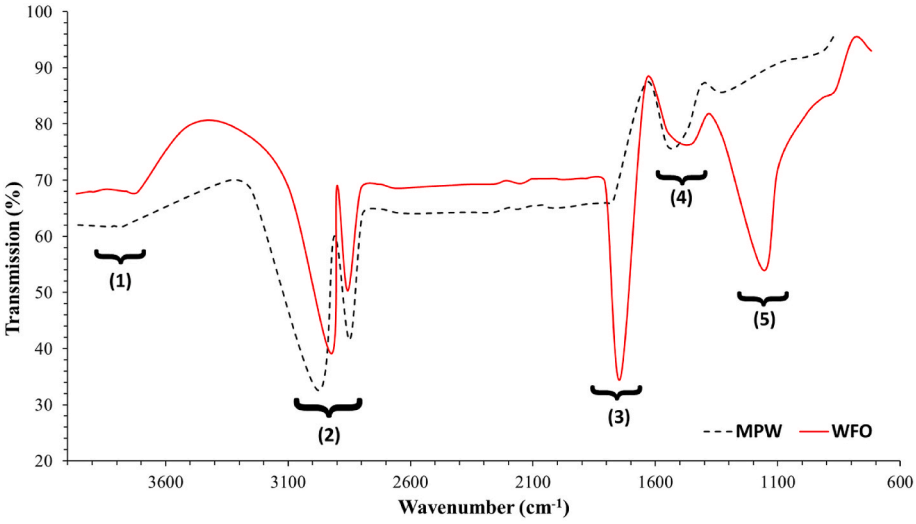

Frequency range (cm^{-1})	Wavenumber (cm^{-1})		Functional group	Classification of compounds
	WFO	MPW		
(1) 3700-3600	3713.0	-	O-H stretching	Alcohol
(2) 3000-2600	2922.2, 2856.6	2912.5, 2848.9	C-H stretching	Aliphatic CH_2 (*e.g.* alkane, alkene)
(3) 1800-1700	1743.7	-	C=O stretching	Carboxylic acid
(4) 1600-1400	1452.4	1548.8	C-H bending	Aliphatic CH_2 and CH_3
(5) 1200-1100	1157.3	-	C-O stretching	Carboxylic acid

Fig. 2. FTIR spectra, functional group and classification of compounds content in waste frying oil and medical plastic waste.

signifying the existence of aliphatic hydrocarbons such as alkanes with C–H stretching vibrations. The presence of aliphatic hydrocarbons was further confirmed by the peak at 1600–1400 cm^{-1} for both WFO and MPW [32]. There was a difference in FTIR spectrum observed between WFO and MPW at 3713.0 cm^{-1}, 1743.7 cm^{-1} and 1157.3 cm^{-1} which can be attributed to O–H stretching, C═O stretching and C–O stretching, respectively, resulting from oxygenated compounds such as carboxylic group in WFO [42]. Additionally, MPW consists of polymers with repeating units and only C and H; thus, no peaks were observed at wavenumbers within the range of 3700–3600 cm^{-1}, 1800–1700 cm^{-1}, and 1200–1100 cm^{-1}. The FTIR results reveal that WFO and MWP consist of aliphatic hydrocarbons such as alkanes and alkenes, exhibiting their potential as carbon sources for the production of bioplastics and biofuels.

3.2. Temperature behaviour and heating rate

Fig. 3 shows the temperature profile versus heating time during microwave co-pyrolysis of the combined WFO and MPW, and WFO and MPW, individually. The microwave power significantly affects the temperature behaviour and heating rate during co-pyrolysis and microwave pyrolysis of all samples. A lower microwave power (600 W) decelerates the heating rate during the pyrolysis process, with the maximum temperature achieved after 30 min. The main decomposition of samples into volatiles and active pyrolysis cracking occurs at maximum temperatures of 300–480 °C [43,44]. This is followed by passive pyrolysis, where the remaining feedstock is transformed into volatiles during declining temperatures, until no more volatiles are formed. The long heating time required to achieve maximum temperature results in a low heating rate (10–15 °C/min) for all samples operated at 600 W. Conversely, a higher microwave power resulted in a higher heating rate, and a maximum temperature of approximately 486 °C for 20 min at 800 W, with the highest heating rate (24 °C/min). This is likely because a high microwave power with a higher energy input results in a faster heating rate [45].

During microwave pyrolysis with only WFO, pyrolytic volatiles were produced at 200–300 °C and 8–10 min after the initiation of the experiments. The maximum temperature of 306–364 °C was observed at 20–30 min of heating time with a slower heating rate (10–12 °C/min) compared to both microwave pyrolysis of only MPW and co-pyrolysis. Microwave pyrolysis of MPW alone generated pyrolytic volatiles at 150–200 °C after 10–15 min, with extended volatiles generation as compared to WFO. MPW is a polymer that possesses high thermal stability and can withstand high temperatures; thus, extended heating times and higher temperatures are needed to break the long MPW polymer chains, especially the C–C bonds, compared to WFO [46].

Interestingly, during microwave co-pyrolysis of WFO and MPW, pyrolytic volatiles generated at 300–350 °C within 4–7 min after initiation of the experiments. Shorter time was needed to heat and pyrolyse WFO and MPW into volatiles, and the maximum temperature was achieved at 438–486 °C. This suggests that microwave co-pyrolysis has a positive synergistic effect on waste materials to reach a high pyrolysis temperature (*i.e.* showing a higher heating rate) compared to microwave pyrolysis of WFO and MPW, individually.

3.3. Production of liquid oil

The liquid oil yield from microwave pyrolysis of WFO, MPW, and co-pyrolysis is shown in Fig. 4. As the production of pyrolytic gases and char is not the focus of this study, these are not discussed. The liquid oil generated from the co-pyrolysis of WFO and MPW was higher than that generated by WFO and MPW, individually. This is attributed to the positive synergistic radical interactions [47] that occur during the co-pyrolysis of WFO and MPW. The interaction of free radicals with other polymers or long hydrocarbon chains in MPW and WFO may stimulate chain breaking reactions (*e.g.* fragmentation and depolymerisation) to produce pyrolytic volatiles containing smaller compounds (*e.g.* light hydrocarbons) that additionally condense into liquid oil products [48]. Furthermore, previous research reported that MPW contained a higher volatile matter content (97–98 wt%) compared to WFO (~90 wt%) [49,50]. The high content of volatile matter likely increases the formation of pyrolytic volatiles, and consecutively enhances condensation to generate more liquid oil [51]. This explains the high yield of liquid oil attained using microwave co-pyrolysis of WFO and MPW.

As the microwave power increased from 600 to 700 W, the liquid oil produced from all the samples increased significantly. Nevertheless, as the microwave power increased to 800 W, the liquid oil produced individually from WFO and MPW decreased likely because of secondary cracking reactions that normally occur at high microwave power, leading to high process temperatures [52–54]. As discussed in Section 3.2, the process temperature increases with microwave power, which promotes secondary cracking reactions (*e.g.* decarboxylation, decarbonylation, depolymerisation, and carbonisation). These reactions convert pyrolytic volatiles into gases or char [55,56], thus reducing liquid oil production. Surprisingly, the liquid oil produced from the microwave co-pyrolysis of WFO and MPW increased to approximately 81.1 wt% with an increase in microwave power up to 800 W. Perhaps, the increased production and interactions between free radicals generated at higher microwave power during the co-pyrolysis of WFO and MPW stimulated chain-breaking reactions and volatile formation that condensed into liquid oil.

3.4. Elemental and chemical composition of liquid oils

The elemental compositions of liquid oils are shown in Table 4. Liquid oils are mainly composed of carbon, oxygen, and hydrogen produced at a lower microwave power (600–700 W) with a higher carbon content (72.4–77.1 wt%) compared to those obtained at a higher microwave power of 800 W (68.2 wt%). The carbon content is likely derived from aliphatic hydrocarbon compounds found in liquid oil, which corroborates with the GCMS analysis of the liquid oil, indicating a higher concentration of aliphatic hydrocarbons in liquid oil obtained at 600 and 700 W (~96%) as compared to 800 W (~90%). In addition, the higher temperature at higher microwave power increases the occurrence of intensive secondary cracking reactions, such as decarbonylation, polymerisation, and decarboxylation, which convert hydrocarbon compounds into gases (*e.g.* CO, CO_2, C_2H_2, C_2H_4). Conversely, a lower temperature at a lower microwave power may reduce the extent of secondary cracking reactions, thereby producing liquid oil with higher amounts of carbon and hydrogen compounds.

Sulphur was absent in the original feedstock and liquid oils, while lower nitrogen was detected in the liquid oils compared to the original WFO. Similarly, a lower oxygen content was observed in liquid oils compared to the original WFO, indicating that the interaction between MPW (containing low oxygen with almost no nitrogen content) and WFO reduced the nitrogen and oxygen-containing compounds in the oils. The presence of free radicals during co-pyrolysis reactions may convert nitrogen-containing compounds into nitrogen oxides (NOx) or nitrogen gasthat can be released into the atmosphere. Nevertheless, the composition of the gases needs to be verified in future studies. Additionally, the role of MPW as a hydrogen-rich material stimulates the formation of hydrogen radicals, thereby increasing decarbonylation and decarboxylation. The oxygen-containing compounds in the liquid oil are likely reduced because of the elimination of compounds with carbonyl group (C═O) and carboxyl group (COOH) in MPW and WFO, while oxygen-containing compounds are converted into aliphatic hydrocarbons and gases such as CO and CO_2 [10].

Fig. 5 shows the chemical components of the liquid oil produced from microwave co-pyrolysis of MPW and WFO. The liquid oils primarily comprise of aliphatic hydrocarbons (*e.g.* alkanes and alkenes), carboxylic acids (*e.g.* fatty acids), aromatics (*e.g.* benzenes), and other

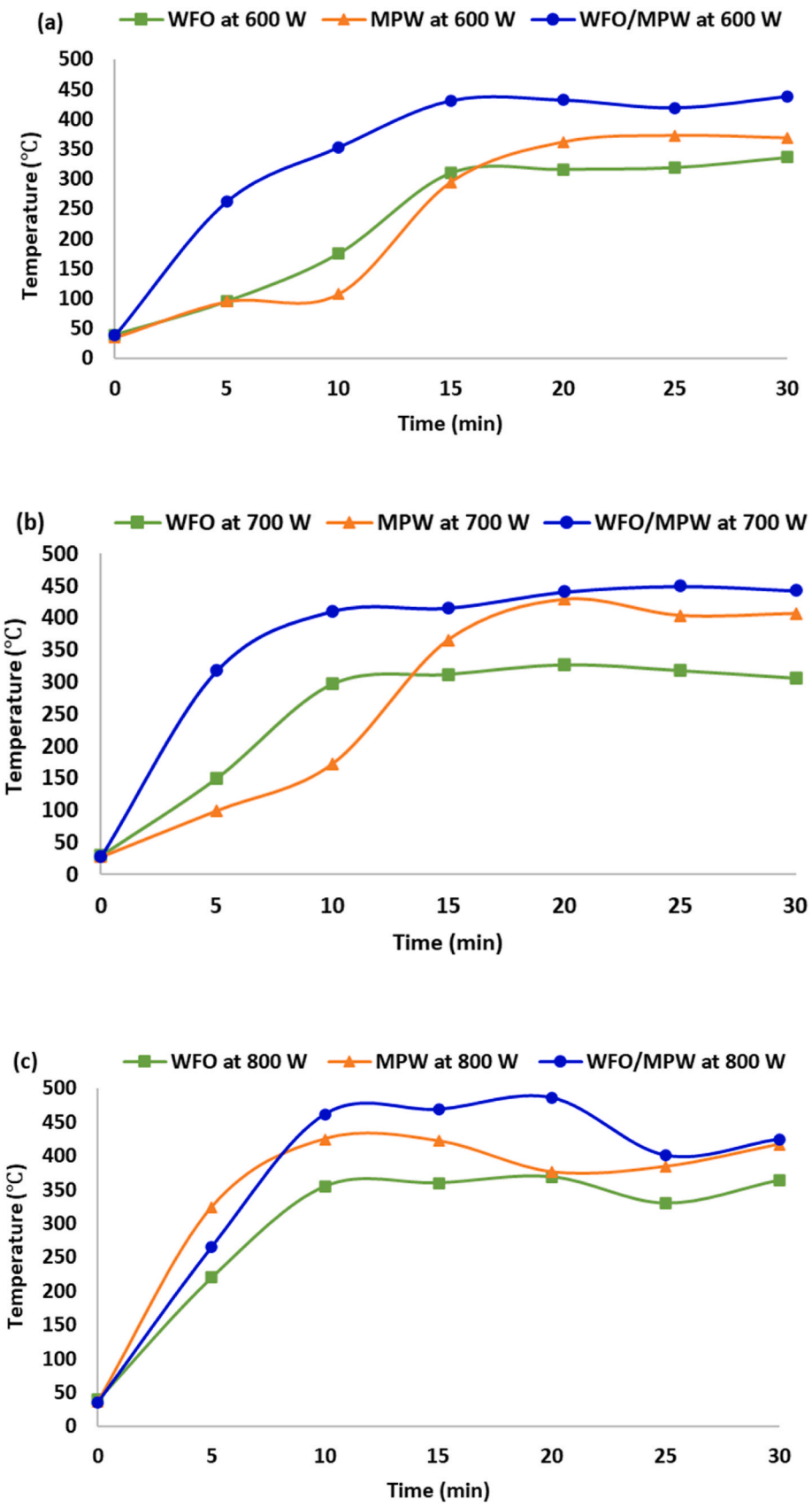

Fig. 3. Temperature behavior versus heating time. (a) pyrolysis performed at microwave power of 600 W, (b) pyrolysis performed at microwave power of 700 W, (c) pyrolysis performed at microwave power of 800 W.

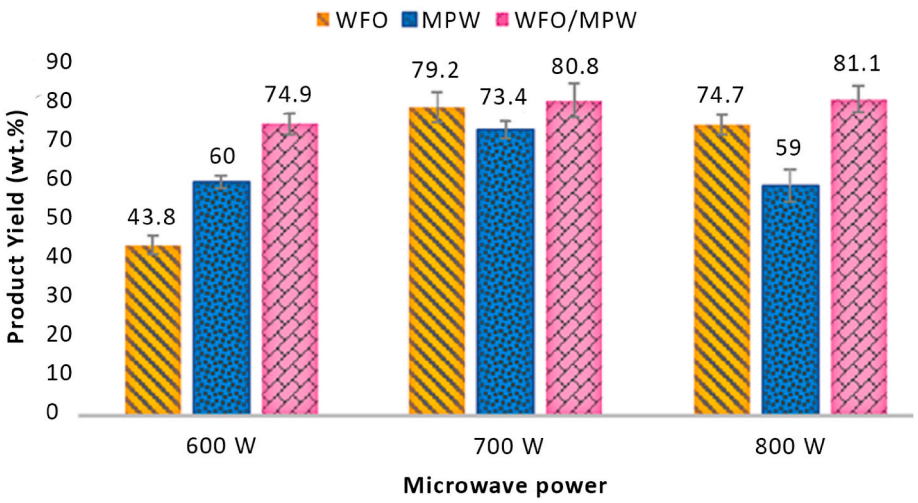

Fig. 4. Yield of liquid oil obtained at various microwave power.

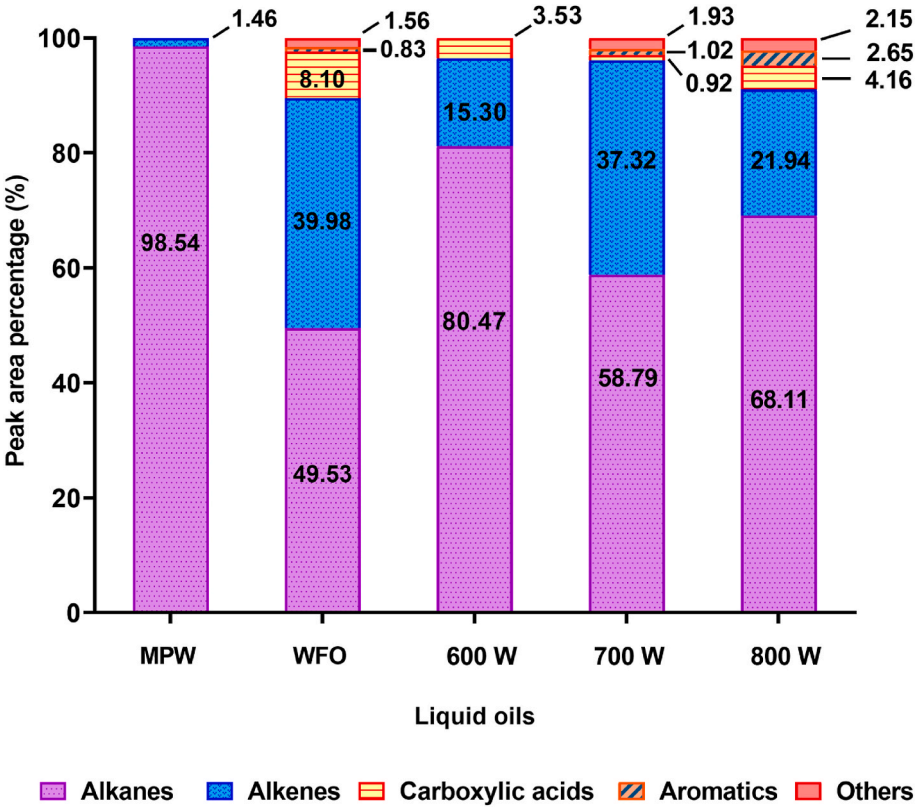

Fig. 5. Chemical composition of liquid oil obtained from microwave pyrolysis of MPW alone, WFO alone and microwave co-pyrolysis of MPW and WFO at 600 W, 700 W, and 800 W of microwave power.

unidentified compounds. Liquid oil produced at 700 W had the highest aliphatic hydrocarbons (96.1%), followed by liquid oil produced at 600 W (95.8%) and 800 W (90.1%). The aliphatic hydrocarbons are mainly decane ($C_{10}H_{22}$) to octacosane ($C_{28}H_{58}$). Octadecane ($C_{18}H_{38}$) and pentacosane ($C_{25}H_{52}$) were the major compounds found in the liquid oil produced at 600 W, whereas heptadecane ($C_{17}H_{34}$) and heneicosane ($C_{21}H_{44}$) were the major compounds found in liquid oil produced at 700 and 800 W (Table S1). This suggests that high process temperatures enhance the thermal cracking reactions of hydrocarbon molecules in MPW and triglyceride molecules in WFO, subsequently cracking heavier hydrocarbon compounds into lighter ones. In addition, higher microwave power may stimulate the production of hydrogen radicals during the random scission polymer degradation reaction, which normally occurs during co-pyrolysis. Other polymer chains may interact with free radicals to break the chains of the polymer into lighter hydrocarbon components.

Aromatic compounds were absent in the liquid oil produced at a lower microwave power (600 W). At a higher microwave power (700 W), 1.02% of aromatics was produced, while oil produced at 800 W had the highest content of aromatics. This signifies the occurrence of secondary cracking reactions, such as the depolymerisation of polyethylene, along with increased microwave power, converting aliphatic hydrocarbons into aromatics such as benzenes [31]. This is also corroborated by the lower aliphatic hydrocarbons in the liquid oil

produced at 800 W (90.1%) compared to other liquid oils produced at a lower microwave power.

Carboxylic acids in liquid oils include hexadecanoic acid, octadecanoic acid, and 9-octadecenoic acid, which is derived from the original WFO, with the highest content of carboxylic acids in the liquid oil produced at 800 W, followed by 600 W and 700 W. At 700 W, intensive deoxygenation of oxygenated compounds (*e.g.* aldehydes, ketones, and fatty acids) enhances its conversion into aliphatic hydrocarbons, especially alkanes and alkenes. Low carboxylic acids detected in the liquid oil following 700 W treatment are desirable for use as alternative fuels, because the characteristics of carboxylic acids degrade liquid oil quality during storage, thus reducing the stability of the oil [10]. Nevertheless, the higher carboxylic acids detected in the liquid oil produced at 800 W is desirable as a supplement for microbial fermentation to produce bioplastics, because the fatty acids can serve as a bacterial food source, creating the ester bond during PHA formation.

The results show the strong potential of the liquid oil produced from the microwave co-pyrolysis of plastic waste and waste frying oil for its use as an alternative fuel, as reflected in our previous studies [10,32,51]. In the subsequent section, we emphasize the use of liquid oil as an energy source and growth substrate to produce bioplastics.

3.5. Production of polyhydroxyalkanoate using liquid oil produced from microwave co-pyrolysis of medical plastic waste and waste frying oil

A negligible growth of *B. megaterium* UMTKB-1 was observed with limited PHA accumulation when the liquid oil generated from microwave pyrolysis of MPW and WFO, individually, was used as the energy source and carbon substrate for bacterial growth (Table 5). Probably, the deficiency of WFO carbon (52.6 wt%, Table 4) inhibits bacterial growth and PHA accumulation. Additionally, WFO also contains the antimicrobial compound, i-Propyl 11,12-methylene-octadecanoate, which can inhibit bacterial growth [57]. The non-existence of nitrogen content in the liquid oil produced from MPW likely contributes to the absence of bacterial growth and PHA. In addition, excessive carbon content can inhibit the pathway of PHA synthesis, revealing that extreme conditions, such as excessive and deficient nutrient content (e.g. carbon and nitrogen), inhibit bacterial growth and PHA accumulation [58].

Interestingly, *B. megaterium* UMTKB-1 strain accumulated PHA in the form of P(3HB) using the liquid oil obtained from the microwave co-pyrolysis of MPW and WFO. The liquid oil served as carbon substrate and energy source for the bacteria to grow and accumulate PHA simultaneously (Table 5). This implies that the encouraging synergistic effect between MPW and WFO increases the carbon and nitrogen content in liquid oil, resulting in a higher carbon to nitrogen ratio that facilitates the growth of *B. megaterium,* and subsequently, the accumulation of PHA. More specifically, the highest PHA content was observed while using liquid oil produced at 600 W, followed by liquid oil produced at 800 and 700 W (Table 4). This was likely due to the desirable properties of liquid oil produced at 600 W, such as higher carbon content (77.1 wt%), lower carbon to nitrogen ratio content (27.9), and slightly higher carboxylic acid (3.52%) content compared to other liquid oils. PHA is a linear polyester comprising monomers of hydroxy acid linked to an ester bond produced by linking the carboxylic group of a monomer to the hydroxyl group of a compound [59].

The levels of PHA accumulation observed using the liquid oils obtained from 600 W to 800 W of microwave power was expected because the C/N ratio of liquid oil obtained at 700 W was the highest compared to the C/N ratio obtained at 600 and 800 W (Table 3). Previous studies reported that PHA accumulation occurred in a limited nitrogen-excess carbon environment, which agrees with our current finding [60–62]. Notably, higher cell dry weight (CDW) was observed when the liquid oil obtained at both 700 and 800 W were used as the energy source compared to the liquid oil obtained at 600 W. Sufficient amounts of nitrogen and carbon facilitate bacterial growth, rather than accumulate PHA [41]. However, the limitation of nitrogen in the culture medium is an important factor for PHA production; therefore, the liquid oil obtained at 600 W is the best carbon source, because of its high carbon and low nitrogen content, which fits the criteria for PHA accumulation.

The fatty acids in liquid oil serve as an energy source for bacterial propagation mainly through the following biosynthesis pathways. The adenosine triphosphate (ATP) molecules, coenzyme A (CoASH), and acyl-CoA synthetase activate fatty acids into acyl-CoA before entering the β-oxidation cycle [63]. Although the acetyl-CoA produced from the β-oxidation cycle usually enters the Krebs cycle for ATP production, nutrient-deficiency decrease the electron transport activity and hence generating lesser ATP and triggering PHA accumulation as an alternative energy storage approach [64]. The metabolic pathway of P(3HB) accumulation in *B. megaterium* UMTKB-1 naturally competes for the β-oxidation of fatty acids to produce acetyl-CoA that is not only used in development of growth but also vital for P(3HB) production, which may explain the reasons of the low PHA accumulation (Fig. 6) [65]. Two acetyl-CoA molecules are formed into acetoacetyl-CoA and subsequently (*R*)-3-hydroxybutyryl-CoA by β-ketothiolase (PhaA) and NADPH-dependent acetoacetyl-CoA reductase (PhaB), then polymerized by PHA synthase (PhaC), thus releasing CoA to be used for P(3HB) synthesis replacing the Krebs cycle. However, during normal conditions without malnourishment, CoA prevents the generation of PhaA in the Krebs cycle.

In liquid oil, these fatty acids help to promote bacterial growth by utilising the readily available alkanes. The alkane is degraded by oxygenases that introduce oxygen atoms into alkane substrates and target the terminal methyl group of alkanes to produce fatty alcohols. Subsequently, alcohol dehydrogenases oxidise alcohols to form fatty acids that then enter the β-oxidation pathway, hence allowing liquid oils to be utilised with other substrates, such as reducing and non-reducing sugars [66]. Although there have been reports of PHA conversion from waste oils, not all PHA-producing bacteria produce the necessary enzymes to perform the biological syntheses and conversions from waste oils and plastic wastes needed for PHA synthesis and ATP production, thus making the mentioned conversion ability observed in this study considered as valuable [9,11,15]. Furthermore, microwave-pyrolyzed waste oils and plastics have altered properties and compositions compared to non-pyrolyzed wastes [40,42,47]. To date and to our knowledge, this is the first report of PHA production from medical plastic waste and waste frying oil using *B. megaterium*. Further studies are needed to further optimize the approach in producing higher yield of PHA.

FTIR analysis provides further insights into the chemical structure of the P(3HB) homopolymer. Fig. 7 shows the functional groups of P(3HB) produced by *B. megaterium* UMTKB-1. The IR spectra recorded peaks at 2978.09 (-CH group), 1737.86 (C═O stretch), and 1286.52–1068.56 (C–O stretch) cm^{-1}, which corresponded with the previous studies [15,28,70]. Absorption bands detected at 2735.06, 2384.02, and

Table 3
Properties of waste frying oil and medical plastic waste.

Feedstock	Elemental analyses (wt.%)					Proximate analyses (wt.%)			
	C	H	N	S	O	Moisture	Volatile matter	Fixed carbon	Char residue
WFO	52.6	17.8	3.33	0	26.3	0	99.8	0.2	0
MPW	86.2	13.3	0.02	0	0.48	0	99.5	0.5	0

Table 4
Elemental composition of the liquid oils.

Elemental Analysis	Carbon (wt%)	Hydrogen (wt%)	Nitrogen (wt%)	Sulphur (wt%)	Oxygen (wt%)	H/C	C/N
Original WFO	52.6	17.8	3.33	0	26.3	4.06	18.4
Original MPW	86.2	13.3	0.02	0	0.48	1.81	–
600 W (1:1)	77.1	10.3	3.18	0	9.82	1.60	27.9
700 W (1:1)	72.4	7.22	2.19	0	18.8	1.19	38.5
800 W (1:1)	68.2	9.14	2.28	0	20.7	1.61	34.9

(–) not available.

Table 5
Biosynthesis of P(3HB) by *B. megaterium* UMTKB-1 using pyrolysis liquid oil as growth substrate.

Liquid oil	PHA content [% (w/w)]	Cell dry weight, CDW (g/L)
MPW	Trace amount[a]	Trace amount[b]
WFO	Trace amount	Trace amount
MPW + WFO (600 W)	11.03	0.13 ± 0.04
MPW + WFO (700 W)	0.80	0.16 ± 0.04
MPW + WFO (800 W)	1.54 ± 0.13	0.16 ± 0.07

CDW = cell dry weight; MPW = medical plastic waste; WFO = waste frying oil.
[a] PHA content <5 wt%.
[b] Cell dry weight <0.05 g/L.

964.41–509.21 cm^{-1} correspond to –CH stretching, C≡C stretching, and –OH groups, respectively. The detection of the C═O bond at 1737.86 cm^{-1} represents the character of P(3HB). Additionally, DSC was conducted to investigate the melting temperature (T_m), glass transition (T_g), crystallization temperature (T_c), and degree of crystallinity of P(3HB). The T_g of the P(3HB) obtained was 2.00 °C, which was comparable with previous studies by Wellen et al. [71] and Gunaratne et al. [72]. The T_m and T_c of the P(3HB) obtained was 172.65 °C and 48.20 °C, respectively. The T_m was comparable to that reported in previous studies by Mohanrasu et al. [73] and Trakunjae et al. [74] while T_c was in agreement with Wellen et al. [71]. The degree of crystallinity of P(3HB) was 55.75% in the present study, which exhibited results approximately similar to the previous studies [75,76]. These analyses provided sufficient data to confirm the identity of the synthesised polymer, P(3HB).

Numerous studies have been performed on the valorisation of waste

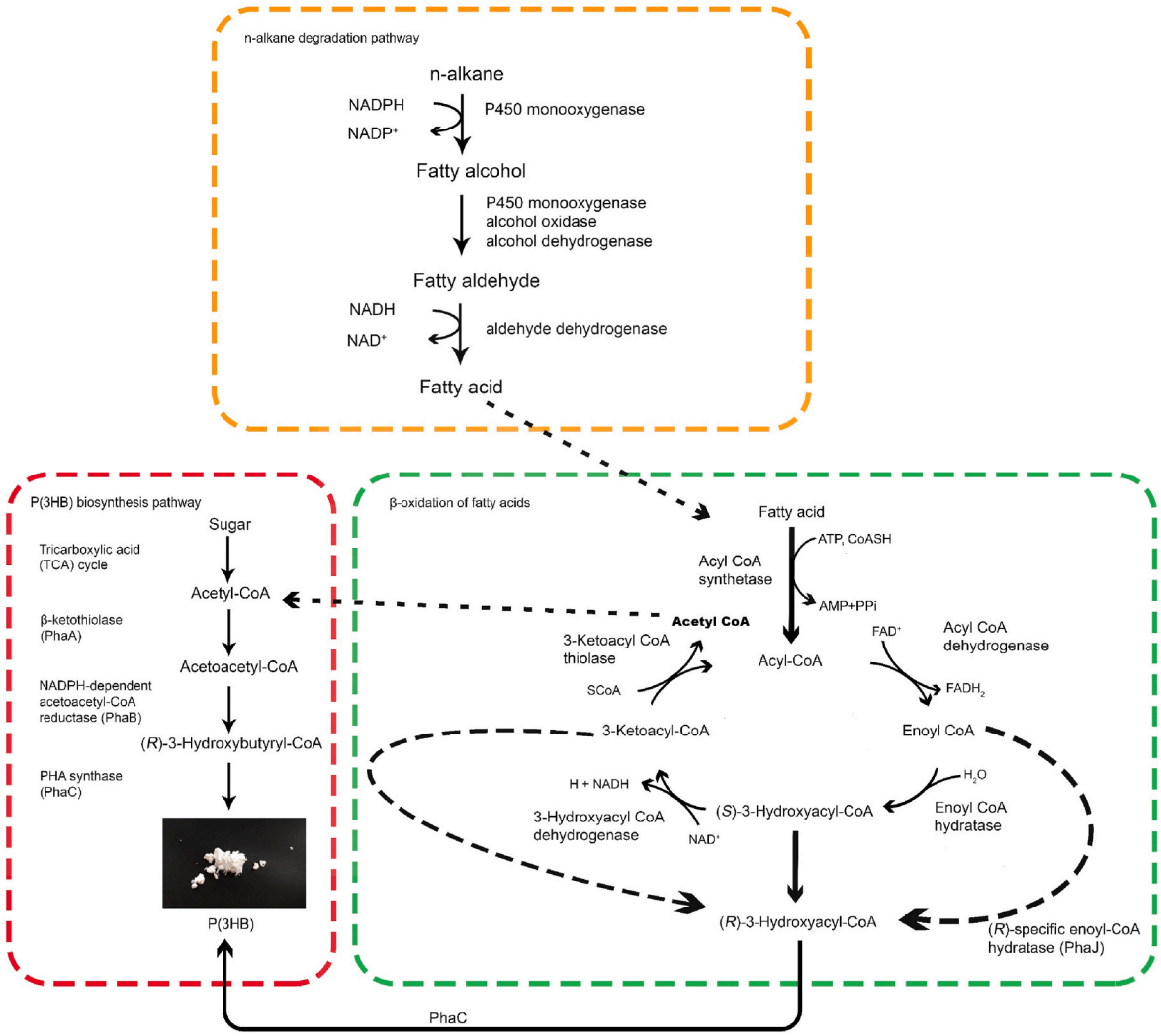

Fig. 6. n-alkane degradation pathway, β-oxidation of fatty acids pathway and P(3HB) biosynthesis pathway. Reproduced from previous studies [67–69].

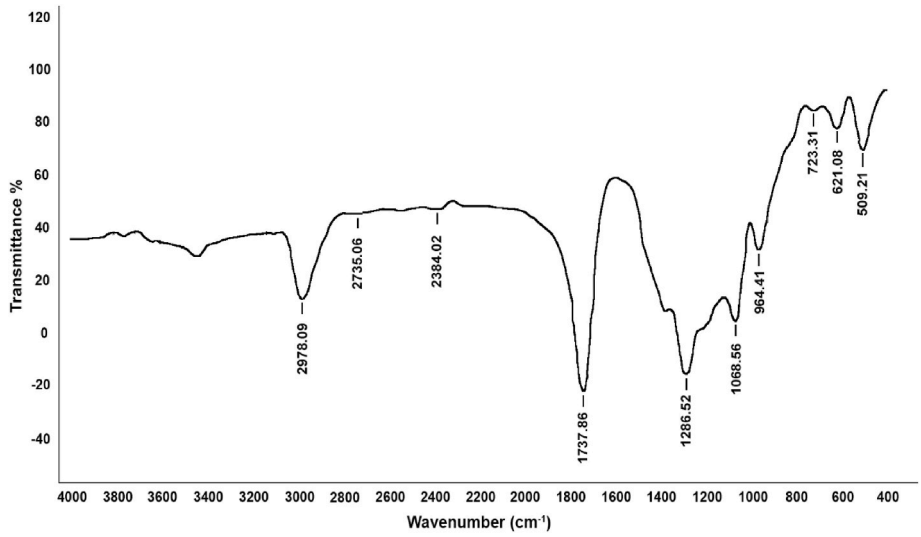

Fig. 7. FTIR spectrum of P(3HB) homopolymer generated by *B. megaterium* UMTKB-1. Resolution = 4 cm^{-1}; 50 scans.

as the sole energy and carbon source for PHA production. Table 5 shows the various bacteria, and wastes used as carbon sources and growth substrates for PHA production. Although previous studies (Table 6) had similar purpose of valorising wastes to produce PHA, the carbon was mainly sourced from organic wastes. The novel aspect that sets our study apart from the previous studies is that P(3HB) was produced from the liquid oil generated by the microwave co-pyrolysis of medical plastic wastes and waste frying oil. However, the P(3HB) yield [11% (w/w)] obtained in our study was lower than that obtained in other studies, which suggests the need for further optimisation of the biosynthesis processes using the feedstock obtained in this study.

The liquid oil produced from the pyrolysis of MPW and WFO has potential and is beneficial as an energy source and carbon substrate for P(3HB) production. This is the first initiative where plastic waste combined with waste cooking oil can be converted into biodegradable P(3HB). One of the main challenges in a circular economy is reducing the generation of solid wastes [77]. Studies on PHA production utilising different organic wastes as an energy source and carbon substrate have been performed, but none to date on synthetic wastes or a combination of organic and synthetic wastes. The potential of waste has yet to be uncovered, and the combination of MPW and WFO can be one of the alternatives to reduce plastic waste and carbon footprint (Table 6).

Table 6
Previous studies of polyhydroxyalkanoate production using various bacteria and different energy feedstocks.

Bacteria	Carbon feedstock	PHA type	PHA yield [% (w/w)]	Refs.
Bacillus megaterium UMTKB-1	Microwave co-pyrolyzed MPW and WFO	P(3HB)	11	This study
B. megaterium R11	Oil palm empty fruit bunch hydrolysate	P(3HB)	58	[78]
B. megaterium NCIM 5472	Cheese whey permeate	P(3HB-*co*-3HV)	87	[79]
B. megaterium NCIM 5472	Ultrafiltered cheese whey	P(3HB)	75	[80]
B. megaterium	Glucose Glycerol	P(3HB) P(3HB)	59 62	[81]
B. megaterium UMTKB-1	Sugarcane molasses Sweetwater Glycerol	P(3HB) P(3HB) P(3HB)	12 7 49	[21]
Defluviicoccus vanus	Sugarcane molasses	PHA	37	[82]
Burkholderia sacchari DSM17165	Wheat straw hydrolysate Glucose	P(3HB) P(3HB-*co*-4HB) P(3HB)	57 27	[83]
Cupravidus necator DSM 428	Used cooking oil	P(3HB)	37	[84]
Haloferax mediterranei DSM1411	Whey	PHA	70	[25]
Bacillus cereus suaeda B-001	Glucose Oil palm empty fruit bunch	P(3HB) P(3HB)	43 40	[15]
Bacillus subtilis RS1	Pre-treated sugarcane molasses	P(3HB)	45	[23]
Recombinant *C. necator* RE2058/pCB113	Sludge palm oil	P(3HB-*co*-3HHx)	74	[85]
Pseudomonas aeruginosa STN-10	Frying oil	P(3HB)	53	[86]

4. Practical implications of the study

This work was initiated due to massive accumulation of MPW at hospitals in Malaysia, which require high cost for disposal via incineration and specific sanitary landfill. The COVID-19 pandemic has led to sudden upsurge of MPW and this exacerbates the problem for its disposal. The current disposal approach such as incineration and sanitary landfill could escalate environmental pollution due to the release of harmful gases including dioxins, furans and CO_2 [87]. Therefore, the present work demonstrates the practicality of applying microwave co-pyrolysis to simultaneously reduce waste materials (MPW and WFO) while recovering energy from these wastes.

The addition of WFO into MPW during microwave co-pyrolysis is effective to reduce the production of undesirable wax and increase the yield of liquid oil compared to pyrolysis of plastic waste alone (Fig. 4). The MPW also represents other types of plastic waste produced from household and industry sectors. This study also demonstrated the capability of MPW to facilitate the pyrolysis of WFO, leading to the reduction of oxygenated compounds and increase the carbon, hydrogen and aliphatic hydrocarbons composition in the liquid oil, thereby showing potential to be upgraded into fuel. The high carbon content in the liquid oil is also desirable to be used as energy source during bacterial fermentation for producing bioplastics. This suggests that microwave co-pyrolysis is a desirable approach to enhance the quantity and quality of the liquid oil product, thereby showing support to the United Nations Sustainable Development Goals (SDGs) in producing affordable and clean energy (Goal#7) and ensuring sustainable consumption and production (Goal #12). The feedstocks used during microwave co-pyrolysis are not limited to MPW and WFO only, but other feedstocks

that exhibit similar properties could be used to generate a liquid oil product with desirable properties. This study could be a suitable reference for researchers or industrial operators who seek for a sustainable approach in using waste materials as feedstocks to produce energy.

Further research is needed to optimize and scale up the technology for industrial application. A microwave co-pyrolysis system can be developed and constructed at hospital so that the MPW can be converted into energy on-site, thus reducing transportation cost for waste disposal. In addition, the liquid oil may be further converted into fuel or ignited in boilers to generate power and electricity. Nevertheless, more research is needed to assess the environmental sustainability of the developed technology via exergetic, exergoenvironmental and exergoeconomic assessments.

5. Concluding remarks and future perspectives

Microwave co-pyrolysis of MPW and WFO produced liquid oil significantly higher than the microwave pyrolysis of MPW and WFO individually, and at higher heating rates and reduced process time. Liquid oil consists of light aliphatic hydrocarbons ranging from C_{10} to C_{28} and contains low oxygen, thus exhibiting potential for use as an alternative fuel. The liquid oil produced from the microwave co-pyrolysis at 600 W with a C/N ratio of 27.9, acts as an energy source for microbial fermentation and produces higher P(3HB) content compared to the range of microwave power considered. The production of bioplastics from synthetic plastic waste is possible using the microwave co-pyrolysis technique. Since this finding is relatively new, the future direction of related research includes optimisation of microwave pyrolysis parameters such as microwave temperature, retention time, presence of catalyst, physical and chemical fermentation parameters, and bioreactor production scale-up for increased yields of P(3HB). Moreover, future research on co-polymer production should also be considered.

This study showed that microwave co-pyrolysis reduced the content of heteroatoms (*e.g.* oxygen and nitrogen) and increased the composition of aliphatic hydrocarbons compounds in the liquid oil, which can potentially be applied as fuel. Nevertheless, it should be mentioned that the presence of heteroatoms such as oxygen and nitrogen could generate nitrogen-containing and oxygen-containing compounds, which could deteriorate the quality of the liquid oil. For instance, the oxygen-containing compounds (*e.g.* carboxylic acids) could cause corrosiveness to the engine if the liquid oil is applied as fuel. In addition, the nitrogen-containing compounds could emit harmful NOx during the combustion of the liquid oil as fuel. Therefore, future studies should be performed to further improve this pyrolysis technique and the composition of the liquid oil:

1. Upgrading techniques to reduce or eliminate the content of heteroatoms in the liquid oil. For example, ionic liquids can be applied as extraction solvents for the reduction of nitrogen compounds from the liquid fuel [88].
2. Examination of microwave co-pyrolysis models using uncertainty analyses that identify and quantify possible faults of this approach. By performing this analysis, the range of possible outputs can be determined based on the uncertainty of the inputs applied to scrutinize the impact of the errors or lack of knowledge of the model.
3. This study showed that *B. megaterium* UMTKB-1 was able to accumulate PHA when fed with microwave co-pyrolyzed MPW and WFO liquid oil. However, the yield is relatively low when compared to previous studies. The liquid oil contains oxygen which can be oxidized and polymerized to generate unfavourable compounds for bacteria growth. Post-treatment can be considered to further stabilize the oil. The bioavailability of carbon from the liquid oil also affects its utilization by the bacteria to accumulate PHA. It was observed from the biosynthesis that solidified liquid oils still present after 48 h. The bacteria were likely not able to fully utilize the liquid oil due to low total surface area. This phenomenon was common when oily substrates with high melting point compared to the bacteria fermentation temperature were used as carbon source. To 'break' the oil higher agitation speed, addition of biosurfactant or biological or physicochemical treatments can be considered to increase the bioavailability of the carbon from the liquid oil. Nonetheless the effect of this factors on the PHA yield is yet to be fully understood.
4. Find other factors that could affect the PHA yield such as the type of strains, genes and enzyme produced [89]. The *B. megaterium* UMTKB-1 strain may not be the most suitable candidate to accumulate PHA when fed with liquid oil produced from microwave pyrolysis. It is important to emphasize that the carbon source utilization is strain dependent. Hence, a quest to search for a more suitable wild-type strain or a robust genetically engineered strain can be considered that can withstand the impurities of the liquid oil is necessary and accustomed to utilising liquid oil for PHA accumulation purposes [30]. Additionally, the gaps in the physiology and complete metabolic pathways of bacterial PHA-producers using liquid oil as carbon source still pose question regarding other competing pathways or inhibitors. Therefore, the findings here show the possible conversion of pyrolyzed bio-oil into PHA but this requires future research in the optimisation of culture conditions and treatment of feedstocks for higher PHA yield.

Declaration of competing interest

The authors declare that they have no known competing financial interests or personal relationships that could have appeared to influence the work reported in this paper.

Acknowledgments

The authors would like to thank the Universiti Malaysia Terengganu and Henan Mingbo New Energy Technology Co. Ltd, China for financial support under the International Partnership Research Grant (UMT/CRIM/2-2/2/23 (23), Vot 55302). We are thankful for the support from the Ministry of Higher Education, Malaysia, under the Higher Institution Centre of Excellence (HICoE), Institute of Tropical Aquaculture and Fisheries (AKUATROP) program (Vot. No. 63933 & Vot. No. 56051, UMT/CRIM/2-2/5 Jilid 2 (10)). The work is also supported by Program for Innovative Research Team (in Science and Technology) in University of Henan Province (No. 21IRTSTHN020) and Central Plain Scholar Funding Project of Henan Province (No. 212101510005). The authors would like to thank KPJ Penang Specialist Hospital, Malaysia for providing the medical plastic waste for this project. We are gratefully acknowledged Henan Agricultural University for the financial, facility, and technical support throughout this research under a Research Collaboration Agreement (RCA) with Universiti Malaysia Terengganu.

Appendix A. Supplementary data

Supplementary data to this article can be found online at https://doi.org/10.1016/j.rser.2021.111790.

Credit author statement

Wan Adibah Wan Mahari: Methodology, Data curation, Formal analysis, Validation, Writing - original draft. **Kee Seng Hon:** Data curation, Formal analysis, Investigation, Visualization, Writing - original draft. **Shin Ying Foong:** Formal analysis, Visualization, Writing - review & editing. **Tan Suet May Amelia:** Formal analysis, Visualization, Writing - review & editing. **Kesaven Bhubalan:** Conceptualization, Supervision, Investigation, Validation, Writing - review & editing. **Mustafa Man:** Conceptualization, Writing - review & editing. **YaFeng Yang:** Writing - review & editing. **Hwai Chyuan Ong:** Writing - review

& editing. **Meththika Vithanage:** Writing - review & editing. **Prof. Dr. Su Shiung Lam:** Conceptualization, Supervision, Methodology, Writing - review & editing, Funding acquisition, Project administration. **Prof. Christian Sonne:** Investigation, Conceptualization, Methodology, Writing - review & editing.

References

[1] Benson NU, Bassey DE, Palanisami T. COVID pollution: impact of COVID-19 pandemic on global plastic waste footprint. Heliyon 2021;7:e06343.
[2] Ansari M, Ehrampoush MH, Farzadkia M, Ahmadi E. Dynamic assessment of economic and environmental performance index and generation, composition, environmental and human health risks of hospital solid waste in developing countries; A state of the art of review. Environ Int 2019;132:105073.
[3] Blahuskova V, Vlcek J, Jancar D. Study connective capabilities of solid residues from the waste incineration. J Environ Manag 2019;231:1048–55.
[4] Liu J, Dai X, Wu Z, Weng X. Unveiling the secondary pollution in the catalytic elimination of chlorinated organics: the formation of dioxins. Chin Chem Lett 2020;31:1410–4.
[5] Xia C, Cai L, Zhang H, Zuo L, Shi SQ, Lam SS. A review on the modeling and validation of biomass pyrolysis with a focus on product yield and composition. Biofuel Research Journal 2021;8:1296–315.
[6] Soltanian S, Lee CL, Lam SS. A review on the role of hierarchical zeolites in the production of transportation fuels through catalytic fast pyrolysis of biomass. Biofuel Research Journal 2020;7:1217–34.
[7] Russell AD, Antreou EI, Lam SS, Ludlow-Palafox C, Chase HA. Microwave-assisted pyrolysis of HDPE using an activated carbon bed. RSC Adv 2012;2:6756.
[8] Suriapparao DV, Boruah B, Raja D, Vinu R. Microwave assisted co-pyrolysis of biomasses with polypropylene and polystyrene for high quality bio-oil production. Fuel Process Technol 2018;175:64–75.
[9] Tang C-Y, Zhang D-X. Mechanisms of aliphatic hydrocarbon formation during co-pyrolysis of coal and cotton stalk. Chin Chem Lett 2016;27:1607–11.
[10] Lam SS, Wan Mahari WA, Ok YS, Peng W, Chong CT, Ma NL, et al. Microwave vacuum pyrolysis of waste plastic and used cooking oil for simultaneous waste reduction and sustainable energy conversion: recovery of cleaner liquid fuel and techno-economic analysis. Renew Sustain Energy Rev 2019;115:109359.
[11] Ben Hassen Trabelsi A, Zaafouri K, Baghdadi W, Naoui S, Ouerghi A. Second generation biofuels production from waste cooking oil via pyrolysis process. Renew Energy 2018;126:888–96.
[12] Wu Q, Wang Y, Peng Y, Ke L, Yang Q, Jiang L, et al. Microwave-assisted pyrolysis of waste cooking oil for hydrocarbon bio-oil over metal oxides and HZSM-5 catalysts. Energy Convers Manag 2020;220:113124.
[13] Zhou N, Dai L, Lv Y, Li H, Deng W, Guo F, et al. Catalytic pyrolysis of plastic wastes in a continuous microwave assisted pyrolysis system for fuel production. Chem Eng J 2021;418:129412.
[14] Rathi DN, Amir H, Abed R, Kosugi A, Arai T, Sulaiman O, et al. Polyhydroxyalkanoate biosynthesis and simplified polymer recovery by a novel moderately halophilic bacterium isolated from hypersaline microbial mats. J Appl Microbiol 2013;114:384–95.
[15] Yustinah Hidayat N, Alamsyah R, Roslan AM, Hermansyah H, Gozan M. Production of polyhydroxybutyrate from oil palm empty fruit bunch (OPEFB) hydrolysates by Bacillus cereus suaeda B-001. Biocatalysis and Agricultural Biotechnology 2019;18:101019.
[16] Sridewi N, Bhubalan K, Sudesh K. Degradation of commercially important polyhydroxyalkanoates in tropical mangrove ecosystem. Polym Degrad Stabil 2006;91:2931–40.
[17] Salim Y, Sharon A, Vigneswari S, Ibrahim MM, Amirul A. Environmental degradation of microbial polyhydroxyalkanoates and oil palm-based composites. Appl Biochem Biotechnol 2012;167:314–26.
[18] Nakayama A, Yamano N, Kawasaki N. Biodegradation in seawater of aliphatic polyesters. Polym Degrad Stabil 2019;166:290–9.
[19] Vigneswari S, Amirul A. Biodegradability and cellular compatibility of poly (3-hydroxybutyrate-co-4-hydroxybutyrate) via subcutaneous implantation in rat model. Malays Appl Biol 2017;46:205–12.
[20] Bhubalan K, Lee W-H, Sudesh K. Polyhydroxyalkanoate. In: Domb AJ, Kumar N, Ezra A, editors. Biodegradable polymers in clinical use and clinical development. New Jersey: John Wiley & Sons, Inc; 2011. p. 249–315.
[21] Yatim AFM, Syafiq IM, Huong KH, Amirul A-A, Effendy AWM, Bhubalan K. Bioconversion of novel and renewable agro-industry by-products into a biodegradable poly (3-hydroxybutyrate) by marine Bacillus megaterium UMTKB-1 strain. BioTechnologia Journal of Biotechnology Computational Biology and Bionanotechnology 2017;98.
[22] Solaiman DK, Ashby RD, Hotchkiss AT, Foglia TA. Biosynthesis of medium-chain-length poly (hydroxyalkanoates) from soy molasses. Biotechnol Lett 2006;28:157–62.
[23] Rathika R, Janaki V, Shanthi K, Kamala-Kannan S. Bioconversion of agro-industrial effluents for polyhydroxyalkanoates production using Bacillus subtilis RS1. Int J Environ Sci Technol 2019;16:5725–34.
[24] Zhang C, Wang C, Cao G, Wang D, Ho S-H. A sustainable solution to plastics pollution: an eco-friendly bioplastic film production from high-salt contained Spirulina sp. residues. J Hazard Mater 2020;388:121773.
[25] Koller M. Biodegradable and biocompatible polyhydroxy-alkanoates (PHA): auspicious microbial macromolecules for pharmaceutical and therapeutic applications. Molecules 2018;23:362.
[26] Yeo JCC, Muiruri JK, Thitsartarn W, Li Z, He C. Recent advances in the development of biodegradable PHB-based toughening materials: approaches, advantages and applications. Mater Sci Eng C 2018;92:1092–116.
[27] Amelia TSM, Govindasamy S, Tamothran AM, Vigneswari S, Bhubalan K. Applications of PHA in agriculture. Biotechnological applications of Polyhydroxyalkanoates. Springer; 2019. p. 347–61.
[28] Mohapatra S, Mohanta P, Sarkar B, Daware A, Kumar C, Samantaray D. Production of polyhydroxyalkanoates (PHAs) by Bacillus strain isolated from waste water and its biochemical characterization. Proc Natl Acad Sci India B Biol Sci 2017;87:459–66.
[29] Tsang YF, Kumar V, Samadar P, Yang Y, Lee J, Ok YS, et al. Production of bioplastic through food waste valorization. Environ Int 2019;127:625–44.
[30] Kee SH, Chiongson JBV, Saludes JP, Vigneswari S, Ramakrishna S, Bhubalan K. Bioconversion of agro-industry sourced biowaste into biomaterials via microbial factories–a viable domain of circular economy. Environ Pollut 2020:116311.
[31] Lam SS, Wan Mahari WA, Ma NL, Azwar E, Kwon EE, Peng W, et al. Microwave pyrolysis valorization of used baby diaper. Chemosphere 2019;230:294–302.
[32] Wan Mahari WA, Chong CT, Cheng CK, Lee CL, Hendrata K, Yuh Yek PN, et al. Production of value-added liquid fuel via microwave co-pyrolysis of used frying oil and plastic waste. Energy 2018;162:309–17.
[33] Lam SS, Liew RK, Lim XY, Ani FN, Jusoh A. Fruit waste as feedstock for recovery by pyrolysis technique. Int Biodeterior Biodegrad 2016;113:325–33.
[34] Vigneswari S, Abdul Khalil H, Amirul A. Designing of collagen based poly (3-hydroxybutyrate-co-4-hydroxybutyrate) scaffolds for tissue engineering. International Journal of Polymer Science 2015;2015.
[35] Salim YS, Abdullah AA-A, Nasri CSSM, Ibrahim MNM. Biosynthesis of poly(3-hydroxybutyrate-co-3-hydroxyvalerate) and characterisation of its blend with oil palm empty fruit bunch fibers. Bioresour Technol 2011;102:3626–8.
[36] Gumel AM, Annuar MSM, Heidelberg T. Biosynthesis and characterization of polyhydroxyalkanoates copolymers produced by Pseudomonas putida Bet 001 isolated from palm oil mill effluent. PLoS One 2012;7:e45214.
[37] Wang Y, Dai L, Fan L, Cao L, Zhou Y, Zhao Y, et al. Catalytic co-pyrolysis of waste vegetable oil and high density polyethylene for hydrocarbon fuel production. Waste Manag 2017;61:276–82.
[38] Awogbemi O, Onuh EI, Inambao FL. Comparative study of properties and fatty acid composition of some neat vegetable oils and waste cooking oils. Int J Low Carbon Technol 2019;14:417–25.
[39] Portugal-Nunes DJ, Pawar SS, Lidén G, Gorwa-Grauslund MF. Effect of nitrogen availability on the poly-3-d-hydroxybutyrate accumulation by engineered Saccharomyces cerevisiae. AMB Express; 2017. p. 7.
[40] Ganesh Saratale R, Cho S-K, Dattatraya Saratale G, Kadam AA, Ghodake GS, Kumar M, et al. A comprehensive overview and recent advances on polyhydroxyalkanoates (PHA) production using various organic waste streams. Bioresour Technol 2021;325:124685.
[41] Ntaikou I, Koumelis I, Kamilari M, Iatridi Z, Tsitsilianis C, Lyberatos G. Effect of nitrogen limitation on polyhydroxyalkanoates production efficiency, properties and microbial dynamics using a soil-derived mixed continuous culture. International Journal of Biobased Plastics 2019;1:31–47.
[42] Alshuiael SM, Al-Ghouti MA. Multivariate analysis for FTIR in understanding treatment of used cooking oil using activated carbon prepared from olive stone. PLoS One 2020:15.
[43] Huang Y-F, Chiueh P-T, Kuan W-H, Lo S-L. Microwave pyrolysis of lignocellulosic biomass: heating performance and reaction kinetics. Energy 2016;100:137–44.
[44] Foong SY, Liew RK, Yang Y, Cheng YW, Yek PNY, Wan Mahari WA, et al. Valorization of biomass waste to engineered activated biochar by microwave pyrolysis: progress, challenges, and future directions. Chem Eng J 2020;389:124401.
[45] Ao W, Fu J, Mao X, Kang Q, Ran C, Liu Y, et al. Microwave assisted preparation of activated carbon from biomass: a review. Renew Sustain Energy Rev 2018;92:958–79.
[46] Miandad R, Barakat MA, Aburiazaiza AS, Rehan M, Nizami AS. Catalytic pyrolysis of plastic waste: a review. Process Saf Environ Protect 2016;102:822–38.
[47] Ryu HW, Kim DH, Jae J, Lam SS, Park ED, Park YK. Recent advances in catalytic co-pyrolysis of biomass and plastic waste for the production of petroleum-like hydrocarbons. Bioresour Technol 2020;310:123473.
[48] Mahari WAW, Azwar E, Ying Foong S, Ahmed A, Peng W, Tabatabaei M, et al. Valorization of municipal wastes using co-pyrolysis for green energy production, energy security, and environmental sustainability: a review. Chem Eng J 2021:129749.
[49] Anuar Sharuddin SD, Abnisa F, Wan Daud WMA, Aroua MK. A review on pyrolysis of plastic wastes. Energy Convers Manag 2016;115:308–26.
[50] Lam SS, Wan Mahari WA, Cheng CK, Omar R, Chong CT, Chase HA. Recovery of diesel-like fuel from waste palm oil by pyrolysis using a microwave heated bed of activated carbon. Energy 2016;115:791–9.
[51] Wan Mahari WA, Chong CT, Lam WH, Anuar TNST, Ma NL, Ibrahim MD, et al. Microwave co-pyrolysis of waste polyolefins and waste cooking oil: influence of N2 atmosphere versus vacuum environment. Energy Convers Manag 2018;171:1292–301.
[52] Song Z, Yang Y, Sun J, Zhao X, Wang W, Mao Y, et al. Effect of power level on the microwave pyrolysis of tire powder. Energy 2017;127:571–80.
[53] Tripathi M, Sahu JN, Ganesan P. Effect of process parameters on production of biochar from biomass waste through pyrolysis: a review. Renew Sustain Energy Rev 2016;55:467–81.
[54] Dai M, Xu H, Yu Z, Fang S, Chen L, Gu W, et al. Microwave-assisted fast co-pyrolysis behaviors and products between microalgae and polyvinyl chloride. Appl Therm Eng 2018;136:9–15.

[55] Ahmed MHM, Batalha N, Mahmudul HMD, Perkins G, Konarova M. A review on advanced catalytic co-pyrolysis of biomass and hydrogen-rich feedstock: insights into synergistic effect, catalyst development and reaction mechanism. Bioresour Technol 2020;310:123457.
[56] Yang J, Rizkiana J, Widayatno WB, Karnjanakom S, Kaewpanha M, Hao X, et al. Fast co-pyrolysis of low density polyethylene and biomass residue for oil production. Energy Convers Manag 2016;120:422–9.
[57] Sun L, Atkinson K, Zhu M, D'Amico DJ. Antimicrobial effects of a bioactive glycolipid on spore-forming spoilage bacteria in milk. J Dairy Sci 2021;104:4002–11.
[58] Sánchez Valencia AI, Rojas Zamora U, Meraz Rodríguez M, Álvarez Ramírez J, Salazar Peláez ML, Fajardo Ortiz C. Effect of C/N ratio on the PHA accumulation capability of microbial mixed culture fed with leachates from the organic fraction of municipal solid waste (OFMSW). Journal of Water Process Engineering 2021;40:101975.
[59] Sharma V, Sehgal R, Gupta R. Polyhydroxyalkanoate (PHA): properties and modifications. Polymer 2021;212:123161.
[60] Montiel-Jarillo G, Carrera J, Suárez-Ojeda ME. Enrichment of a mixed microbial culture for polyhydroxyalkanoates production: effect of pH and N and P concentrations. Sci Total Environ 2017;583:300–7.
[61] Morgan-Sagastume F, Karlsson A, Johansson P, Pratt S, Boon N, Lant P, et al. Production of polyhydroxyalkanoates in open, mixed cultures from a waste sludge stream containing high levels of soluble organics, nitrogen and phosphorus. Water Res 2010;44:5196–211.
[62] Silva F, Campanari S, Matteo S, Valentino F, Majone M, Villano M. Impact of nitrogen feeding regulation on polyhydroxyalkanoates production by mixed microbial cultures. N Biotechnol 2017;37:90–8.
[63] Kumari A. Beta oxidation of fatty acids. In: Sweet biochemistry: remembering structures, cycles, and pathways by mnemonics. London: Academic press; 2018. p. 17–9.
[64] García G, Sosa-Hernández JE, Rodas-Zuluaga LI, Castillo-Zacarías C, Iqbal H, Parra-Saldívar R. Accumulation of PHA in the microalgae scenedesmus sp. under nutrient-deficient conditions. Polymers 2021;13:131.
[65] Tarrahi R, Fathi Z, Seydibeyoğlu MÖ, Doustkhah E, Khataee A. Polyhydroxyalkanoates (PHA): from production to nanoarchitecture. Int J Biol Macromol 2020;146:596–619.
[66] Chen G-Q. Plastics completely synthesized by bacteria: polyhydroxyalkanoates. Plastics from bacteria. Springer; 2010. p. 17–37.
[67] Broadway NM, Dickinson FM, Ratledge C. The enzymology of dicarboxylic acid formation by Corynebacterium sp. strain 7E1C grown on n-alkanes. Microbiology 1993;139:1337–44.
[68] Eschenfeldt WH, Zhang Y, Samaha H, Stols L, Eirich LD, Wilson CR, et al. Transformation of fatty acids catalyzed by cytochrome P450 monooxygenase enzymes of Candida tropicalis. Appl Environ Microbiol 2003;69:5992–9.
[69] Huf S, Krügener S, Hirth T, Rupp S, Zibek S. Biotechnological synthesis of long-chain dicarboxylic acids as building blocks for polymers. Eur J Lipid Sci Technol 2011;113:548–61.
[70] Shah K. FTIR analysis of polyhydroxyalkanoates by a locally isolated novel Bacillus sp. AS 3-2 from soil of Kadi region, North Gujarat, India. J Biochem Technol 2012;3:380–3.
[71] Wellen RM, Canedo EL, Rabello MS. Melting and crystallization of poly (3-hydroxybutyrate)/carbon black compounds. Effect of heating and cooling cycles on phase transition. J Mater Res 2015;30:3211.
[72] Gunaratne LWK, Shanks R. Miscibility, melting, and crystallization behavior of poly (hydroxybutyrate) and poly (D, L-lactic acid) blends. Polym Eng Sci 2008;48:1683–92.
[73] Mohanrasu K, Rao RGR, Dinesh GH, Zhang K, Prakash GS, Song D-P, et al. Optimization of media components and culture conditions for polyhydroxyalkanoates production by Bacillus megaterium. Fuel 2020;271:117522.
[74] Trakunjae C, Boondaeng A, Apiwatanapiwat W, Kosugi A, Arai T, Sudesh K, et al. Enhanced polyhydroxybutyrate (PHB) production by newly isolated rare actinomycetes Rhodococcus sp. strain BSRT1-1 using response surface methodology. Sci Rep 2021;11:1–14.
[75] El-Hadi A, Schnabel R, Straube E, Müller G, Henning S. Correlation between degree of crystallinity, morphology, glass temperature, mechanical properties and biodegradation of poly (3-hydroxyalkanoate) PHAs and their blends. Polym Test 2002;21:665–74.
[76] da Silva Moura A, Demori R, Leão RM, Frankenberg CLC, Santana RMC. The influence of the coconut fiber treated as reinforcement in PHB (polyhydroxybutyrate) composites. Materials Today Communications 2019;18:191–8.
[77] Liguori R, Faraco V. Biological processes for advancing lignocellulosic waste biorefinery by advocating circular economy. Bioresour Technol 2016;215:13–20.
[78] Zhang Y, Sun W, Wang H, Geng A. Polyhydroxybutyrate production from oil palm empty fruit bunch using Bacillus megaterium R11. Bioresour Technol 2013;147:307–14.
[79] Suhazsini P, Keshav R, Narayanan S, Chaudhuri A, Radha P. A study on the synthesis of poly (3-hydroxybutyrate-co-3-hydroxyvalerate) by Bacillus megaterium utilizing cheese whey permeate. J Polym Environ 2020;28:1390–405.
[80] Das S, Majumder A, Shukla V, Suhazsini P, Radha P. Biosynthesis of poly (3-hydroxybutyrate) from cheese whey by Bacillus megaterium NCIM 5472. J Polym Environ 2018;26:4176–87.
[81] Naranjo JM, Posada JA, Higuita JC, Cardona CA. Valorization of glycerol through the production of biopolymers: the PHB case using Bacillus megaterium. Bioresour Technol 2013;133:38–44.
[82] Bengtsson S, Pisco AR, Johansson P, Lemos PC, Reis MA. Molecular weight and thermal properties of polyhydroxyalkanoates produced from fermented sugar molasses by open mixed cultures. J Biotechnol 2010;147:172–9.
[83] Cesário MT, Raposo RS, de Almeida MCM, Van Keulen F, Ferreira BS, Telo JP, et al. Production of poly (3-hydroxybutyrate-co-4-hydroxybutyrate) by Burkholderia sacchari using wheat straw hydrolysates and gamma-butyrolactone. Int J Biol Macromol 2014;71:59–67.
[84] Martino L, Cruz MV, Scoma A, Freitas F, Bertin L, Scandola M, et al. Recovery of amorphous polyhydroxybutyrate granules from Cupriavidus necator cells grown on used cooking oil. Int J Biol Macromol 2014;71:117–23.
[85] Thinagaran L, Sudesh K. Evaluation of sludge palm oil as feedstock and development of efficient method for its utilization to produce polyhydroxyalkanoate. Waste and biomass valorization 2019;10:709–20.
[86] Tufail S, Munir S, Jamil N. Variation analysis of bacterial polyhydroxyalkanoates production using saturated and unsaturated hydrocarbons. Braz J Microbiol 2017;48:629–36.
[87] Mallick SK, Pramanik M, Maity B, Das P, Sahana M. Plastic waste footprint in the context of COVID-19: reduction challenges and policy recommendations towards sustainable development goals. Sci Total Environ 2021;796:148951.
[88] Fan Y, Cai D, Zhang S, Wang H, Guo K, Zhang L, et al. Effective removal of nitrogen compounds from model diesel fuel by easy-to-prepare ionic liquids. Separ Purif Technol 2019;222:92–8.
[89] Li M, Wilkins MR. Recent advances in polyhydroxyalkanoate production: feedstocks, strains and process developments. Int J Biol Macromol 2020;156:691–703.

About UMT Faculty SDI

Selective Dissemination of Information (SDI) service is a current-awareness service offered by the PSNZ for UMT Faculty Members. The contents selection criteria include current publications (last 5 years), highly cited and most viewed/downloaded documents. The contents with pdf full text from subscribed databases are organized and compiled according to a monthly theme which is determined based on the topics of specified interest.

For more information or further assistance, kindly contact us at 09-6684185/4298 or email to psnz@umt.edu.my/sh_akmal@umt.edu.my

Thank you.

Perpustakaan Sultanah Nur Zahirah
Universiti Malaysia Terengganu
21030 Kuala Nerus, Terengganu.
Tel. : 09-6684185 (Kaunter Utama)
Fax : 09-6684179
Email : psnz@umt.edu.my